ACS central science

http://pubs.acs.org/journal/acscii

Research Article

The Interplay of Electrostatics and Chemical Positioning in the Evolution of Antibiotic Resistance in TEM β-Lactamases

Samuel H. Schneider,[#] Jacek Kozuch,[#] and Steven G. Boxer*

Cite This: *ACS Cent. Sci.* 2021, 7, 1996–2008

Read Online

ACCESS | Metrics & More | Article Recommendations | Supporting Information

ABSTRACT: The interplay of enzyme active site electrostatics and chemical positioning is important for understanding the origin(s) of enzyme catalysis and the design of novel catalysts. We reconstruct the evolutionary trajectory of TEM-1 β-lactamase to TEM-52 toward extended-spectrum activity to better understand the emergence of antibiotic resistance and to provide insights into the structure−function paradigm and noncovalent interactions involved in catalysis. Utilizing a detailed kinetic analysis and the vibrational Stark effect, we quantify the changes in rates and electric fields in the Michaelis and acyl-enzyme complexes for penicillin G and cefotaxime to ascertain the evolutionary role of electric fields to modulate function. These data are combined with MD simulations to interpret and quantify the substrate-dependent structural changes during evolution. We observe that this evolutionary trajectory utilizes a large preorganized electric field and substrate-dependent chemical positioning to facilitate catalysis. This governs the evolvability, substrate promiscuity, and protein fitness landscape in TEM β-lactamase antibiotic resistance.

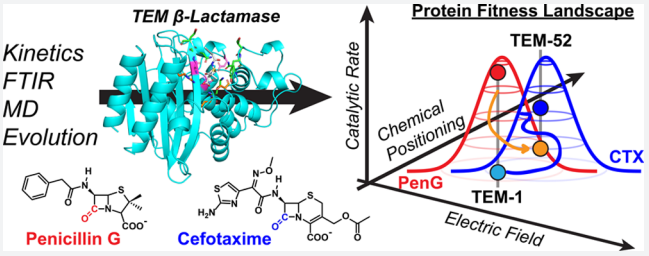

INTRODUCTION

The origins of the enormous catalytic capacity of enzymes remain a long-standing question. Unraveling these origins is essential to our ability to design and engineer proteins with diverse functions, as well as rationalize the evolutionarily acquired mutations that lead to altered functions such as novel substrate scopes and chemistry, solvent adaptation, thermal stability, and improved rates, as demonstrated with the many successes of directed evolution.[1,2] A physical picture of enzyme evolution requires new observables that can link evolutionary changes in catalysis to local interactions arising from mutations.

Recent experimental work, based on the electrostatic catalysis model and the vibrational Stark effect (VSE), has quantified the electrostatic contribution to catalysis in the model enzyme, ketosteroid isomerase (KSI),[3,4] and more generally for enzymes such as serine proteases and 4-chlorobenzoyl-CoA dehalogenase.[5,6] The VSE method utilizes high-frequency and local vibrational reporters, such as carbonyls (C═O), to quantify the electric field created by functional groups in enzyme active sites. Carbonyls are the functional moieties of many enzymatic reactions, including KSI and the β-lactamases discussed in detail in the following, making them ideal for investigating electrostatic catalysis.

Measurement of the active site electric field is achieved through calibration of the carbonyl-containing molecule by VSE spectroscopy, using a well-defined external electric field, vibrational solvatochromism, and MD simulations.[5,7] This approach provides an electric field-frequency calibration curve from which the environment's electric field projected onto the probe bond can be directly quantified using vibrational (IR or Raman) spectroscopy.[6] By combining the free-energy barrier of activation, $\Delta G^{\ddagger}$, from steady-state kinetics and transition-state (TS) theory with measurements of the active site electric field ($\vec{F}_{enz}$) for a series of wild-type (WT) and mutant enzymes, the contribution of electrostatic catalysis to accelerate a reaction ($\Delta\Delta G^{\ddagger}$) can be modeled according to[6,8]

$$\Delta\Delta G^{\ddagger} = -[(\vec{F}_{enz,TS}\cdot\vec{\mu}_{TS}) - (\vec{F}_{enz,RS}\cdot\vec{\mu}_{RS})] \quad (1)$$

where $\vec{\mu}_{TS}$ and $\vec{\mu}_{GS}$ are the TS and reactant-state (RS) dipole moment for bonds that change charge distribution over the course of the reaction coordinate (see SI Section 3a for further discussion).

All previous studies using the VSE approach have been performed on wild-type and site-directed mutant enzymes,[6] where the latter were all deleterious to the overall enzymatic function and do not necessarily reflect those acquired over the course of evolution. However, the multidimensional evolutionary fitness landscape can modulate favorable enthalpic and entropic effects by improving the electrostatic environment and chemical positioning within the enzyme active site. Chemical positioning refers to both entropic and enthalpic

Received: July 21, 2021
Published: November 22, 2021

Downloaded via STANFORD UNIV on December 22, 2021 at 19:40:46 (UTC).
See https://pubs.acs.org/sharingguidelines for options on how to legitimately share published articles.

ACS Publications

© 2021 The Authors. Published by American Chemical Society

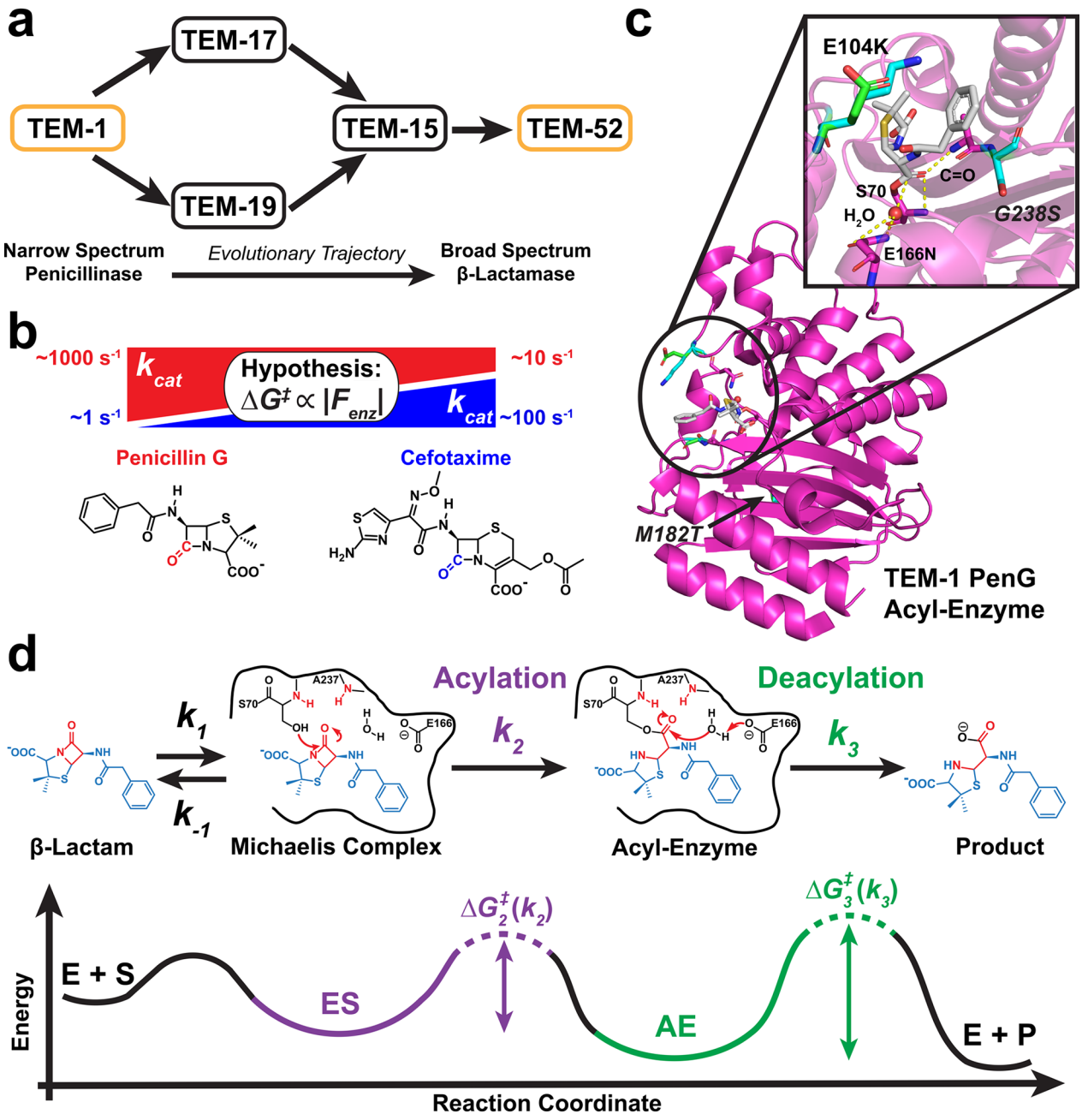

Figure 1. Evolutionary trajectory and reaction mechanism of TEM-1 to TEM-52 β-lactamase. (a) Most probable evolutionary trajectory from TEM-1 to TEM-52 with the acquisition of three mutations (E104K, G238S, and M182T) which alters the substrate scope of TEM β-lactamase from narrow spectrum to broad spectrum activity against β-lactam antibiotics.[10,16,26] (b) Order of magnitude change in rate-constant for the hydrolysis (k_{cat}) of penicillin G (PenG; red) and cefotaxime (CTX; blue) over the course of evolution from TEM-1 to TEM-52[30] with the hypothesized change in free energy barrier of activation ($\Delta G^{\ddagger}$ from TS-theory) proportional to the active site electric field, $|F_{enz}|$. Reactive carbonyls of the β-lactams are highlighted for clarity. (c) Crystal structure (PDB ID: 1fqg) of the TEM-1 E166N acyl-enzyme complex with PenG (gray) highlighting the E104K, M182T, and G238S positions (blue) relative to TEM-1 (green) with the functional β-lactam and other catalytic moieties labeled near the oxyanion hole (see SI Discussion Section 1). (d) Mechanism of class A β-lactamases and reaction coordinate diagram for PenG hydrolysis. The Michaelis complex (ES; noncovalent) and acyl-enzyme (AE; covalent) are illustrated in reference to functionally important active site residues formed via the amide backbone nitrogens of S70 and A237 as well as key catalytic residues, S70 and E166, necessary for the acylation and deacylation reactions, respectively. The functional β-lactam ring and oxyanion hole are shown in red and all other substrate moieties in blue, where chemical functionalization is altered across antibiotic classes (e.g., penicillins, cephalosporins, monobactams, etc.). The two chemical steps, acylation (k_2; purple) and deacylation (k_3; green), can be related to their respective activation free energy barriers through transition-state theory which proceed through tetrahedral intermediates at each step (dotted lines, see Scheme S1 for details). Barrier heights not drawn to scale.

effects on catalysis of placing reactive groups in close proximity and correct orientations relative to the bound substrate. While both electrostatic catalysis and chemical positioning are important, we start with the hypothesis that, similar to KSI,[6] if electrostatic TS-stabilization is the primary driving force for navigating the evolutionary fitness landscape, then an enzyme's evolution toward improved function (i.e., lower $\Delta G^{\ddagger}$) would correspond to a proportional increase in the active site electric

https://doi.org/10.1021/acscentsci.1c00880
ACS Cent. Sci. 2021, 7, 1996−2008

field (note that negative electric fields correspond to stabilizing interactions).

The enzymes we have chosen to test this hypothesis are β-lactamases, which play a clinical role in the emergence of antibiotic resistance.[9,10] TEM-1, a class A and the first isolated and genetically characterized β-lactamase, has served as a model enzyme for understanding protein evolution toward extended-spectrum β-lactamase (ESBL) activity, one of the mechanisms for achieving antibiotic resistance.[11−22] There are now over 240 TEM β-lactamase clinical variants (and over 7100 identified β-lactamases in total[23]) that endow extended-spectrum activity against multiple β-lactams (including penicillins, cephalosporins, and monobactams) as well as inhibitor-resistance (e.g., clavulanic acid).[24] TEM-1 has narrow spectrum penicillinase activity, i.e., against penicillin G (PenG) and ampicillin, and its evolution toward new function against other classes of β-lactam antibiotics, such as cephalosporins, has been observed both in clinical isolates and in directed evolution.[25,26]

One of the most well-studied ESBL evolutionary trajectories is from TEM-1 over the course of three mutations, E104K, G238S, and M182T, to TEM-52 (E104K/G238S/M182T Ambler notation;[27] Figure 1a−c, SI Discussion S1), resulting in both decreased penicillinase activity and increased hydrolysis of the third-generation cephalosporin, cefotaxime (CTX). We use the functionally critical β-lactam C═O (Figure 1b,d)[25,28,29] as an IR probe of the active site electric field. The general mechanism and reaction coordinate for class A β-lactamases are shown in Figure 1d. Upon binding, the β-lactam antibiotic forms the noncovalent enzyme−substrate complex (ES) which is first acylated via ring-opening of the β-lactam by the active site serine (S70), forming an acyl-enzyme intermediate (AE). The AE complex is subsequently deacylated via a nucleophilic water molecule activated by a nearby glutamate (E166), followed by product release.[10] These two reaction steps are associated with two distinct activation barriers, i.e., $\Delta G_2^{\ddagger}$ and $\Delta G_3^{\ddagger}$, which give rise to two catalytic rate constants k_2 and k_3, respectively. Note that in contrast to KSI which uses amino acid side-chains to H-bond with the substrate/inhibitor, TEM β-lactamases interact with the bound β-lactam C═O through the backbone amides of S70 and A237. These backbone amides serve as hydrogen-bond donors and are maintained throughout the course of natural evolution, although slight changes in their position may result from the three mutations at more distant positions acquired from TEM-1 to TEM-52 (Figure 1c).

In the following, we use two substrates, PenG and CTX, to monitor the evolutionary changes to catalytic rates, the electric fields sensed by the reactive β-lactam in response to the charge distribution of the active site, and chemical positioning throughout the active sites. In order to understand the mechanistic implications of these evolutionary changes we measured the Michaelis−Menten kinetic parameters and the corresponding acylation (k_2) and deacylation (k_3) rate constants for all mutants utilizing both PenG and CTX as substrates. Using the VSE to monitor local catalysis-relevant electric fields and molecular dynamics (MD) simulations to evaluate changes in chemical positioning, we expand upon the physical origins of antibiotic resistance and catalysis in TEM β-lactamases.

RESULTS AND DISCUSSION

Kinetic Decomposition of β-Lactamase Activity. Given the mechanism for class A β-lactamases (Figure 1d)

$$E + S \underset{k_{-1}}{\overset{k_1}{\rightleftarrows}} ES \xrightarrow{k_2} AE \xrightarrow{k_3} E + P$$

the conventional Michaelis−Menten parameters, k_{cat} and K_M, correspond to

$$k_{cat} = \frac{k_2 k_3}{k_2 + k_3} \tag{2}$$

$$K_M = \frac{k_3(k_{-1} + k_2)}{k_1(k_2 + k_3)} \tag{3}$$

To determine the acylation (k_2) and deacylation (k_3) rate constants, we followed the previously described steady-state mass spectrometry approach (Figures S2−5).[31] At steady-state conditions, the relative concentrations of the AE and ES complexes can be directly related to the corresponding rate constants according to (Figures S3−4)

$$\frac{[AE]}{[ES]} = \frac{k_2}{k_3} \tag{4}$$

The kinetic results are presented pictorially in Figure 2 and summarized in Table S1 (see Methods and Figure S2−5).

As seen in Figure 2, the rate constants all change in accordance with the observed ESBL phenotype as TEM-1 evolves toward TEM-52. In the case of PenG hydrolysis (Figure 2a), the mutations generally decrease the rate constants in accordance with the loss of function as a narrow-spectrum penicillinase; however, the K_M decreases significantly going from TEM-1 to TEM-52, primarily as a result of the G238S mutation (Table S1). As has been previously observed with TEM-1 and PenG,[31,32] the rate-limiting step for all variants is deacylation (k_3). The extent to which acylation and deacylation change (i.e., k_2/k_3) is differentially affected by the mutations. All of the mutations, with the exception of TEM-19 (G238S), lead to k_2/k_3 being perturbed away from that of TEM-1 ($k_2 \approx k_3$),[32] with the double mutant TEM-15 being the most perturbed ($k_2/k_3 > 10$). The ratio is then partially recovered with the global suppressor mutation, M182T, which is distant from the active site but thermodynamically stabilizing,[16] leading to TEM-52 ($k_2/k_3 \approx 5$). This kinetic evaluation deconvolves some of the epistatic relationship of these mutations on function, supplementing previous studies.[12,13]

In the case of the evolutionarily improved CTX hydrolysis (Figure 2b), we observe an improvement in both binding and turnover with the two distal active site mutations, E104K and G238S, and minimal effect of M182T, relative to TEM-1. Significantly, and in contrast to that of PenG hydrolysis, the rate-limiting step for each variant is the acylation (k_2) step, such that $k_2 \approx k_{cat}$, as previously suspected by several authors.[10,31,33] Furthermore, the relative ratio of k_2/k_3 generally improves (i.e., toward unity) as TEM-1 evolves toward the ESBL TEM-52, primarily as a result of the G238S mutation. In terms of TEM-52's phenotype as an ESBL, i.e., increased promiscuity, the final corresponding rate constants for both PenG and CTX converge toward the same order of magnitude, consistent with the broad-spectrum activity profile.

https://doi.org/10.1021/acscentsci.1c00880
ACS Cent. Sci. 2021, 7, 1996−2008

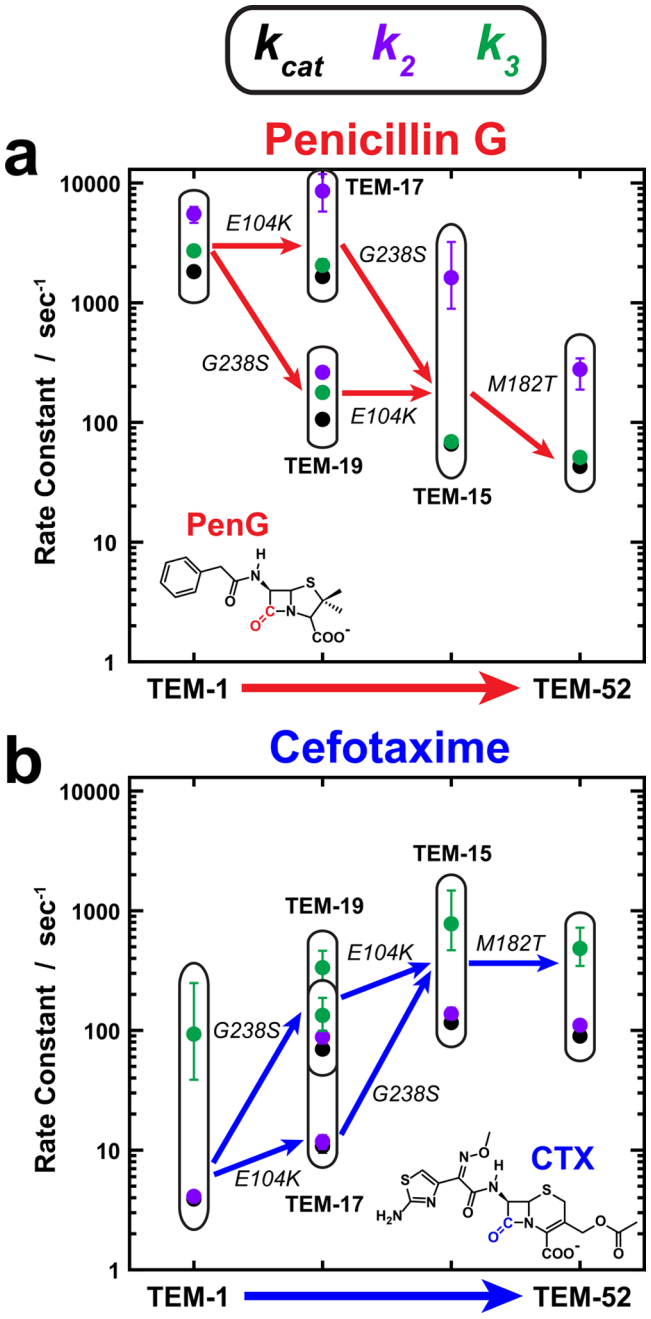

Figure 2. Evolution of the catalytic rates of β-lactam hydrolysis from TEM-1 to TEM-52. The absolute rate constants for (a) PenG (red) and (b) CTX (blue) hydrolysis are shown for k_{cat} (black), k_2 (purple), and k_3 (green), for each TEM β-lactamase mutant along the evolutionary trajectory from TEM-1 to TEM-52 as denoted by directional arrows. Error bars represent the equivalent of 1 standard deviation (68.25% confidence interval (CI)), see the Methods section, Table S1, and Figures S2−5 for details.

VSE Measurements of β-Lactamase Complexes. We utilized isotope-edited $^{12}C-^{13}C$ difference spectroscopy to determine the active site electric fields using the VSE, made possible by site-specific isotope incorporation of ^{13}C into common β-lactam antibiotics.[34] This method enables detection of a single C═O stretching frequency even amid the extensive protein backbone signal (Figures S6,7).[35] In order to trap the ES and AE species for the intrinsically slow IR measurements, we introduce the S70G and E166N mutations, respectively, to monitor the mechanistic intermediates. These kinetically incompetent background S70G or E166N mutations are denoted "TEM-# S70G" or "TEM-# E166N" relative to the evolutionary and clinically observed WT proteins TEM-1, -17, -19, -15, and -52. We infer the projected electric fields based on the observed frequency shifts using the electric-field/frequency calibration of model compounds.[36] We use the smallest and chemically simplest rigid functional moieties of the β-lactam substrate's C═O, namely, the bicyclic penam/cephem core and the acylated ester for the ES and AE complexes, respectively (see ref 36 and Figure S7).

Isotope-edited difference IR measurements of PenG and CTX in the S70G ES and E166N AE complexes with TEM β-lactamases are shown in Figure 3 (see Figure S9 for further details of spectral processing and Figure S10 for additional S70 and E166N variant spectra). Across all of the enzyme−substrate complexes, we observe multiple sets of narrow (fwhm 5−16 cm^{-1}) vibrational features, with corresponding sets of ^{12}C (positive) and ^{13}C (negative) features (shown only on the bottom spectrum in each panel for clarity, Figure 3c−f) that exhibit the expected isotope frequency shift of $\Delta\bar{\nu} \sim 40$ cm^{-1} (Tables S3−6). These peaks are significantly narrower than the β-lactam C═O frequency in aqueous buffer (D_2O, Figure S6), which is observed at 1762 cm^{-1} with fwhm ~35 cm^{-1}. The multiple features are indicative of conformational heterogeneity upon binding. Previous studies with β-lactamases have indicated the possibility of multiple peaks upon substrate binding, but they could not be confidently assigned in the absence of isotopic labels.[37,38]

As shown in Figure 3c−f, where the upper axis translates the observed frequencies into electric fields (Figure S7), we observe predominantly two distinct electric field environments for both PenG and CTX: a major population (by integrated area) in a small electric field conformation (ca. −30 to −70 MV/cm), and minor populations at significantly larger and more stabilizing (i.e., more negative) electric fields (ca. −140 to −175 MV/cm). The lineshapes of the lower electric field species are broad compared to the minor species experiencing much larger electric fields. The simplest interpretation of line width variations in proteins is that they reflect the heterogeneity of the environment around the probe.[39] For PenG, we observe minimal changes in the peak position/electric field over the course of (de)evolution for either the small or large electric field species, with the largest electric field species consistently observed at ca. −175 and −140 MV/cm (Figure 3c,d) for the ES and AE complexes, respectively. However, there is an increase in conformational heterogeneity as evidenced by additional populations with fields of ca. −160 and −30 MV/cm with introduction of G238S (i.e., TEM-19, TEM-15, and TEM-52). For PenG, the negligible effect on the electric field sensed by the reactive C═O over evolution contradicts the hypothesized changes expected based on the observed rate decrease; the implications of this are discussed below. For CTX (Figure 3e,f), we observe minimal changes in the small electric field species but significantly larger electric fields detected over the course of evolution toward TEM-52, with the largest improvement in field (ΔF(TEM-52 − TEM-1) ≈ −40 MV/cm) corresponding to the ES complex (k_2 is rate-limiting). Interestingly, the largest electric fields projected onto the CTX C═O converge toward the maximum fields experienced by PenG's C═O of ca. −175 and −145 MV/cm for the ES and AE complexes, respectively; the corresponding conformational heterogeneities converge in a

https://doi.org/10.1021/acscentsci.1c00880
ACS Cent. Sci. 2021, 7, 1996−2008

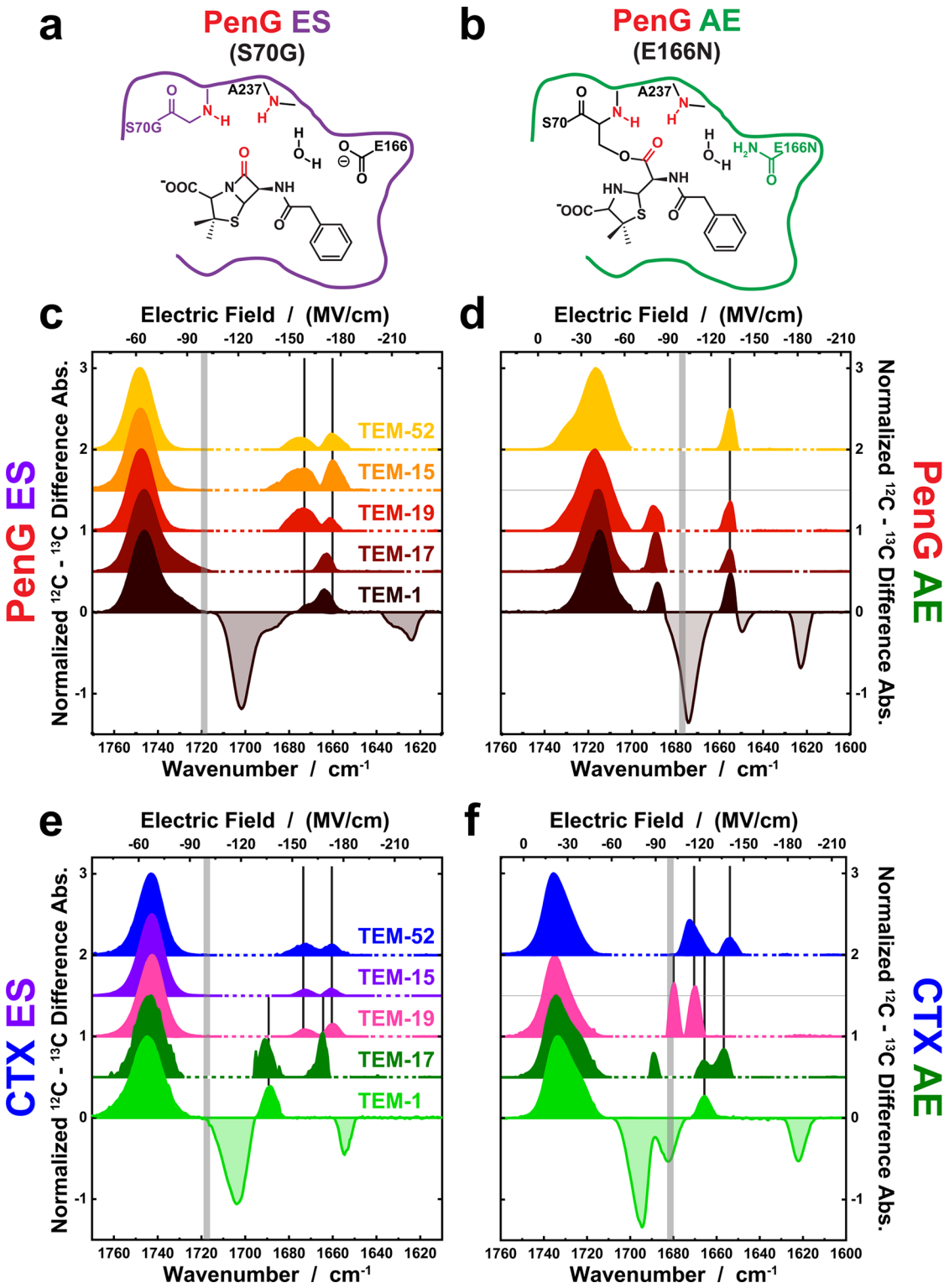

Figure 3. Isotope-edited IR difference spectroscopy of the TEM β-lactamases. (a,b) Schematic illustration of the active site environment of TEM β-lactamases in the (a) ES and (b) AE complexes with PenG and the background mutations S70G and E166N required for FTIR spectroscopy. The oxyanion hole, composed of backbone amides from S70 and A237, relative to the substrate C═O are shown in red. (c−f) Vibrational frequencies and corresponding electric fields for (c,d) PenG and (e,f) CTX in the (c,e) ES (S70G) and (d,f) AE (E166N) complexes across evolutionary variants from TEM-1 to TEM-52. IR spectra are shown as a ^{12}C-normalized difference absorbance with an example ^{12}C−^{13}C spectra shown for TEM-1 complexes and otherwise depicted with only the positive (^{12}C) features for clarity with dashed horizontal axes indicating negative features that have been removed for simplicity (see Figure S8 for full ^{12}C−^{13}C difference spectra). The top axis is the electric field corresponding to the ^{12}C-isotope of the corresponding VSE calibrated probe (Figure S7). The panels are subdivided between those C═O species corresponding to small or large electric fields (−100 MV/cm; vertical gray bars) to broadly classify the results. Vertical black lines indicate large electric field species changes between evolutionary mutations. The TEM-15 E166N mutant was not measured due to the protein's instability and likely aggregation, observed as increasing protein-specific spectral changes and a loss of 280 nm absorbance over time.

https://doi.org/10.1021/acscentsci.1c00880
ACS Cent. Sci. 2021, 7, 1996−2008

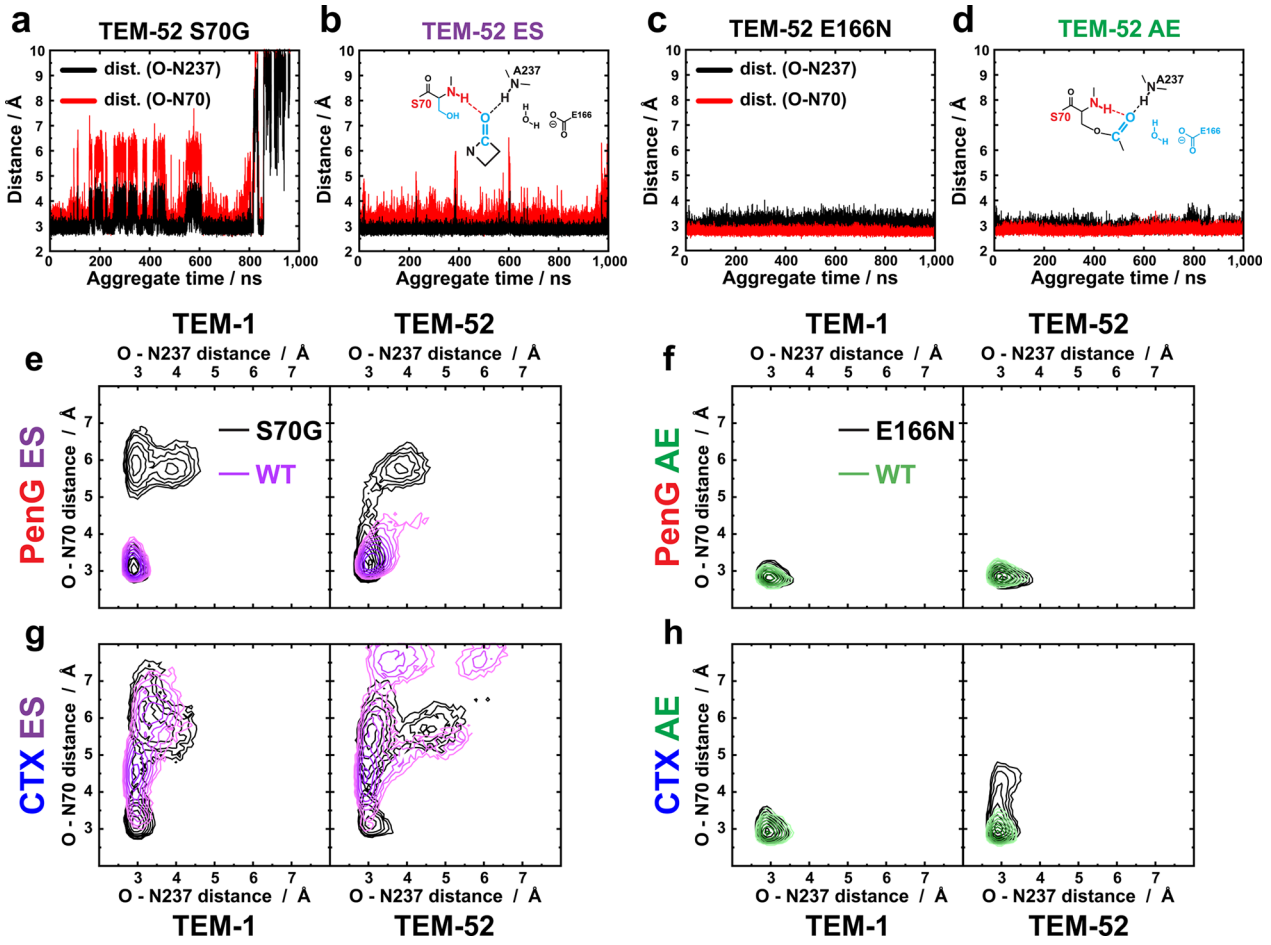

Figure 4. MD structure-guided approach to assess the effect of background and evolutionary mutations on the ES and AE complexes. (a–d) Example MD trajectories of the TEM-52 $O_{\beta lactam\ C=O}$–N distances between the oxyanion hole composed of the backbone N–H of S70 (red) and A237 (black), and the β-lactam C=O of PenG in the ES and AE complexes. Comparison of the background mutations (a) TEM-52 S70G ES and (c) TEM-52 E166N AE relative to the (b,d) TEM-52 WT ES and AE complexes, respectively, provides a means to assess perturbations to the active site environment, e.g., conformational sampling, structural fluctuations, and effects of evolutionary mutations. (e–h) 2D correlation plots of the O–N distances as a function of background mutants (black contours) relative to the WT for the (e,g) ES (purple) and (f,h) AE (green) complexes of TEM-1 and TEM-52 with (e,f) PenG and (g,h) CTX. Contours represent dwell times ≥400 ps on a log-scale. Average structures of overlapping conformational species were evaluated for structural similarity (see main text).

similar way. The magnitude of the electric field in the high-field population in TEM is consistent with or even considerably larger than that of other proteins with similar oxyanion holes composed of backbone amides (ca. −90 to −120 MV/cm).[5]

MD Simulations of β-Lactamase Complexes—Effects of S70G and E166N Mutations. We utilized MD simulations to provide a structural basis for interpreting the IR and kinetic results as well as monitoring changes in chemical positioning between the start and end points of the evolutionary trajectory (TEM-1 and TEM-52; 1 μs MD runs of each). The MD simulations provide two primary results (Figure S11): (1) they compare and contrast the extent to which the necessary background mutations, S70G and E166N, bias the conformational sampling relative to their WT variants and assess the functional relevance of the species detected by IR; and (2) they help elucidate the structural origins and effects of chemical positioning on catalysis and evolution, which cannot be fully described by electrostatics as evidenced by the VSE results. While QM/MM(MD) calculations would allow us, in principle, to predict activation barriers, the current accuracy of such approaches[40] would be insufficient given the experimentally observed changes of barriers of ca. ± 2 kcal/mol along the evolutionary pathway, and particularly in light of the high degree of conformational heterogeneity and fluctuations described below.

Protein–ligand complexes were simulated starting from an initial ligand pose based on crystallographic coordinates of PenG-acylated TEM-1 E166N (PDB ID: 1FQG) and CTX-acylated Toho-1 E166A (PDB ID: 1IYO), which were modeled into the corresponding variants in both the noncovalent ES and covalent AE states (see Methods). We focus on the oxyanion hole interactions that are important for function and most directly relevant to interpreting the VSE results,[41] namely, the O–N distances between the β-lactam C=O and the backbone amide nitrogens of S70 and A237. To compare the background mutants with WT, the O–N distances were measured for the ES complexes of WT and S70G, and the AE complexes of the WT and E166N; the comparison is made for both TEM-1 and TEM-52 (Figure 4a-d). Based on these MD trajectories, 2D-correlation plots of the $O_{\beta lactam\ C=O} - N_{A237}$ ("O − N237") versus the $O_{\beta lactam\ C=O} - N_{S70}$ ("O − N70") distances were generated for each protein–ligand complex (Figure 4e-h), and the average structures for

https://doi.org/10.1021/acscentsci.1c00880
ACS Cent. Sci. 2021, 7, 1996−2008

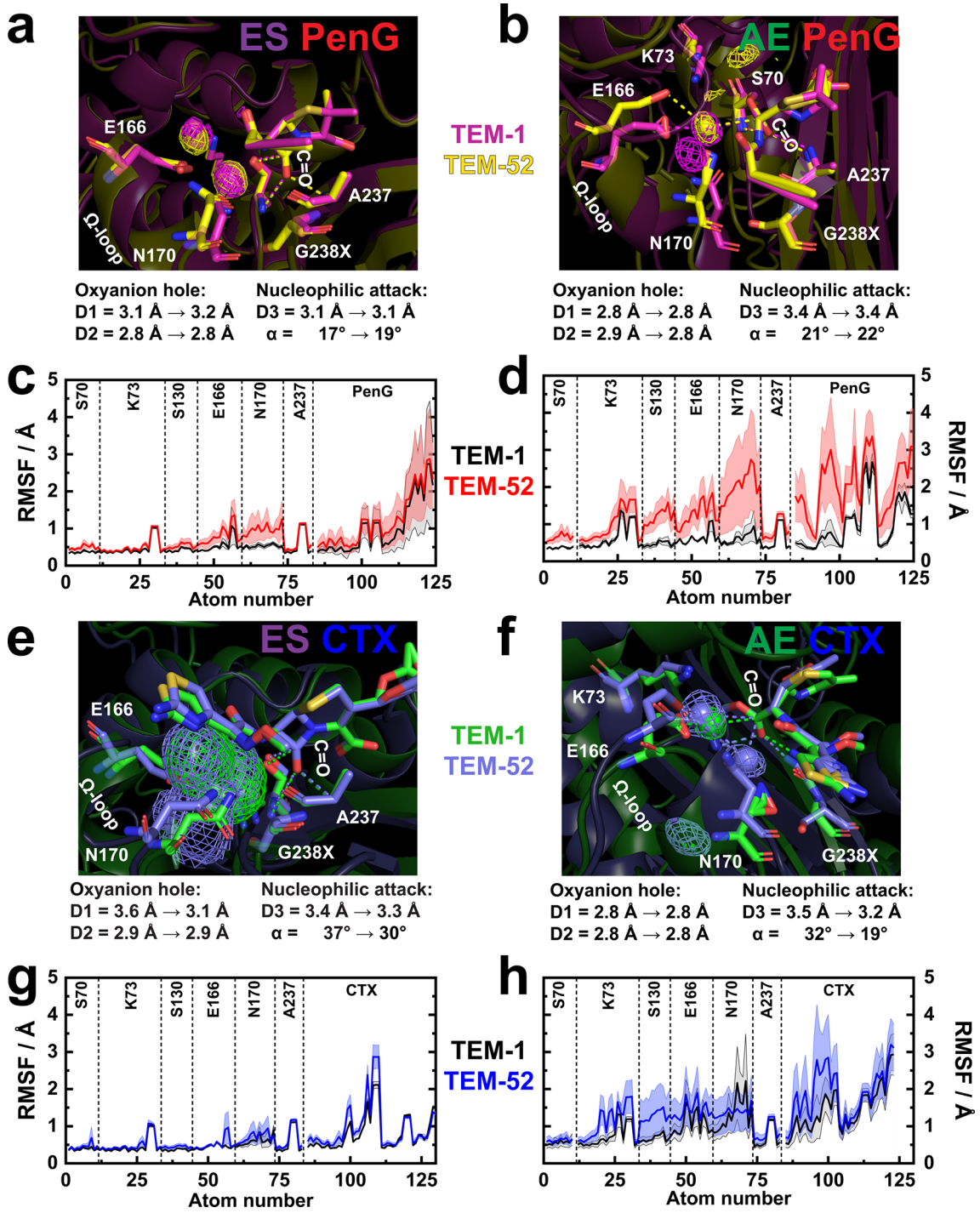

Figure 5. Catalytic interactions and active site structural heterogeneity in TEM β-lactamases as quantified via MD simulations. (a,b,e,f) Average active site structural overlay of (a,b) PenG and (e,f) CTX in complex with TEM-1 (pink or green) and TEM-52 (yellow or purple) in the ES and AE complexes, respectively. D1 and D2 refer to the $N_{backbone}-O_{\beta lactam\ C=O}$ distances of the oxyanion hole between the β-lactam C═O and the S70 and A237 backbone amides, respectively. D3 and α refer to the distance and angle of the nucleophilic S70 side chain O atom or catalytic water O atom in the ES- or AE-complex, respectively, the latter relative to the substrate C═O (the plane of the β-lactam and ester C═O in the ES and AE complexes, respectively, Scheme S4). Structures are aligned according to the substrate's C═O to indicate evolutionary changes from the perspective of the reactive functional group. Averaged structures as well as extracted observables/values refer to MD aggregate times of 1 μs, except for CTX ES complexes where a total of 200 ns was used. Comparison of catalytic interactions with the oxyanion hole and nucleophilic S70 or reactive water are indicated by dotted lines and values. Solid spheres in the AE complexes represent the average water positions, and isomeshed density represents the active site regions where waters are observed in the vicinity of E166 and the substrate. (c,d,g,h) Absolute RMSF of active site residues and substrate atoms with respect to TEM-1 (black) and TEM-52 (red or blue) for (c,d) PenG and (g,h) CTX in the ES and AE complexes. Solid lines represent the average RMSF of a given atom across the MD trajectories with the 95% CI shown with dotted lines and shaded regions. See SI Scheme S3, Tables S7−12, Figures S16−18 for further details on active site RMSF and distance changes between TEM-1 and TEM-52 with PenG and CTX.

https://doi.org/10.1021/acscentsci.1c00880
ACS Cent. Sci. 2021, 7, 1996−2008

each conformation were compared between the mutants and WT protein complexes (Figure S11−13). Comparison of the commonly observed conformations, for both the S70G and E166N mutants and the respective WT proteins, enables a structure-guided approach to interpret the IR and kinetic results as discussed below. While it is tempting to directly calculate the active site electric field as experienced by the β-lactam C═O in the MD simulations, accurate calculation of electric fields when short H-bonds are involved in catalysis requires more advanced simulation force fields and levels of theory.[42−47]

A comparison of MD simulations of the S70G and E166N background mutants with WT complexes, which are inaccessible to our IR measurements, provides insights into states that are due to the required background mutations versus those that are catalytically permissive (Figure 4). In these simulations, the background mutations introduce exaggerated conformational heterogeneity relative to the WT, primarily evident in the ES complexes, where the functional β-lactam C═O is displaced from the oxyanion hole due to increased water accessibility (Figure S13). This results in the C═O forming H-bonds to structured water located in the active site, which would be expected to result in smaller electric fields than those observed in the oxyanion hole, consistent with the VSE measurements and vibrational solvatochromism in water (Figure 3, Figures S7, 13−14).[36] When we biased the WT ES complexes to start from structures resembling these long O−N states in the S70G mutant, we find that these conformations are not maintained, and generally converge toward the shortest O−N distance species (Figure S15). This suggests that the removal of the S70 side chain can induce additional substrate binding modes within the active site oxyanion hole, as previously suggested in the TEM-1 S70G crystal structure.[48] Importantly, the species with the shortest oxyanion hole distances (<4 Å), likely the catalytically permissive states, are commonly observed in both the background mutants and WT TEM-1 and TEM-52 simulations for the ES and AE complexes with PenG and CTX. The average structures are similar to the crystallographic binding geometry as observed for the TEM-1 S70G and E166N complexes with PenG (Figures S12, 13).[48,49] We consider only those species shared in common as the biologically relevant and catalytically permissive species.

MD Simulations of β-Lactamase Complexes—Evolutionary Changes and Structural Plasticity. Based on the MD results, we quantify the significant ($p < 0.05$ in two-tailed t test) and substrate-dependent structural changes from TEM-1 to TEM-52 in terms of the changes in interatom distances and root-mean square fluctuations (RMSF) of key atoms and residues in the active site (Figure 5, Scheme S3, Tables S7−12). We emphasize in Figure 5 only those residues directly involved in the extended H-bond network to nucleophilic groups, i.e., the first coordination sphere, with other potentially important residues reported in Tables S7−12 and Figures S16−18. These structural and dynamic changes are generally involved in modulating interactions with the catalytic residues and/or water, binding of the β-lactams' amide side-chains or carboxylates, or the extensive H-bond network in the active site. Alignment of the reactive substrate C═O in TEM-1 and TEM-52 for the corresponding ES and AE complexes provides a functional and structural glimpse into how the evolutionarily acquired mutations modulate catalytic turnover of PenG and CTX (Figure 5a,b,e,f), complementary to the VSE measurements. The changes in structural heterogeneity of key active site atoms and residues, in terms of RMSFs, are graphically presented in Figure 5c,d,g,h to identify key differences between TEM-1 and TEM-52 in a substrate-dependent and ES- and AE-dependent manner.

The introduction of the evolutionarily acquired mutations E104K and G238S leads to substrate-dependent structural changes across the active site (see also SI Discussion S2,3). These changes primarily affect H-bonding interactions in the Ω-loop[10,50] (E166 and N170) and surrounding H-bond network, which modulate the positioning of S70, E166, and the catalytic water with respect to the reactive C═O (Figure 5). For example, the average structures from MD simulations illustrate how the G238S mutation contributes to disrupting the backbone interaction of N170−G238 in TEM-1, which results in the Ω-loop becoming more flexible and expanding the active site to accommodate larger substrates such as CTX (Figure 5).[10] We generally observe an increase in structural heterogeneity for interactions with PenG and CTX in TEM-52 relative to TEM-1 as evident in the RMSF, which is also associated with additional active site water molecules (Figure 5b,e,f). For CTX, interactions in ES and AE are differently affected. In the ES complex, we observe minimal changes in the active site RMSFs, but there is a significant shortening of the distance of the β-lactam C═O to the S70 backbone amide ($\Delta D_1 = -0.5$ Å) as well as improved positioning of the S70 side-chain hydroxyl group for the nucleophilic attack ($\alpha = 37° \rightarrow 30°$; Figure 5e, Scheme S4), which approaches those observed in the TEM-1 ES-complex with PenG (Figure 5a). The shortened distance of the β-lactam C═O to the backbone amide would be predicted to lead to an increase in the electric field of the highest-field (most red-shifted) component, consistent with the VSE results (Figure 3). In the AE complex with CTX, there is increased solvent accessibility as evident from the presence of an additional water molecule in the vicinity of E166, N170, and CTX, which exhibits improved positioning in terms of attack distance and angle relative to those found in TEM-1 (Figure 5f), again approaching those observed in the AE-complex with PenG (Figure 5b). There are additional significant structural changes, in terms of both interatom distances and RMSFs that are observed more globally around the active site, consistent with the aforementioned observations and, thus, likely to support the positioning of reactive groups as well as modulating substrate binding into the oxyanion hole (Scheme S3, Table S7−14, Figure S16−18). This is a result of the substrate-specific geometry of the bicyclic core (i.e., penam versus cephem), including the carboxylate geometry relative to the β-lactam C═O, and the amide side-chain, which together differentially influence and are influenced by the evolutionary trajectory (Table S13, 14, Figure S19).

Role of Electric Fields and Structural Changes for Catalysis. Based on our initial hypothesis that electrostatic catalysis underlies the evolution of β-lactamases, we assumed that activation barriers and active site electric fields (at the β-lactam C═O) would follow a clear linear trend along the chosen evolutionary trajectory, similar to the trends observed in our previous studies on KSI, serine proteases, and 4-chlorobenzoyl-CoA dehalogenase.[3−5] However, despite the presence of remarkably high electric fields in the active site exerted on the β-lactam C═O, the correlation of the two observables for both substrates and for both reaction steps does not exhibit a straightforward linear trend (Figure 6a,b).

https://doi.org/10.1021/acscentsci.1c00880
ACS Cent. Sci. 2021, 7, 1996−2008

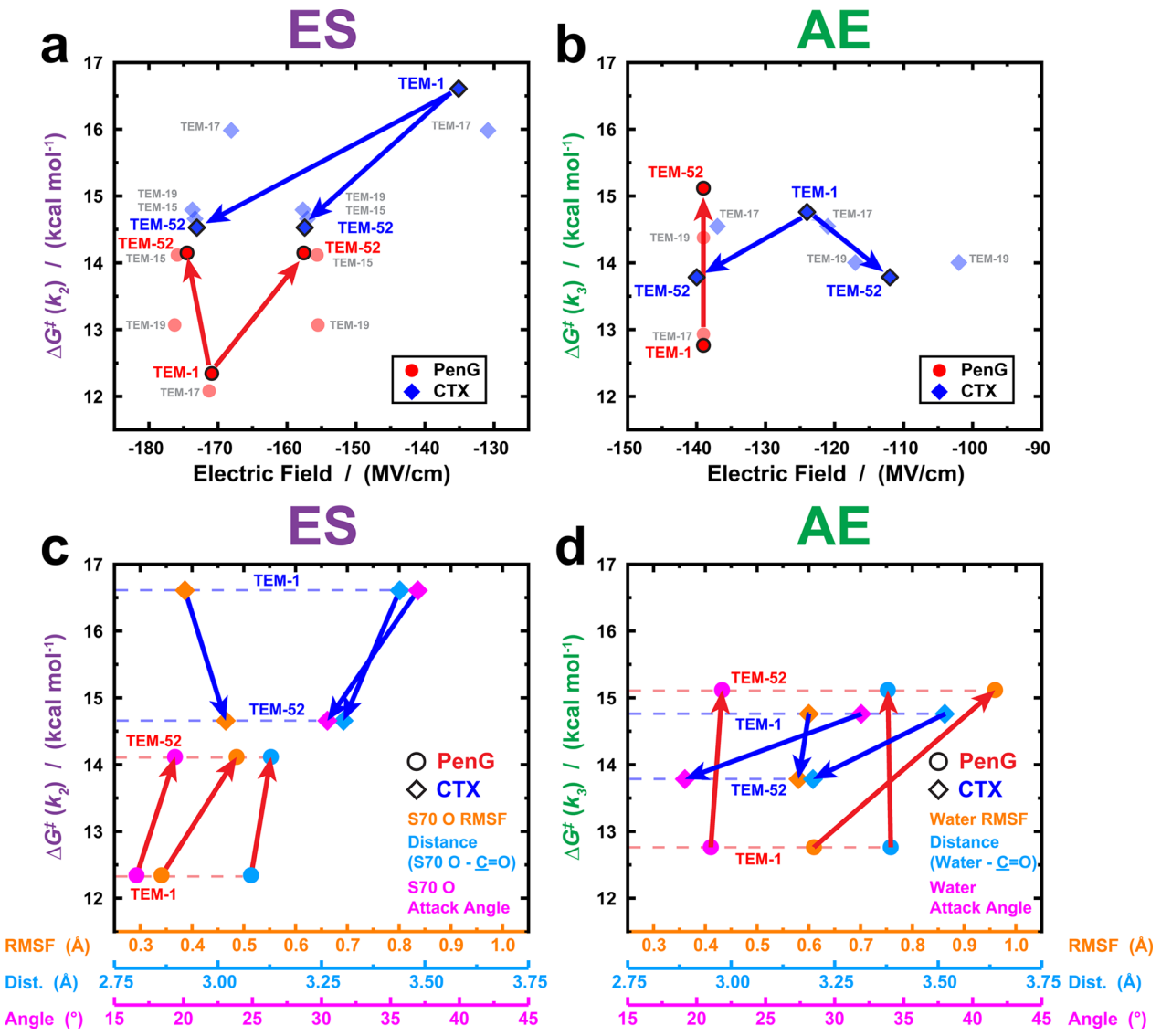

Figure 6. Substrate-dependent evolution of active site electric fields and chemical positioning in the catalysis of TEM β-lactamase. (a,b) Nonmonotonic correlation between the large catalytically relevant electric field species and free energy barriers of activation from steady-state kinetics and TS-theory for (a) acylation (ES) and (b) deacylation (AE) with respect to PenG (red) and CTX (blue). (c,d) Correlation between the free energy barriers of activation and absolute changes in chemical positioning (RMSF, distances to β-lactam C=O, and attack angle) for nucleophilic attack of (c) S70 or (d) active site water from MD simulations of the ES and AE complex, respectively, for hydrolysis of PenG (circles) and CTX (diamonds). The RMSF (orange), distance to β-lactam C=O (light blue), and nucleophilic attack angle (pink; defined according to the plane of the C=O, Scheme S4) represent averages across the MD trajectories as discussed in Figures 4–5. Catalytic waters are assigned according to their proximity to E166, K73, N170, and the substrate C=O as described according to Figure 5. Arrows denote the direction of evolution from TEM-1 to TEM-52 for either PenG (red) or CTX (blue).

Instead, we observe rather scattered and diverging tendencies, shown by the blue and red arrows, pointing toward other contributions beyond the framework of electrostatic catalysis that underlie the catalytic activity changes observed in the evolutionary trajectory from TEM-1 to TEM-52. In order to assess these additional contributions, we analyzed the MD results to combine the electrostatic picture with the roles of chemical positioning and conformational (fluctuation) effects in modulating the activation free energy barrier ($\Delta G^{\ddagger}$ from k_{cat} and TS-theory) (Figure 6, Table S2, SI Discussion S3).

In the case of the evolved improvements in cefotaximase activity of TEM-52, relative to TEM-1, we observe changes in *both* the catalytically relevant active site electric field and the positioning of the nucleophilic atoms, i.e., the side-chain of S70 and active site water involved in acylation (ES state) and deacylation (AE state), respectively, as summarized in Figure 6. Contrary to our expectations based on the kinetics, even in TEM-1 we observe in the IR spectra a catalytically relevant population with a high electric field projected onto the β-lactam C=O of CTX; MD simulations indicate that the catalytic inefficiency can be ascribed to mispositioned catalytic residues. Over the course of evolution, in the rate-limiting ES state, the three mutations result in nonmonotonic increases in the magnitude of the largest electric fields experienced by the C=O (Figure 6a, blue arrows). This is consistent with E104K and G238S leading to an expansion of the active site to accommodate CTX,[10] allowing an improved alignment of the β-lactam C=O with the backbone amide N–H's of S70 and A237 as observed using MD and expected to generate large electric fields, consistent with what is observed by the VSE

https://doi.org/10.1021/acscentsci.1c00880
ACS Cent. Sci. 2021, 7, 1996–2008

(Figure 6a, blue arrows). In addition, we observe small increases in the RMSFs of the S70 side-chain that are compensated by shortened distances and a better attack angle, i.e., improved chemical positioning, approaching those observed in the PenG complexes (Figure 6c, blue arrows). In the deacylation step, we detect improved *and* worsened electric fields over the course of evolution (Figure 6b, blue arrows), which is in line with the overall increased RMSFs of the active site (Figure 5h). At the same time, better positioning of the nucleophilic water, in terms of distance and attack angle with respect to the acyl ester C═O (Figure 6d, blue arrows), is achieved through increased solvent accommodation and entry of a second water molecule (Figure 5e,f).

Based on previous investigations of enzymes with the VSE that employ similar reaction mechanisms (e.g., serine proteases),[6] a reduction of the activation free energy barrier by 1 kcal/mol corresponds to more stabilizing electric fields by 10−20 MV/cm if modulated primarily by electrostatic TS-stabilization. The observed improvements of electric field are consistent with this relative change in activation free energy barrier for acylation (rate-limiting) and deacylation (in reference to the blue arrow denoting an increasing field) for CTX hydrolysis, so that increased RMSFs are compensated by improved distances and attack angle of nucleophilic atoms via global structural changes throughout the enzyme active site (Figures S16−18, Tables S7−14). For deacylation, the divergence of electric fields over the course of evolution may suggest that improved chemical positioning is the major contribution to improved rates.

In the case of the PenG hydrolysis, where deacylation is rate-limiting (Figure 2a), there is no obvious selective pressure to preserve the catalytic efficiency of TEM-1 during the evolutionary trajectory to TEM-52. We observe that the E104K mutation greatly alters the k_2/k_3 ratio, resulting in $k_3 \approx k_{cat}$, consistent with either a reduced electric field magnitude at the β-lactam C═O or mispositioning of E166 and the nucleophilic water molecule for deacylation. The β-lactam C═O vibration is only sensitive to the electric field projected onto its bond axis, and therefore changes occurring orthogonal to or far from the reactive C═O probe, such as changes in the positioning of E166, S70, or the catalytic water, cannot be spectroscopically observed (SI Discussion S3). Therefore, the apparent absence of a change in electric field for the catalytically relevant high-field population in the IR spectra (Figure 6a,b) suggests that the changes in chemical positioning of active site residues are a more likely basis for the observed rate changes. This is consistent with the changes in the RMSFs of the nucleophilic atoms (Figure 6c,d, orange, red arrows), such as the acylating serine, in line with decreased k_2, and overall increased active site heterogeneity as observed in the MD that accompany the evolution from TEM-1 to TEM-52 (e.g., K73, E166, N170; Figures 5c,d, S16−18, Table S7−12). This is also consistent with the observation that G238S is primarily responsible for the reduction in both k_2 and k_3, which are the primary contribution to lowering K_M (Figure S20 and Table S15). Recently reported studies using time-resolved electrospray ionization with H/D exchange on TEM-1 with ampicillin and cephalexin are consistent with these structural changes and implications in the AE complex, with efficient deacylation (i.e., TEM-1 with PenG) being associated with tighter active site interactions as evident from decreased deuterium uptake.[51] This increased active site heterogeneity results in PenG becoming more inhibitor-like for TEM-52 relative to TEM-1, i.e., a high on-rate (k_1) but lower turnover ($k_{cat} \approx k_3$). The increased structural displacement and heterogeneity of the S70 and E166 side-chains and nucleophilic water are expected to break one essential aspect of the preorganized active site for acylation and deacylation, namely, proper chemical positioning for catalysis.

Taken together, we see that changes in the chemical positioning of the side-chains of S70 and the catalytic water have significant kinetic consequences (Figure 6c,d) without necessarily perturbing the electric field as sensed by the β-lactam C═O (Figure 6a,b; SI Discussion S2,3). This observation is reminiscent of the D40N mutation in KSI, which ablates the catalytic base from proton abstraction (i.e., changing the mechanism), thereby lowering the catalytic rate by 6 orders of magnitude, but has a minimal effect on the electric field projected onto the functionally important carbonyl for TS-stabilization relative to the WT enzyme.[3] In summary, despite the complexity of the structure−function relationship in TEM β-lactamase activity, we generally observe that the evolution toward cefotaximase activity is achieved through an interplay between the improvement of electrostatic catalysis and chemical positioning of nucleophilic groups. Conversely, we observe that the (de)evolution of penicillinase specificity, i.e., toward broad spectrum or promiscuous activity, is modulated primarily through fluctuations of the active site environment.

Implications for the Role of Electric Fields, the Protein Fitness Landscape, and Antibiotic Resistance. We observe that the natural evolution from TEM-1 to TEM-52 in response to new antibiotics utilizes both electrostatic effects directed at the reactive β-lactam C═O and chemical positioning to modulate catalysis in a substrate-dependent manner. This is in contrast to prior studies of KSI, serine proteases, and 4-chlorobenzoyl-CoA dehalogenase,[6] where the observed catalytic effect could be ascribed largely to mutations that were in close contact (e.g., H-bonding) with the reactive C═O bonds. These laboratory mutations do not necessarily recapitulate the natural evolutionary trajectory of these enzymes. The observed linear free energy relationship with the active site electric field in these enzymes indicates that there is a minimal (or constant) effect of each mutation on the overall active site structural heterogeneity, so the dominant effect is through electrostatic interaction with the reactive C═O bond. In contrast, the mutations along the evolutionary trajectory from TEM-1 to TEM-52 are not directly involved in the dominant noncovalent interactions between the β-lactam C═O and backbone amides of S70 and A237, which are difficult to perturb except as a secondary consequence of changes in backbone positioning. Rather, these mutations modulate binding interactions across the active site in a substrate-dependent manner, indicative of the structural plasticity of the TEM scaffold. These can propagate to changes in the alignment of the reactive C═O with respect to the oxyanion hole electric field, as observed using the VSE with CTX (i.e., partially attributed to the 4,6-bicyclic ring), as a result of increased active site accommodation for improved binding.

Substrate promiscuity and structural plasticity enable a starting point for evolutionary improvement,[1,2,52,53] which in the case of TEM-1 takes three mutations to achieve the robust cefotaximase activity in the ESBL TEM-52. As demonstrated across all the TEM variants with both PenG and CTX, the maximum observed electric fields experienced by the C═O of

https://doi.org/10.1021/acscentsci.1c00880
ACS Cent. Sci. 2021, 7, 1996−2008

the functional β-lactam in both the ES and AE complexes are surprisingly large throughout the enzyme's evolution. This might be expected given that the backbone amides of S70 and A237 are difficult to perturb without deformation of the active site's secondary and tertiary structure, and only a single mutation, either E104K or G238S, is necessary for the β-lactam C═O of CTX to achieve the largest electric fields observed with PenG of −140 to −175 MV/cm. If we were not starting with the evolved oxyanion hole of TEM-1 for penicillinase activity, mutations would be required to both position the C═O of CTX into the oxyanion hole (i.e., if it could not fit or bind correctly) and to increase the overall magnitude of the electric field experienced by the carbonyl group of the β-lactam ring. This hypothesis could be explored further in ancestral variants of TEM using ancestral sequence reconstruction (ASR)[54] to compare and contrast more long-term evolutionary changes in structure, function, and fields. During the evolution of CTX hydrolysis from TEM-1 to TEM-52, the large pre-existing oxyanion hole electric field simplifies the mutational search along the fitness landscape for improved catalytic rates—via improved alignment of the reactive C═O into the active site and correct positioning of the reactive water, S70, and E166 residues—thereby enabling the ESBL phenotype to be acquired over the course of three mutations and driving the emergence of antibiotic resistance. This implies that for a new β-lactam antibiotic to be effective against a given class of β-lactamases, i.e., to minimize the risk of resistance, it must bind in a manner that is able to simultaneously avoid the large active site electric field and unproductively position the catalytic side-chains. Across class A β-lactamases, the overall active site architectures, including the oxyanion hole and active site amino acids, are well conserved, and therefore it is not surprising that many families of β-lactamase have been observed (and/or have the potential) to rapidly evolve activity toward hydrolysis of penicillins, cephalosporins, and monobactams.

Our findings of large electric fields in the oxyanion hole of TEM β-lactamases may help to rationalize how structural plasticity leads to substrate promiscuity.[53,54] The evolutionary history leading to TEM-1 resulted in an enzyme scaffold and active site that is capable of exerting large stabilizing electric fields necessary for TSS of chemical reactions with similar substrate geometries and mechanisms. This may be the case for hydrolases and many other enzymes,[55] which utilize pre-existing catalytic architectures, such as oxyanion holes, to enable catalysis of a large substrate scope for further improvements via directed evolution.[56] As evident in the evolution of cefotaximase activity from TEM-1 to TEM-52, there is some basal level of binding and catalysis in the inherited protein scaffold (as required for evolution), which is supported by the large electric fields observed even in TEM-1 with CTX. Instead of electric field optimization, subsequent mutations are focused on accommodating and chemical repositioning of reactive side-chains and the substrate, with only small perturbations to the electric field sensed by the reactive C═O, to fully utilize these naturally evolved electric fields for catalysis. This interplay of electrostatic and chemical positioning to modulate the protein fitness landscape may be a general observation, as evident in the changes in active site heterogeneity in the directed evolution of *de novo* Kemp eliminases and ancestrally reconstructed β-lactamases.[53,57,58] Combining the complementary approaches of MD simulations and the VSE with kinetic studies enables a more comprehensive molecular picture of the parameters modulating an enzyme's evolution toward new and/or improved function with implications in protein design, enzyme evolution, and antibiotic resistance.

■ ASSOCIATED CONTENT

Supporting Information

The Supporting Information is available free of charge at https://pubs.acs.org/doi/10.1021/acscentsci.1c00880.

Experimental details and methods for protein expression and purification, kinetics, steady-state MS, FTIR spectroscopy, and MD simulations. Additional discussions of the solvatochromic calibration for the VSE, difference spectra processing, IR peak determination and evaluation, choice of mutations for VSE experiments, and utilization of MD simulations to guide experimental findings. Additional figures, tables, and schemes relating to the kinetics, activation free energy barriers, FTIR spectral processing, FTIR line shape parameters, structural comparisons from MD simulations, analysis of MD simulations, and alternative representations of evolutionary changes from MD simulations (PDF)

■ AUTHOR INFORMATION

Corresponding Author

Steven G. Boxer − *Chemistry Department, Stanford University, Stanford, California 94305, United States;* orcid.org/0000-0001-9167-4286; Email: sboxer@stanford.edu

Authors

Samuel H. Schneider − *Chemistry Department, Stanford University, Stanford, California 94305, United States;* Present Address: Department of Pharmaceutical Chemistry, University of California San Francisco, San Francisco, CA, 94158, USA; orcid.org/0000-0002-5792-4015

Jacek Kozuch − *Chemistry Department, Stanford University, Stanford, California 94305, United States;* Present Address: Experimental Molecular Biophysics, Department of Physics, Freie Universitat Berlin, Arnimallee 14, 14195 Berlin, Germany; orcid.org/0000-0002-2115-4899

Complete contact information is available at: https://pubs.acs.org/10.1021/acscentsci.1c00880

Author Contributions

#S.H.S. and J.K. contributed equally to this work.

Notes

The authors declare no competing financial interest.

■ ACKNOWLEDGMENTS

We acknowledge helpful discussions with Peter Kasson at the UVA and the Vincent Coates Foundation Mass Spectrometry Laboratory at Stanford University. We thank extensive feedback from Dr. Zhe Ji, Jacob Kirsh, and Jared Weaver during the drafting process. J.K. acknowledges the Deutsche Forschungsgemeinschaft for a Research Fellowship (KO5464/1). This work is supported in part by NIH Grant GM118044 (to S.G.B.).

REFERENCES

(1) Bloom, J. D.; Arnold, F. H. In the Light of Directed Evolution: Pathways of Adaptive Protein Evolution. *Proc. Natl. Acad. Sci. U. S. A.* **2009**, *106*, 9995−10000.

(2) Romero, P. A.; Arnold, F. H. Exploring Protein Fitness Landscapes by Directed Evolution. *Nat. Rev. Mol. Cell Biol.* **2009**, *10* (12), 866−876.

(3) Fried, S. D.; Bagchi, S.; Boxer, S. G. Extreme Electric Field Power Catalysis in the Active Site of Ketosteroid Isomerase. *Science* **2014**, *346*, 1510−1514.

(4) Wu, Y.; Boxer, S. G. A Critical Test of the Electrostatic Contribution to Catalysis with Noncanonical Amino Acids in Ketosteroid Isomerase. *J. Am. Chem. Soc.* **2016**, *138* (36), 11890−11895.

(5) Schneider, S. H.; Boxer, S. G. Vibrational Stark Effects of Carbonyl Probes Applied to Reinterpret IR and Raman Data for Enzyme Inhibitors in Terms of Electric Fields at the Active Site. *J. Phys. Chem. B* **2016**, *120*, 9672−9684.

(6) Fried, S. D.; Boxer, S. G. Electric Fields and Enzyme Catalysis. *Annu. Rev. Biochem.* **2017**, *86*, 387−415.

(7) Fried, S. D.; Boxer, S. G. Measuring Electric Fields and Noncovalent Interactions Using the Vibrational Stark Effect. *Acc. Chem. Res.* **2015**, *48*, 998−1006.

(8) Wu, Y.; Fried, S. D.; Boxer, S. G. A Preorganized Electric Field Leads to Minimal Geometrical Reorientation in the Catalytic Reaction of Ketosteroid Isomerase. *J. Am. Chem. Soc.* **2020**, *142* (22), 9993−9998.

(9) Bush, K. The Importance of β-Lactamases to the Development of New β-Lactams. In *Antimicrobial Drug Resistance. Mechanisms of Drug Resistance*, Mayers, D. L., Ed.; Humana Press: Totowa, NJ, 2009; Vol. *1*, pp 135−144.

(10) Palzkill, T. Structural and Mechanistic Basis for Extended-Spectrum Drug-Resistance Mutations in Altering the Specificity of TEM, CTX-M, and KPC β-lactamases. *Front. Mol. Biosci.* **2018**, *5*, 16.

(11) Orencia, M. C.; Yoon, J. S.; Ness, J. E.; Stemmer, W. P. C.; Stevens, R. C. Predicting the Emergence of Antibiotic Resistance by Directed Evolution and Structural Analysis. *Nat. Struct. Biol.* **2001**, *8*, 238−242.

(12) Dellus-Gur, E.; Elias, M.; Caselli, E.; Prati, F.; Salverda, M. L.; de Visser, J. A.; Fraser, J. S.; Tawfik, D. S. Negative Epistasis and Evolvability in TEM-1 β-Lactamase - The Thin Line between an Enzyme's Conformational Freedom and Disorder. *J. Mol. Biol.* **2015**, *427* (14), 2396−2409.

(13) Steinberg, B.; Ostermeier, M. Shifting Fitness and Epistatic Landscapes Reflect Trade-offs along an Evolutionary Pathway. *J. Mol. Biol.* **2016**, *428* (13), 2730−2743.

(14) Stiffler, M. A.; Hekstra, D. R.; Ranganathan, R. Evolvability as a Function of Purifying Selection in TEM-1 β-Lactamase. *Cell* **2015**, *160* (5), 882−892.

(15) Bershtein, S.; Goldin, K.; Tawfik, D. S. Intense Neutral Drifts Yield Robust and Evolvable Consensus Proteins. *J. Mol. Biol.* **2008**, *379* (5), 1029−1044.

(16) Brown, N. G.; Pennington, J. M.; Huang, W.; Ayvaz, T.; Palzkill, T. Multiple Global Suppressors of Protein Stability Defects Facilitate the Evolution of Extended-Spectrum TEM β-Lactamases. *J. Mol. Biol.* **2010**, *404* (5), 832−846.

(17) Zimmerman, M. I.; Hart, K. M.; Sibbald, C. A.; Frederick, T. E.; Jimah, J. R.; Knoverek, C. R.; Tolia, N. H.; Bowman, G. R. Prediction of New Stabilizing Mutations Based on Mechanistic Insights from Markov State Models. *ACS Cent. Sci.* **2017**, *3* (12), 1311−1321.

(18) Bowman, G. R.; Bolin, E. R.; Hart, K. M.; Maguire, B. C.; Marqusee, S. Discovery of Multiple Hidden Allosteric Sites by Combining Markov State Models and Experiments. *Proc. Natl. Acad. Sci. U. S. A.* **2015**, *112*, 2734−2739.

(19) Bowman, G. R.; Geissler, P. L. Equilibrium Fluctuations of a Single Folded Protein Reveal a Multitude of Potential Cryptic Allosteric Sites. *Proc. Natl. Acad. Sci. U. S. A.* **2012**, *109* (29), 11681−11686.

(20) Hart, K. M.; Ho, C. M.; Dutta, S.; Gross, M. L.; Bowman, G. R. Modelling Proteins' Hidden Conformations to Predict Antibiotic Resistance. *Nat. Commun.* **2016**, *7*, 12965.

(21) Campitelli, P.; Modi, T.; Kumar, S.; Ozkan, S. B. The Role of Conformational Dynamics and Allostery in Modulating Protein Evolution. *Annu. Rev. Biophys.* **2020**, *49*, 267−290.

(22) Yang, J.; Naik, N.; Patel, J. S.; Wylie, C. S.; Gu, W.; Huang, J.; Ytreberg, F. M.; Naik, M. T.; Weinreich, D. M.; Rubenstein, B. M. Predicting the Viability of Beta-Lactamase: How Folding and Binding Free Energies Correlate with Beta-Lactamase Fitness. *PLoS One* **2020**, *15* (5), e0233509.

(23) Naas, T.; Oueslati, S.; Bonnin, R. A.; Dabos, M. L.; Zavala, A.; Dortet, L.; Retailleau, P.; Iorga, B. I. Beta-Lactamase Database (BLDB) - Structure and Function. *J. Enzyme Inhib. Med. Chem.* **2017**, *32* (1), 917−919.

(24) Bush, K. The ABCD's of β-Lactamase Nomenclature. *J. Infect. Chemother.* **2013**, *19* (4), 549−559.

(25) Weinreich, D. M.; Delaney, N. F.; DePristo, M. A.; Hartl, D. L. Darwinian Evolution Can Follow Only Very Few Mutational Paths to Fitter Proteins. *Science* **2006**, *312*, 111−114.

(26) Gniadkowski, M. Evolution of Extended-Spectrum β-Lactamases by Mutation. *Clin. Microbiol. Infect.* **2008**, *14*, 11−32.

(27) Ambler, R. P. In *Beta-Lactamases*, Hamilton-Miller, J. M. T.; Smith, J. T., Eds.; Academic Press: London, 1979.

(28) Guthrie, V. B.; Allen, J.; Camps, M.; Karchin, R. Network Models of TEM β-Lactamase Mutations Coevolving Under Antibiotic Selection Show Modular Structure and Anticipate Evolutionary Trajectories. *PLoS Comput. Biol.* **2011**, *7* (9), e1002184.

(29) Salverda, M. L.; De Visser, J. A.; Barlow, M. Natural Evolution of TEM-1 β-Lactamase: Experimental Reconstruction and Clinical Relevance. *FEMS Microbiol. Rev.* **2010**, *34* (6), 1015−1036.

(30) Wang, X.; Minasov, G.; Shoichet, B. K. Evolution of an Antibiotic Resistance Enzyme Constrained by Stability and Activity Trade-offs. *J. Mol. Biol.* **2002**, *320* (1), 85−95.

(31) Saves, I.; Burlet-Schiltz, O.; Maveyraud, L.; Samama, J.-P.; Promé, J.-C.; Masson, J.-M. Mass Spectral Kinetic Study of Acylation and Deacylation during the Hydrolysis of Penicillins and Cefotaxime by β-Lactamase TEM-1 and G238S Mutant. *Biochemistry* **1995**, *34*, 11660−11667.

(32) Christensen, H.; Martin, M. T.; Waley, S. G. β-Lactamases as Fully Efficient Enzymes. Determination of all the Rate Constants in the Acyl-Enzyme Mechanism. *Biochem. J.* **1990**, *266*, 853−861.

(33) Singh, M. K.; Dominy, B. N. The Evolution of Cefotaximase Activity in the TEM β-Lactamase. *J. Mol. Biol.* **2012**, *415* (1), 205−220.

(34) Kozuch, J.; Schneider, S. H.; Boxer, S. G. Biosynthetic Incorporation of Site-Specific Isotopes in β-Lactam Antibiotics Enables Biophysical Studies. *ACS Chem. Biol.* **2020**, *15* (5), 1148−1153.

(35) Buchner, G. S.; Kubelka, J. Isotope-Edited Infrared Spectroscopy. In *Intrinsically Disored Protein Analysis. Methods in Molecular Biology (Methods and Protocols)*, Uversky, V.; Dunker, A., Eds.; Humana Press: Totowa, NJ, 2012; Vol. *895*, pp 347−358.

(36) Kozuch, J.; Schneider, S. H.; Zheng, C.; Ji, Z.; Bradshaw, R. T.; Boxer, S. G. Testing the Limitations of MD-based Local Electric Fields Using the Vibrational Stark Effect in Solution: Penicillin G as a Test Case. *J. Phys. Chem. B* **2021**, *125* (17), 4415−4427.

(37) Wilkinson, A.-S.; Bryant, P. K.; Meroueh, S. O.; Page, M. G. P.; Mobashery, S.; Wharton, C. W. A Dynamic Structure for the Acyl-Enzyme Species of the Antibiotic Aztreonam with the *Citrobacter freundii* β-Lactamase Revealed by Infrared Spectroscopy and Molecular Dynamics Simulations. *Biochemistry* **2003**, *42*, 1950−1957.

(38) Wilkinson, A.-S.; Simon, W.; Kania, M.; Page, M. G. P.; Wharton, C. W. Multiple Conformations of the Acylenzyme Formed in the Hydrolysis of Methicillin by *Citrobacter freundii* β-Lactamase: A Time-Resolved FTIR Spectroscopic Study. *Biochemistry* **1999**, *38*, 3851−3856.

https://doi.org/10.1021/acscentsci.1c00880
ACS Cent. Sci. 2021, 7, 1996−2008

(39) Schneider, S. H.; Kratochvil, H. T.; Zanni, M. T.; Boxer, S. G. Solvent-Independent Anharmonicity for Carbonyl Oscillators. *J. Phys. Chem. B* **2017**, *121*, 2331−2338.
(40) Jindal, G.; Warshel, A. Exploring the Dependence of QM/MM Calculations of Enzyme Catalysis on the Size of the QM Region. *J. Phys. Chem. B* **2016**, *120* (37), 9913−9921.
(41) Knox, J. R. Extended-Spectrum and Inhibitor-Resistant TEM-Type β-Lactamases: Mutations, Specificity, and Three-Dimensional Structure. *Antimicrob. Agents Chemother.* **1995**, *39*, 2593−2601.
(42) Richard, A. M.; Gascón, J. A. Protein Polarization Effects in the Thermodynamic Computation of Vibrational Stark Shifts. *Theor. Chem. Acc.* **2020**, *139* (1), 9.
(43) Wang, X.; He, X. An Ab Initio QM/MM Study of the Electrostatic Contribution to Catalysis in the Active Site of Ketosteroid Isomerase. *Molecules* **2018**, *23* (10), 2410.
(44) Wang, L.; Fried, S. D.; Markland, T. E. Proton Network Flexibility Enables Robustness and Large Electric Fields in the Ketosteroid Isomerase Active Site. *J. Phys. Chem. B* **2017**, *121* (42), 9807−9815.
(45) Welborn, V. V.; Head-Gordon, T. Fluctuations of Electric Fields in the Active Site of the Enzyme Ketosteroid Isomerase. *J. Am. Chem. Soc.* **2019**, *141* (32), 12487−12492.
(46) Zoi, I.; Antoniou, D.; Schwartz, S. D. Electric Fields and Fast Protein Dynamics in Enzymes. *J. Phys. Chem. Lett.* **2017**, *8* (24), 6165−6170.
(47) Bhowmick, A.; Sharma, S. C.; Head-Gordon, T. The Importance of the Scaffold for de Novo Enzymes: A Case Study with Kemp Eliminase. *J. Am. Chem. Soc.* **2017**, *139* (16), 5793−5800.
(48) Stec, B.; Holtz, K. M.; Wojciechowski, C. L.; Kantrowitz, E. R. Structure of the Wild-Type TEM-1 β-Lactamase at 1.55 Å and the Mutant Enzyme Ser70Ala at 2.1 Å Suggest the Mode of Noncovalent Catalysis for the Mutant Enzyme. *Acta Crystallogr., Sect. D: Biol. Crystallogr.* **2005**, *61*, 1072−1079.
(49) Strynadka, N. C. J.; Adachi, H.; Jensen, S. E.; Johns, K.; Sielecki, A.; Betzel, C.; Sutoh, K.; James, M. N. G. Molecular Structure of the Acyl-Enzyme Intermediate in β-Lactam Hydrolysis at 1.7 Å Resolution. *Nature* **1992**, *359*, 700−705.
(50) Banerjee, S.; Pierper, U.; Kapadia, G.; Pannell, L. K.; Herzberg, O. Role of the Ω-Loop in the Activity, Substrate Specificity, and Structure of Class A β-Lactamase. *Biochemistry* **1998**, *37*, 3286−3296.
(51) Knox, R.; Lento, C.; Wilson, D. J. Mapping Conformational Dynamics to Individual Steps in the TEM-1 β-Lactamase Catalytic Mechanism. *J. Mol. Biol.* **2018**, *430*, 3311−3322.
(52) Leveson-Gower, R. B.; Mayer, C.; Roelfes, G. The Importance of Catalytic Promiscuity for Enzyme Design and Evolution. *Nat. Rev. Chem.* **2019**, *3* (12), 687−705.
(53) Modi, T.; Risso, V. A.; Martinez-Rodriguez, S.; Gavira, J. A.; Mebrat, M. D.; Van Horn, W. D.; Sanchez-Ruiz, J. M.; Banu Ozkan, S. Hinge-Shift Mechanism as a Protein Design Principle for the Evolution of β-Lactamases from Substrate Promiscuity to Specificity. *Nat. Commun.* **2021**, *12* (1), 1852.
(54) Risso, V. A.; Gavira, J. A.; Mejia-Carmona, D. F.; Gaucher, E. A.; Sanchez-Ruiz, J. M. Hyperstability and Substrate Promiscuity in Laboratory Resurrections of Precambrian β-Lactamases. *J. Am. Chem. Soc.* **2013**, *135* (8), 2899−2902.
(55) Khersonsky, O.; Tawfik, D. S. Enzyme Promiscuity: A Mechanistic and Evolutionary Perspective. *Annu. Rev. Biochem.* **2010**, *79*, 471−505.
(56) Chen, K.; Arnold, F. H. Engineering New Catalytic Activities in Enzymes. *Nat. Catal.* **2020**, *3*, 203.
(57) Broom, A.; Rakotoharisoa, R. V.; Thompson, M. C.; Zarifi, N.; Nguyen, E.; Mukhametzhanov, N.; Liu, L.; Fraser, J. S.; Chica, R. A. Ensemble-Based Enzyme Design can Recapitulate the Effects of Laboratory Directed Evolution *In Silico*. *Nat. Commun.* **2020**, *11* (1), 4808.
(58) Otten, R.; Pádua, R. A. P.; Bunzel, H. A.; Nguyen, V.; Pitsawong, W.; Patterson, M.; Sui, S.; Perry, S. L.; Cohen, A. E.; Hilvert, D.; et al. How Directed Evolution Reshapes the Energy Landscape in an Enzyme to Boost Catalysis. *Science* **2020**, *370* (6523), 1442−1446.

https://doi.org/10.1021/acscentsci.1c00880
ACS Cent. Sci. 2021, 7, 1996−2008

Supplementary Information for

The Interplay of Electrostatics and Chemical Positioning in the Evolution of Antibiotic Resistance in TEM β-Lactamases

Samuel H. Schneider,[1,2] Jacek Kozuch,[1,3] Steven G. Boxer*

Chemistry Department, Stanford University, Stanford, CA, 94305, USA

[1] These authors contributed equally to this work.

* Email: sboxer@stanford.edu

[2] Present address: Department of Pharmaceutical Chemistry, University of California San Francisco, San Francisco, CA, 94158, USA

[3] Present address: Experimental Molecular Biophysics, Department of Physics, Freie Universitat Berlin, Arnimallee 14, 14195 Berlin, Germany

Table of Contents:

Materials & Methods: pg. 6-17

Nucleotide sequence for TEM-1 β-lactamase. pg. 6

Protein expression and purification. pg. 7-8

UV-vis kinetics. pg. 9-10

Steady-state mass spectrometry. pg. 11-12

FTIR spectroscopy. pg. 13-14

MD simulation parameterization. pg. 15

MD simulations. pg. 16-17

Supplementary Discussion: pg. 18-29

Section 1. Interactions of E104 and G238 in the TEM-1 PenG AE crystal structure and implications of the MD simulations of TEM-52. **pg. 18**

Section 2. The proximity of E104K and G238S to the oxyanion hole and substrate-dependent effects. **pg. 19-21**

Figure S1. Proximity of E104K and G238S to the oxyanion hole of TEM β-lactamases in MD simulations. **pg. 19**

Section 3. The local and global effects of electric fields and chemical positioning on catalysis. **pg. 22-29**

Section 3a. The physical origins of electrostatic catalysis. **pg. 22-24**

Scheme S1. Expanded reaction mechanism for TEM β-lactamase with PenG. **pg. 23**

Section 3b. The effects of chemical positioning on enzyme catalysis. **pg. 25-29**

Scheme S2. Accounting for the possibility of conformational heterogeneity in enzyme catalysis. **pg. 26**

Extended Figures, Tables, and Schemes: pg. 30-75

Table S1. Kinetics of TEM β-lactamase-catalyzed hydrolysis of PenG and CTX from steady-state kinetics and mass spectrometry. **pg. 30**

Table S2. Activation free energy barriers for the TEM β-lactamase reaction with PenG and CTX. **pg. 31**

Figure S2. Absorbance spectra and extinction coefficient determination for PenG and CTX. **pg. 32**

Figure S3. Representative time-trace data for PenG hydrolysis by TEM-1 S70A β-lactamase. **pg. 33**

Figure S4. Representative steady-state MS charge envelope of TEM-1 with PenG. **pg. 34**

Figure S5. Example kinetic parameter distributions determined using bootstrapping algorithm for TEM-1 β-lactamase with CTX. **pg. 36**

Figure S6. FTIR spectra of $^{12}C_{CO}$ and $^{13}C_{CO}$ β-lactams in aqueous buffer. **pg. 37**

Figure S7. Electric field-frequency calibration for model compounds and their β-lactam antibiotic mechanistic equivalents. **pg. 38**

Figure S8. Full isotope-edited IR difference spectroscopy of the TEM β-lactamases with PenG and CTX. **pg. 39**

Figure S9. Representative example of FTIR data processing and assignment with TEM-52 E166N and CTX. **pg. 40**

Table S3. TEM-# S70G PenG vibrational frequencies and lineshape -parameters from curve-fitting. **pg. 42**

Table S4. TEM-# S70G CTX vibrational frequencies and lineshape parameters from curve-fitting. **pg. 44**

Table S5. TEM-# E166N PenG vibrational frequencies and lineshape parameters from curve-fitting. **pg. 46**

Table S6. TEM-# E166N CTX vibrational frequencies and lineshape parameters from curve-fitting. **pg. 48**

Figure S10. Mutational effect on IR spectra of TEM-1 β-lactamase with PenG. **pg. 50**

Figure S11. MD Methodology for Structure-Guided Interpretation of Kinetic and VSE Results. **pg. 51**

Figure S12. Structural comparison of tight-binding PenG complexes with S70G and E166N background mutants and WT TEM β-lactamases. **pg. 52**

Figure S13. Structural comparison of weak-binding PenG complexes with S70G background mutations and WT TEM β-lactamases. **pg. 53**

Figure S14. Structure-guided approach to inferring catalytically relevant electric fields. **pg. 54**

Figure S15. Biased MD simulations of WT TEM β-lactamases as informed from kinetically compromised variants. **pg. 55**

Scheme S3. Atoms and Interactions Considered in the MD Analysis. **pg. 56**

Table S7. PenG-dependent average changes in active site RMSFs due to evolution. **pg. 58**

Table S8. CTX-dependent average changes in active site RMSFs due to evolution. **pg. 60**

Table S9. Collective RMSF changes in the evolution of TEM-1 to TEM-52 for PenG and CTX. **pg. 62**

Table S10. PenG-dependent average changes in active site distances due to evolution. **pg. 63**

Table S11. CTX-dependent average changes in active site distances due to evolution. **pg. 64**

Table S12. Collective distance changes in the evolution of TEM-1 to TEM-52 for PenG and CTX. **pg. 65**

Scheme S4. Angle of nucleophilic attack in the ES and AE complexes. **pg. 66**

Figure S16. Alternative probability density representation of significant active site distance changes over the course of evolution from TEM-1 to TEM-52 for PenG and CTX. **pg. 67**

Figure S17. Alternative probability density representation of significant active site RMSF changes over the course of evolution from TEM-1 to TEM-52 for PenG and CTX. **pg. 69**

Figure S18. Alternative representation of significant active site RMSF and distances changes over the course of evolution from TEM-1 to TEM-52 for PenG and CTX. **pg. 70**

Table S13. Average changes in active site RMSFs between TEM-1 and TEM-52 with PenG and CTX, respectively. **pg. 72**

Table S14. Average changes in active site distances between TEM-1 and TEM-52 with PenG and CTX, respectively. **pg. 73**

Figure S19. Structural comparison of TEM-1 PenG versus TEM-52 CTX complexes. **pg. 74**

Figure S20. Viscosity-dependence of PenG hydrolysis by TEM β-lactamases. **pg. 75**

Table S15. Evolutionary change in on- and off-rates of PenG hydrolysis with TEM-1 and TEM-52. **pg. 75**

Supplementary References: pg. 76-80

Extended Data and Scripts for Analysis: pg. 81-125

MD Files and Parameters: pg. 81-115

MATLAB Code: pg. 116-125

- MATLAB script for kinetic fitting of β-lactam hydrolysis using the Lambert function.
- MATLAB script for quantifying the [ES]/[AE] ratios from steady-state MS.
- MATLAB script for kinetic determination of k_2 and k_3 using boot-strapping algorithm.

Methods:

Nucleotide sequence for TEM-1 β-Lactamase:

The pBAD plasmid containing TEM-1 (pBAD-TEM-1) β-lactamase was kindly given to us by Patrice Soumillion at the Université Catholique de Louvain.[1-2] Standard PCR site-directed mutagenesis was performed on the plasmid using commercial QuikChange Lightning (Agilent) kits and protocols, which was transformed into DH10B *E. coli* cells with 15 μg/mL tetracycline HCl selection on agar plates. This was used to introduce the evolutionarily derived mutations (E104K, G238S, M182T) and kinetically incompetent variants (S70G or E166N) in addition to a cleavable His-tag in TEM-1 β-lactamase.

ATGGGTAGTCAACATTTCCGTGTCGCCCTTATTCCCTTTTTTGCGGCATTTTGCCTTCCTGT
TTTTGCTCACCCAGAAACGCTGGTGAAAGTAAAAGATGCTGAAGATCAGTTGGGTGCACGA
GTGGGTTACATCGAACTGGATCTCAACAGCGGTAAGATCCTTGAGAGTTTTCGCCCCGAAG
AACGTTTTCCAATGATGAGCACTTTTAAAGTTCTGCTATGTGGCGCGGTATTATCCCGTGTT
GACGCCGGGCAAGAGCAACTCGGTCGCCGCATACACTATTCTCAGAATGACTTGGTTGAG
TACTCACCAGTCACAGAAAAGCATCTTACGGATGGCATGACAGTAAGAGAATTATGCAGTG
CTGCCATAACCATGAGTGATAACACTGCGGCCAACTTACTTCTGACAACGATCGGAGGACC
GAAGGAGCTAACCGCTTTTTTGCACAACATGGGGGATCATGTAACTCGCCTTGATCGTTGG
AATCCGGAGCTGAATGAAGCCATACCAAACGACGAGCGTGACACCACGATGCCTGTAGCA
ATGGCAACAACGTTGCGCAAACTATTAACTGGCGAACTACTTACTCTAGCTTCCCGGCAAC
AATTAATAGACTGGATGGAGGCGGATAAAGTTGCAGGACCACTTCTGCGCTCGGCCCTTC
CGGCTGGCTGGTTTATTGCTGATAAATCTGGAGCCGGTGAGCGTGGGTCTCGCGGTATCA
TTGCAGCACTGGGGCCAGATGGTAAGCCCTCCCGTATCGTAGTTATCTACACGACGGGGA
GTCAGGCAACTATGGATGAACGAAATAGACAGATCGCTGAGATAGGTGCCTCACTGATTAA
GCATTGGGCTCTAGTACCAAGAGGCAGCTCAGAAGAGGATCTGAATAGCGCCGTCGACCA
TCATCATCATCATCAT

Protein Expression and Purification:

The pBAD-TEM plasmids were transformed into One Shot TOP10 Chemically Competent *E. coli* cells (Thermo-Fisher) using selection with 15 µg/mL Tetracycline HCl on Luria Broth (Fisher) agar plates. Unless otherwise specified, all variants of TEM β-lactamase, wild-type (S70S, E166E), acylation-impaired (S70G), and deacylation-impaired (E166N), were prepared and purified identically. A single-colony of transformed cells was grown into 5 mL overnight cultures using Terrific Broth (Fisher) with 15 µg/mL Tetracycline HCl at 37C. Overnight cultures were then inoculated into 1 L of Terrific Broth (Fisher) media with 10 µg/mL Tetracycline HCl shaking at 200 rpm and 37C until they reached an OD600 ~ 0.6 at which point protein expression was induced with 2 g per L of L-(+)-Arabinose (Sigma), and grown for 4-5 hrs at 27 C. Cells were harvested by centrifugation at 6000x g's for 30 mins and resuspended in lysis buffer (50 mM potassium phosphate, 20 mM imidazole, 500 mM sodium chloride, 10% (v/v) glycerol, pH 7.4). Cells were lysed by homogenization, and the lysate centrifuged twice for 90 mins each at 15,000x g's before sterile filtering the supernatant. The crude protein was then purified using a Ni-NTA affinity resin column, washing with 50 mM potassium phosphate (pH 7.4), 50 mM imidazole, 500 mM sodium chloride and eluted using 50 mM potassium phosphate (pH 7.4), 200 mM imidazole, 500 mM sodium chloride. Further purification was performed using anion exchange chromatography on a 5 mL HiTrap-Q HP (GE Healthcare) column and eluted using a 0-40% gradient of Buffer A (25 mM Tris (pH 8.4) 25 mM sodium chloride) to Buffer B (25 mM Tris (pH 8.4) 1 M sodium chloride) over 25 column volumes. Purified protein was exchanged into a cryoprotectant-containing storage buffer (50 mM KP_i (pH 7.4), 100 mM NaCl, 10% (v/v) glycerol) for long-term storage at -80C.

TEM-1 (WT) β-Lactamase with all permutation sites (Ambler numbering[3]) highlighted for clarity based on the key.

Key: Cyan = Signal Peptide (removed *in situ*); Red = S70; Pink = E166; Green = E104; Blue = G238; Yellow = M182.

MGSQHFRVALIPFFAAFCLPVFAHPETLVKVKDAEDQLGARVGYIELDLNSGKILESFRPEERFP
MMSTFKVLLCGAVLSRVDAGQEQLGRRIHYSQNDLVEYSPVTEKHLTDGMTVRELCSAAITMS
DNTAANLLLTTIGGPKELTAFLHNMGDHVTRLDRWEPELNEAIPNDERDTTMPVAMATTLRKLL
TGELLTLASRQQLIDWMEADKVAGPLLRSALPAGWFIADKSGAGERGSRGIIAALGPDGKPSRI
VVIYTTGSQATMDERNRQIAEIGASLIKHWALVPRGSSEEDLNSAVDHHHHHH

UV-vis kinetics:

All TEM kinetics with either PenG or CTX were performed using identical buffers and preparations unless otherwise mentioned. Before kinetic measurements, the concentration of the original purified TEM β-lactamase was determined using the absorbance at 280 nm (ε_{280} = 28,085 M^{-1} cm^{-1})[4] in 50 mM potassium phosphate (pH 7.0). All buffer solutions for kinetic measurements contained 50 – 200 mM potassium phosphate (pH 7.0) and bovine serum albumin (BSA; Sigma) at 0.02 – 0.05% (w/v) in order to assist with passivation of all cuvette surfaces for the low TEM concentrations used, typically between 10 – 50 nM for PenG and 10 – 500 nM for CTX hydrolysis. Substrate concentrations were determined from extinction coefficient measurements as shown in Figure S2. Prior to use, all cuvettes and rapid-mixing tubing were passivated for at least 30 mins with a 1% (w/v) BSA solution. We assume the simplest mechanism of class A β-lactamase-catalyzed hydrolysis according to (c.f. Figure 1):[5-6]

$$E + S \underset{k_{-1}}{\overset{k_1}{\rightleftharpoons}} ES \xrightarrow{k_2} EA \xrightarrow{k_3} E + P$$

E, S, ES, AE, and P correspond to the free enzyme, substrate, non-covalent Michaelis complex, covalent acyl-enzyme complex, and product, respectively. The apparent rate constant from steady-state kinetics (k_{cat} and K_M) corresponds to the microscopic rate constants according to Eq. 2 and 3:

Hydrolysis of PenG by TEM β-lactamases was monitored on a Cary6000i UV-vis-NIR spectrometer equipped with a stopped-flow accessory (SFA-20 Rapid Mixing Accessory from TgK Scientific). Substrate loss was monitored at 232 nm ($\Delta\varepsilon_{232}$ = -940 M^{-1} cm^{-1})[7] every 0.2 secs until completion of the reaction (i.e. $\Delta A/\Delta t = 0$). A full kinetic decomposition into k_{cat} and K_M was determined using the closed-form solution to the Michaelis-Menten equation (Eq. S1), which utilizes the Lambert function (W) to solve for the time-dependent change in substrate concentration (S_t and S_0),[8-9]

$$S_t = K_M * W\left[\frac{S_0}{K_M} exp\left(\frac{S_0 - k_{cat} t}{K_M}\right)\right] \quad \text{(Eq. S1)}$$

Kinetic parameters k_{cat} and K_M were evaluated using a MATLAB script (see SI) and measurements were repeated 7 – 9 times and for at least two solute concentrations (see Figure S3 for example kinetic trace). Kinetic parameters presented in Table S1 represent the average and standard deviation across all measurements and solute concentrations.

Hydrolysis of CTX by TEM β-lactamases was monitored on a Lambda 25 (Perkin-Elmer) UV-vis spectrometer at 262 nm, corresponding to ring-opening of the β-lactam ($\Delta\varepsilon_{262}$ = -7250 M^{-1} cm^{-1}),[7] for 16 substrate concentrations (15-1500 μM). Initial rates were determined for the first 10-30 secs of the single-wavelength kinetic trace for all substrate concentrations. Standard Michaelis-Menten plots were utilized to determine kinetic parameters for TEM-19, -15, and -52. Kinetic constants for TEM-1 and TEM-17 were determined using Lineweaver-Burke analysis because of the high K_M (ca. 1-2 mM), such that rates corresponding to saturating substrate concentrations (i.e. rate approaches k_{cat}) could not be measured. Kinetic parameters were averaged from three separate fits and errors represent the standard deviations across measurements.

Steady-state mass spectrometry:

Mass spectrometry (MS) was performed in the Stanford University Mass Spectrometry facility on a Waters Single Quadrupole LC-ESI/MS instrument. All protein LC-MS for assessing purity was performed at ~ 20 μM concentrations in water following ion-exchange chromatography and assessed using either the Intact Mass (Protein Metrics) or MassLynx (Waters) software suites.

Measurement of the proportions of non-covalent and covalent TEM-substrate complexes were performed similarly to that of Saves *et al*.[10] TEM β-lactamase was added to a solution containing an excess of substrate in 50 – 200 mM potassium phosphate buffer (pH 7.0), mixed gently, and then the reaction was quenched through addition of one volume equivalent of methanol. Concentrations were chosen to ensure that the steady-state reaction would be observed for at least 20 – 40 secs and final enzyme concentrations would be approximately 20-50 μM in at least 50 μL for sufficient LC-MS signal-to-noise. After quenching the reaction, the solution was buffer exchanged using a 3,000 Da MWCO Amicon (Millipore) spin filter to achieve a 1:1 (v/v) mixture of water/methanol before quantification using LC-MS on a reverse-phase C8 column (2.1 x 30 mm Agilent Zorbax columns with 3.5 μm Stablebond stationary phases; ESI+, 50-2000 m/z, standard cone voltage). The HPLC mobile phases consists of water and acetonitrile with 0.1% formic acid.

The relative abundance of non-covalent (ES) and covalent (AE) complexes (+ 334 or +413 Da, respectively) was determined from analysis of the unprocessed m/z data extracted using the MassLynx software and the mass envelope intensities quantified using a MATLAB script (see Figure S4 and SI MATLAB code).

While quantification of the [AE]/[ES] ratios may be normally distributed, the distributions of rate constants are not necessarily since both k_2 and $k_3 > k_{cat}$, i.e. $0 \leq [AE]/[ES] \leq$ infinity. As such, we utilize the uncertainty in both k_{cat} and [AE]/[ES] ratios to bootstrap a distribution of possible k_2 and k_3 values and determine the median and appropriate confidence intervals. For

comparison to normally distributed statistics we report the 68% (corresponding to 1 standard deviation in a normal distribution) and 95% confidence intervals (CI) to determine k_2 and k_3 and corresponding uncertainties. Example distributions are shown Figure S5 and the MATLAB scripts used to perform the bootstrapping is presented in the SI.

Control experiments to determine the ionization efficiency of the ES and AE complexes were performed by mixing an equal amount of kinetically incompetent protein TEM-1 E166N (which is not observed to deacylate) in the presence or absence of PenG or CTX, but otherwise treated identically as above. An equal concentration of protein treated with and without β-lactam were mixed and measured via LC-MS in order to quantify the ratio of ionization efficiencies ([AE]/[ES]), which was observed to be 1.0 ± 0.1 (n=3) based on the ratio of integrated peak intensities, as quantified above (see Figure S4,5). Similarly, no hydrolysis of the acylated TEM-1 E166N complex with either PenG or CTX was observed in the water:methanol mixtures, as no detectable non-covalent TEM-1 E166N was observed via LC-MS.

Note that the less thermodynamically stable TEM variants, i.e. TEM-19 and TEM-15, were more prone to unfolding in water/methanol solutions as determined via loss of concentration after buffer exchange. This could be ameliorated through lower methanol concentrations, thereby reducing the extent of unfolding, and no change in [AE]/[ES] ratios as determined from LC-MS were observed with water:methanol ratios (v/v) of 3:1 or 7:1.

FTIR spectroscopy:

FTIR spectra were recorded on a Bruker Vertex 70 spectrometer with a liquid nitrogen-cooled mercury cadmium telluride (MCT) detector; all data processing was performed using the OPUS program (Bruker). A liquid cell was prepared using two CaF_2 optical windows (19.05 mm diameter, 3 mm thickness, Lambda Research Optics, Inc.), separated by two semicircular Teflon spacers (25 and 50 μm thickness). FTIR spectra of ^{12}C- and ^{13}C-PenG and CTX, and all TEM-substrate complexes were acquired in a D_2O buffer (50 mM KP_i, 100 mM NaCl, pD 7.0) through averaging 256-512 scans from 4000-1000 cm^{-1} with 1 cm^{-1} resolution after 600 secs of dry air purging.[11]

All protein-substrate measurements were performed similarly with a final concentration of ca. 2.3 mM TEM and a slight excess of substrate (ca. 2.5 – 3.0 mM). In the case of the TEM S70G mutants with PenG, where slow hydrolysis can be observed on the timescale of the FTIR measurements, an excess of substrate was added (ca. 10 – 25 mM PenG). Before FTIR measurements, proteins were exchanged overnight into the D_2O buffer at 4 C and were exchanged again the following day into fresh D_2O buffer to achieve optimal H/D exchange of the protein.

In order to obtain isotope-edited difference spectra (^{12}C – ^{13}C), measurements were performed on the same day from a single batch of doubly-D_2O-exchanged protein, which ensures minimal difference between the two measurements. A brief description of the process for generating the final isotope-edited difference spectra is described below. First, the ^{13}C spectrum was scaled and subtracted from the ^{12}C spectrum to remove the protein absorption. Second, residual unbound ^{12}C- and ^{13}C-β-lactam was subtracted from the difference spectra using either PenG or CTX in D_2O buffer as a reference. Third, residual changes due to H/D back-exchange of either the bound or unbound protein complex was subtracted using either (^{12}C – ^{12}C) or (^{13}C – ^{13}C) difference spectrum in the former and a protein-only reference spectrum in D_2O buffer in the latter. Finally, based on 2nd-derivative analysis and the ^{12}C – ^{13}C

β-lactam C=O isotope frequency shift of ~45 cm^{-1}, sets of peaks (a positive and a negative feature) were identified and baselined conservatively. This process was repeated for multiple difference spectra and subsequent baselined spectra were averaged ($n \geq 5$) to generate those presented in Figure 3 (see Table S3-6). For further details and specific examples of the spectral processing see Figure S9.

MD simulation parameterization:

The initial structures for all simulations were based on the crystal structure of the TEM1(E166N)-Penicillin G acyl-enzyme complex (PDB id: 1FQG)[12]; mutants of interest were generated via the mutation option in PyMOL 2.3.2. Then, the PenG-acylated S70 was exchanged to a serine residue and amber99-ffSBildn parameters for the resulting 6 structures (TEM-1, TEM1-S70G, TEM-1 E166N, TEM-52, TEM-52 S70G, TEM-52 E166N) containing the nucleophilic active site water were obtained using the pbd2gmx option in GROMACS 2018.[13-14] Parameters for the ligands PenG and CTX were generated using AmberTools18 (ff99SB-ildn force field and AM1-BCC) based on optimized structures from DFT simulations in Gaussian09.A (b3lyp/6-311g**(2d,2p)).[15] The PenG-acylated and CTX-acylated serine residues, needed for the simulations of the acyl-enzyme states, were parameterized analogously using acetyl and methyl amine caps on the N- and C-termini of the serine group. In order to import the parameters into the protein topology files the caps were removed to obtain the acylated PenG-serine and CTX-serine building blocks. Then, backbone partial charges were adjusted to those of the serine parameters, and finally the charges of C_β and its H atoms were minimally adjusted to ensure a correct net charge of the acylated serines. Finally, when implementing the new acylated serines into the respective protein topology file, the original structural parameters of serine (besides those containing the hydroxyl H) were maintained and all additional parameters that include the PenG or CTX moiety, but exclude the serine fragment, were added to the topology file.

MD simulations:

MD simulations were performed using GROMACS 2018,[16] and were closely related to the work of the Kasson lab.[17-19] Protein structures of all variants were based on the structure of TEM-1 E166N PenG acyl-enzyme complex (PDB ID: 1FQG) as explained above. For all acyl-enzyme simulations, the starting structure for the PenG-acylated S70 was taken as is from the PDB file. PenG's starting structure in the ES complex was adapted to the same conformation: starting from the DFT optimized geometry, PenG's core was positioned such that the β-lactam C=O was located in the oxyanion hole, similar to the acyl-enzyme, and torsion angles of side-chains were changed to resemble those in the PenG-acylated case. The CTX-acylated S70 geometry was taken from the acyl-enzyme structure of Toho-1 E166A (PDB ID: 1IYO).[20] CTX's ES geometry was adapted from 1IYO using the same approach as for PenG. In this way, in all structures the β-lactam C=O was located at H-bond length of ca. 3 Å to both nitrogens of A237 and S/G70. Each protein was positioned in the center of a box with a dodecahedral unit cell of a size corresponding to a cube with walls located at distance of at least 2 nm from the protein surface. The box was filled with ca. 20500 water molecules (tip3p) and an ion strength of 0.175 M (similar to experiments) was generated using sodium and chloride ions, such that the system is net charge neutral. Each system was energy minimized using the steepest descent algorithm until all forces were below 1000 kJ mol^{-1} nm^{-1}, and then equilibrated (NVT and NPT steps, 100 ps each with protein and ligand heavy atoms restrained; second NPT over 100 ps with Cα atoms and ligand heavy atoms restrained). Here, the velocity-rescaling theromostat and Berendsen barostat were used (300K and 1 bar) with short range interactions truncated to 1.2 nm, long range electrostatics treated with Particle Mesh Ewald, and hydrogen bonds constrained used LINCS. MD production runs (using the Parrinello-Rahman barostat) were carried out over a total of 1 μs for each of the 16 structures. If the substrate left the active site (in simulations of ES states), the simulation was aborted and continued from a structure with bound ligand. In order to test (a) the stability of each of the observed conformations of the substrate

(assessed via the 2D correlation plots of the oxyanion H-bond distances; Fig 4) and (b) the possibility to access additional conformations due to possible sampling of a local minimum, for example starting WT TEM-1 in a conformation only observed in TEM-1 S70G, representative structures were extracted, and ligand conformations were implanted into proteins for additional MD simulations. Each structure was then newly minimized and equilibrated, and then underwent five 50 ns MD simulations. Average structures, rms fluctuations, distances, etc. were extracted using the tools present in the GROMACS package and additional add-ons (e.g. GROmaps[21]). 2D correlation plots were generated in OriginLabs2018.

The quantification of changes in structural displacement, either in terms of the root mean square fluctuations (RMSF) or distances between atoms, were quantified from representative trajectories and average structures (n = 3-5, each 50-200 ns), respectively, from the WT MD simulations of TEM-1 and TEM-52 with PenG and CTX in the ES and AE states (see Scheme S3 and Tables S7-12 for further details). Across each comparison, either RMSF or distance, values that were statistically significant ($p < 0.05$) were determined from a two-tailed student's t-test (see t-values for given degrees of freedom (df). Significant values were then utilized in the corresponding averages for each set of regions or interactions in the active site: K73/N132/E166/N170, oxyanion hole, β-lactam carboxylate, or β-lactam (Figure 5, 6). This approach highlights the complexity of evaluating structural perturbations arising from both mutational changes over evolution and those that are substrate specific.

Supplementary Discussion Section 1. Interactions of E104 and G238 in the TEM-1 PenG AE crystal structure and implications of the MD simulations of TEM-52.

The evolutionary trajectory of TEM-1 to TEM-52, and the three mutations that are acquired, have been the subject of extensive investigation but only understood in a general structural context of X-ray crystallography.[5, 12, 22] Among the three mutations, only E104K and G238S are within 10 Å of the substrate and M182T, located approx. 17 Å away from the active site, has long been reported as a global suppressor of protein stability defects. E104 is a solvent-exposed position on the loop region located directly above the enzyme active site with backbone H-bonding to the side-chain carboxamide of N132, which engages with the amide side-chain C=O of the substrates. It is worth noting that the adjacent Y105 position also engages with backbone H-bonding to α-helix containing S130 and N132 which are involved in the active site H-bonding interactions. Towards the other side of the active site is G238, which is directly adjacent to the β-sheet containing A237 (one of the two oxyanion hole amide H-bonds) and the backbone H-bond of E240 (note that E240 is adjacent to G238 in Ambler notation) to the backbone of N170 on the Ω-loop, which also contains E166. G238 also forms a backbone H-bond of S242 on the adjacent beta sheet. As observed in the acyl-enzyme crystal structure of TEM-1 with PenG, there is no space to accommodate the hydroxyl group of G238S, which is often correlated to the notion that the combination of E104K and G238S expands the active site as would be required for achieving substrate promiscuity and accommodating larger substrates such as CTX.

Supplementary Discussion Section 2. The proximity of E104K and G238S to the oxyanion hole and substrate-dependent effects.

As described above, the role of the E104K and G238S mutations in the evolution of extended spectrum antibiotic resistance in TEM-52 against cephalosporins remains poorly understood.[5, 22-25] In the absence of crystallographic data with multiple substrates, the MD results presented in this study provide further insights for how these two mutations, which do not directly interact with either the β-lactam C=O, or the side-chains of S70 and E166, can potentially modulate the catalytic activity and substrate promiscuity.

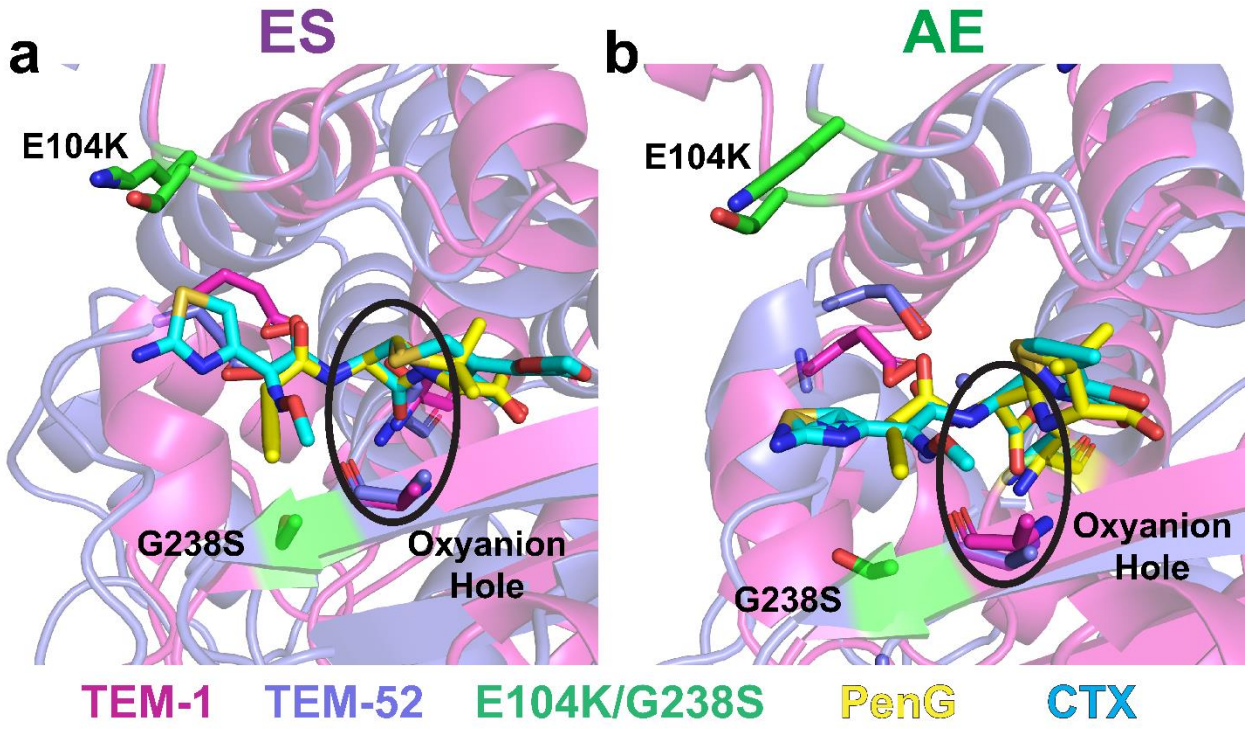

Figure S1. Proximity of E104K and G238S to the oxyanion hole of TEM β-lactamases in MD simulations. *The relative proximity and orientation of the evolutionary mutations E104K and G238S (green) in the (a) ES and (b) AE complexes with PenG (yellow) and CTX (blue) relative to the oxyanion hole from by the backbone amides of S70 and A237 of the oxyanion hole (black circle). Only the average TEM-1 (pink) PenG complexes and TEM-52 (purple) CTX complexes are shown for simplicity. See Supplementary Discussion S1 for details about the structural implications of these two positions.*

As observed in the kinetic analysis and MD simulations, the G238S mutation is responsible for the largest changes to both structure and catalysis (including k_2, k_3, and K_M) as evident in the comparison of TEM-1 relative to TEM-17 and TEM-19 for both PenG and CTX (Table S1). As described above, this can be understood in terms of the clash between the G238S hydroxyl and the terminus of the Ω-loop containing E166 and N170 which are involved in catalysis and substrate binding, respectively (Figure S1). Introduction of G238S leads to a breaking of the E240 – N170 backbone interactions in favor of the side-chain H-bond to G238S for both PenG and CTX in the ES and AE states, with the exception of the ES complex with CTX in TEM-52 (Figure 5e; the carboxamide side chain of N170 H-bonds to the backbone amide of E240). This destabilization of the backbone H-bonding leads to increased RMSF of the adjacent beta-sheet, which includes the backbone amide of A237 (see Table S7,8) and might be expected to alter the oxyanion hole fluctuations and/or electric field projected onto the β-lactam C=O. Additionally, G238S, through displacement of the Ω-loop, introduces sufficient space and mobility in the active site (see Tables S7,8,10,11 for significant RMSF and distance changes to residues 170, 237, 238, and 240), and this allows for binding of the larger and more polar CTX relative to PenG.

Although the E104K mutation is less perturbative catalytically and in terms of the VSE, its effects in combination with G238S can be readily observed in Tables S7-12. While both E104 and E104K result in a solvent-exposed side-chain, the introduction of E104K and G238S introduces significant conformational heterogeneity, as quantified by the increased RMSF and distances across the active site for both PenG and CTX in the ES and AE complexes. As discussed above, the E104K and Y105 form a loop above the active site and backbone H-bond to the side-chain and backbone amide of N132 (on the same loop as S130), which is directly implicated in H-bonding to the active site water, the side-chain of K73, and the amide-side chain of either PenG or CTX. As observed in Table S7-12, the combined effect is to alter the distances and RMSF of many residues surrounding the active site cleft that are generally

orthogonal to the backbone amide interactions that comprise the oxyanion hole. The combined changes in dynamics and alteration of non-covalent interactions leads to greater mobility across the active site as evident at K73, S130, N132, E166, and N170, which result in substrate- and complex-dependent (i.e. ES and AE) changes to the chemical positioning. It is for this reason that we focus on the propagated effects of these two mutations on the chemical positioning of S70 and the nucleophilic water, as they are essential for catalysis (Figure 6c,d).

Supplementary discussion section 3. The local and global effects of electric fields and chemical positioning on catalysis.

Section 3a. *The physical origins of electrostatic catalysis.*

As extensively described,[26-29] electrostatic catalysis describes the process by which an electric field, such as that originating from the protein environment, can preferentially stabilize the transition-state (TS) relative to the reactant-state (RS) to lower the activation free energy barrier between a series of enzymes sharing the same substrate and mechanism according to (Eq. 1),

$$\Delta\Delta G^{\ddagger} = -\left[\left(\vec{F}_{enz,TS} \cdot \vec{\mu}_{TS}\right) - \left(\vec{F}_{enz,RS} \cdot \vec{\mu}_{RS}\right)\right]$$

where $\vec{\mu}_{TS}$ and $\vec{\mu}_{GS}$ are the TS and RS dipole moments for bonds that change charge distribution over the course of the reaction coordinate, i.e. a summation over all bonds that change over the reaction coordinate (Scheme S1). In other words, for any atoms, bonds, or chemical moieties that undergo a change in geometry or electronic structure in going from the RS to the TS (described in terms of changes in dipoles) can serve as an electrostatic handle by which the active site electric field can exert a biased force to alter catalysis. This principle underlies the phenomenon of TS stabilization and preorganization, whereby an enzyme's folded state is on average able to achieve more favorable interactions with the TS relative to the RS. Note that a more general description of electrostatic catalysis would involve not dipoles in an electric field, but charges (distributions) in an electrostatic potential. We have demonstrated the validity of the electric field-based simplification in our previous work on KSI, serine proteases and 4-chlorobenzoyl-CoA dehalogenase.[26, 28, 30] Importantly, the electric field-based framework can be tested using the VSE experimentally, whereas the electrostatic potential is only accessible using computational methods. In particular, the case of serine proteases is interesting for this work, since it involves a similar chemical mechanism and utilize a similar oxyanion hole composed of backbone amides.

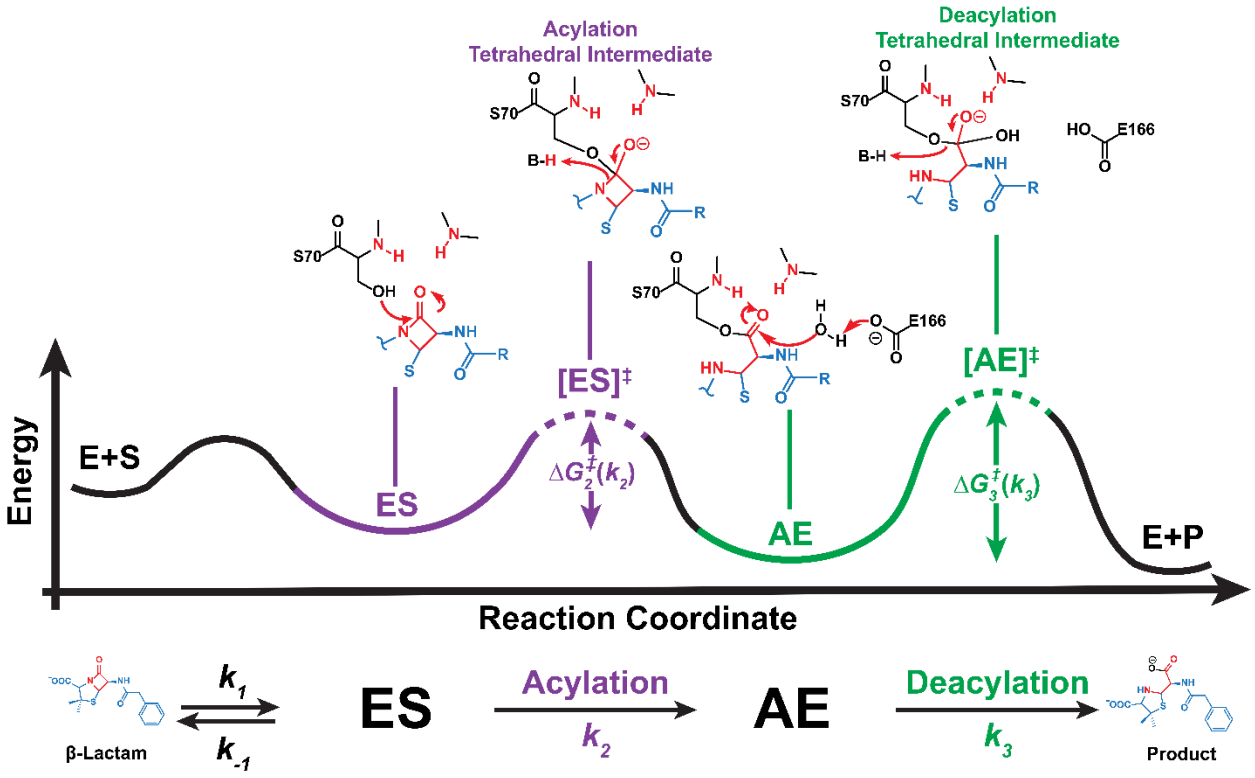

Scheme S1. Expanded reaction mechanism for TEM β-lactamase with PenG. *The mechanism, proposed tetrahedral intermediates, and reaction coordinate involved in the acylation and deacylation processes.[1] The alkoxide tetrahedral intermediates are presumed to be similar, i.e. in terms of both chemical and electronic structure, to the TS for each chemical transformation (dotted lines) and illustrate the mechanism by which an electric field and the oxyanion hole can preferentially stabilize the TS relative to the reactant-state via electrostatic preorganization (Eq. 1). Barrier heights are not drawn to scale.*

In the context of the acylation and deacylation steps of catalysis for class A β-lactamases such as TEM, there are several bonds that undergo a change between the RS and TS, first and foremost being the β-lactam C=O where the two chemical steps (i.e. nucleophilic attack) occur. It is presumed that for this reason the enzyme has evolved an oxyanion hole, which is a common active site feature for enzymes such as proteases, amidases, ligases, etc., which achieve catalysis through nucleophilic substitution at C=O groups. The obvious involvement and charge displacement of the C=O over the reaction is one of the central reasons

that we chose to monitor the electric field at the functional β-lactam C=O using the VSE as it may be the most sensitive and/or experience one of the largest electric fields. Additionally, the β-lactam substrates undergo significant changes over the reaction coordinate, notably upon breaking of the four-membered β-lactam ring, but these interactions are difficult to quantify using the current VSE methodology. As described in the main text, the VSE is not technically accessible with all types of bonds, and cannot be readily applied to monitor the change in electric field at the catalytic residues such as S70 and E166, nor the catalytic water, even though these residues undergo changes in the RS and TS. Therefore, when monitoring the effects of the evolutionary mutations, i.e. which are distant from the oxyanion hole as described in the Supplementary Discussion Section 1, to the active site electric field as projected along the β-lactam C=O, we may invariably not see effects that either 1) do not propagate from the mutational changes to the backbone amides of S70 and A237 to modify the projected field along the C=O bond axis or 2) involve changes to the electric field experienced at other residues or chemical groups involved in the catalysis (e.g. the entire β-lactam ring, S70, E166, or the catalytic water). In addition, it is worth mentioning that mutational changes that change the net charge of the protein, e.g. E104K, do not necessarily have to be treated via changes in the electrostatic potential as long as the reaction mechanism is unperturbed. This is because such changes occur in the environment of the chemical reaction, i.e. in the dielectric surrounding the dipolar changes described by the reaction coordinate. We have demonstrated this situation using the N155R mutation in serine proteases[28] and the D103N and D103L mutations in KSI[26, 30] where each of these mutations was remarkably consistent with the linear correlation between the activation free energy barrier and the electric fields as described by electrostatic catalysis.

Section 3b. *The effects of chemical positioning on enzyme catalysis.*

The original conception of the model for electrostatic catalysis as demonstrated with KSI does not include any observable influence from chemical positioning.[26] However, the mutations under investigation were those chosen to directly ablate specific non-covalent interactions, primarily H-bonds, to the functional C=O for catalysis rather than those observed in the recent evolutionary trajectory from TEM-1 to TEM-52. The observation of multiple species of electric fields using VSE spectroscopy and altered dynamics and conformational heterogeneity as interpreted by the MD simulations would potentially suggest a further role for conformational sampling in the evolution of enzymatic catalysis. As described extensively above in Supplementary Discussion 1 and 2, the evolutionary mutations E104K, G238S, and M182T are distant from the functional β-lactam C=O, which may be one reason that a large electric field at the β-lactam C=O in both TEM-1 and TEM-52 with PenG and CTX may be observed and/or preserved throughout the investigated evolutionarily trajectory. As evident from the MD simulations, these distant mutations perturb the relative dynamics and inter-atom distances of residues across the active site and the substrates in a substrate-dependent manner that can potentially be orthogonal to the electric field projected onto the β-lactam C=O (Supplementary Discussion Section 2,3a). We discuss below how changes in chemical positioning and/or conformational heterogeneity may factor into the observed rate constants and provide a potential interpretation within the framework for electrostatic catalysis.

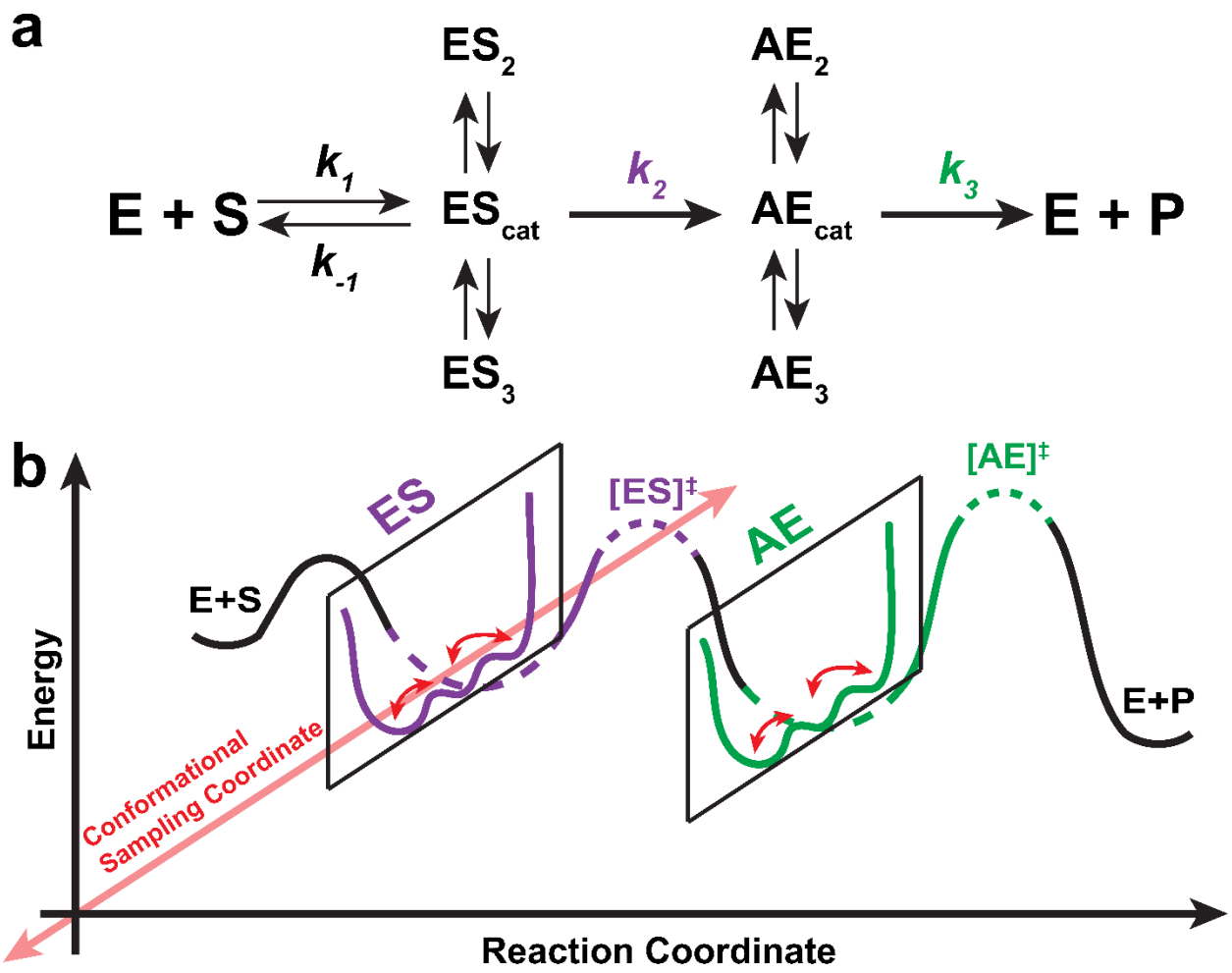

Scheme S2. Accounting for the possibility of conformational heterogeneity in enzyme catalysis. *(a) An expanded model for TEM β-lactamase catalysis that accounts for conformational sampling (ES_2, ES_3, …, AE_2, AE_3) of the ES- and AE-complex relative to a single catalytic conformation (ES_{cat} and AE_{cat}). It should be noted that further mechanistic complexity could be considered if sufficient evidence was experimentally or computationally observed. (b) Expansion of the reaction coordinate diagram along the conformational sampling coordinate (red axis) that would describe the mechanism shown in (a). The sampling of conformations (red arrows) in either the ES (purple) or AE (green) complexes lead to altered rates via changing the relative amount of enzyme in a catalytically permissive state, i.e. ES_{cat} and AE_{cat}, that has some combination of the correct chemical positioning and/or electric field for catalysis.*

A way to rationalize the absence of the linear free energy barrier correlation with the electric field in Figure 6a,b in a more quantitative manner is based on an expansion of the two-

step mechanism of class A β-lactamases, such as TEM-1 (see Figure 1), by adding an orthogonal axis (relative to the reaction coordinate, red axis in Scheme S2) that captures the effect of conformational sampling or structural fluctuations. This model assumes that there are multiple conformational states that are in rapid equilibrium with the catalytically permissive states (i.e. ES_{cat} and AE_{cat}); these equilibria are associated with very low activation barriers and, thus, represent a very fast exchange. Note that in relation to thermal energy at room temperature, the indicated model of multiple ES-like and AE-like states in equilibrium is essentially equal to highly conformationally fluctuating states. These additional conformational states (or increased fluctuations) can relate to structures with perturbed electrostatics and/or chemical positioning of atoms across the active site (both in terms of the protein and substrates). This expanded kinetic picture is supported by the observation of several high field states along the evolutionary trajectory towards TEM-52, as well as the increased fluctuations of nucleophilic atoms and the entire active site from MD simulations. The rather low barriers are supported by the observation that there is complete turnover of either PenG or CTX, indicative of no dead-end conformations, as evident from the time-course UV-vis kinetics and the MS data, which indicates no residual acyl-enzyme. This is also supported by MD results where active site fluctuations are observed for the wild-type enzymes, rather than off-pathway states.

Based on such an interpretation, if there were discrete conformations that are able to interconvert (see red arrows in Scheme S2) and only one of which is catalytically permissive, this would lead to an underestimation of the true rate constant for each chemical step, according to,

$$k_{2,app} = k_2 \left(\frac{[ES_{cat}]}{[ES_{Total}]}\right) \quad \text{and} \quad k_{3,app} = k_3 \left(\frac{[AE_{cat}]}{[AE_{Total}]}\right)$$

where the ratio of catalytic protein to total protein (ES_{cat}/ES_{Total} and AE_{cat}/AE_{Total}) leads to a population-weighted scaling of the apparent rate as determined via UV-vis and steady-state MS. In the alternative picture invoking extensive fluctuations (instead of discrete conformations) a

similar effect would be observed due to limited sampling of the conformation with optimal electrostatics and chemical positioning but would be more difficult to quantify. Therefore, returning to the rationale for the missing linear trend in barrier-electric field correlation, we can outline several scenarios:

- If electrostatics at the β-lactam C=O were the sole change along evolution from TEM-1 to TEM-52, we would observe a linear trend.
- If, as additional effect, chemical positioning was changed along evolution, divergence from the linear barrier-electric field correlation would be observed, via changes of the activation barriers that are orthogonal to the electric field projected along the β-lactam C=O.
- If, instead, fluctuations are increased to the extent describe above, then the above model would apply and the measured apparent rate constants would represent the relative fraction of the enzyme population that is in the catalytic conformation with the true rate constants, k_2 and/or k_3, respectively. Interpreting this result in the context of electrostatic catalysis or any model in which conformational states are interconverting and exhibit differential catalytic activities, would require more sensitive techniques that could monitor and/or detect the individual species, possibly time-resolved IR spectroscopy or single-molecule kinetics, rather than bulk steady-state measurements as performed in most enzymatic studies.

We suggest that a mixture of these situations happens where, along with electrostatics, chemical positioning and fluctuations evolve and thus lead to a complicated activation barrier-electric field trend. A worsening of the chemical positioning, for example increased heterogeneity of the hydroxyl group of S70 for acylation of PenG, can directly impede catalysis by increasing the relative amount of time in which the nucleophilic oxygen is not at the appropriate distance or attack angle with respect to the β-lactam C=O. Such a notion is the basis for many examples in enzyme evolution whereby an increasing catalytic rate can be

attributed to rigidification (i.e. improved preorganization) of the active site. It should be noted that active site rigidification does not necessitate an improvement to catalysis since one could imagine that the consequence of rigidifying an unproductive conformation for catalysis could be more deleterious to function. This discussion is consistent with numerous studies that indicate protein scaffolds with greater structural plasticity, i.e. conformational sampling or more fluctuation chemical positioning such as β-lactamases, are better starting points for directed evolution.[17, 31-36]

Extended Figures, Tables, and Schemes:

Table S1. Summary of kinetic data for TEM β-lactamase-catalyzed hydrolysis of PenG and CTX based on steady-state kinetics and mass spectrometry.

	PenG				CTX			
Variant	k_{cat} (s^{-1})	K_M (μM)	k_2 (s^{-1})[b]	k_3 (s^{-1})[b]	k_{cat} (s^{-1})	K_M (μM)	k_2 (s^{-1})[b]	k_3 (s^{-1})[b]
TEM-1	1816.2 ± 18.0	25.6 ± 8.0	5514.7 [4641.0, 6318.2]	2707.5 [2545.4, 2985.6]	3.9 ± 0.2	2051.3 ± 168.2	4.1 [3.8, 4.4]	93.1 [38.7, 248.9]
TEM-17	1650.5 ± 36.9	30.6 ± 0.3	8559.5 [5779.5, 11898.6]	2047.0 [1908.3, 2314.7]	10.8 ± 1.4	1189.0 ± 214.9	11.8 [10.2, 13.3]	133.3 [99.0, 187.2]
TEM-19	105.9 ± 4.4	2.5 ± 0.5	262.1 [236.6, 291.3]	177.7 [165.2, 192.4]	69.7 ± 7.1	281.2 ± 40.4	88.1 [77.7, 99.4]	334.1 [259.1, 462.7]
TEM-15	65.8 ± 2.6	1.9 ± 0.7	1620.1 [891.0, 3218.2][a]	68.9 [65.7, 72.8][a]	116.1 ± 3.6	76.3 ± 8.2	137.6 [125.7, 154.8]	777.2 [467.2, 1477.6]
TEM-52	42.9 ± 0.2	1.3 ± 0.2	276.8 [188.2, 342.4]	50.9 [49.1, 55.6]	89.6 ± 2.5	71.8 ± 11.5	110.4 [101.9, 121.9]	483.1 [345.7, 721.4]

[a] *Minimal detectable non-covalent species, such that $k_3 \approx k_{cat}$, only values of [AE]/[ES] < 50 were considered in rate-constant determination due to the signal-to-noise of LC-MS data.*

[b] *Rate-constants and uncertainties (68.25% confidence interval (CI) equivalent to 1σ) for k_2 and k_3 are the median value as determined through propagation of k_{cat} values as well as the distribution of [AE]/[ES] values for each charge state of the protein charge envelope via LC-MS (see Figure S4,5).*

Table S2. Activation free energy barriers for the TEM β-lactamase reaction with PenG and CTX.

	PenG			CTX		
Variant	**Overall** $\Delta G^{\ddagger}_{kcat}$ **(kcal/mol)[a]**	**Acylation** $\Delta G^{\ddagger}_{k2}$ **(kcal/mol)[a,b]**	**Deacylation** $\Delta G^{\ddagger}_{k3}$ **(kcal/mol)[a,b]**	**Overall** $\Delta G^{\ddagger}_{kcat}$ **(kcal/mol)[a]**	**Acylation** $\Delta G^{\ddagger}_{k2}$ **(kcal/mol)[a,b]**	**Deacylation** $\Delta G^{\ddagger}_{k3}$ **(kcal/mol)[a,b]**
TEM-1	**13.00 ± 0.01**	**12.34 [12.44, 12.26]**	**12.76 [12.80, 12.70]**	**16.64 ± 0.04**	**16.61 [16.65, 16.57]**	**14.76 [15.28, 14.18]**
TEM-17	**13.06 ± 0.02**	**12.08 [12.31, 11.89]**	**12.93 [12.97, 12.86]**	**16.04 ± 0.04**	**15.98 [16.07, 15.91]**	**14.55 [14.72, 14.34]**
TEM-19	**14.68 ± 0.02**	**14.15 [14.21, 14.08]**	**14.38 [14.42, 14.33]**	**14.93 ± 0.06**	**14.79 [14.87, 14.72**	**14.00 [14.15, 13.81]**
TEM-15	**14.96 ± 0.02**	**13.07 [13.42, 12.66]**	**14.94 [14.96, 14.90]**	**14.63 ± 0.02**	**14.53 [14.58, 14.46]**	**13.50 [13.80, 13.12]**
TEM-52	**15.22 ± 0.01**	**14.11 [14.34, 13.99]**	**15.12 [15.14, 16.06]**	**14.78 ± 0.02**	**14.66 [14.70, 14.60]**	**13.78 [13.98, 13.55]**

[a] *Activation free energy barriers are calculated using TS-theory at 298 K according to* $\Delta G^{\ddagger} = -RT \ln\left(k \frac{h}{k_B T}\right)$*, where k is the observed rate-constant, k_B is the Boltzmann constant, h is Planck's constant, T is temperature (K), R is the gas constant.*

[b] *Activation free energy barrier values and uncertainties (68.25% confidence interval (CI) equivalent to 1σ) for k_2 and k_3 are the median value as determined through propagation of k_{cat} values as well as the distribution of [AE]/[ES] values for each charge state of the protein charge envelope via LC-MS (see Figure S4,5, Table S1).*

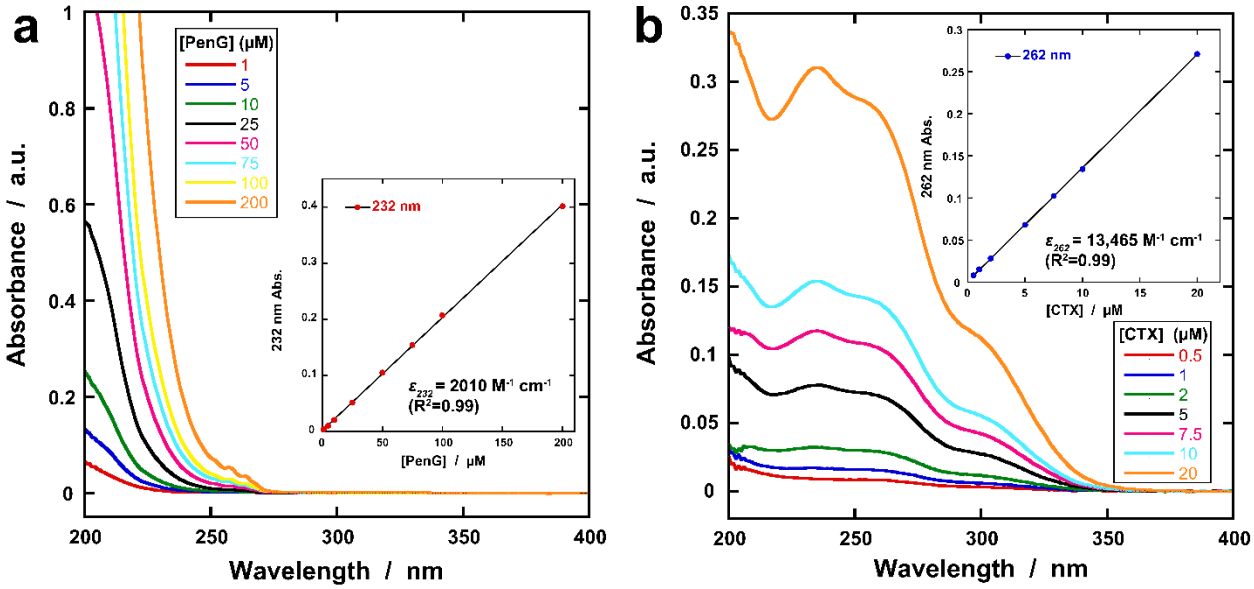

Figure S2. Absorbance spectra and extinction coefficient determination for PenG and CTX. *Increasing concentrations of* ***(a)*** *PenG and* ***(b)*** *CTX in phosphate buffer (pH 7.0). Insets contain extinction coefficient determination information as determined from single-wavelength analysis as a function of concentration. The extinction coefficients at 232 and 262 nm, for PenG and CTX, respectively, are approximately 2-fold higher than those utilized for monitoring hydrolysis (i.e. substrate loss is quantified based on* $\Delta\varepsilon$ *= -940 and -7250* M^{-1} cm^{-1}*, respectively).*[2]

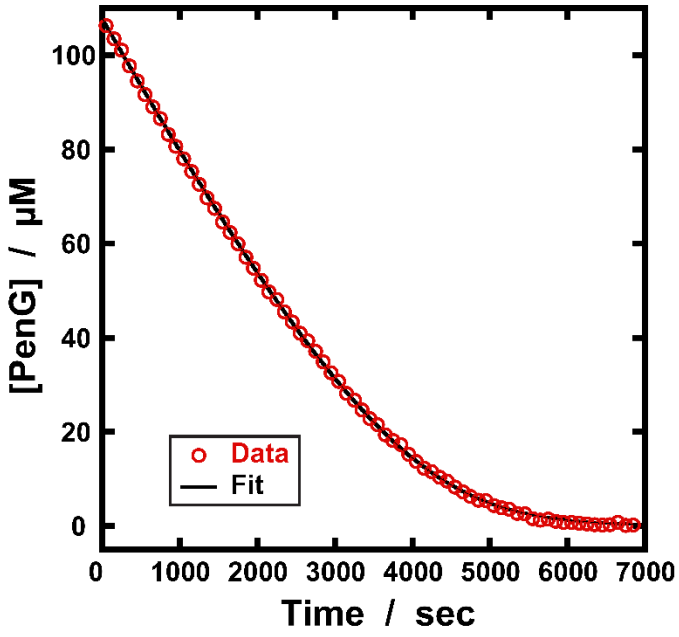

Figure S3. Representative time-trace data for PenG hydrolysis by TEM-1 S70A β-lactamase. *Data (red circles) is shown relative to the analytical fit (black line) based on the closed-form solution to the Michaelis-Menten equation. Kinetic parameters: k_{cat} = 0.0105 ± 0.0001 sec^{-1}, K_M = 23.35 ± 0.04 µM were determined using analytical solution (see MATLAB scripts) and errors are determined from the Jacobian and covariance matrix.*

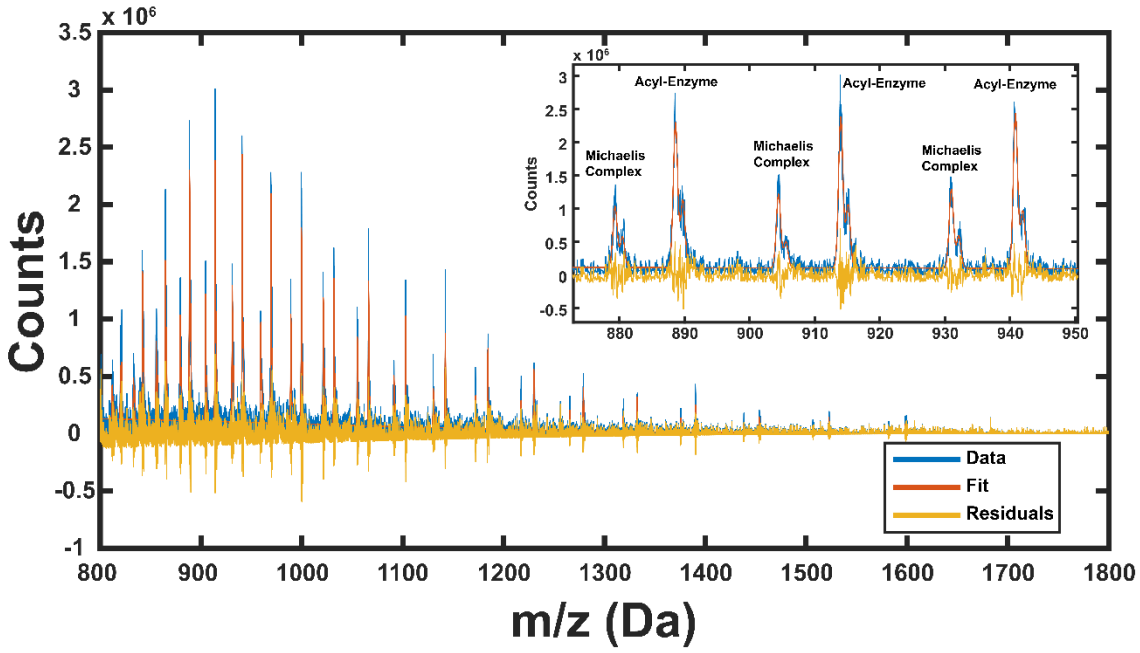

Figure S4. Representative steady-state MS charge envelope of TEM-1 with PenG for kinetic deconvolution. *The relative abundance of the ES and AE complexes can be followed in MS following the general approach and methods of Saves et al.[3] The corresponding raw data (blue), overall fit (orange), and fitting residuals (yellow) for the steady-state quenched TEM-1 with PenG. Inset displays distribution pattern for Michaelis complex and acyl-enzyme for a given charge state of the overall protein charge envelope. The relative abundance of non-covalent (ES) and covalent (AE) complexes (+ 334 or +413 Da for PenG and CTX, respectively) was determined similarly to Saves et al.[3] from analysis of the unprocessed m/z data extracted using the MassLynx software and the mass envelope intensities quantified using a MATLAB script (See SI MATLAB code) for each charge state (z=20 – 39) of the charge envelope (also referred to as charge state distribution). For each charge state in the protein charge envelope, a series of gaussian bands corresponding to the non-covalent and covalent complexes were fit with equal width but adjustable intensities in order to compare the integrated peak areas within a given charge state for [AE]/[ES] determination. A broad gaussian baseline was applied throughout to improve the fits. Ratios of [AE]/[ES] were acquired across 3-5 independent sample preparations, and [AE]/[ES] values from each charge state were utilized to determine the overall [AE]/[ES] ratios and subsequently k_2 and k_3 using a bootstrapping algorithm as described in Figure S5. The relative ionization efficiencies of the complexes ([AE]/[ES]), was determined to be 1.0 ± 0.1 (n=3) by mixing an equal amount of kinetically incompetent protein TEM-1 E166N (which is not observed to deacylate) both with and without PenG or CTX, but*

otherwise treated as described in the Methods, and measured via LC-MS. There was no apparent hydrolysis of the acylated TEM-1 E166N complex with either PenG or CTX in the water:methanol mixtures, as no detectable non-covalent TEM-1 E166N was observed via LC-MS. Note that the less thermodynamically stable TEM variants, i.e. TEM-19 and TEM-15, were more prone to unfolding in water/methanol solutions as determined via loss of concentration after buffer exchange, indicated by transfer through the 3k molecular weight cut-off (MWCO) filter. This could be ameliorated through lower methanol concentrations, thereby reducing the extent of unfolding, and no change in [AE]/[ES] ratios as determined from LC-MS were observed with water:methanol ratios of 3:1 or 7:1.

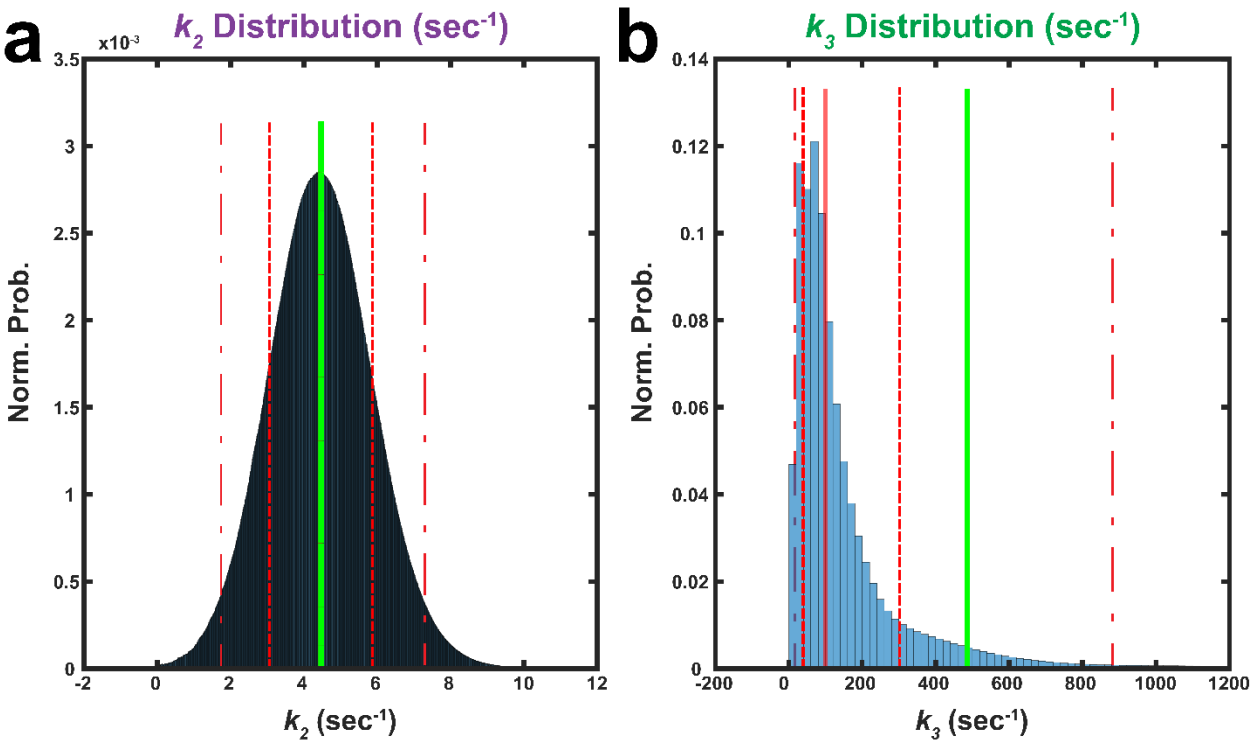

Figure S5. Example kinetic parameter distributions determined using bootstrapping algorithm for TEM-1 β-lactamase with CTX. *Normalized probability distribution of* ***(a)*** k_2 *and* ***(b)*** k_3 *values from analytical bootstrapping using Michaelis-Menten parameters and measured [AE]/[ES]ratios. While quantification of the [AE]/[ES] ratios may be normally distributed, the distributions of rate constants are not necessarily since both* k_2 *and* $k_3 > k_{cat}$*, i.e.* $0 \leq$ *[AE]/[ES]* $\leq$ *infinity. As such, we utilize the uncertainty in both* k_{cat} *and [AE]/[ES] ratios to bootstrap a distribution of possible* k_2 *and* k_3 *values and determine the median and appropriate confidence intervals. The solid green and red lines indicate the average and median, respectively. The 68% CI (red dashed lines; 15.865 and 84.135 quantiles) and 95% CI (red double dashed lines; 2.5 and 95 quantiles), equivalent to 1σ and 2σ for normal distributions, respectively, are shown in red dashed lines. See SI MATLAB code.*

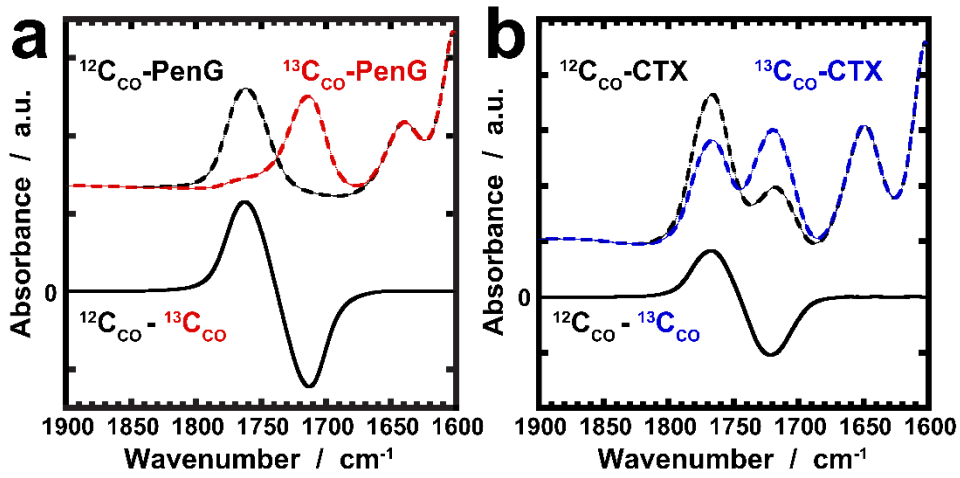

Figure S6. FTIR spectra of $^{12}C_{CO}$ and $^{13}C_{CO}$ β-lactams in aqueous buffer.[4] (a) *PenG (black and red dashed lines, respectively) and* ***(b)*** *CTX (black and blue dashed lines, respectively) and corresponding isotope-edited difference spectra ($^{12}C_{CO}$ – $^{13}C_{CO}$; solid black line) in deuterated aqueous buffer (50 mM KP_i, 100 mM NaCl, pD 7.0), offset for clarity. Note that the ^{12}C-component of the 50:50 $^{12/13}C$-CTX basis spectrum is first removed using a reference ^{12}C-CTX spectrum in aqueous buffer. Figure adapted from Kozuch et al.[4] Note that the IR features for both PenG and CTX are much narrower when associated with the protein (Fig. 3) so that the positive (^{12}C=O) and negative (^{13}C=O) features are well separated.*

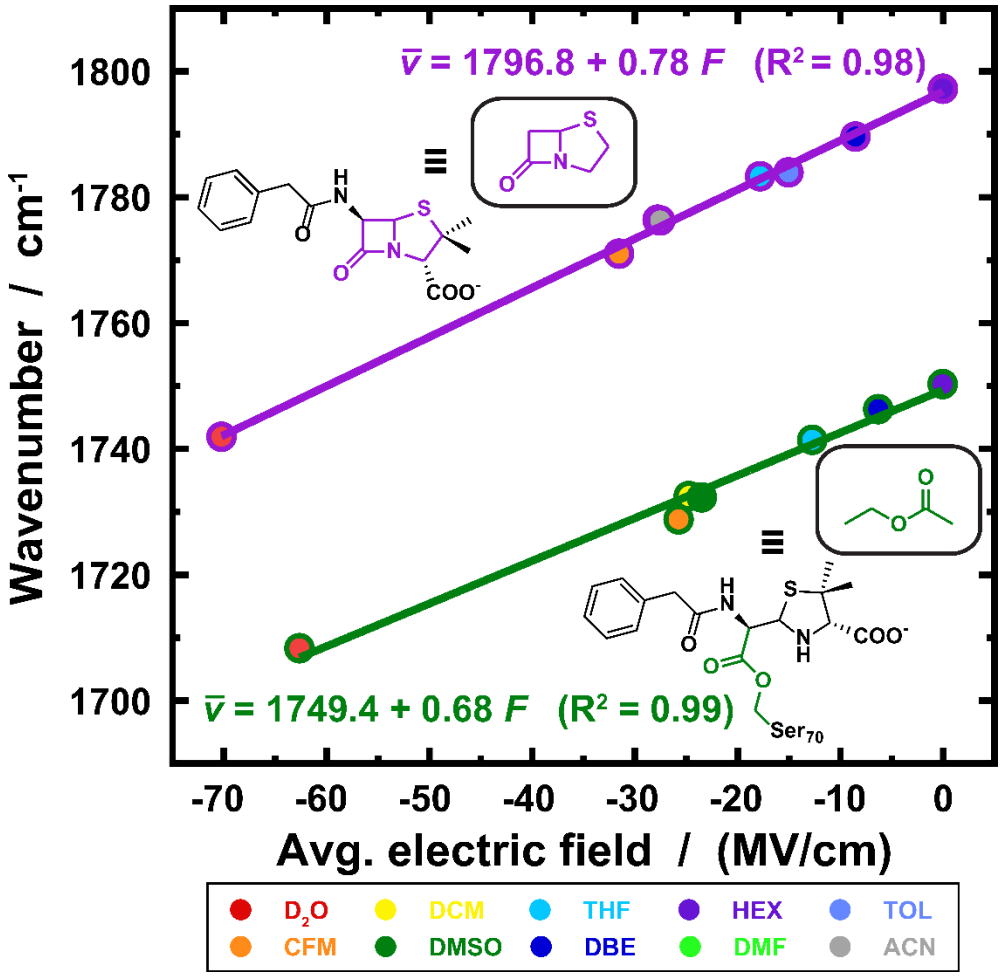

Figure S7. Electric field-frequency calibration for model compounds and their β-lactam antibiotic mechanistic equivalents.[5] *Top line (purple) corresponds to the penam core (inset) and bottom line (green) to ethyl acetate, which correspond to the Michaelis complex and acyl-enzyme, respectively. Best fit lines and equations are shown in terms of the VSE based on fixed-charge MD simulations. Solvent legend: CFM = chloroform, DCM = dichloromethane, DMSO = dimethylsulfoxide, THF = tetrahydrofuran, DBE = dibutyl ether, HEX = hexanes, DMF = dimethylformamide, TOL = toluene, ACN = acetonitrile. In order to establish an analogous comparison for CTX's cephem-core (ES complex), DFT vibrational frequency calculations were used to predict the harmonic frequencies for the penam and cephem β-lactam C=O, which were scaled according to the scaling factor of 0.9679 for B3LYP/6-311(p,d) to 6-311G**(3pd,3df), resulting in corrected frequencies of 1781.1 and 1779.8 cm^{-1}. We utilize this frequency offset ($\Delta\bar{\nu} = 1.3$ cm^{-1}) and the Stark tuning rate for the penam-core (|Δμ| = 0.78 cm^{-1}/(MV/cm); purple line), based on their similar bicyclic structures, to determine the VSE field-frequency calibration of intact CTX as $\bar{\nu} = 0.78F + 1795.5$. Figure adapted from Kozuch et al.*[5]

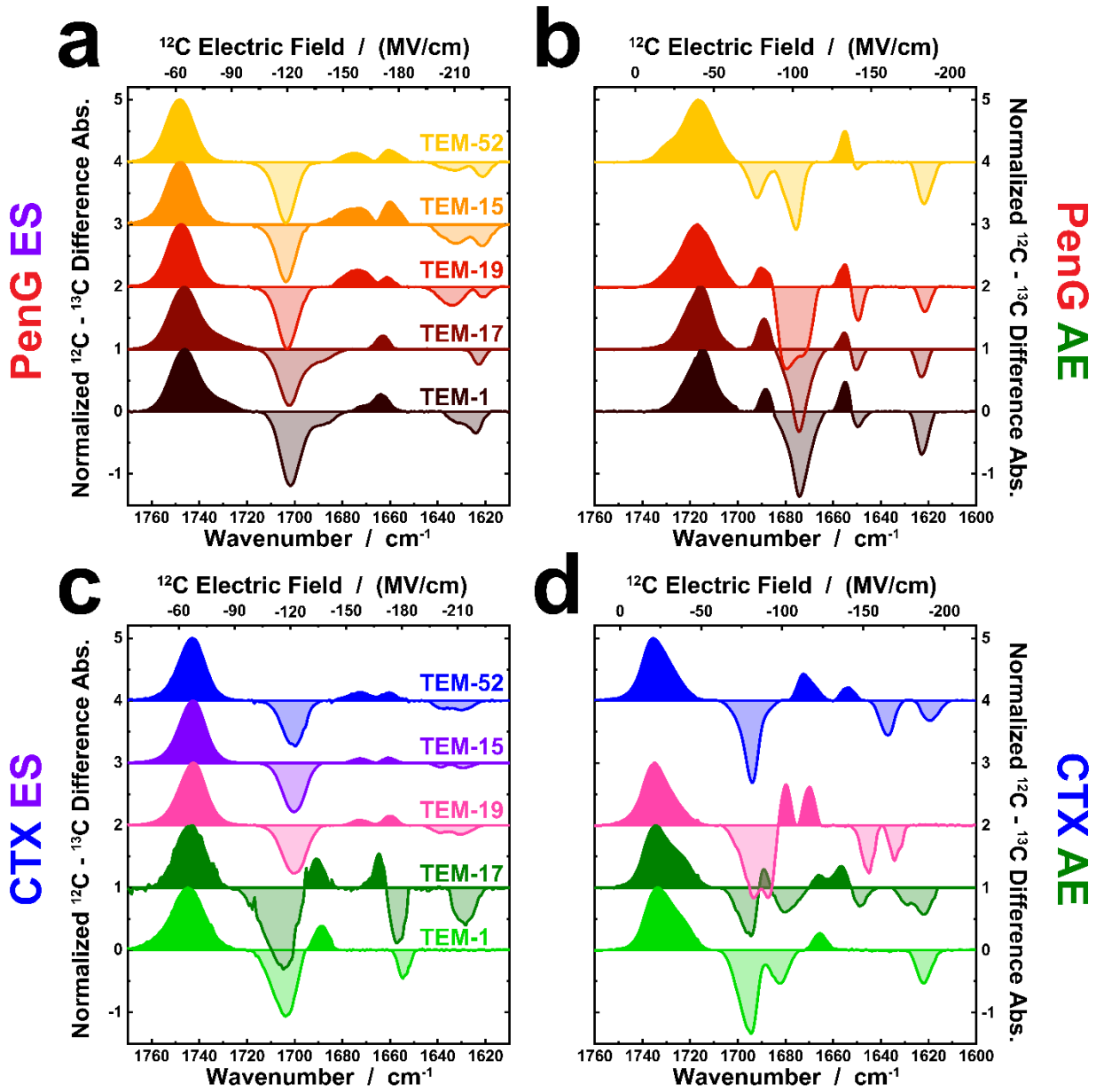

Figure S8. ***Full isotope-edited IR difference spectroscopy of the TEM β-lactamases with PenG and CTX. (a-d)*** *The vibrational frequencies and corresponding ^{12}C-electric fields for* ***(a, b)*** *PenG and* ***(c, d)*** *CTX in the* ***(a,c)*** *ES (S70G) and* ***(b,d)*** *AE (E166N) complexes across evolutionary variants from TEM-1 to TEM-52. IR spectra are shown as a ^{12}C-normalized ^{12}C-^{13}C difference spectra (see Figure 3) with ^{13}C spectral components (negative absorbance) being shown with faded color. The top axis is the electric field corresponding to the ^{12}C-isotope of the corresponding VSE calibrated probe (Figure S7). The TEM-15 E166N mutant was not measured due to the protein's instability and likely aggregation, observed as increasing protein-specific spectral changes and loss of 280 nm absorbance over time.*

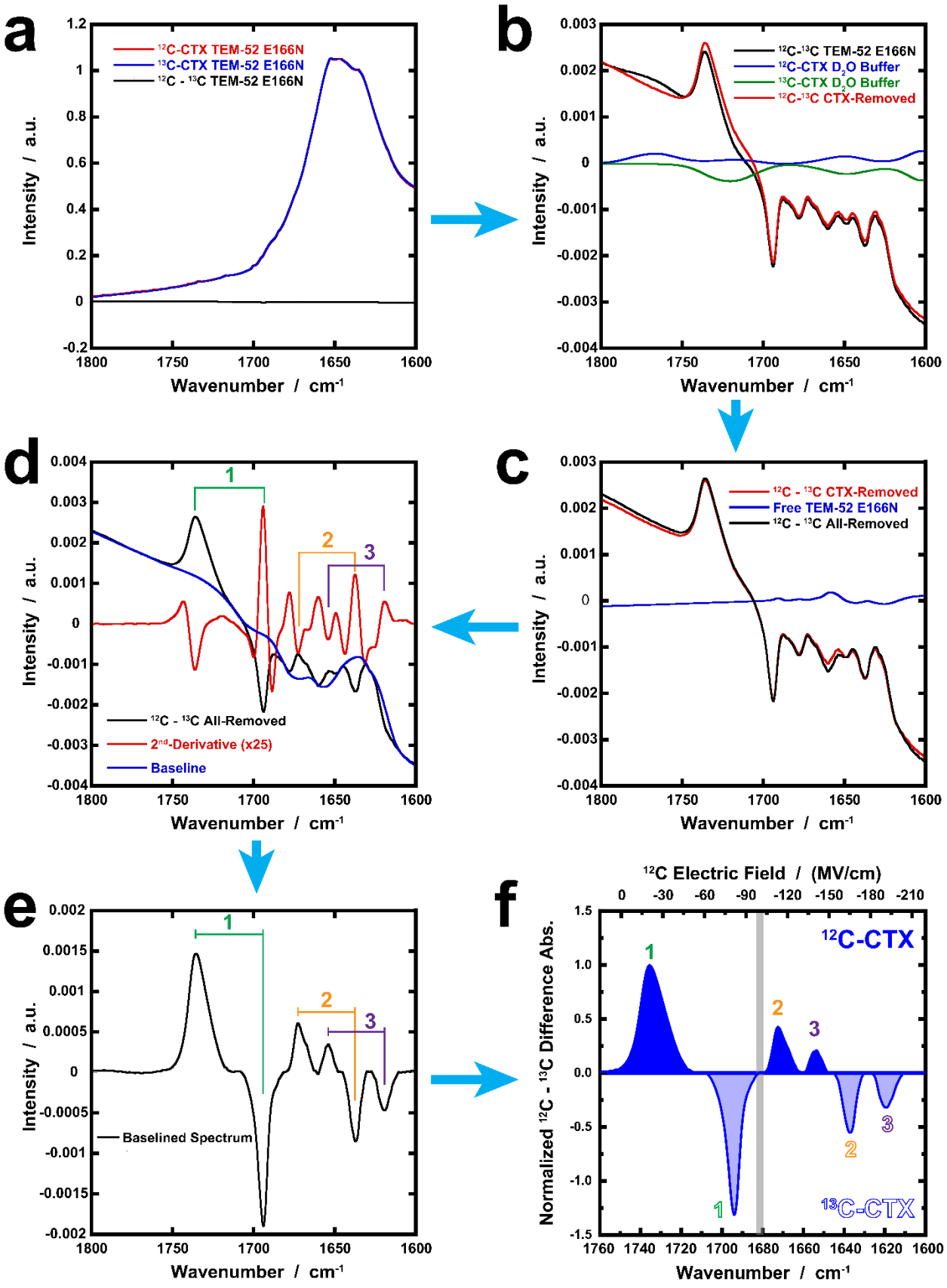
a
^{12}C-CTX TEM-52 E166N
^{13}C-CTX TEM-52 E166N
^{12}C - ^{13}C TEM-52 E166N
Intensity / a.u.
Wavenumber / cm^{-1}
b
^{12}C-^{13}C TEM-52 E166N
^{12}C-CTX D$_2$O Buffer
^{13}C-CTX D$_2$O Buffer
^{12}C-^{13}C CTX-Removed
Intensity / a.u.
Wavenumber / cm^{-1}
c
^{12}C - ^{13}C CTX-Removed
Free TEM-52 E166N
^{12}C - ^{13}C All-Removed
Intensity / a.u.
Wavenumber / cm^{-1}
d
1
2
3
^{12}C - ^{13}C All-Removed
2nd-Derivative (x25)
Baseline
Intensity / a.u.
Wavenumber / cm^{-1}
e
1
2
3
Baselined Spectrum
Intensity / a.u.
Wavenumber / cm^{-1}
f
^{12}C Electric Field / (MV/cm)
0 -30 -60 -90 -120 -150 -180 -210
^{12}C-CTX
^{13}C-CTX
Normalized ^{12}C - ^{13}C Difference Abs.
Wavenumber / cm^{-1}

Figure S9. Representative example of FTIR data processing and assignment with TEM-52 E166N and CTX. (a) *^{12}C- and ^{13}C- spectra are scaled to minimize all protein absorbances and then subtracted to produce the isotope-edited difference spectrum (black).* ***(b)*** *All unbound CTX (^{12}C in blue, ^{13}C- in green) is then removed from the preliminary difference spectra using basis spectra of free CTX acquired in aqueous (D_2O) buffer (Fig. S6).* ***(c)*** *Additional features due to H/D exchange of the protein backbone and side-chains are also removed using basis spectra of the unbound protein acquired in identical aqueous buffer.* ***(d)*** *2nd-derivative analysis (red) is utilized to determine the sets of positive and negative features and then the spectrum is baselined resulting in the* ***(e)*** *final spectrum.* ***(f)*** *Multiple difference spectra were conservatively baselined and averaged to generate the final spectra shown in Figure 3 and S8. There was no evidence of spectral features corresponding to the β-lactam C=O below 1600 cm^{-1}. In the TEM-# S70G mutants with PenG, as previously observed,[6] these mutants exhibit a residual slow level of hydrolytic activity leading to time-dependent changes on the timescale of the FTIR measurements. Measurements were acquired until nearly all PenG was hydrolyzed and difference spectra were taken between an early and late spectrum (timescale of ~ 1-3 hrs apart) of identical isotopes, i.e. $^{12}C_{early} - {}^{12}C_{late}$ and $^{13}C_{early} - {}^{13}C_{late}$. An isotope-edited difference spectrum was then achieved through scaled subtraction, i.e. $(^{12}C_{early} - {}^{12}C_{late}) - (^{13}C_{early} - {}^{13}C_{late})$, which was further processed according to the protocol described above. Hydrolysis leads to formation of the ^{12}C and ^{13}C-penicilloic acid product species (1599.8 and 1554.5 cm^{-1}), which have opposite signs relative to the peaks assigned to the Michaelis complex due to the inverse correlation between substrate and product concentrations as a function of time. An increasing amount of bound product is observed over time with sharp peaks at ca. 1582 and 1545 cm^{-1} across all the TEM variants, corresponding to the ^{12}C- and ^{13}C-species, respectively, and assigned to the asymmetric carboxylate stretching frequency.*

Table S3. TEM-# S70G PenG vibrational frequencies and lineshape parameters from curve-fitting.

TEM-# S70G **PenG**	Frequency (cm^{-1})[a,b]	FWHM (cm^{-1})[a,b]	Integral (OD/cm^{-1})	Lineshape (%L+G)[c]
1	1746.4 (1701.8)	13.4 (9.6)	0.0142 (-0.0115)	5 (0)
	1732.2 (1689.3)	13.3 (14.3)	0.0028 (-0.0052)	20 (100)
	1671.2 (1631.0)	14.2 (8.1)	0.0024 (-0.0016)	99 (0)
	1663.5 (1624.0)	6.8 (5.7)	0.0017 (-0.0019)	0 (0)
	1582.8 (1546.1)	9.2 (9.9)	-0.0080 (0.0053)	0 (0)
17	1746.6 (1702.5)	14.1 (10.1)	0.0189 (-0.0142)	4 (28)
	1731.7 (1690.3)	15.9 (12.2)	0.0057 (-0.0030)	86 (0)
	1663.2 (1622.8)	5.9 (5.2)	0.0019 (-0.0017)	8 (0)
	1585.0 (1546.4)	8.7 (10.1)	-0.0075 (0.0072)	0 (3)
19	1747.7 (1703.1)	13.3 (9.6)	0.0482 (-0.0345)	10 (12)
	1673.9 (1634.2)	12.5 (10.9)	0.0121 (-0.0113)	0 (0)
	1660.7 (1620.5)	5.0 (5.2)	0.0024 (-0.0029)	0 (0)
	1582.3 (1544.5)	8.5 (11.4)	-0.0182 (0.0240)	0 (3)
15	1748.0 (1703.8)	13.7 (9.1)	0.0495 (-0.0319)	17 (26)
	1675.5 (1633.0)	14.6 (12.5)	0.0177 (-0.0125)	64 (0)
	1659.3 (1620.8)	6.7 (7.6)	0.0073 (-0.0085)	0 (12)
	1582.8 (1545.7)	9.0 (12.5)	-0.0207 (0.0264)	0 (2)
52	1748.3 (1703.8)	13.7 (9.6)	0.0796 (-0.0566)	10 (20)
	1675.4 (1633.5)	10.3 (11.3)	0.0101 (-0.0082)	30 (0)
	1659.6 (1621.1)	7.7 (6.2)	0.0081 (-0.0079)	0 (0)

	1582.6 (1544.8)	9.7 (13.0)	-0.0304 (0.0439)	0 (4)

[a] *Uncertainties in peak positions are ca. ± 1 cm^{-1} based on comparison of multiple spectral comparisons within a given protein-ligand complex. There are greater uncertainties in the FWHM, integrations, and lineshapes due to curve-fitting of multiple overlapping peaks in many protein spectra.*

[b] *Values in parentheses correspond to those of the ^{13}C-substrate peaks. Note that the ^{13}C peaks are generally narrower than the corresponding ^{12}C peak and that as the frequencies shift to lower frequencies, the isotope frequency offset (^{12}C-^{13}C) gets smaller. These changes may arise due to differential effects of normal mode coupling, slight variations in the Stark tuning rate, and homogeneous broadening, respectively.*

[c] *The pseudo-Voigt lineshape was used to fit all peaks, where the % corresponds to the linear combination of Lorentzian (L) and Gaussian (G) lineshapes.*

Table S4. TEM-# S70G CTX vibrational frequencies and lineshape parameters from curve-fitting.

TEM-# S70G **CTX**	Frequency (cm^{-1})[a,b]	FWHM (cm^{-1})[a,b]	Integral (OD/cm^{-1})	Lineshape (%L+G)[c]
1	1744.9 (1704.2)	16.3 (11.9)	0.0035 (-0.0028)	32 (33)
	1690.1 (1654.3)	10.0 (5.0)	0.0007 (-0.0004)	0 (0)
17	1743.7 (1703.6)	14.8 (18.8)	0.0040 (-0.0072)	0 (12)
	1693.4 (1657.0)	11.2 (6.5)	0.0028 (-0.0017)	0 (0)
	1664.4 (1628.7)	5.0 (8.9)	0.0010 (-0.0014)	63 (0)
19	1751.2 (1704.9)	11.6 (8.4)	0.0039 (-0.0079)	0 (43)
	1742.4 (1699.2)	12.4 (9.8)	0.0448 (-0.0234)	18 (0)
	1672.5 (1639.4)	7.4 (6.9)	0.0023 (-0.0026)	9 (0)
	1660.0 (1630.1)	6.1 (9.1)	0.0032 (-0.0049)	0 (0)
15	1749.5 (1704.9)	13.9 (7.7)	0.0061 (-0.0071)	0 (38)
	1742.5 (1699.5)	12.1 (9.4)	0.0451 (-0.0255)	13 (0)
	1672.7 (1639.0)	6.8 (5.1)	0.0019 (-0.0013)	8 (0)
	1660.5 (1629.2)	5.6 (7.4)	0.0018 (-0.0022)	0 (0)
52	1750.1 (1704.2)	14.2 (7.6)	0.0076 (-0.0153)	4 (58)
	1742.7 (1699.0)	12.2 (8.0)	0.0552 (-0.0210)	17 (0)
	1673.0 (1638.6)	11.0 (6.5)	0.0071 (-0.0032)	21 (0)
	1660.3 (1629.9)	7.0 (9.6)	0.0038 (-0.0065)	5 (0)

[a] *Uncertainties in peak positions are ca. ± 1 cm^{-1} based on comparison of multiple spectral comparisons within a given protein-ligand complex. There are greater uncertainties in the FWHM, integrations, and lineshapes due to curve-fitting of multiple overlapping peaks in many protein spectra.*

[b] *Values in parentheses correspond to those of the ^{13}C-substrate peaks. Note that the ^{13}C peaks are generally narrower than the corresponding ^{12}C peak and that as the frequencies shift to lower frequencies, the isotope frequency offset (^{12}C-^{13}C) gets smaller. These changes may arise due to differential effects of normal mode coupling, slight variations in the Stark tuning rate, and homogeneous broadening, respectively.*

[c] *The pseudo-Voigt lineshape was used to fit all peaks, where the % corresponds to the linear combination of Lorentzian (L) and Gaussian (G) lineshapes.*

Table S5. TEM-# E166N PenG vibrational frequencies and lineshape parameters from curve-fitting.

TEM-# E166N **PenG**	Frequency (cm^{-1})[a,b]	FWHM (cm^{-1})[a,b]	Integral (OD/cm^{-1})	Lineshape (%L+G)[c]
1	1722.3 (***)[d]	9.1	0.0046	0
	1714.6 (1673.9)	11.2 (9.0)	0.0320 (-0.0384)	49 (66)
	1688.2 (1650.6)	5.0 (6.6)	0.0051 (-0.0063)	0 (0)
	1654.5 (1622.6)	5.5 (5.4)	0.0130 (-0.0089)	100 (0)
17	1722.5 (***)[d]	10.0	0.0119	23
	1715.1 (1674.2)	10.7 (8.7)	0.0443 (-0.0566)	31 (60)
	1688.9 (1650.6)	6.1 (5.2)	0.0126 (-0.0102)	0 (18)
	1654.4 (1622.9)	6.6 (4.7)	0.0143 (-0.0084)	100 (0)
19	1729.2 (***)[b, d]	10.7	0.0060	0
	1717.1 (1680.4)[b]	14.0 (9.9)	0.0469 (-0.0588)	0 (4)
	1708.1 (1671.5)[b]	8.2 (6.4)	0.0038 (-0.0195)	0 (0)
	1685.2 (1649.7)	10.1 (4.5)	0.0277 (-0.0090)	1 (0)
	1655.1 (1621.5)	5.0 (5.0)	0.0075 (-0.0068)	35 (0)
52	1730.6 (1691.9)	7.4 (7.4)	0.0026 (-0.0161)	0 (100)
	1716.3 (1676.3)	16.1 (7.5)	0.0437 (-0.0190)	19 (0)
	*** (1650.5)[a, d]	(4.5)	(-0.0018)	(0)
	1655.0 (1621.6)	5.0 (6.4)	0.0071 (-0.0108)	26 (0)

[a] *Uncertainties in peak positions are ca. ± 1 cm^{-1} based on comparison of multiple spectral comparisons within a given protein-ligand complex. There are greater uncertainties in the FWHM, integrations, and lineshapes due to curve-fitting of multiple overlapping peaks in many protein spectra.*

[b] *Values in parentheses correspond to those of the ^{13}C-substrate peaks. Note that the ^{13}C peaks are generally narrower than the corresponding ^{12}C peak and that as the frequencies shift to lower frequencies, the isotope frequency offset (^{12}C-^{13}C) gets smaller. These changes may arise due to differential effects of normal mode coupling, slight variations in the Stark tuning rate, and homogeneous broadening, respectively.*

[c] *The pseudo-Voigt lineshape was used to fit all peaks, where the % corresponds to the linear combination of Lorentzian (L) and Gaussian (G) lineshapes.*

[d] *"***" corresponds to either a ^{12}C or ^{13}C feature that cannot be resolved due to spectral overlap and cancellation.*

Table S6. TEM# E166N CTX vibrational frequencies and lineshape parameters from curve-fitting.

TEM-# E166N **CTX**	Frequency (cm^{-1})[a,b]	FWHM (cm^{-1})[a,b]	Integral (OD/cm^{-1})	Lineshape (%L+G)[c]
1	1734.3 (1695.6)	11.2 (9.0)	0.0139 (-0.0168)	6 (18)
	1724.4 (1682.1)	12.0 (7.0)	0.0074 (-0.0048)	0 (0)
	1665.6 (1621.9)	6.2 (6.8)	0.0024 (-0.0047)	12 (0)
17[d]	1735.6 (1694.7)			
	1722.5 (1681.3)			
	1689.0 (1649.1)			
	1667.0 (1630.3)			
	1655.8 (1621.0)			
19	1735.1 (1693.0)	11.8 (11.1)	0.0188 (-0.0232)	16 (32)
	1725.5 (1686.5)	10.8 (4.2)	0.0056 (-0.0045)	77 (0)
	1680.0 (1645.5)	4.7 (5.6)	0.0054 (-0.0067)	0 (0)
	1670.0 (1633.9)	5.0 (5.2)	0.0051 (-0.0044	0 (0)
52	1735.9 (1694.3)	10.6 (7.2)	0.0168 (-0.0195)	29 (66)
	1727.8 (***)[e]	11.4	0.0080	41
	1672.7/1668.2 (1637.3)	5.7/5.7 (6.6)	0.0053/0.0014 (-0.0058)	86/0 (0)
	1653.8 (1619.2)	5.9 (7.5)	0.0019 (-0.0039)	0 (0)

[a] *Uncertainties in peak positions are ca. ± 1 cm^{-1} based on comparison of multiple spectral comparisons within a given protein-ligand complex. There are greater uncertainties in the FWHM, integrations, and lineshapes due to curve-fitting of multiple overlapping peaks in many protein spectra.*

[b] *Values in parentheses correspond to those of the ^{13}C-substrate peaks. Note that the ^{13}C peaks are generally narrower than the corresponding ^{12}C peak and that as the frequencies shift to lower frequencies, the isotope frequency offset (^{12}C-^{13}C) gets smaller. These changes may arise due to differential effects of normal mode coupling, slight variations in the Stark tuning rate, and homogeneous broadening, respectively.*

[c] *The pseudo-Voigt lineshape was used to fit all peaks, where the % corresponds to the linear combination of Lorentzian (L) and Gaussian (G) lineshapes.*

[d] *Peak positions determined based on 2nd-derivative maxima and minima positions. Uncertainties will be increased for peaks that overlap due to cancellation.*

[e] *"***" corresponds to either a ^{12}C or ^{13}C feature that cannot be resolved due to spectral overlap and cancellation.*

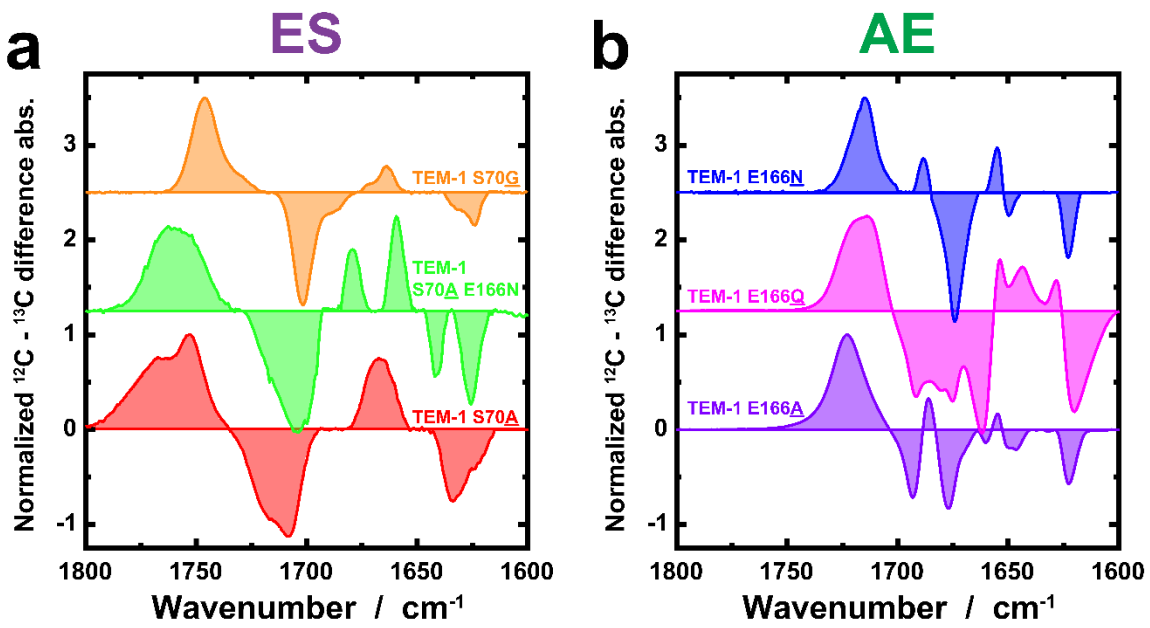

Figure S10. Mutational effect on IR spectra of TEM-1 β-lactamase with PenG. *The mutational choice for the S70X and E166X positions as related to the WT TEM for the* ***(a)*** *ES and* ***(b)*** *AE complex with PenG. Positive peaks correspond to ^{12}C-PenG with corresponding negative peaks for the ^{13}C-PenG with an offset of ca. 35-45 cm^{-1}. Spectra are normalized and offset for clarity. The highest frequency peaks (1800-1700 cm^{-1}) are generally more mutation-dependent than the lower frequency peak(s) (<1675 cm^{-1}), with the simplest spectra corresponding to those of the S70G and E166N, as supported by crystallographic results.[7] Additional variants S70(C/T) and E166D were all considered but either did not express or had rates too fast for FTIR measurements.[8]*

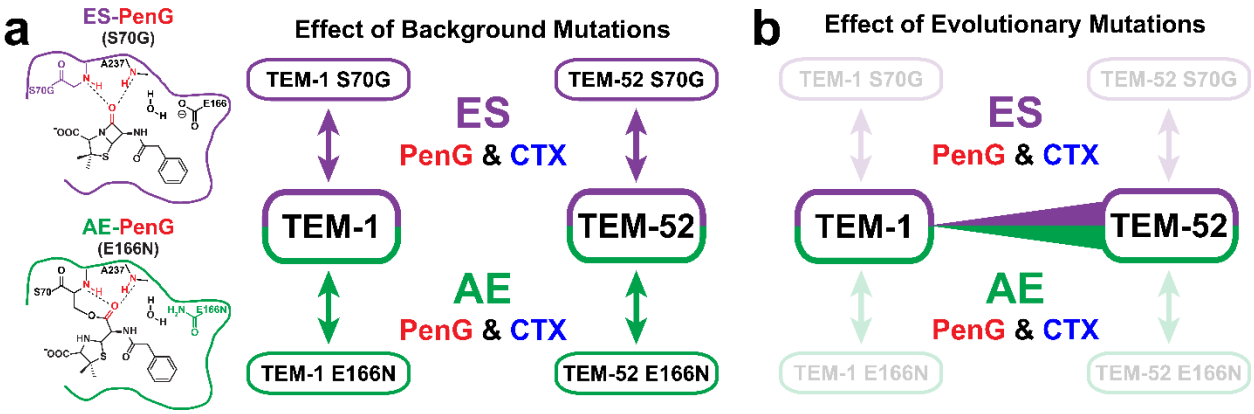

Figure S11. MD Methodology for Structure-Guided Interpretation of Kinetic and VSE Results. *The MD methodology to assess the structural effect of* ***(a)*** *introduction of background mutations S70G and E166N, relative to the WT TEM-1 and TEM-52, on conformational sampling and* ***(b)*** *evolutionary mutations to alter the active site environment in the ES (purple) and AE (green) complexes with PenG (red) and CTX (blue).*

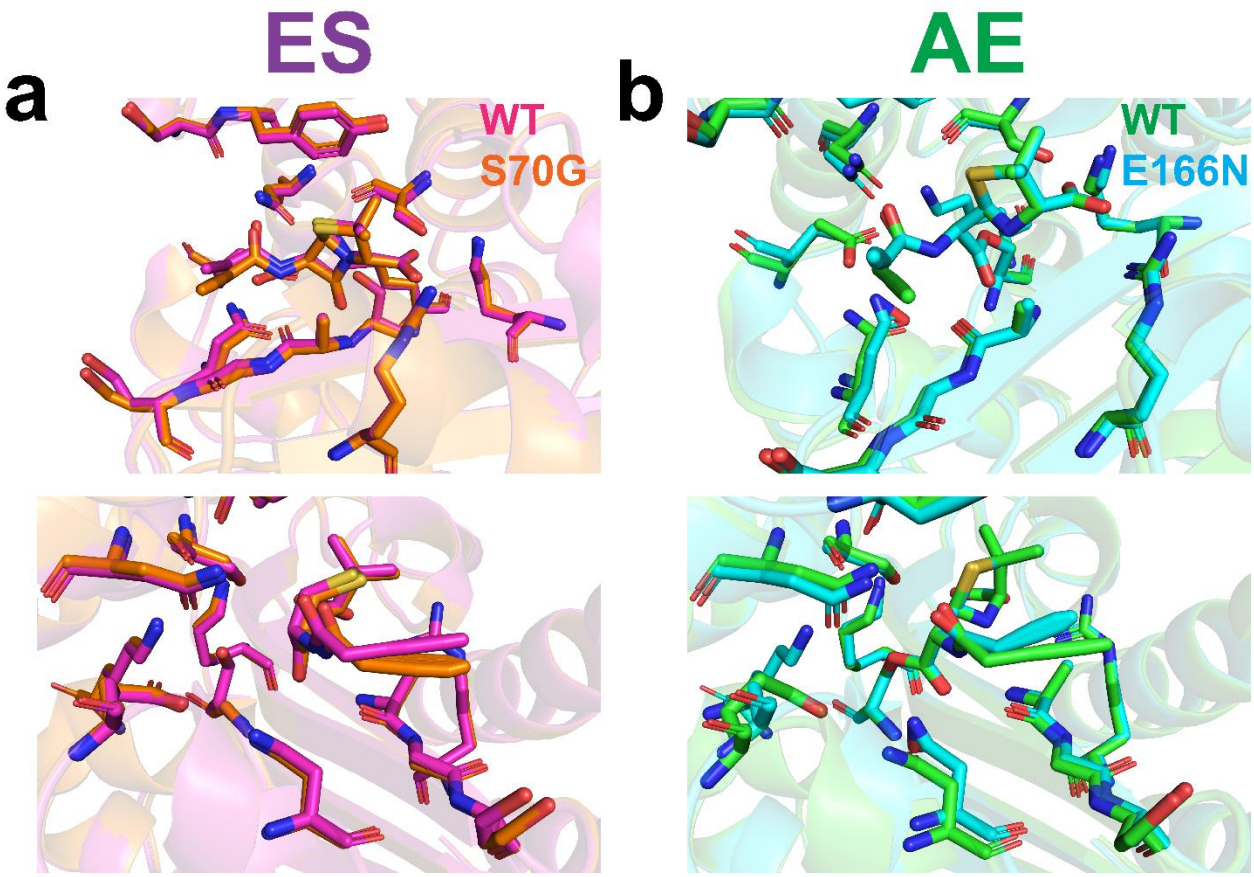

Figure S12. Structural comparison of tight-binding PenG complexes with S70G and E166N background mutants and WT TEM β-lactamases from MD simulations.
Representative structural alignment examples of WT TEM-1 (WT; pink, green) relative to the TEM-1 S70G (orange) and E166N (cyan) shortest oxyanion hole complexes for the ***(a)*** *ES and* ***(b)*** *AE states with PenG. Global alignment between variants (WT vs. S70G and WT vs. E166N) exhibit a RMSD of 0.3 Å for the average structures of those observed with the shortest distances to the S70 andA237 backbone amide N-H.*

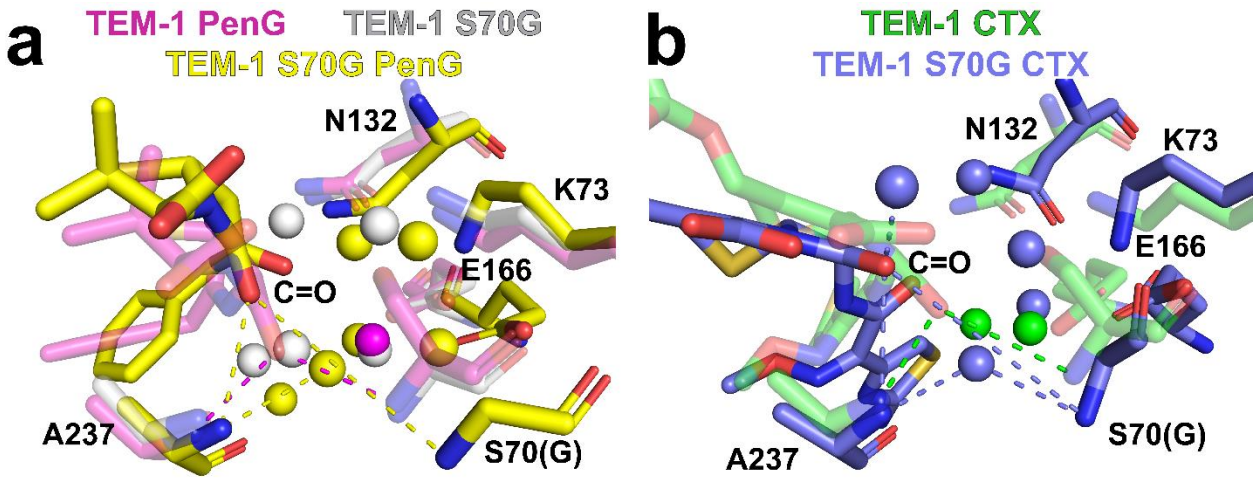

Figure S13. Structural comparison of weak-binding PenG complexes with S70G background mutations and WT TEM β-lactamases from MD simulations. *Representative structural alignment examples of the strong- (WT; pink, green) and weak-binding TEM-1 (S70G; yellow, purple) complexes with* ***(a)*** *PenG (pink, yellow) and* ***(b)*** *CTX (green, purple) relative to the apo crystal structure of TEM-1 S70G (white; PDBID: 1ZG6). Alignments are made on the entire protein structure.*

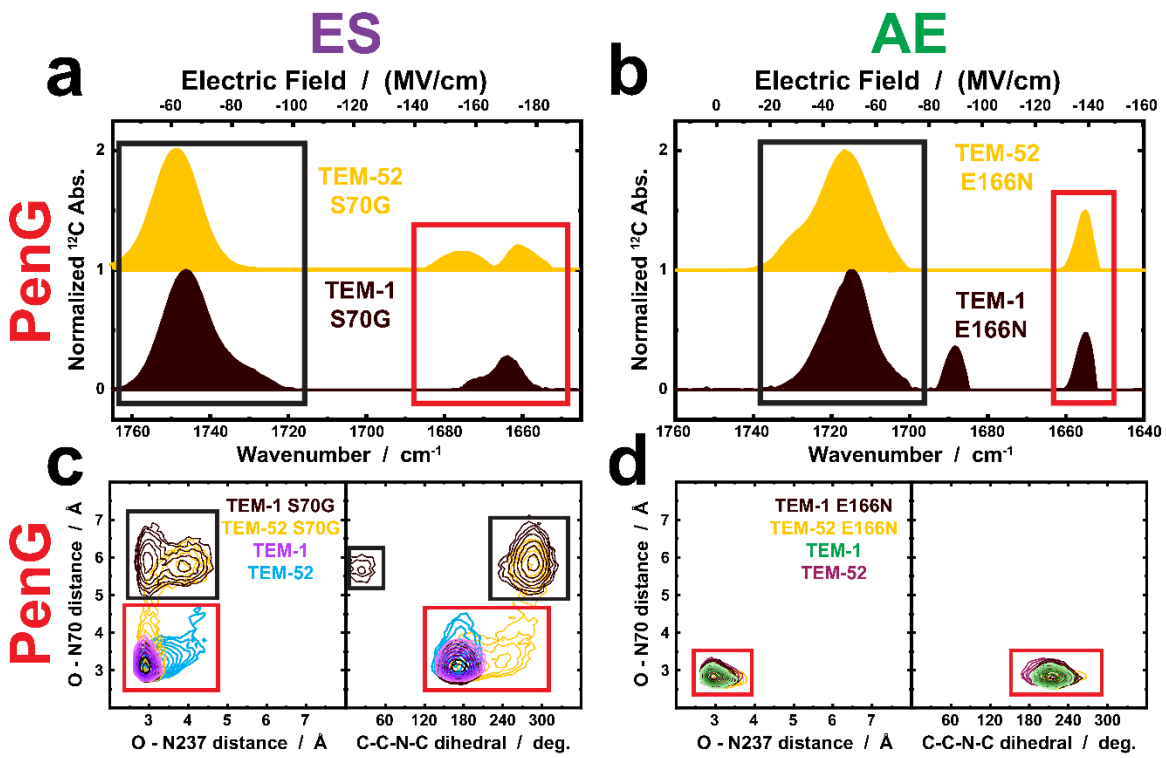

Figure S14. Structure-guided approach to inferring catalytically relevant electric fields. *Representative examples of TEM-1 and TEM-52 with PenG for comparison between the IR spectra of* ***(a)*** *S70G and* ***(b)*** *E166N background mutants relative to MD simulations of the* ***(c)*** *ES and* ***(d)*** *AE complexes.* ^{13}*C PenG (negative intensity) signal removed for clarity. MD simulations are depicted with either the oxyanion hole C=O – N distances (see main text) or dihedral angle (C-C-N-C) of the bound PenG substrate. Background mutants are shown consistently for TEM-1 (brown) and TEM-52 (yellow), relative to their WT species in the ES (pink, cyan) and AE (green, maroon) complexes. Black and red boxes indicate presumed assignment of populations between the VSE results and MD simulations.*

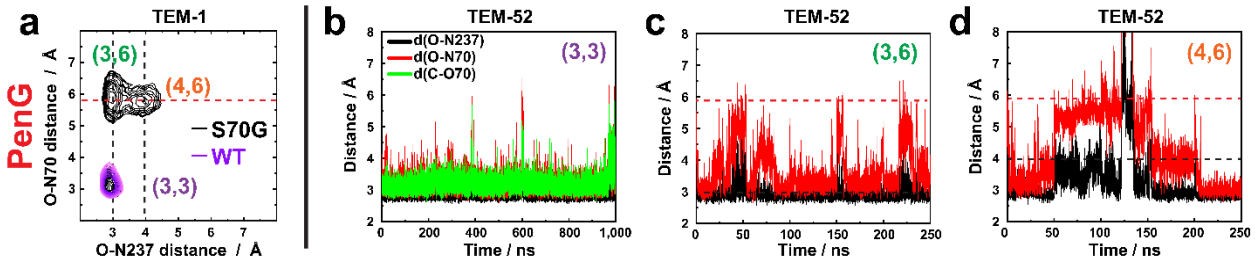

Figure S15. Biased MD simulations of WT TEM β-lactamases as informed from kinetically compromised variants. *A representative* ***(a)*** *overlaid 2D correlation plot of the ES complex of PenG with WT TEM-1 (purple) and S70G TEM-1 to identify additional conformations (cross peaks of black and red dotted lines) relative to those in the shortest oxyanion hole geometry* ***(b)*** *(3, 3). Using these conformations, five 50 ns MD simulations of the WT TEM-52 complex were biased to start from the* ***(c)*** *(3,6) and* ***(d)*** *(4,6) conformations (starting distances indicated with dotted lines), which converge back towards the (3,3) conformation.*

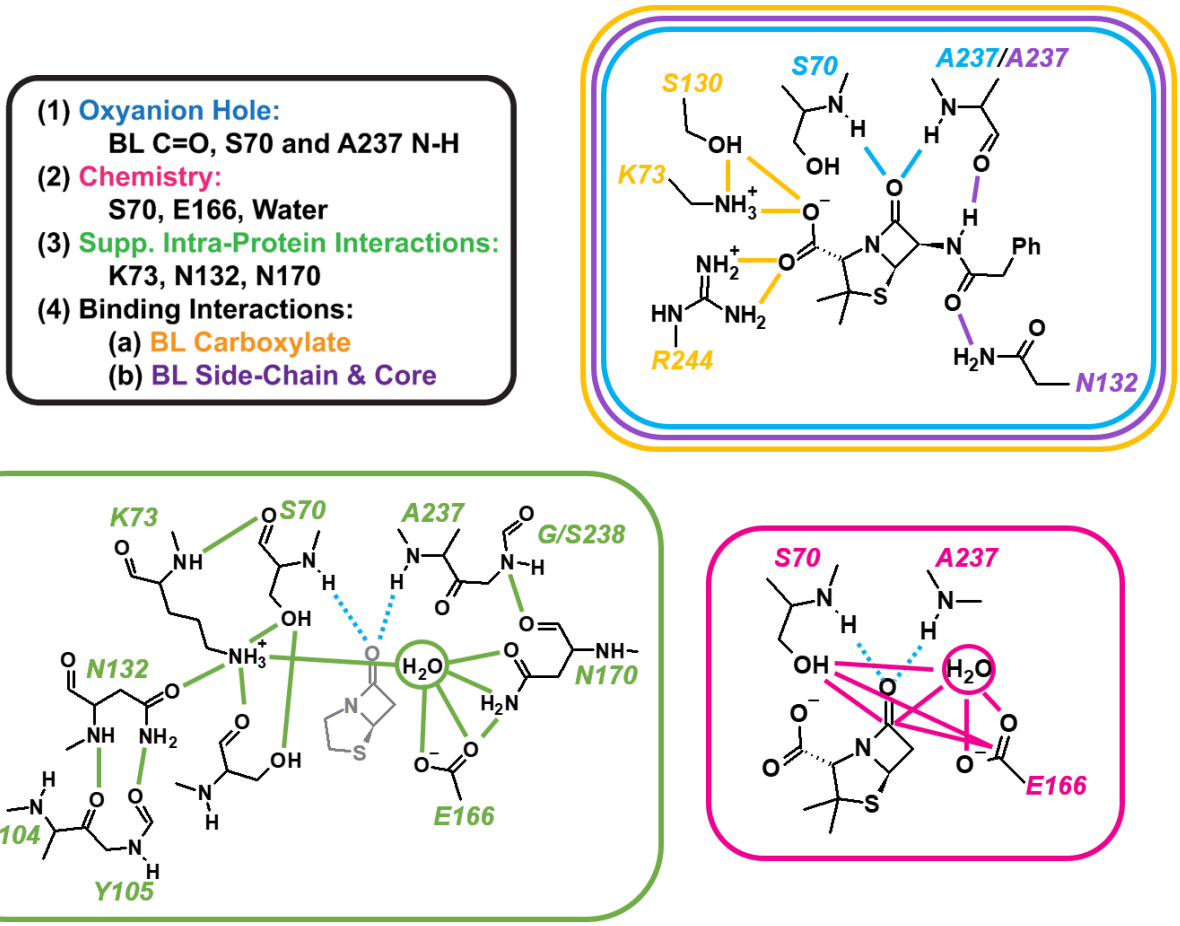

Scheme S3. Atoms and Interactions Considered in the MD Analysis. *Atoms and distances quantified in terms of RMSF and distance changes are indicated by color-coded solid lines and bolded atoms. Colors correspond to the categorization scheme shown in Figure S16b,c, Tables S7-12, and Figure S16-18. The same general scheme is used for the ES and AE complexes of both PenG and CTX. RMSF and distance values were extracted from representative trajectories and average structures (n = 3-5, each 50-200 ns), respectively, from the WT MD simulations of TEM-1 and TEM-52 with PenG and CTX in the ES and AE states. Average values and standard deviations for these complexes are presented below in Tables S7-12; these were used to produce Figure 5-6 and Figure S16-18. Statistically significant changes ($p<0.05$) were determined from a two-tailed student's t-test. Significant values were then utilized in the corresponding averages for each set of discretized regions or interactions in the active site based on proximity or known involvement in catalysis: K73/N132/E166/N170, oxyanion hole, β-lactam carboxylate, or β-lactam (Figure 5,6, Tables S7-12, Figures S16-18). Interactions referred to in the H-bond network of K73/N132/E166/N170 correspond to those side chains listed and those within H-bonding distance (≤3.5 Å) such as K73 to S70, the backbone of N170*

to the backbone of E240, among others. Oxyanion hole interactions are those that connect to S70 and the β-lactam C=O primarily via backbone interactions with S70 and A237. The carboxylate interactions refer to those made to the carboxylate functional group of PenG or CTX primarily from S130, K234 and R244, in addition to the atoms of the substrate itself (COO). Interactions to the β-lactam ,(i.e. backbone amide of A237, N132), as well as the penam or cephem core (either bicyclic or acylated rings), or the respective side chains of PenG (phenylacetamido) and CTX (oxyimino/aminothiazolyl-ring).

Table S7. PenG-dependent average changes in active site RMSFs due to evolution.

PenG RMSF (Å)	ES				AE			
	TEM-1 PenG		TEM-52 PenG		TEM-1 PenG		TEM-52 PenG	
Atom [a,b]	Avg.	Std. Dev.	Avg.	Std. Dev.	Avg.	Std. Dev.	Avg.	Std. Dev.
S70bbN	**0.312**	**0.005**	**0.405**	**0.023**	**0.330**	**0.019**	**0.461**	**0.028**
S70bbH	**0.365**	**0.008**	**0.454**	**0.030**	**0.378**	**0.016**	**0.502**	**0.028**
S70O	**0.341**	**0.009**	**0.486**	**0.049**	**0.347**	**0.028**	**0.553**	**0.063**
S70bbO	**0.359**	**0.008**	**0.476**	**0.038**	**0.396**	**0.024**	**0.563**	**0.036**
K73bbN	**0.330**	**0.017**	**0.379**	**0.015**	**0.384**	**0.048**	**0.497**	**0.057**
K73bbH	**0.372**	**0.020**	**0.418**	**0.015**	**0.426**	**0.051**	**0.519**	**0.022**
K73N	**0.355**	**0.005**	**0.438**	**0.031**	**0.583**	**0.063**	**0.878**	**0.117**
X104bbO	**0.537**	**0.023**	**0.659**	**0.048**	**0.537**	**0.055**	**1.434**	**0.234**
Y105bbO	**0.460**	**0.011**	**0.555**	**0.048**	**0.491**	**0.043**	**1.814**	**0.519**
S130O	0.453	0.015	0.573	0.117	**0.494**	**0.100**	**1.078**	**0.131**
S130bbO	**0.400**	**0.009**	**0.488**	**0.052**	**0.457**	**0.049**	**0.970**	**0.149**
N132bbN	**0.322**	**0.011**	**0.407**	**0.039**	**0.334**	**0.037**	**0.667**	**0.089**
N132bbH	**0.392**	**0.011**	**0.465**	**0.031**	**0.408**	**0.031**	**0.713**	**0.055**
N132O	**0.438**	**0.014**	**0.572**	**0.051**	**0.449**	**0.040**	**1.446**	**0.290**
N132N	**0.553**	**0.022**	**0.679**	**0.052**	**0.473**	**0.056**	**1.278**	**0.164**
E166C	**0.442**	**0.029**	**0.687**	**0.127**	**0.477**	**0.028**	**0.803**	**0.135**
E166O1	**0.561**	**0.090**	**0.985**	**0.239**	**0.968**	**0.250**	**1.321**	**0.159**
E166O2	**0.587**	**0.101**	**0.991**	**0.232**	**0.969**	**0.261**	**1.358**	**0.122**
N170O	**0.517**	**0.040**	**1.019**	**0.379**	**0.662**	**0.231**	**1.296**	**0.533**
N170N	0.535	0.031	0.848	0.187	**0.688**	**0.247**	**1.203**	**0.360**
N170bbO	**0.510**	**0.027**	**1.082**	**0.445**	**0.580**	**0.074**	**1.049**	**0.355**
K234N	0.688	0.137	0.840	0.171	0.793	0.161	1.037	0.689
A237bbN	**0.325**	**0.011**	**0.379**	**0.029**	**0.333**	**0.023**	**0.509**	**0.054**
A237bbH	**0.373**	**0.009**	**0.432**	**0.029**	**0.394**	**0.023**	**0.576**	**0.063**
A237bbO	**0.391**	**0.010**	**0.535**	**0.042**	**0.403**	**0.025**	**0.634**	**0.108**
X238bbN	**0.362**	**0.009**	**0.442**	**0.028**	**0.382**	**0.027**	**0.588**	**0.087**
X238bbH	**0.418**	**0.009**	**0.473**	**0.035**	**0.432**	**0.023**	**0.592**	**0.064**
X238bbC	**0.409**	**0.010**	**0.479**	**0.026**	**0.420**	**0.028**	**0.645**	**0.135**
E240bbN	**0.416**	**0.013**	**0.521**	**0.043**	**0.428**	**0.034**	**0.718**	**0.190**
E240bbH	**0.457**	**0.011**	**0.571**	**0.062**	**0.470**	**0.028**	**0.776**	**0.217**
R244N1	0.411	0.005	0.436	0.032	**0.428**	**0.038**	**1.316**	**0.639**
R244N2	0.461	0.008	0.483	0.034	**0.481**	**0.052**	**1.281**	**0.524**
Water	**0.596**	**0.081**	**1.182**	**0.326**	**0.884**	**0.476**	**19.986**	**5.504**
BL_C	0.318	0.114	0.349	0.077	**0.330**	**0.030**	**0.530**	**0.065**
BL_O	0.372	0.201	0.378	0.145	**0.346**	**0.028**	**0.515**	**0.052**
PNM_C	0.351	0.030	0.352	0.045	**0.452**	**0.064**	**1.153**	**0.317**
PNM_C1	0.362	0.042	0.399	0.030	**0.419**	**0.102**	**1.201**	**0.436**
PNM_C2	0.340	0.054	0.397	0.040	**0.353**	**0.035**	**0.687**	**0.155**

PNM_S	0.427	0.109	0.416	0.066	**0.492**	**0.046**	**1.155**	**0.334**
PNM_N	0.323	0.051	0.363	0.035	**0.390**	**0.066**	**1.040**	**0.356**
PNM_C3	0.320	0.085	0.394	0.063	**0.348**	**0.038**	**0.612**	**0.108**
Amide_N	0.409	0.166	0.423	0.067	**0.384**	**0.044**	**0.647**	**0.104**
Amide_H	0.502	0.240	0.461	0.107	**0.434**	**0.040**	**0.646**	**0.092**
Amide_C	0.448	0.184	0.463	0.103	**0.448**	**0.055**	**0.779**	**0.137**
Amide_O	0.543	0.192	0.565	0.118	**0.482**	**0.059**	**0.919**	**0.148**
Phenyl_C6	0.538	0.322	0.547	0.165	**0.637**	**0.060**	**0.882**	**0.167**
Phenyl_C7	0.568	0.294	0.675	0.239	**0.824**	**0.117**	**1.110**	**0.207**
Phenyl_C8	0.986	0.568	1.079	0.301	1.561	0.110	1.769	0.214
Phenyl_C9	0.711	0.301	1.021	0.373	1.829	0.222	2.161	0.413
Phenyl_C10	1.120	0.575	1.411	0.408	1.582	0.354	2.068	0.589
Phenyl_C11	0.833	0.299	1.313	0.454	1.841	0.245	2.188	0.409
Phenyl_C12	0.890	0.310	1.393	0.413	1.567	0.128	1.799	0.210
COO_C	0.383	0.043	0.348	0.049	**0.465**	**0.181**	**1.539**	**0.688**
COO_O1	0.405	0.034	0.351	0.062	**0.541**	**0.250**	**1.896**	**0.853**
COO_O2	0.475	0.077	0.456	0.074	**0.574**	**0.273**	**1.911**	**0.873**

[a] *Rows are colored according to their interaction groupings.*

[b] *Bold rows indicate those with significant change altered ($p<0.05$ in two-tailed t-test) due to evolution (TEM-52 – TEM-1).*

Abbreviations: BL= β-lactam substrate atom; bb = backbone atom; Amide = substrate amide side-chain atoms; COO = substrate carboxylate side-chain atoms; PNM = atoms of PenG corresponding to the penam core; SC = substrate phenyl side-chain, respectively. See Scheme S3.

Table S8. CTX-dependent average changes in active site RMSFs due to evolution.

CTX RMSF (Å)	ES				AE			
	TEM-1 CTX		TEM-52 CTX		TEM-1 CTX		TEM-52 CTX	
Atom [a,b]	Avg.	Std. Dev.	Avg.	Std. Dev.	Avg.	Std. Dev.	Avg.	Std. Dev.
S70bbN	0.339	0.026	0.353	0.013	0.420	0.056	0.477	0.063
S70bbH	0.422	0.047	0.424	0.016	0.469	0.061	0.517	0.064
S70O	0.386	0.033	0.432	0.047	0.510	0.144	0.530	0.064
S70bbO	**0.380**	**0.023**	**0.446**	**0.030**	0.513	0.085	0.570	0.062
K73bbN	0.346	0.021	0.363	0.019	0.430	0.047	0.574	0.151
K73bbH	**0.392**	**0.020**	**0.421**	**0.017**	0.475	0.047	0.542	0.062
K73N	**0.358**	**0.013**	**0.430**	**0.045**	**0.565**	**0.073**	**0.859**	**0.224**
X104bbO	**0.458**	**0.016**	**0.508**	**0.028**	0.699	0.058	0.895	0.206
Y105bbO	**0.417**	**0.011**	**0.487**	**0.031**	0.674	0.103	0.889	0.197
S130O	0.381	0.010	0.430	0.054	0.719	0.061	0.811	0.339
S130bbO	**0.366**	**0.010**	**0.412**	**0.025**	0.573	0.097	0.662	0.257
N132bbN	**0.301**	**0.007**	**0.335**	**0.022**	0.439	0.041	0.522	0.133
N132bbH	**0.370**	**0.011**	**0.408**	**0.020**	0.512	0.044	0.597	0.126
N132O	**0.401**	**0.018**	**0.435**	**0.026**	0.664	0.098	1.006	0.377
N132N	**0.409**	**0.017**	**0.467**	**0.026**	0.732	0.067	0.910	0.211
E166C	0.448	0.058	0.442	0.045	0.698	0.124	0.789	0.109
E166O1	0.571	0.181	0.747	0.269	1.183	0.299	1.272	0.118
E166O2	0.551	0.215	0.772	0.260	1.054	0.171	1.297	0.189
N170O	0.766	0.245	0.860	0.237	1.236	0.291	1.001	0.346
N170N	0.643	0.276	0.923	0.284	0.884	0.226	0.930	0.256
N170bbO	0.752	0.184	0.795	0.215	1.170	0.319	1.205	0.488
K234N	0.525	0.026	0.503	0.051	**1.048**	**0.159**	**0.700**	**0.130**
A237bbN	**0.331**	**0.021**	**0.361**	**0.020**	**0.402**	**0.019**	**0.484**	**0.058**
A237bbH	0.385	0.018	0.414	0.025	**0.457**	**0.016**	**0.541**	**0.059**
A237bbO	**0.403**	**0.025**	**0.465**	**0.028**	**0.501**	**0.065**	**0.625**	**0.066**
X238bbN	0.379	0.023	0.380	0.012	0.471	0.049	0.527	0.067
X238bbH	0.431	0.024	0.419	0.012	0.529	0.039	0.518	0.069
X238bbC	0.405	0.022	0.383	0.019	0.525	0.054	0.613	0.107
E240bbN	0.417	0.021	0.439	0.025	**0.526**	**0.057**	**0.715**	**0.123**
E240bbH	0.479	0.022	0.506	0.042	**0.581**	**0.058**	**0.813**	**0.139**
R244N1	0.595	0.421	0.513	0.043	0.507	0.023	1.323	0.851
R244N2	0.618	0.384	0.614	0.075	**0.587**	**0.017**	**1.467**	**0.770**
Water	**0.674**	**0.156**	**1.075**	**0.348**	1.510	0.273	1.847	0.348
BL_C	0.410	0.035	0.462	0.082	0.464	0.084	0.536	0.082
BL_O	0.421	0.038	0.465	0.071	0.453	0.082	0.542	0.094
CPM_C	0.440	0.027	0.540	0.114	0.573	0.153	0.604	0.092
CPM_C1	**0.529**	**0.026**	**0.651**	**0.107**	0.707	0.254	0.738	0.154
CPM_C2	0.470	0.035	0.558	0.097	0.788	0.283	0.825	0.203

CPM_S	**0.522**	**0.030**	**0.610**	**0.082**	1.028	0.330	1.099	0.439
CPM_N	0.431	0.032	0.507	0.097	1.327	0.392	1.372	0.378
CPM_C3	0.441	0.037	0.509	0.087	1.134	0.413	1.183	0.259
CPM_C7	**0.592**	**0.032**	**0.718**	**0.095**	0.852	0.395	0.897	0.185
Amide_N	0.439	0.037	0.496	0.079	0.664	0.109	0.699	0.117
Amide_H	0.499	0.051	0.541	0.068	0.816	0.089	0.846	0.136
Amide_C	0.422	0.024	0.472	0.082	0.801	0.169	0.816	0.132
Amide_O	0.487	0.022	0.533	0.085	1.024	0.237	0.951	0.160
SC_C11	0.460	0.029	0.480	0.072	0.918	0.163	0.996	0.148
SC_N2	0.503	0.040	0.488	0.064	0.927	0.110	1.054	0.144
SC_O6	**0.675**	**0.046**	**0.596**	**0.049**	1.059	0.106	1.209	0.112
SC_C12	**0.781**	**0.066**	**0.630**	**0.045**	1.297	0.175	1.321	0.162
SC_C13	0.506	0.034	0.511	0.074	1.233	0.252	1.254	0.236
SC_C14	0.575	0.043	0.585	0.073	1.498	0.330	1.528	0.272
SC_C15	0.763	0.059	0.699	0.073	1.546	0.290	1.636	0.246
SC_S1	0.684	0.065	0.666	0.080	1.965	0.409	1.859	0.413
SC_N3	0.723	0.061	0.657	0.067	1.855	0.361	1.838	0.313
SC_N4	**1.048**	**0.096**	**0.923**	**0.071**	2.239	0.417	2.307	0.382
COO_C	0.428	0.023	0.533	0.135	0.900	0.473	1.075	0.214
COO_O1	0.479	0.042	0.617	0.150	1.062	0.560	1.339	0.300
COO_O2	0.510	0.179	0.538	0.138	0.957	0.430	1.186	0.267

[a] *Rows are colored according to their interaction groupings.*

[b] *Bold rows indicate those with significant change altered ($p<0.05$ in two-tailed t-test) due to evolution (TEM-52 – TEM-1).*

Abbreviations: BL= β-lactam substrate atom; bb = backbone atom; Amide = substrate amide side-chain atoms; COO = substrate carboxylate side-chain atoms; CPM = atoms of CTX corresponding to the cephem core; SC = substrate oxyimino/aminothiazolyl-ring, respectively. See Scheme S3.

Table S9. Collective RMSF changes in the evolution of TEM-1 to TEM-52 for PenG and CTX.

	TEM-1 RMSF (Å)			TEM-52 RMSF (Å)		
State & Substrate	Interaction[a]	Median	68% CI	Interaction[a]	Median	68% CI
ES PenG	**Total**	**0.41**	**[0.33, 0.58]**	**Total**	**0.48**	**[0.38, 0.87]**
	Oxyanion	0.34	[0.31, 0.37]	**Oxyanion**	0.41	[0.37, 0.46]
	Chemistry	0.49	[0.35, 0.64]	**Chemistry**	0.75	[0.49, 1.10]
	Supporting	0.41	[0.35, 0.52]	**Supporting**	0.51	[0.41, 0.73]
	COO			**COO**		
	BL	0.44	[0.38, 0.56]	**BL**	0.60	[0.51, 0.70]
ES CTX	**Total**	**0.44**	**[0.37, 0.66]**	**Total**	**0.49**	**[0.39, 0.68]**
	Oxyanion	0.36	[0.32, 0.39]	**Oxyanion**	0.38	[0.35, 0.43]
	Chemistry	0.44	[0.36, 0.75]	**Chemistry**	0.51	[0.40, 1.24]
	Supporting	0.38	[0.35, 0.42]	**Supporting**	0.43	[0.38, 0.49]
	COO	0.42	[0.38, 0.48]	**COO**	0.50	[0.39, 0.86]
	BL	0.49	[0.41, 0.73]	**BL**	0.58	[0.46, 0.73]
AE PenG	**Total**	**0.45**	**[0.35, 0.83]**	**Total**	**0.88**	**[0.53, 1.68]**
	Oxyanion	0.35	[0.32, 0.39]	**Oxyanion**	0.51	[0.45, 0.58]
	Chemistry	0.65	[0.36, 1.15]	**Chemistry**	1.23	[0.59, 1.62]
	Supporting	0.46	[0.38, 0.64]	**Supporting**	0.87	[0.54, 1.44]
	COO	0.47	[0.37, 0.65]	**COO**	1.38	[0.90, 2.29]
	BL	0.44	[0.35, 0.56]	**BL**	0.84	[0.60, 1.26]
AE CTX	**Total**	**0.70**	**[0.46, 1.31]**	**Total**	**0.85**	**[0.53, 1.42]**
	Oxyanion	0.43	[0.39, 0.46]	**Oxyanion**	0.51	[0.45, 0.58]
	Chemistry			**Chemistry**		
	Supporting	0.56	[0.49, 0.62]	**Supporting**	0.78	[0.63, 0.96]
	COO	0.63	[0.58, 1.12]	**COO**	0.82	[0.60, 1.89]
	BL	0.50	[0.43, 0.56]	**BL**	0.63	[0.56, 0.69]

[a] *Interaction groups and colors according to Scheme S3. COO and BL refer to binding interactions to the substrate carboxylate group and β-lactam core/amide side-chain, respectively.*

Table S10. PenG-dependent average changes in active site distances due to evolution.

PenG Distance (Å)	ES				AE			
	TEM-1 PenG		TEM-52 PenG		TEM-1 PenG		TEM-52 PenG	
Distance Pair [a,b]	Avg.	Std. Dev.	Avg.	Std. Dev.	Avg.	Std. Dev.	Avg.	Std. Dev.
S70bbN – O	3.100	0.100	3.240	0.100	2.740	0.100	2.800	0.100
A237bbN – O	2.800	0.100	2.800	0.100	2.900	0.100	2.900	0.100
S70O – BL_O	3.100	0.100	3.120	0.100				
S70O – BL_C	3.100	0.100	3.160	0.100				
E166C – BL_C	6.660	0.100	6.800	0.100	6.400	0.100	6.780	0.458
Water1 – BL_C	**3.640**	**0.100**	**3.460**	**0.102**	**3.340**	**0.174**	**2.960**	**0.206**
Water1 – BL_O	3.400	0.100	3.240	0.120	3.820	0.117	3.740	0.150
Water1 – E166C	**3.400**	**0.100**	**3.780**	**0.117**	**3.360**	**0.120**	**4.040**	**0.609**
Water1 – S70O	2.700	0.100	2.680	0.194	**3.140**	**0.224**	**2.640**	**0.356**
S70O – E166C	5.200	0.100	5.200	0.167	6.120	0.100	6.180	0.453
S130O – K234N	2.740	0.100	2.880	0.117	**3.000**	**0.253**	**5.660**	**2.207**
S130O – COO_C	3.700	0.100	3.780	0.160	4.040	0.480	5.300	1.134
K234N – COO_C	5.000	0.253	5.020	0.279	**5.620**	**0.640**	**7.500**	**1.003**
R244N1 – COO_C	3.900	0.100	3.900	0.100	2.800	0.100	2.850	0.100
R244N2 – COO_C	5.100	0.100	5.100	0.100	**3.640**	**0.224**	**3.100**	**0.200**
N132N – AmideO	**3.140**	**0.102**	**3.860**	**0.372**	**2.980**	**0.100**	**4.600**	**0.982**
A237bbO – AmideN	3.080	0.100	3.160	0.100	3.000	0.100	2.920	0.100
S70O – S130O	4.000	0.100	4.000	0.110	**3.960**	**0.100**	**5.560**	**0.736**
K73N – N132O	2.800	0.100	2.800	0.100	**2.780**	**0.100**	**5.220**	**1.130**
K73N – S130bbO	2.900	0.100	2.900	0.100	**3.040**	**0.100**	**4.080**	**0.741**
K73N – S70O	2.980	0.100	3.000	0.100	**3.800**	**0.100**	**4.520**	**0.504**
K73N – E166C	3.800	0.100	3.800	0.110	3.760	0.100	3.780	0.538
X104bbO – N132N	2.900	0.100	2.900	0.100	**2.900**	**0.100**	**5.200**	**0.537**
Y105bbO – N132bbN	3.200	0.100	3.200	0.100	**3.240**	**0.100**	**4.980**	**1.139**
E166C – N170N	3.820	0.100	4.080	0.248	**4.060**	**0.100**	**5.300**	**0.965**
N170bbO – E240bbN	**3.000**	**0.100**	**3.340**	**0.224**	3.040	0.100	4.380	1.411
Water1 – K73N	**3.720**	**0.100**	**4.040**	**0.136**	3.260	0.102	3.940	0.734
Water1 – N170N	**3.680**	**0.100**	**4.040**	**0.150**	3.520	0.100	3.780	0.515
Water1 – N170O	**2.800**	**0.100**	**3.160**	**0.280**	2.980	0.100	3.500	0.718

[a] *Abbreviations: BL= β-lactam substrate atom; bb = backbone atom; Amide = substrate amide side-chain atoms; COO = substrate carboxylate side-chain atoms. See Figure 5 and Scheme S3 for color coding of interactions.*

[b] *Bold rows entries indicate those that are significantly altered between TEM-1 and TEM-52 based on a two-tailed t-test ($p<0.05$ in two-tailed t-test) and represented in Figure 5-6.*

Table S11. CTX-dependent average changes in active site distances due to evolution.

CTX Distance (Å)	ES				AE			
	TEM-1 CTX		TEM-52 CTX		TEM-1 CTX		TEM-52 CTX	
Distance Pair [a,b]	Avg.	Std. Dev.	Avg.	Std. Dev.	Avg.	Std. Dev.	Avg.	Std. Dev.
S70bbN – O	3.445	0.223	3.220	0.117	2.820	0.100	2.860	0.100
A237bbN – O	2.873	0.045	2.900	0.100	2.880	0.100	2.900	0.100
S70O – BL_O	3.100	0.100	3.080	0.040				
S70O – BL_C	3.445	0.078	3.380	0.040				
E166C – BL_C	**7.082**	**0.159**	**7.500**	**0.100**	6.700	0.167	7.040	0.472
Water1 – BL_C	3.900	0.230	3.800	0.167	3.180	0.117	3.140	0.273
Water1 – BL_O	3.545	0.188	3.500	0.167	3.840	0.102	3.820	0.542
Water1 – S70O	**2.691**	**0.100**	**2.940**	**0.162**	3.060	0.250	3.020	0.223
Water1 – E166C	**3.500**	**0.141**	**3.780**	**0.133**	3.700	0.210	4.280	0.700
S70O – E166C	**5.200**	**0.085**	**5.880**	**0.040**	6.300	0.155	6.500	0.533
S130O – K234N	2.791	0.029	2.800	0.100	4.180	1.356	3.300	0.100
S130O – COO_C	**3.482**	**0.039**	**3.640**	**0.049**	**5.800**	**0.253**	**4.900**	**0.100**
K234N – COO_C	4.982	0.057	5.000	0.110	**7.980**	**0.618**	**5.640**	**1.031**
R244N1 – COO_C	4.236	1.113	3.920	0.075	3.400	0.179	6.160	2.968
R244N2 – COO_C	5.273	0.377	5.240	0.080	4.060	0.174	6.220	2.500
N132N – AmideO	2.809	0.029	2.820	0.040	**3.760**	**0.615**	**5.020**	**0.926**
A237bbO – AmideN	3.073	0.062	3.040	0.049	3.180	0.040	3.120	0.100
S70O – S130O	**3.645**	**0.078**	**3.560**	**0.049**	4.100	0.329	4.280	0.952
K73N – N132O	**2.855**	**0.050**	**2.800**	**0.100**	**2.840**	**0.049**	**3.680**	**0.806**
K73N – S130bbO	2.855	0.050	2.900	0.100	**2.920**	**0.075**	**3.660**	**0.647**
K73N – S70O	2.955	0.050	3.000	0.100	4.360	0.287	4.520	0.371
K73N – E166C	**3.827**	**0.045**	**4.260**	**0.049**	**3.800**	**0.063**	**3.540**	**0.100**
X104bbO – N132N	2.900	0.100	2.900	0.100	2.920	0.098	3.320	0.445
Y105bbO – N132bbN	3.109	0.029	3.100	0.100	3.160	0.100	3.200	0.100
E166C – N170N	**4.691**	**0.760**	**5.620**	**0.098**	**6.240**	**1.174**	**4.680**	**0.100**
N170bbO – E240bbN	**3.309**	**0.320**	**5.060**	**0.136**	**4.120**	**0.584**	**4.940**	**0.273**
Water1 – K73N	**3.709**	**0.116**	**3.500**	**0.210**	3.700	0.494	3.920	0.991
Water1 – N170N	**3.400**	**0.113**	**4.640**	**0.174**	**4.240**	**0.393**	**3.660**	**0.314**
Water1 – N170O	**3.836**	**0.971**	**6.360**	**0.301**	**5.580**	**1.306**	**3.040**	**0.287**

[a] *Abbreviations: BL= β-lactam substrate atom; bb = backbone atom; Amide = substrate amide side-chain atoms; COO = substrate carboxylate side-chain atoms. See Figure 5 and Scheme S3 for color coding of interactions.*

[b] *Bold rows entries indicate those that are significantly altered between TEM-1 and TEM-52 based on a two-tailed t-test ($p<0.05$ in two-tailed t-test) and represented in Figure 5-6.*

Table S12. Collective distance changes in the evolution of TEM-1 to TEM-52 for PenG and CTX.

	TEM-1 Distances (Å)			TEM-52 Distance (Å)		
State & Substrate	Interaction[a]	Median	68% CI	Interaction[a]	Median	68% CI
ES PenG	Total	3.26	[2.84, 4.01]	Total	3.39	[2.90, 4.23]
	Oxyanion			Oxyanion		
	Chemistry	3.52	[3.35, 3.69]	Chemistry	3.61	[3.41, 3.83]
	Supporting	3.34	[2.82, 3.74]	Supporting	3.76	[3.13, 4.11]
	COO			COO		
	BL	3.14	[3.04, 3.24]	BL	3.86	[3.49, 4.23]
ES CTX	Total	3.44	[2.84, 4.89]	Total	3.56	[2.90, 5.22]
	Oxyanion			Oxyanion		
	Chemistry	4.33	[2.72, 7.03]	Chemistry	4.39	[2.99, 7.46]
	Supporting	3.63	[2.94, 4.00]	Supporting	4.34	[3.37, 5.67]
	COO	3.48	[3.44, 3.52]	COO	3.64	[3.59, 3.69]
	BL			BL		
AE PenG	Total	3.28	[2.87, 4.05]	Total	4.06	[2.88, 6.05]
	Oxyanion			Oxyanion		
	Chemistry	3.3	[3.08, 3.47]	Chemistry	3.01	[2.58, 4.08]
	Supporting	3.25	[2.85, 4.00]	Supporting	4.96	[4.03, 5.94]
	COO	3.64	[3.00, 5.66]	COO	5.55	[3.03, 7.96]
	BL	2.98	[2.88, 3.08]	BL	4.6	[3.62, 5.58]
AE CTX	Total	3.78	[2.93, 5.97]	Total	3.77	[3.00, 5.50]
	Oxyanion			Oxyanion		
	Chemistry			Chemistry		
	Supporting	3.87	[2.88, 5.75]	Supporting	3.69	[3.13, 4.75]
	COO	6.43	[5.68, 8.27]	COO	4.97	[4.78, 6.13]
	BL	3.76	[3.15, 4.37]	BL	5.02	[4.09, 5.94]

[a] *Interaction groups and colors according to Scheme S3. COO and BL refer to binding interactions to the substrate carboxylate group and β-lactam core/amide side-chain, respectively.*

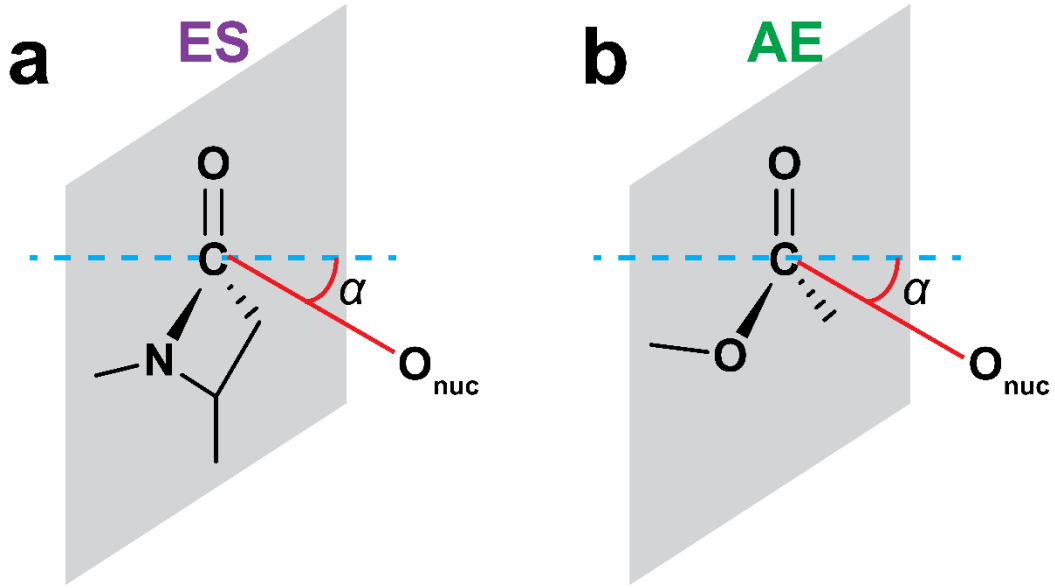

Scheme S4. Angle of nucleophilic attack in the ES and AE complexes. *The angle of nucleophilic attack (α) for the* ***(a)*** *ES and* ***(b)*** *AE complexes are defined as normal to the plane of the four-atoms defining the* sp^2 *hybridized C in the C=O. An angle approaching zero degrees is expected to be indicative of better chemical positioning for nucleophilic addition at the C=O.*

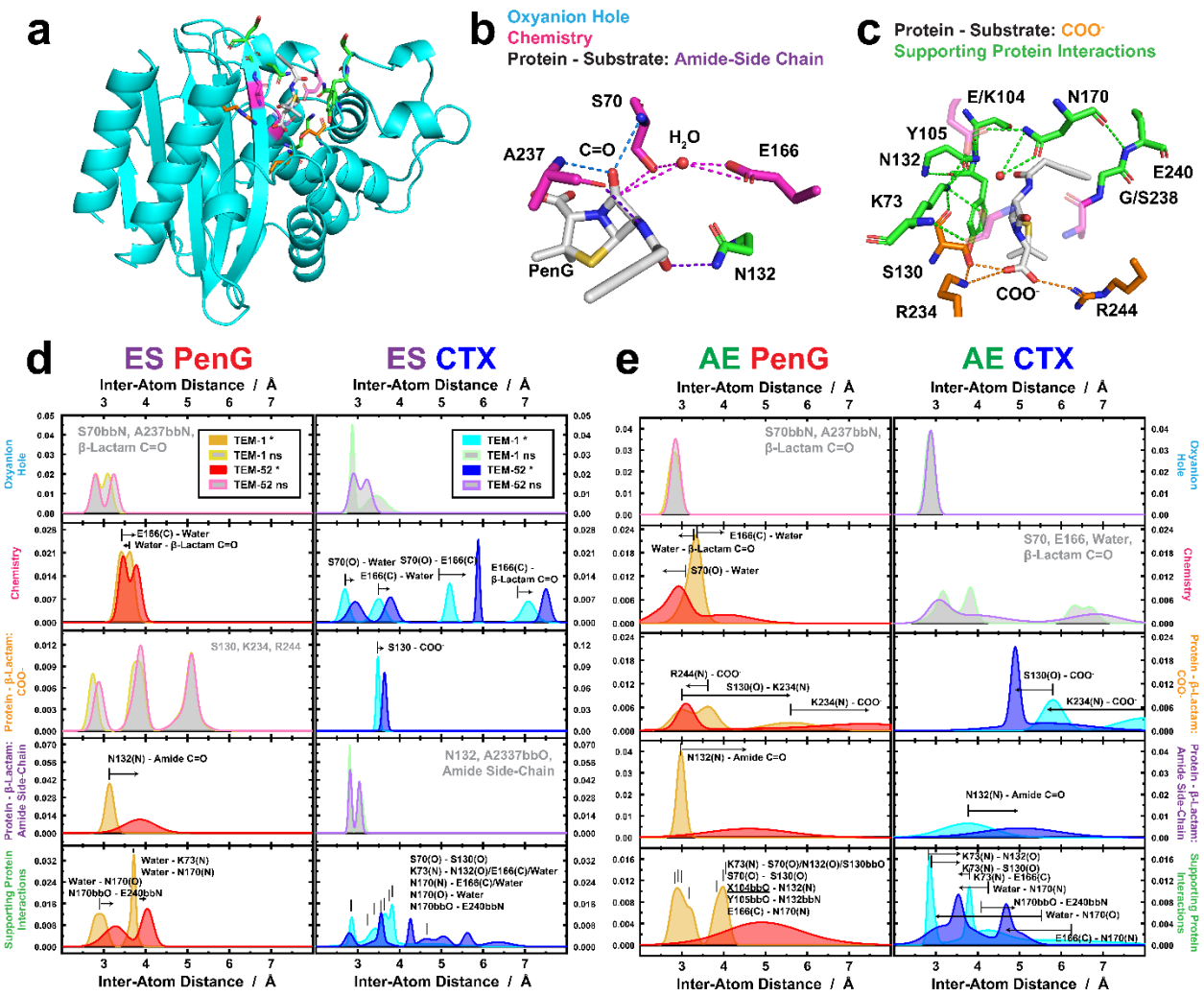

Figure S16. Alternative probability density representation of significant active site distance changes over the course of evolution from TEM-1 to TEM-52 for PenG and CTX. ***(a)*** *Overall structure of the TEM-1 PenG ES complex with active site residues shown according to their broad classifications and role in catalysis.* ***(b,c)*** *Inter-atom interactions are classified according to their role in catalysis for key residues in the active site: oxyanion hole (blue), chemistry (pink), protein-substrate interactions (orange for the substrate COO^- and purple for the amide side-chain), or supporting inter-amino acid interactions that participate in the extended H-bond network for chemical positioning (green). Protons removed for clarity.* ***(d,e)*** *Significant (*) average distances and corresponding heterogeneity of key active site non-covalent interactions shown as a normalized probability distributions for the (b) ES and (c) AE complexes of TEM-1 and TEM-52 with PenG and CTX, respectively. Significant distance changes correspond to $p < 0.05$ in a two-tailed t-test (Scheme S3 and Tables S10-12). Vertical bars represent the average positions observed in TEM-1 for a given complex and arrows denote*

the direction of change in TEM-52. In cases where no significant (ns) changes were observed among a given interaction group, the total probability densities are shown for all interactions and shaded in grey for TEM-1 (green outline) and TEM-52 (purple outline). Averages distances represent comparison across 3-5 average structures each from 50-200 ns of the MD trajectories.

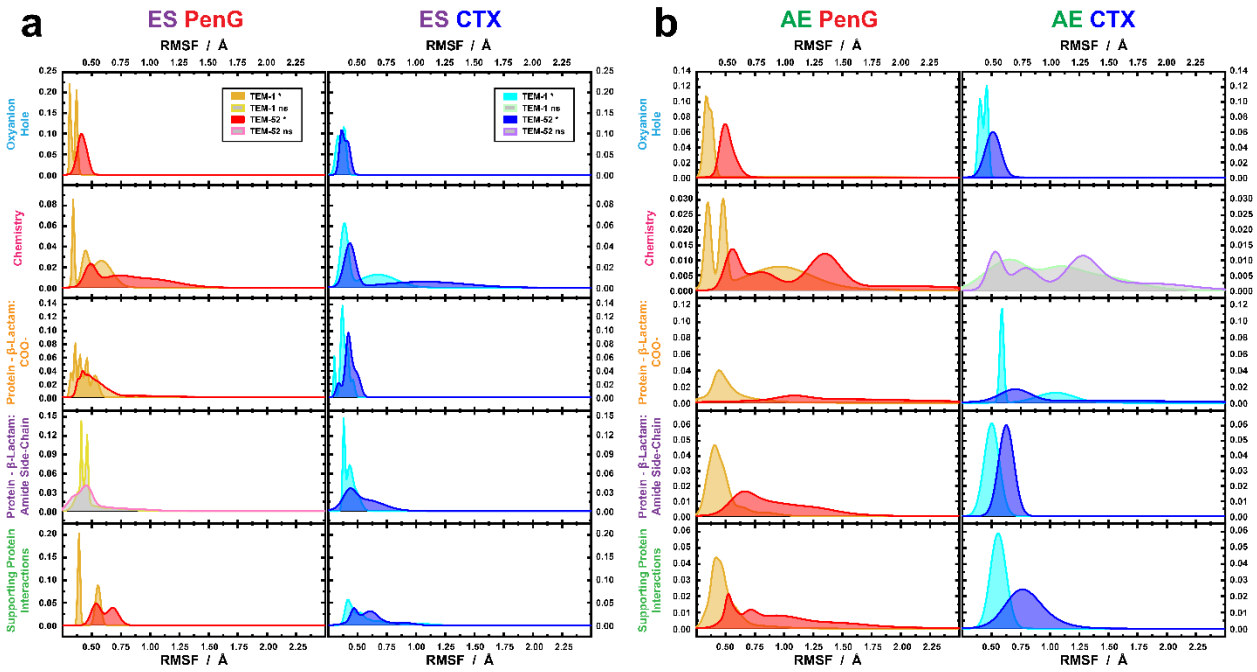

Figure S17. Alternative probability density representation of significant active site RMSF changes over the course of evolution from TEM-1 to TEM-52 for PenG and CTX. (a,b) *Significant (*) average RMSF and corresponding heterogeneity of key active site atoms shown as a normalized probability distributions for the* ***(a)*** *ES and* ***(b)*** *AE complexes of TEM-1 and -52 with PenG (orange, red) and CTX (cyan, blue), respectively. Significant RMSF changes correspond to $p < 0.05$ in a two-tailed t-test (Scheme S3 and Tables S7-9). In cases where no significant (ns) changes were observed among a given interaction group, the total probability densities are shown for all interactions and shaded in grey for TEM-1 (pink outline) and TEM-52 (purple outline). Averages RMSFs and standard deviations represent comparison across 3-5 trajectories of 50-200 ns each from the MD trajectories.*

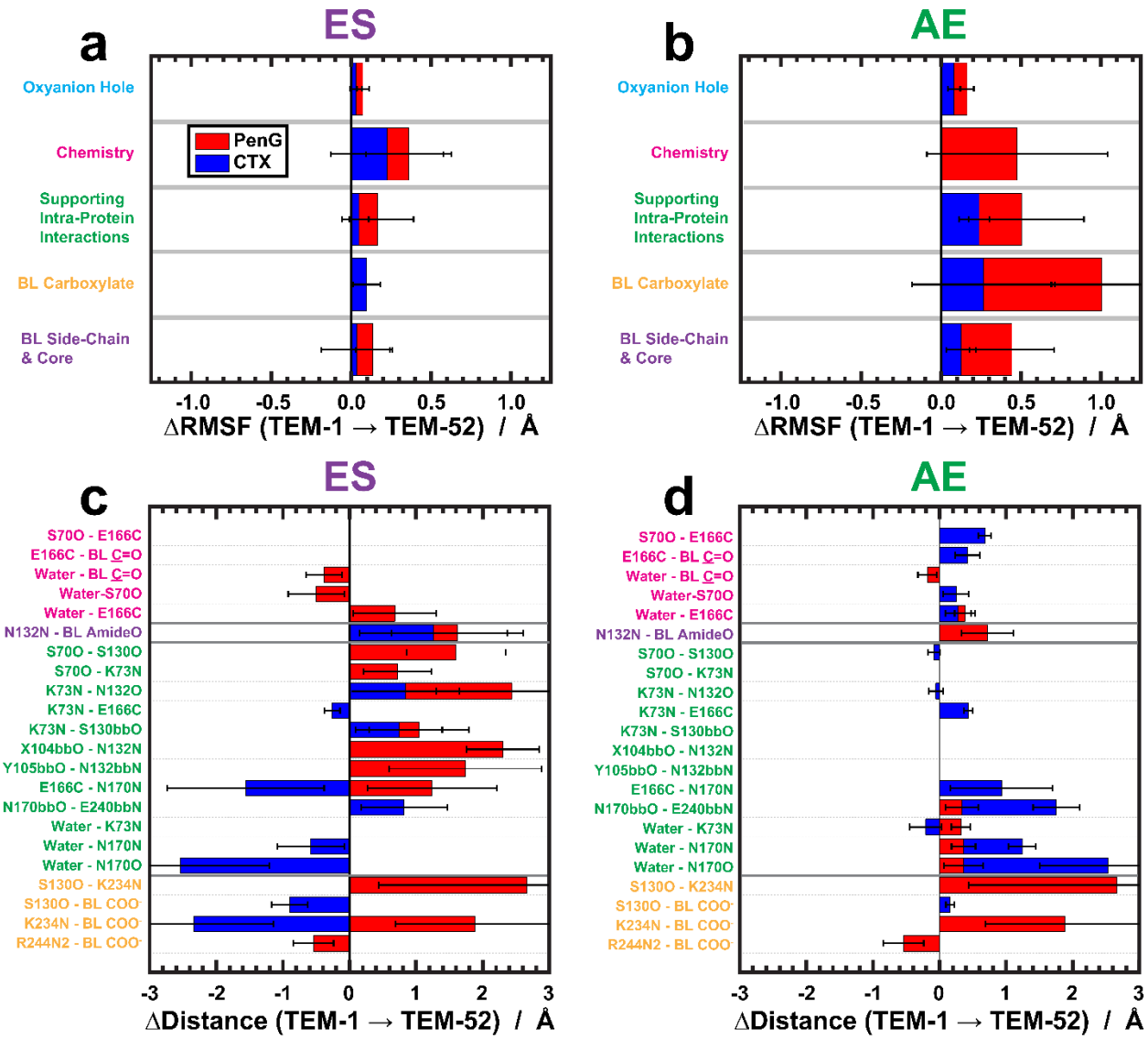

Figure S18. Alternative representation of significant active site RMSF and distances changes over the course of evolution from TEM-1 to TEM-52 for PenG and CTX. (a,b) *Significant average change in RMSF (TEM-52 – TEM-1) and corresponding heterogeneity of key active site atoms for the* ***(a)*** *ES and* ***(b)*** *AE complexes with PenG (red) and CTX (blue), respectively.* ***(c,d)*** *Significant average change in distance (TEM-52 – TEM-1) between key active site atoms for the* ***(c)*** *ES and* ***(d)*** *AE complexes with PenG and CTX. Significant changes correspond to $p < 0.05$ in a two-tailed t-test for the interaction groups according to Scheme S3 (Tables S7-12). Averages RMSFs and standard deviations represent comparison across 3-5 trajectories of 50-200 ns each from the MD trajectories. Standard deviations correspond to*

$\sqrt{\sigma_{TEM1}^2 + \sigma_{TEM52}^2}$. *Abbreviations: BL = substrate β-lactam antibiotic, COO^- = substrate's carboxylate functional group (C-atom), bb = backbone, Amide = substrate's amide side-chain.*

Table S13. Average changes in active site RMSFs between TEM-1 and TEM-52 with PenG and CTX, respectively. (E) and (S) refers to changes occurring on the enzyme or substrate, respectively.

ΔRMSF [(TEM-1 (PenG) – TEM-52 (CTX)]		
Active Site Fluctuations	**ES**	**AE**
Oxyanion Hole (E)	-0.06 ± 0.02	-0.16 ± 0.02
Oxyanion Hole (S)		-0.20 ± 0.01
Chemistry (E)		
Chemistry (S)		
β-Lactam Carboxylate (E)	-0.02 ± 0.15	-0.94 ± 0.04
β-Lactam Carboxylate (S)	-0.18 ± 0.03	-0.67 ± 0.09
β-Lactam Amide Side-Chain (E)	0.01 ± 0.08	-0.33 ± 0.11
β-Lactam Amide Side-Chain (S)		-0.39 ± 0.06
Supporting Protein Interactions		

Standard deviations correspond to the variance across all of the average RMSF changes for a given active site interaction type. See Scheme S3 for interaction groupings and Tables S7-9.

Table S14. Average changes in active site distances between TEM-1 and TEM-52 with PenG and CTX, respectively.

∆dist. [TEM-1 (PenG) – TEM-52 (CTX)] [a]		
Distance Pair	**ES**	**AE**
S70O – [BL-C=O (C)]	-0.28 ± 0.11	
S70O – E166C	-0.68 ± 0.11	
S70 – Water	-0.24 ± 0.19	
E166C – [BL-C=O (C)]	-0.84 ± 0.14	-0.64 ± 0.48
E166C – Water	-0.38 ± 0.17	-0.92 ± 0.71
S130O – K234N		-0.30 ± 0.27
S130O – COO(C)		-0.86 ± 0.49
R244N1 – COO(C)	-0.14 ± 0.13	-3.36 ± 2.97
N132N – [BL-AmideO]	0.32 ± 0.11	-2.04 ± 0.93
S70O – S130O	0.44 ± 0.11	
S70O – K73N		-0.72 ± 0.38
K73N – N132O		-0.90 ± 0.81
K73N – E166C	-0.46 ± 0.11	0.22 ± 0.14
E166C – N170N	-1.80 ± 0.14	-0.62 ± 0.14
N170bbO – E240bbN	-2.06 ± 0.17	-1.90 ± 0.29
N170N – Water	-0.96 ± 0.20	
N170O – Water	-3.56 ± 0.32	

[a] *Standard deviations correspond to* $\sqrt{\sigma_{TEM1}^2 + \sigma_{TEM52}^2}$. *Abbreviations: BL= β-lactam substrate atom; bb = backbone atom; Amide = substrate amide side-chain atoms; COO = substrate carboxylate side-chain atoms; core = atoms of substrate corresponding to the cephem or penam core; side-chain = substrate phenylacetamido or oxyimino/aminothiazolyl-ring, respectively. See Scheme S3 for interaction groupings and Tables S10,11.*

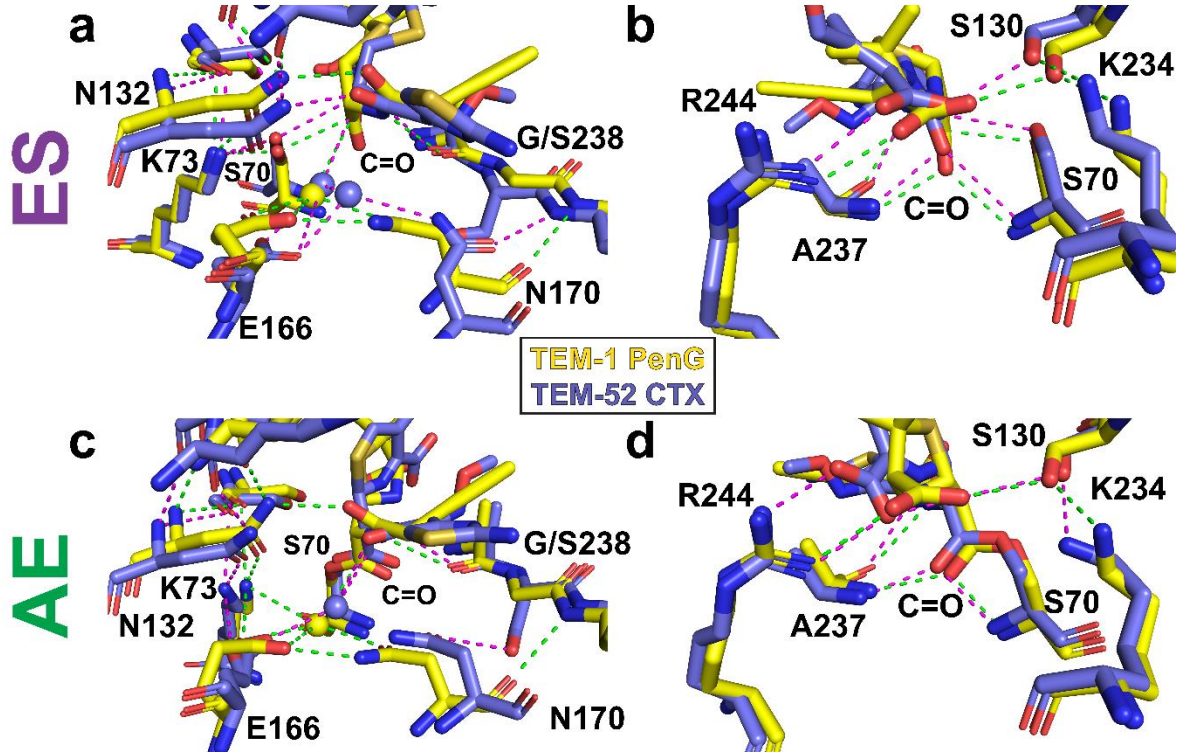

Figure S19. Structural comparison of TEM-1 PenG versus TEM-52 CTX complexes. *Structural overlay of representative average structures of the* ***(a,b)*** *ES complex and* ***(c,d)*** *AE complex of TEM-1 PenG (yellow) relative to TEM-52 CTX (purple).* ***(a,c)*** *The changes in oxyanion hole and extended H-bond network around S70, E166, relative to the β-lactam C=O.* ***(b, d)*** *The substrate-induced changes in structure surrounding the carboxylate functional group of PenG and CTX of the ES and AE states, respectively. Dashed lines show non-covalent interactions ≤ 3.5 Å between nearby interacting functional groups for TEM-1 PenG (green) and TEM-52 CTX (magenta). Changes in structural displacement in terms of the*

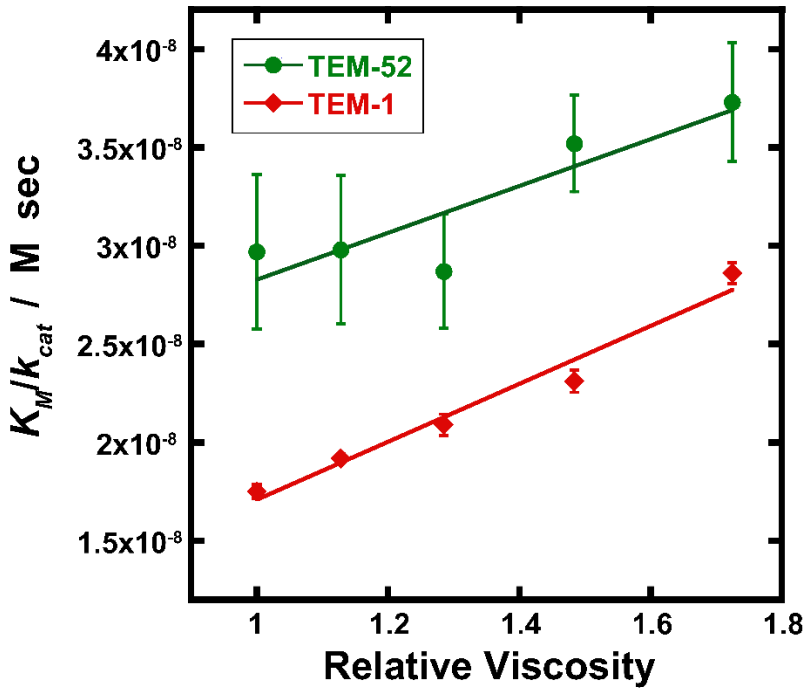

Figure S20. Viscosity-dependence of PenG hydrolysis by TEM β-lactamases. *The change in K_M/k_{cat} as a function of relative viscosity using glycerol as a viscogen (0-20% v/v) enables determination of kinetic parameters as shown in Table S15.*[9,10] *Error bars reflect the standard deviation across 10 measurements (see Methods section).*

Table S15. Evolutionary change in on- and off-rates of PenG hydrolysis with TEM-1 and TEM-52.

Enzyme with PenG	k_1 (μM^{-1} s^{-1})	k_{-1} (s^{-1}) [a]	k_2 (s^{-1})	k_3 (s^{-1})
TEM-1	78.1 ± 3.6	553	5529	2702
TEM-52	84.0 ± 41.5	349	249	52

[a] *Propagated errors of k_{-1} are of a similar magnitude as the values due to the uncertainty in the y-intercept of Figure S20.*

Supplementary References:

1. Deschuyteneer, G.; Garcia, S.; Michiels, B.; Baudoux, B.; Degand, H.; Morsomme, P.; Soumillion, P., Intein-Mediated Cyclization of Randomized Peptides in the Periplasm of *Escherichia coli* and Their Extracellular Secretion. *ACS Chem. Biol.* **2010,** *5* (7), 691-700.
2. Mathonet, P.; Deherve, J.; Soumillion, P.; Fastrez, J., Active TEM-1 β-Lactamase Mutants with Random Peptides Inserted in Three Contiguous Surface Loops. *Protein Sci.* **2006,** *15* (10), 2323-2334.
3. Ambler, R. P., In *Beta-Lactamases*, Hamilton-Miller, J. M. T.; Smith, J. T., Eds. Academic Press: London, 1979.
4. Gasteiger, E.; Hoogland, C.; Gattiker, A.; Duvaud, S.; Wilkins, M. R.; Appel, R. D.; Bairoch, A., Protein Identification and Analysis Tools on the ExPASy Server. In *The Proteomics Protocols Handbook*, Walker, J. M., Ed. Humana Press: Totowa, NJ, 2005; pp 571-607.
5. Palzkill, T., Structural and Mechanistic Basis for Extended-Spectrum Drug-Resistance Mutations in Altering the Specificity of TEM, CTX-M, and KPC β-lactamases. *Front. Mol. Biosci.* **2018,** *5*, 16.
6. Fisher, J.; Belasco, J. G.; Khosla, S.; Knowles, J. R., B-Lactamase Proceeds via an Acyl-Enzyme Intermediate. Interaction of the *Escherichia coli* RTEM Enzyme with Cefoxitin. *Biochemistry* **1980,** *19*, 2895-2901.
7. Banerjee, S.; Pierper, U.; Kapadia, G.; Pannell, L. K.; Herzberg, O., Role of the Ω-Loop in the Activity, Substrate Specificity, and Structure of Class A β-Lactamase. *Biochemistry* **1998,** *37*, 3286-3296.
8. Schnell, S.; Mendoza, C., Closed Form Solution for Time-Dependent Enzyme Kinetics. *J. Theor. Biol.* **1997,** *187*, 207-212.

9. Goličnik, M., On the Lambert W Function and its Utility in Biochemical Kinetics. *Biochem. Eng.* **2012,** *63*, 116-123.

10. Saves, I.; Burlet-Schiltz, O.; Maveyraud, L.; Samama, J.-P.; Promé, J.-C.; Masson, J.-M., Mass Spectral Kinetic Study of Acylation and Deacylation during the Hydrolysis of Penicillins and Cefotaxime by β-Lactamase TEM-1 and G238S Mutant. *Biochemistry* **1995,** *34*, 11660-11667.

11. Kozuch, J.; Schneider, S. H.; Boxer, S. G., Biosynthetic Incorporation of Site-Specific Isotopes in β-Lactam Antibiotics Enables Biophysical Studies. *ACS Chem. Biol.* **2020,** *15* (5), 1148-1153.

12. Strynadka, N. C. J.; Adachi, H.; Jensen, S. E.; Johns, K.; Sielecki, A.; Betzel, C.; Sutoh, K.; James, M. N. G., Molecular Structure of the Acyl-Enzyme Intermediate in β-Lactam Hydrolysis at 1.7 Å Resolution. *Nature* **1992,** *359*, 700-705.

13. Abraham, M. J.; Murtola, T.; Schulz, R.; Páll, S.; Smith, J. C.; Hess, B.; Lindahl, E., GROMACS: High Performance Molecular Simulations through Multi-Level Parallelism from Laptops to Supercomputers. *SoftwareX* **2015,** *1-2*, 19-25.

14. Páll, S.; Abraham, M. J.; Kutzner, C.; Hess, B.; Lindahl, E., Tackling Exascale Software Challenges in Molecular Dynamics Simulations with GROMACS. In *Solving Software Challenges for Exascale*, Markidis, S.; Laure, E., Eds. Springer International Publishing: Switzerland 2015; Vol. 8759, pp 3-27.

15. Frisch, M. J.; Trucks, G. W.; Schlegel, H. B.; Scuseria, G. E.; Robb, M. A.; Cheeseman, J. R.; Scalmani, G.; Barone, V.; Petersson, G. A.; Nakatsuji, H., et al., Gaussian 09, Rev E.01. Gaussian 09, Rev E.01, Gaussian, Inc.: Wallingford, CT, 2016.

16. Lemkul, J., From Proteins to Perturbed Hamiltonians: A Suite of Tutorials for the GROMACS-2018 Molecular Simulation Package [Article v1.0]. *Living J. Comp. Mol. Sci* **2019,** *1* (1), 5068.

17. Cortina, G. A.; Hays, J. M.; Kasson, P. M., Conformational Intermediate That Controls KPC-2 Catalysis and Beta-Lactam Drug Resistance. *ACS Catal.* **2018,** *8* (4), 2741-2747.

18. Cortina, G. A.; Kasson, P. M., Predicting Allostery and Microbial Drug Resistance with Molecular Simulations. *Curr. Opin. Struct. Biol.* **2018,** *52*, 80-86.

19. Latallo, M. J.; Cortina, G. A.; Faham, S.; Nakamoto, R. K.; Kasson, P. M., Predicting Allosteric Mutants that Increase Activity of a Major Antibiotic Resistance Enzyme. *Chem. Sci.* **2017,** *8* (9), 6484-6492.

20. Shimamura, T.; Ibuka, A.; Fushinobu, S.; Wakagi, T.; Ishiguro, M.; Ishii, Y.; Matsuzawa, H., Acyl-Intermediate Structures of the Extended-Spectrum Class A β-lactamase, Toho-1, in Complex with Cefotaxime, Cephalothin, and Benzylpenicillin. *J. Biol. Chem.* **2002,** *277* (48), 46601-46608.

21. Briones, R.; Blau, C.; Kutzner, C.; de Groot, B. L.; Aponte-Santamaria, C., GROmaps: A GROMACS-Based Toolset to Analyze Density Maps Derived from Molecular Dynamics Simulations. *Biophys. J.* **2019,** *116* (1), 4-11.

22. Brown, N. G.; Pennington, J. M.; Huang, W.; Ayvaz, T.; Palzkill, T., Multiple Global Suppressors of Protein Stability Defects Facilitate the Evolution of Extended-Spectrum TEM β-Lactamases. *J. Mol. Biol.* **2010,** *404* (5), 832-846.

23. Guthrie, V. B.; Allen, J.; Camps, M.; Karchin, R., Network Models of TEM β-Lactamase Mutations Coevolving Under Antibiotic Selection Show Modular Structure and Anticipate Evolutionary Trajectories. *PLoS Comput. Biol.* **2011,** *7* (9), e1002184.

24. Knox, J. R., Extended-Spectrum and Inhibitor-Resistant TEM-Type β-Lactamases: Mutations, Specificity, and Three-Dimensional Structure. *Antimicrob. Agents Chemother.* **1995,** *39*, 2593-2601.

25. Page, M. G., Extended-Spectrum β-Lactamases: Structure and Kinetic Mechanism. *Clin. Microbiol. Infect.* **2008,** *14 Suppl 1*, 63-74.

26. Fried, S. D.; Bagchi, S.; Boxer, S. G., Extreme Electric Field Power Catalysis in the Active Site of Ketosteroid Isomerase. *Science* **2014,** *346*, 1510-1514.

27. Fried, S. D.; Boxer, S. G., Electric Fields and Enzyme Catalysis. *Annu. Rev. Biochem.* **2017,** *86*, 387-415.

28. Schneider, S. H.; Boxer, S. G., Vibrational Stark Effects of Carbonyl Probes Applied to Reinterpret IR and Raman Data for Enzyme Inhibitors in Terms of Electric Fields at the Active Site. *J. Phys. Chem. B* **2016,** *120*, 9672-9684.

29. Wu, Y.; Fried, S. D.; Boxer, S. G., A Preorganized Electric Field Leads to Minimal Geometrical Reorientation in the Catalytic Reaction of Ketosteroid Isomerase. *J. Am. Chem. Soc.* **2020,** *142* (22), 9993-9998.

30. Wu, Y.; Boxer, S. G., A Critical Test of the Electrostatic Contribution to Catalysis with Noncanonical Amino Acids in Ketosteroid Isomerase. *J. Am. Chem. Soc.* **2016,** *138* (36), 11890-11895.

31. Modi, T.; Risso, V. A.; Martinez-Rodriguez, S.; Gavira, J. A.; Mebrat, M. D.; Van Horn, W. D.; Sanchez-Ruiz, J. M.; Banu Ozkan, S., Hinge-Shift Mechanism as a Protein Design Principle for the Evolution of β-Lactamases from Substrate Promiscuity to Specificity. *Nat. Commun.* **2021,** *12* (1), 1852.

32. Risso, V. A.; Gavira, J. A.; Mejia-Carmona, D. F.; Gaucher, E. A.; Sanchez-Ruiz, J. M., Hyperstability and Substrate Promiscuity in Laboratory Resurrections of Precambrian β-Lactamases. *J. Am. Chem. Soc.* **2013,** *135* (8), 2899-2902.

33. Broom, A.; Rakotoharisoa, R. V.; Thompson, M. C.; Zarifi, N.; Nguyen, E.; Mukhametzhanov, N.; Liu, L.; Fraser, J. S.; Chica, R. A., Ensemble-Based Enzyme Design can Recapitulate the Effects of Laboratory Directed Evolution *In Silico*. *Nat. Commun.* **2020,** *11* (1), 4808.

34. Otten, R.; Pádua, R. A. P.; Bunzel, H. A.; Nguyen, V.; Pitsawong, W.; Patterson, M.; Sui, S.; Perry, S. L.; Cohen, A. E.; Hilvert, D., et al., How Directed Evolution Reshapes the

Energy Landscape in an Enzyme to Boost Catalysis. *Science* **2020,** *370* (6523), 1442-1446.

35. Wang, F.; Zhou, H.; Wang, X.; Tao, P., Dynamical Behavior of β-Lactamases and Penicillin-Binding Proteins in Different Functional States and Its Potential Role in Evolution. *Entropy* **2019,** *21* (11), 1130.

36. Crean, R. M.; Gardner, J. M.; Kamerlin, S. C. L., Harnessing Conformational Plasticity to Generate Designer Enzymes. *J. Am. Chem. Soc.* **2020**.

MD Files and Parameters:

PEN.gro

```
  289PEN      C 4061   4.665   3.745   3.526
  289PEN     C1 4062   4.812   3.780   3.558
  289PEN     C2 4063   4.653   3.974   3.635
  289PEN      H 4064   4.633   3.668   3.597
  289PEN     H1 4065   4.692   4.058   3.576
  289PEN      S 4066   4.791   3.877   3.711
  289PEN      N 4067   4.588   3.867   3.559
  289PEN     C3 4068   4.517   3.997   3.710
  289PEN     H2 4069   4.467   4.090   3.681
  289PEN     C4 4070   4.467   3.876   3.628
  289PEN      O 4071   4.370   3.803   3.631
  289PEN     N1 4072   4.507   3.983   3.854
  289PEN     H3 4073   4.472   3.895   3.892
  289PEN     C5 4074   4.546   4.075   3.947
  289PEN     O1 4075   4.589   4.185   3.915
  289PEN     C6 4076   4.537   4.026   4.091
  289PEN     H4 4077   4.474   3.937   4.094
  289PEN     H5 4078   4.485   4.104   4.148
  289PEN     C7 4079   4.673   3.995   4.153
  289PEN     C8 4080   4.684   3.992   4.293
  289PEN     C9 4081   4.788   3.974   4.074
  289PEN    C10 4082   4.810   3.978   4.353
  289PEN     H6 4083   4.596   4.006   4.355
  289PEN    C11 4084   4.914   3.957   4.135
  289PEN     H7 4085   4.783   3.974   3.966
  289PEN    C12 4086   4.924   3.962   4.274
  289PEN     H8 4087   4.819   3.982   4.461
  289PEN     H9 4088   5.003   3.943   4.074
  289PEN    H10 4089   5.022   3.955   4.321
  289PEN    C13 4090   4.644   3.685   3.388
  289PEN     O2 4091   4.582   3.748   3.303
  289PEN     O3 4092   4.681   3.570   3.370
  289PEN    C14 4093   4.881   3.861   3.445
  289PEN    H11 4094   4.984   3.883   3.472
  289PEN    H12 4095   4.884   3.803   3.352
  289PEN    H13 4096   4.829   3.955   3.425
  289PEN    C15 4097   4.897   3.657   3.594
  289PEN    H14 4098   4.852   3.601   3.676
  289PEN    H15 4099   4.909   3.589   3.508
  289PEN    H16 4100   4.998   3.688   3.626
```

PEN.top

```
[ defaults ]
; nbfunc        comb-rule       gen-pairs       fudgeLJ fudgeQQ
1               2               yes             0.5     0.8333

[ atomtypes ]
;name   bond_type     mass     charge   ptype   sigma         epsilon       Amb
 c3       c3          0.00000  0.00000   A     3.39967e-01   4.57730e-01 ; 1.91  0.1094
 cy       cy          0.00000  0.00000   A     3.39967e-01   3.59824e-01 ; 1.91  0.0860
 h1       h1          0.00000  0.00000   A     2.47135e-01   6.56888e-02 ; 1.39  0.0157
 h2       h2          0.00000  0.00000   A     2.29317e-01   6.56888e-02 ; 1.29  0.0157
 ss       ss          0.00000  0.00000   A     3.56359e-01   1.04600e+00 ; 2.00  0.2500
 nj       nj          0.00000  0.00000   A     3.25000e-01   7.11280e-01 ; 1.82  0.1700
 c        c           0.00000  0.00000   A     3.39967e-01   3.59824e-01 ; 1.91  0.0860
 o        o           0.00000  0.00000   A     2.95992e-01   8.78640e-01 ; 1.66  0.2100
 n        n           0.00000  0.00000   A     3.25000e-01   7.11280e-01 ; 1.82  0.1700
 hn       hn          0.00000  0.00000   A     1.06908e-01   6.56888e-02 ; 0.60  0.0157
 hc       hc          0.00000  0.00000   A     2.64953e-01   6.56888e-02 ; 1.49  0.0157
 ca       ca          0.00000  0.00000   A     3.39967e-01   3.59824e-01 ; 1.91  0.0860
 ha       ha          0.00000  0.00000   A     2.59964e-01   6.27600e-02 ; 1.46  0.0150
```

```
[ moleculetype ]
;name            nrexcl
 PEN             3

[ atoms ]
;   nr  type  resi  res  atom  cgnr     charge      mass       ; qtot   bond_type
    1   c3    1   PEN     C    1    -0.080300     12.01000 ; qtot -0.080
    2   c3    1   PEN    C1    2     0.091100     12.01000 ; qtot 0.011
    3   cy    1   PEN    C2    3     0.132800     12.01000 ; qtot 0.144
    4   h1    1   PEN     H    4     0.080700      1.00800 ; qtot 0.224
    5   h2    1   PEN    H1    5     0.121700      1.00800 ; qtot 0.346
    6   ss    1   PEN     S    6    -0.436200     32.06000 ; qtot -0.090
    7   nj    1   PEN     N    7    -0.337800     14.01000 ; qtot -0.428
    8   cy    1   PEN    C3    8    -0.015300     12.01000 ; qtot -0.443
    9   h1    1   PEN    H2    9     0.112700      1.00800 ; qtot -0.331
   10   c     1   PEN    C4   10     0.650501     12.01000 ; qtot 0.320
   11   o     1   PEN     O   11    -0.572501     16.00000 ; qtot -0.253
   12   n     1   PEN    N1   12    -0.534901     14.01000 ; qtot -0.788
   13   hn    1   PEN    H3   13     0.337500      1.00800 ; qtot -0.450
   14   c     1   PEN    C5   14     0.662101     12.01000 ; qtot 0.212
   15   o     1   PEN    O1   15    -0.623101     16.00000 ; qtot -0.411
   16   c3    1   PEN    C6   16    -0.112100     12.01000 ; qtot -0.523
   17   hc    1   PEN    H4   17     0.077200      1.00800 ; qtot -0.446
   18   hc    1   PEN    H5   18     0.077200      1.00800 ; qtot -0.369
   19   ca    1   PEN    C7   19    -0.088300     12.01000 ; qtot -0.457
   20   ca    1   PEN    C8   20    -0.120000     12.01000 ; qtot -0.577
   21   ca    1   PEN    C9   21    -0.120000     12.01000 ; qtot -0.697
   22   ca    1   PEN   C10   22    -0.129000     12.01000 ; qtot -0.826
   23   ha    1   PEN    H6   23     0.140000      1.00800 ; qtot -0.686
   24   ca    1   PEN   C11   24    -0.129000     12.01000 ; qtot -0.815
   25   ha    1   PEN    H7   25     0.140000      1.00800 ; qtot -0.675
   26   ca    1   PEN   C12   26    -0.131000     12.01000 ; qtot -0.806
   27   ha    1   PEN    H8   27     0.130500      1.00800 ; qtot -0.676
   28   ha    1   PEN    H9   28     0.130500      1.00800 ; qtot -0.545
   29   ha    1   PEN   H10   29     0.127000      1.00800 ; qtot -0.418
   30   c     1   PEN   C13   30     0.940604     12.01000 ; qtot 0.523
   31   o     1   PEN    O2   31    -0.811801     16.00000 ; qtot -0.289
   32   o     1   PEN    O3   32    -0.811801     16.00000 ; qtot -1.101
   33   c3    1   PEN   C14   33    -0.089100     12.01000 ; qtot -1.190
   34   hc    1   PEN   H11   34     0.046533      1.00800 ; qtot -1.144
   35   hc    1   PEN   H12   35     0.046533      1.00800 ; qtot -1.097
   36   hc    1   PEN   H13   36     0.046533      1.00800 ; qtot -1.050
   37   c3    1   PEN   C15   37    -0.089100     12.01000 ; qtot -1.140
   38   hc    1   PEN   H14   38     0.046533      1.00800 ; qtot -1.093
   39   hc    1   PEN   H15   39     0.046533      1.00800 ; qtot -1.047
   40   hc    1   PEN   H16   40     0.046533      1.00800 ; qtot -1.000

[ bonds ]
;   ai     aj funct   r             k
    1      2   1    1.5375e-01    2.5179e+05 ;     C - C1
    1      4   1    1.0969e-01    2.7665e+05 ;     C - H
    1      7   1    1.4520e-01    2.8359e+05 ;     C - N
    1     30   1    1.5241e-01    2.6192e+05 ;     C - C13
    2      6   1    1.8392e-01    1.8067e+05 ;    C1 - S
    2     33   1    1.5375e-01    2.5179e+05 ;    C1 - C14
    2     37   1    1.5375e-01    2.5179e+05 ;    C1 - C15
    3      5   1    1.0930e-01    2.8108e+05 ;    C2 - H1
    3      6   1    1.8500e-01    1.7598e+05 ;    C2 - S
    3      7   1    1.4750e-01    2.6426e+05 ;    C2 - N
    3      8   1    1.5580e-01    2.3732e+05 ;    C2 - C3
    7     10   1    1.4010e-01    3.3313e+05 ;     N - C4
    8      9   1    1.0950e-01    2.7874e+05 ;    C3 - H2
    8     10   1    1.5520e-01    2.4150e+05 ;    C3 - C4
    8     12   1    1.4330e-01    3.0091e+05 ;    C3 - N1
   10     11   1    1.2183e-01    5.3363e+05 ;    C4 - O
   12     13   1    1.0129e-01    3.3740e+05 ;    N1 - H3
   12     14   1    1.3789e-01    3.5782e+05 ;    N1 - C5
   14     15   1    1.2183e-01    5.3363e+05 ;    C5 - O1
   14     16   1    1.5241e-01    2.6192e+05 ;    C5 - C6
   16     17   1    1.0969e-01    2.7665e+05 ;    C6 - H4
```

```
   16    18   1    1.0969e-01    2.7665e+05 ;    C6 - H5
   16    19   1    1.5156e-01    2.6861e+05 ;    C6 - C7
   19    20   1    1.3984e-01    3.8585e+05 ;    C7 - C8
   19    21   1    1.3984e-01    3.8585e+05 ;    C7 - C9
   20    22   1    1.3984e-01    3.8585e+05 ;    C8 - C10
   20    23   1    1.0860e-01    2.8937e+05 ;    C8 - H6
   21    24   1    1.3984e-01    3.8585e+05 ;    C9 - C11
   21    25   1    1.0860e-01    2.8937e+05 ;    C9 - H7
   22    26   1    1.3984e-01    3.8585e+05 ;   C10 - C12
   22    27   1    1.0860e-01    2.8937e+05 ;   C10 - H8
   24    26   1    1.3984e-01    3.8585e+05 ;   C11 - C12
   24    28   1    1.0860e-01    2.8937e+05 ;   C11 - H9
   26    29   1    1.0860e-01    2.8937e+05 ;   C12 - H10
   30    31   1    1.2183e-01    5.3363e+05 ;   C13 - O2
   30    32   1    1.2183e-01    5.3363e+05 ;   C13 - O3
   33    34   1    1.0969e-01    2.7665e+05 ;   C14 - H11
   33    35   1    1.0969e-01    2.7665e+05 ;   C14 - H12
   33    36   1    1.0969e-01    2.7665e+05 ;   C14 - H13
   37    38   1    1.0969e-01    2.7665e+05 ;   C15 - H14
   37    39   1    1.0969e-01    2.7665e+05 ;   C15 - H15
   37    40   1    1.0969e-01    2.7665e+05 ;   C15 - H16

[ pairs ]
;   ai    aj    funct
    1     5     1 ;     C - H1
    1     8     1 ;     C - C3
    1    11     1 ;     C - O
    1    34     1 ;     C - H11
    1    35     1 ;     C - H12
    1    36     1 ;     C - H13
    1    38     1 ;     C - H14
    1    39     1 ;     C - H15
    1    40     1 ;     C - H16
    2     5     1 ;    C1 - H1
    2     8     1 ;    C1 - C3
    2    10     1 ;    C1 - C4
    2    31     1 ;    C1 - O2
    2    32     1 ;    C1 - O3
    3    11     1 ;    C2 - O
    3    13     1 ;    C2 - H3
    3    14     1 ;    C2 - C5
    3    33     1 ;    C2 - C14
    3    37     1 ;    C2 - C15
    4     3     1 ;     H - C2
    4     6     1 ;     H - S
    4    10     1 ;     H - C4
    4    31     1 ;     H - O2
    4    32     1 ;     H - O3
    4    33     1 ;     H - C14
    4    37     1 ;     H - C15
    5     9     1 ;    H1 - H2
    5    10     1 ;    H1 - C4
    5    12     1 ;    H1 - N1
    6     9     1 ;     S - H2
    6    10     1 ;     S - C4
    6    12     1 ;     S - N1
    6    34     1 ;     S - H11
    6    35     1 ;     S - H12
    6    36     1 ;     S - H13
    6    38     1 ;     S - H14
    6    39     1 ;     S - H15
    6    40     1 ;     S - H16
    7     9     1 ;     N - H2
    7    12     1 ;     N - N1
    7    31     1 ;     N - O2
    7    32     1 ;     N - O3
    7    33     1 ;     N - C14
    7    37     1 ;     N - C15
    8    15     1 ;    C3 - O1
    8    16     1 ;    C3 - C6
```

```
    9    11     1 ;    H2 - O
    9    13     1 ;    H2 - H3
    9    14     1 ;    H2 - C5
   10    13     1 ;    C4 - H3
   10    14     1 ;    C4 - C5
   11    12     1 ;     O - N1
   12    17     1 ;    N1 - H4
   12    18     1 ;    N1 - H5
   12    19     1 ;    N1 - C7
   13    15     1 ;    H3 - O1
   13    16     1 ;    H3 - C6
   14    20     1 ;    C5 - C8
   14    21     1 ;    C5 - C9
   15    17     1 ;    O1 - H4
   15    18     1 ;    O1 - H5
   15    19     1 ;    O1 - C7
   16    22     1 ;    C6 - C10
   16    23     1 ;    C6 - H6
   16    24     1 ;    C6 - C11
   16    25     1 ;    C6 - H7
   17    20     1 ;    H4 - C8
   17    21     1 ;    H4 - C9
   18    20     1 ;    H5 - C8
   18    21     1 ;    H5 - C9
   19    26     1 ;    C7 - C12
   19    27     1 ;    C7 - H8
   19    28     1 ;    C7 - H9
   20    24     1 ;    C8 - C11
   20    25     1 ;    C8 - H7
   20    29     1 ;    C8 - H10
   21    22     1 ;    C9 - C10
   21    23     1 ;    C9 - H6
   21    29     1 ;    C9 - H10
   22    28     1 ;   C10 - H9
   23    26     1 ;    H6 - C12
   23    27     1 ;    H6 - H8
   24    27     1 ;   C11 - H8
   25    26     1 ;    H7 - C12
   25    28     1 ;    H7 - H9
   27    29     1 ;    H8 - H10
   28    29     1 ;    H9 - H10
   30     3     1 ;   C13 - C2
   30     6     1 ;   C13 - S
   30    10     1 ;   C13 - C4
   30    33     1 ;   C13 - C14
   30    37     1 ;   C13 - C15
   33    38     1 ;   C14 - H14
   33    39     1 ;   C14 - H15
   33    40     1 ;   C14 - H16
   34    37     1 ;   H11 - C15
   35    37     1 ;   H12 - C15
   36    37     1 ;   H13 - C15

[ angles ]
;   ai    aj    ak    funct   theta         cth
    1     2     6     1    1.1027e+02    5.1296e+02 ;     C - C1    - S
    1     2    33     1    1.1151e+02    5.2635e+02 ;     C - C1    - C14
    1     2    37     1    1.1151e+02    5.2635e+02 ;     C - C1    - C15
    1     7     3     1    1.1718e+02    5.2300e+02 ;     C - N     - C2
    1     7    10     1    1.2760e+02    5.1463e+02 ;     C - N     - C4
    1    30    31     1    1.2320e+02    5.6400e+02 ;     C - C13   - O2
    1    30    32     1    1.2320e+02    5.6400e+02 ;     C - C13   - O3
    2     1     4     1    1.0956e+02    3.8828e+02 ;    C1 - C     - H
    2     1     7     1    1.0694e+02    5.6484e+02 ;    C1 - C     - N
    2     1    30     1    1.1104e+02    5.2969e+02 ;    C1 - C     - C13
    2     6     3     1    9.4240e+01    5.1547e+02 ;    C1 - S     - C2
    2    33    34     1    1.0980e+02    3.8744e+02 ;    C1 - C14   - H11
    2    33    35     1    1.0980e+02    3.8744e+02 ;    C1 - C14   - H12
    2    33    36     1    1.0980e+02    3.8744e+02 ;    C1 - C14   - H13
    2    37    38     1    1.0980e+02    3.8744e+02 ;    C1 - C15   - H14
```

```
  2    37    39     1    1.0980e+02    3.8744e+02 ;    C1 - C15    - H15
  2    37    40     1    1.0980e+02    3.8744e+02 ;    C1 - C15    - H16
  3     7    10     1    9.4020e+01    5.9413e+02 ;    C2 - N      - C4
  3     8     9     1    1.1317e+02    3.7740e+02 ;    C2 - C3     - H2
  3     8    10     1    8.5160e+01    5.9496e+02 ;    C2 - C3     - C4
  3     8    12     1    1.1987e+02    5.3220e+02 ;    C2 - C3     - N1
  4     1     7     1    1.0852e+02    4.2007e+02 ;    H - C       - N
  4     1    30     1    1.0822e+02    3.9330e+02 ;    H - C       - C13
  5     3     6     1    1.0966e+02    3.4811e+02 ;    H1 - C2     - S
  5     3     7     1    1.1454e+02    4.0334e+02 ;    H1 - C2     - N
  5     3     8     1    1.1679e+02    3.7154e+02 ;    H1 - C2     - C3
  6     2    33     1    1.1027e+02    5.1296e+02 ;    S - C1      - C14
  6     2    37     1    1.1027e+02    5.1296e+02 ;    S - C1      - C15
  6     3     7     1    1.0514e+02    5.4141e+02 ;    S - C2      - N
  6     3     8     1    1.1827e+02    4.9120e+02 ;    S - C2      - C3
  7     1    30     1    1.1019e+02    5.5982e+02 ;    N - C       - C13
  7     3     8     1    8.8640e+01    6.1170e+02 ;    N - C2      - C3
  7    10     8     1    9.1680e+01    6.1588e+02 ;    N - C4      - C3
  7    10    11     1    1.3306e+02    5.9078e+02 ;    N - C4      - O
  8    10    11     1    1.3523e+02    5.3053e+02 ;    C3 - C4     - O
  8    12    13     1    1.1885e+02    3.8828e+02 ;    C3 - N1     - H3
  8    12    14     1    1.2171e+02    5.3388e+02 ;    C3 - N1     - C5
  9     8    10     1    1.1297e+02    3.7907e+02 ;    H2 - C3     - C4
  9     8    12     1    1.0799e+02    4.2593e+02 ;    H2 - C3     - N1
 10     8    12     1    1.1738e+02    5.3974e+02 ;    C4 - C3     - N1
 12    14    15     1    1.2305e+02    6.2091e+02 ;    N1 - C5     - O1
 12    14    16     1    1.1518e+02    5.5898e+02 ;    N1 - C5     - C6
 13    12    14     1    1.1755e+02    4.0417e+02 ;    H3 - N1     - C5
 14    16    17     1    1.0877e+02    3.9246e+02 ;    C5 - C6     - H4
 14    16    18     1    1.0877e+02    3.9246e+02 ;    C5 - C6     - H5
 14    16    19     1    1.1101e+02    5.3304e+02 ;    C5 - C6     - C7
 15    14    16     1    1.2320e+02    5.6400e+02 ;    O1 - C5     - C6
 16    19    20     1    1.2077e+02    5.3137e+02 ;    C6 - C7     - C8
 16    19    21     1    1.2077e+02    5.3137e+02 ;    C6 - C7     - C9
 17    16    18     1    1.0758e+02    3.2970e+02 ;    H4 - C6     - H5
 17    16    19     1    1.1047e+02    3.9162e+02 ;    H4 - C6     - C7
 18    16    19     1    1.1047e+02    3.9162e+02 ;    H5 - C6     - C7
 19    20    22     1    1.2002e+02    5.5731e+02 ;    C7 - C8     - C10
 19    20    23     1    1.1988e+02    4.0334e+02 ;    C7 - C8     - H6
 19    21    24     1    1.2002e+02    5.5731e+02 ;    C7 - C9     - C11
 19    21    25     1    1.1988e+02    4.0334e+02 ;    C7 - C9     - H7
 20    19    21     1    1.2002e+02    5.5731e+02 ;    C8 - C7     - C9
 20    22    26     1    1.2002e+02    5.5731e+02 ;    C8 - C10    - C12
 20    22    27     1    1.1988e+02    4.0334e+02 ;    C8 - C10    - H8
 21    24    26     1    1.2002e+02    5.5731e+02 ;    C9 - C11    - C12
 21    24    28     1    1.1988e+02    4.0334e+02 ;    C9 - C11    - H9
 22    20    23     1    1.1988e+02    4.0334e+02 ;    C10 - C8    - H6
 22    26    24     1    1.2002e+02    5.5731e+02 ;    C10 - C12   - C11
 22    26    29     1    1.1988e+02    4.0334e+02 ;    C10 - C12   - H10
 24    21    25     1    1.1988e+02    4.0334e+02 ;    C11 - C9    - H7
 24    26    29     1    1.1988e+02    4.0334e+02 ;    C11 - C12   - H10
 26    22    27     1    1.1988e+02    4.0334e+02 ;    C12 - C10   - H8
 26    24    28     1    1.1988e+02    4.0334e+02 ;    C12 - C11   - H9
 31    30    32     1    1.3025e+02    6.5187e+02 ;    O2 - C13    - O3
 33     2    37     1    1.1151e+02    5.2635e+02 ;    C14 - C1    - C15
 34    33    35     1    1.0758e+02    3.2970e+02 ;    H11 - C14   - H12
 34    33    36     1    1.0758e+02    3.2970e+02 ;    H11 - C14   - H13
 35    33    36     1    1.0758e+02    3.2970e+02 ;    H12 - C14   - H13
 38    37    39     1    1.0758e+02    3.2970e+02 ;    H14 - C15   - H15
 38    37    40     1    1.0758e+02    3.2970e+02 ;    H14 - C15   - H16
 39    37    40     1    1.0758e+02    3.2970e+02 ;    H15 - C15   - H16

[ dihedrals ] ; propers
; treated as RBs in GROMACS to use combine multiple AMBER torsions per quartet
;   i     j     k     l   func    C0          C1          C2          C3          C4          C5
    1     2     6     3     3   1.39467    4.18400    0.00000   -5.57867    0.00000    0.00000 ;     C-   C1-   S-   C2
    1     2    33    34     3   0.66944    2.00832    0.00000   -2.67776    0.00000    0.00000 ;     C-   C1-   C14-  H11
    1     2    33    35     3   0.66944    2.00832    0.00000   -2.67776    0.00000    0.00000 ;     C-   C1-   C14-  H12
    1     2    33    36     3   0.66944    2.00832    0.00000   -2.67776    0.00000    0.00000 ;     C-   C1-   C14-  H13
    1     2    37    38     3   0.66944    2.00832    0.00000   -2.67776    0.00000    0.00000 ;     C-   C1-   C15-  H14
```

```
1   2   37  39   3   0.66944   2.00832   0.00000  -2.67776   0.00000   0.00000 ;   C-   C1-  C15-  H15
1   2   37  40   3   0.66944   2.00832   0.00000  -2.67776   0.00000   0.00000 ;   C-   C1-  C15-  H16
1   7   3   5    3   0.00000   0.00000   0.00000   0.00000   0.00000   0.00000 ;   C-   N-   C2-   H1
1   7   3   6    3   0.00000   0.00000   0.00000   0.00000   0.00000   0.00000 ;   C-   N-   C2-   S
1   7   3   8    3   0.00000   0.00000   0.00000   0.00000   0.00000   0.00000 ;   C-   N-   C2-   C3
1   7   10  8    3  20.92000   0.00000 -20.92000   0.00000   0.00000   0.00000 ;   C-   N-   C4-   C3
1   7   10  11   3  20.92000   0.00000 -20.92000   0.00000   0.00000   0.00000 ;   C-   N-   C4-   O
2   1   7   3    3   0.00000   0.00000   0.00000   0.00000   0.00000   0.00000 ;  C1-   C-   N-   C2
2   1   7   10   3   2.84512  -4.10032  16.73600   2.51040 -16.73600   0.00000 ;  C1-   C-   N-   C4
2   1   30  31   3   0.00000   0.00000   0.00000   0.00000   0.00000   0.00000 ;  C1-   C-  C13-   O2
2   1   30  32   3   0.00000   0.00000   0.00000   0.00000   0.00000   0.00000 ;  C1-   C-  C13-   O3
2   6   3   5    3   1.39467   4.18400   0.00000  -5.57867   0.00000   0.00000 ;  C1-   S-   C2-   H1
2   6   3   7    3   1.39467   4.18400   0.00000  -5.57867   0.00000   0.00000 ;  C1-   S-   C2-   N
2   6   3   8    3   1.39467   4.18400   0.00000  -5.57867   0.00000   0.00000 ;  C1-   S-   C2-   C3
3   6   2   33   3   1.39467   4.18400   0.00000  -5.57867   0.00000   0.00000 ;  C2-   S-   C1-  C14
3   6   2   37   3   1.39467   4.18400   0.00000  -5.57867   0.00000   0.00000 ;  C2-   S-   C1-  C15
3   7   10  8    3  20.92000   0.00000 -20.92000   0.00000   0.00000   0.00000 ;  C2-   N-   C4-   C3
3   7   10  11   3  20.92000   0.00000 -20.92000   0.00000   0.00000   0.00000 ;  C2-   N-   C4-   O
3   8   10  7    3   0.00000   0.00000   0.00000   0.00000   0.00000   0.00000 ;  C2-   C3-   C4-   N
3   8   10  11   3   0.00000   0.00000   0.00000   0.00000   0.00000   0.00000 ;  C2-   C3-   C4-   O
3   8   12  13   3   0.00000   0.00000   0.00000   0.00000   0.00000   0.00000 ;  C2-   C3-   N1-   H3
3   8   12  14   3   0.00000   0.00000   0.00000   0.00000   0.00000   0.00000 ;  C2-   C3-   N1-   C5
4   1   2   6    3   0.65084   1.95253   0.00000  -2.60338   0.00000   0.00000 ;   H-   C-   C1-   S
4   1   2   33   3   0.65084   1.95253   0.00000  -2.60338   0.00000   0.00000 ;   H-   C-   C1-  C14
4   1   2   37   3   0.65084   1.95253   0.00000  -2.60338   0.00000   0.00000 ;   H-   C-   C1-  C15
4   1   7   3    3   0.00000   0.00000   0.00000   0.00000   0.00000   0.00000 ;   H-   C-   N-   C2
4   1   7   10   3   0.00000   0.00000   0.00000   0.00000   0.00000   0.00000 ;   H-   C-   N-   C4
4   1   30  31   3   3.68192  -4.35136   0.00000   1.33888   0.00000   0.00000 ;   H-   C-  C13-   O2
4   1   30  32   3   3.68192  -4.35136   0.00000   1.33888   0.00000   0.00000 ;   H-   C-  C13-   O3
5   3   7   10   3   0.00000   0.00000   0.00000   0.00000   0.00000   0.00000 ;  H1-  C2-   N-   C4
5   3   8   9    3   0.65084   1.95253   0.00000  -2.60338   0.00000   0.00000 ;  H1-  C2-   C3-   H2
5   3   8   10   3   0.65084   1.95253   0.00000  -2.60338   0.00000   0.00000 ;  H1-  C2-   C3-   C4
5   3   8   12   3   0.65084   1.95253   0.00000  -2.60338   0.00000   0.00000 ;  H1-  C2-   C3-   N1
6   2   33  34   3   0.65084   1.95253   0.00000  -2.60338   0.00000   0.00000 ;   S-   C1-  C14-  H11
6   2   33  35   3   0.65084   1.95253   0.00000  -2.60338   0.00000   0.00000 ;   S-   C1-  C14-  H12
6   2   33  36   3   0.65084   1.95253   0.00000  -2.60338   0.00000   0.00000 ;   S-   C1-  C14-  H13
6   2   37  38   3   0.65084   1.95253   0.00000  -2.60338   0.00000   0.00000 ;   S-   C1-  C15-  H14
6   2   37  39   3   0.65084   1.95253   0.00000  -2.60338   0.00000   0.00000 ;   S-   C1-  C15-  H15
6   2   37  40   3   0.65084   1.95253   0.00000  -2.60338   0.00000   0.00000 ;   S-   C1-  C15-  H16
6   3   7   10   3   0.00000   0.00000   0.00000   0.00000   0.00000   0.00000 ;   S-   C2-   N-   C4
6   3   8   9    3   0.65084   1.95253   0.00000  -2.60338   0.00000   0.00000 ;   S-   C2-   C3-   H2
6   3   8   10   3   0.65084   1.95253   0.00000  -2.60338   0.00000   0.00000 ;   S-   C2-   C3-   C4
6   3   8   12   3   0.65084   1.95253   0.00000  -2.60338   0.00000   0.00000 ;   S-   C2-   C3-   N1
7   1   2   6    3   0.65084   1.95253   0.00000  -2.60338   0.00000   0.00000 ;   N-   C-   C1-   S
7   1   2   33   3   0.65084   1.95253   0.00000  -2.60338   0.00000   0.00000 ;   N-   C-   C1-  C14
7   1   2   37   3   0.65084   1.95253   0.00000  -2.60338   0.00000   0.00000 ;   N-   C-   C1-  C15
7   1   30  31   3   0.00000   0.00000   0.00000   0.00000   0.00000   0.00000 ;   N-   C-  C13-   O2
7   1   30  32   3   0.00000   0.00000   0.00000   0.00000   0.00000   0.00000 ;   N-   C-  C13-   O3
7   3   8   9    3   0.65084   1.95253   0.00000  -2.60338   0.00000   0.00000 ;   N-  C2-   C3-   H2
7   3   8   10   3   0.65084   1.95253   0.00000  -2.60338   0.00000   0.00000 ;   N-  C2-   C3-   C4
7   3   8   12   3   0.65084   1.95253   0.00000  -2.60338   0.00000   0.00000 ;   N-  C2-   C3-   N1
7   10  8   9    3   0.00000   0.00000   0.00000   0.00000   0.00000   0.00000 ;   N-  C4-   C3-   H2
7   10  8   12   3   0.00000   0.00000   0.00000   0.00000   0.00000   0.00000 ;   N-  C4-   C3-   N1
8   3   7   10   3   0.00000   0.00000   0.00000   0.00000   0.00000   0.00000 ;  C3-  C2-   N-   C4
8   12  14  15   3  20.92000   0.00000 -20.92000   0.00000   0.00000   0.00000 ;  C3-  N1-  C5-   O1
8   12  14  16   3  20.92000   0.00000 -20.92000   0.00000   0.00000   0.00000 ;  C3-  N1-  C5-   C6
9   8   10  11   3   0.00000   0.00000   0.00000   0.00000   0.00000   0.00000 ;  H2-  C3-  C4-   O
9   8   12  13   3   0.00000   0.00000   0.00000   0.00000   0.00000   0.00000 ;  H2-  C3-  N1-   H3
9   8   12  14   3   0.00000   0.00000   0.00000   0.00000   0.00000   0.00000 ;  H2-  C3-  N1-   C5
10  8   12  13   3   0.00000   0.00000   0.00000   0.00000   0.00000   0.00000 ;  C4-  C3-  N1-   H3
10  8   12  14   3   0.00000   0.00000   0.00000   0.00000   0.00000   0.00000 ;  C4-  C3-  N1-   C5
11  10  8   12   3   0.00000   0.00000   0.00000   0.00000   0.00000   0.00000 ;   O-  C4-  C3-   N1
12  14  16  17   3   0.00000   0.00000   0.00000   0.00000   0.00000   0.00000 ;  N1-  C5-  C6-   H4
12  14  16  18   3   0.00000   0.00000   0.00000   0.00000   0.00000   0.00000 ;  N1-  C5-  C6-   H5
12  14  16  19   3   0.00000   0.00000   0.00000   0.00000   0.00000   0.00000 ;  N1-  C5-  C6-   C7
13  12  14  15   3  29.28800  -8.36800 -20.92000   0.00000   0.00000   0.00000 ;  H3-  N1-  C5-   O1
13  12  14  16   3  20.92000   0.00000 -20.92000   0.00000   0.00000   0.00000 ;  H3-  N1-  C5-   C6
14  16  19  20   3   0.00000   0.00000   0.00000   0.00000   0.00000   0.00000 ;  C5-  C6-  C7-   C8
14  16  19  21   3   0.00000   0.00000   0.00000   0.00000   0.00000   0.00000 ;  C5-  C6-  C7-   C9
15  14  16  17   3   3.68192  -4.35136   0.00000   1.33888   0.00000   0.00000 ;  O1-  C5-  C6-   H4
```

```
   15    14    16    18     3    3.68192   -4.35136    0.00000    1.33888    0.00000    0.00000 ;    O1-   C5-   C6-   H5
   15    14    16    19     3    0.00000    0.00000    0.00000    0.00000    0.00000    0.00000 ;    O1-   C5-   C6-   C7
   16    19    20    22     3   30.33400    0.00000  -30.33400    0.00000    0.00000    0.00000 ;    C6-   C7-   C8-  C10
   16    19    20    23     3   30.33400    0.00000  -30.33400    0.00000    0.00000    0.00000 ;    C6-   C7-   C8-   H6
   16    19    21    24     3   30.33400    0.00000  -30.33400    0.00000    0.00000    0.00000 ;    C6-   C7-   C9-  C11
   16    19    21    25     3   30.33400    0.00000  -30.33400    0.00000    0.00000    0.00000 ;    C6-   C7-   C9-   H7
   17    16    19    20     3    0.00000    0.00000    0.00000    0.00000    0.00000    0.00000 ;    H4-   C6-   C7-   C8
   17    16    19    21     3    0.00000    0.00000    0.00000    0.00000    0.00000    0.00000 ;    H4-   C6-   C7-   C9
   18    16    19    20     3    0.00000    0.00000    0.00000    0.00000    0.00000    0.00000 ;    H5-   C6-   C7-   C8
   18    16    19    21     3    0.00000    0.00000    0.00000    0.00000    0.00000    0.00000 ;    H5-   C6-   C7-   C9
   19    20    22    26     3   30.33400    0.00000  -30.33400    0.00000    0.00000    0.00000 ;    C7-   C8-  C10-  C12
   19    20    22    27     3   30.33400    0.00000  -30.33400    0.00000    0.00000    0.00000 ;    C7-   C8-  C10-   H8
   19    21    24    26     3   30.33400    0.00000  -30.33400    0.00000    0.00000    0.00000 ;    C7-   C9-  C11-  C12
   19    21    24    28     3   30.33400    0.00000  -30.33400    0.00000    0.00000    0.00000 ;    C7-   C9-  C11-   H9
   20    19    21    24     3   30.33400    0.00000  -30.33400    0.00000    0.00000    0.00000 ;    C8-   C7-   C9-  C11
   20    19    21    25     3   30.33400    0.00000  -30.33400    0.00000    0.00000    0.00000 ;    C8-   C7-   C9-   H7
   20    22    26    24     3   30.33400    0.00000  -30.33400    0.00000    0.00000    0.00000 ;    C8-  C10-  C12-  C11
   20    22    26    29     3   30.33400    0.00000  -30.33400    0.00000    0.00000    0.00000 ;    C8-  C10-  C12-  H10
   21    19    20    22     3   30.33400    0.00000  -30.33400    0.00000    0.00000    0.00000 ;    C9-   C7-   C8-  C10
   21    19    20    23     3   30.33400    0.00000  -30.33400    0.00000    0.00000    0.00000 ;    C9-   C7-   C8-   H6
   21    24    26    22     3   30.33400    0.00000  -30.33400    0.00000    0.00000    0.00000 ;    C9-  C11-  C12-  C10
   21    24    26    29     3   30.33400    0.00000  -30.33400    0.00000    0.00000    0.00000 ;    C9-  C11-  C12-  H10
   22    26    24    28     3   30.33400    0.00000  -30.33400    0.00000    0.00000    0.00000 ;   C10-  C12-  C11-   H9
   23    20    22    26     3   30.33400    0.00000  -30.33400    0.00000    0.00000    0.00000 ;    H6-   C8-  C10-  C12
   23    20    22    27     3   30.33400    0.00000  -30.33400    0.00000    0.00000    0.00000 ;    H6-   C8-  C10-   H8
   24    26    22    27     3   30.33400    0.00000  -30.33400    0.00000    0.00000    0.00000 ;   C11-  C12-  C10-   H8
   25    21    24    26     3   30.33400    0.00000  -30.33400    0.00000    0.00000    0.00000 ;    H7-   C9-  C11-  C12
   25    21    24    28     3   30.33400    0.00000  -30.33400    0.00000    0.00000    0.00000 ;    H7-   C9-  C11-   H9
   27    22    26    29     3   30.33400    0.00000  -30.33400    0.00000    0.00000    0.00000 ;    H8-  C10-  C12-  H10
   28    24    26    29     3   30.33400    0.00000  -30.33400    0.00000    0.00000    0.00000 ;    H9-  C11-  C12-  H10
   30     1     2     6     3    0.65084    1.95253    0.00000   -2.60338    0.00000    0.00000 ;   C13-   C-   C1-    S
   30     1     2    33     3    0.65084    1.95253    0.00000   -2.60338    0.00000    0.00000 ;   C13-   C-   C1-  C14
   30     1     2    37     3    0.65084    1.95253    0.00000   -2.60338    0.00000    0.00000 ;   C13-   C-   C1-  C15
   30     1     7     3     3    0.00000    0.00000    0.00000    0.00000    0.00000    0.00000 ;   C13-   C-   N-   C2
   30     1     7    10     3   10.46000   -3.34720   -7.11280    0.00000    0.00000    0.00000 ;   C13-   C-   N-   C4
   33     2    37    38     3    0.66944    2.00832    0.00000   -2.67776    0.00000    0.00000 ;   C14-   C1-  C15-  H14
   33     2    37    39     3    0.66944    2.00832    0.00000   -2.67776    0.00000    0.00000 ;   C14-   C1-  C15-  H15
   33     2    37    40     3    0.66944    2.00832    0.00000   -2.67776    0.00000    0.00000 ;   C14-   C1-  C15-  H16
   34    33     2    37     3    0.66944    2.00832    0.00000   -2.67776    0.00000    0.00000 ;   H11-  C14-   C1-  C15
   35    33     2    37     3    0.66944    2.00832    0.00000   -2.67776    0.00000    0.00000 ;   H12-  C14-   C1-  C15
   36    33     2    37     3    0.66944    2.00832    0.00000   -2.67776    0.00000    0.00000 ;   H13-  C14-   C1-  C15

[ dihedrals ] ; impropers
; treated as propers in GROMACS to use correct AMBER analytical function
;    i     j     k     l  func   phase     kd      pn
     1    31    30    32     1  180.00   4.60240   2 ;    C-    O2-   C13-    O3
     8     7    10    11     1  180.00  43.93200   2 ;    C3-    N-    C4-     O
    10     1     7     3     1  180.00   4.60240   2 ;    C4-    C-    N-    C2
    14     8    12    13     1  180.00   4.60240   2 ;    C5-    C3-    N1-    H3
    16    12    14    15     1  180.00  43.93200   2 ;    C6-    N1-    C5-    O1
    19    22    20    23     1  180.00   4.60240   2 ;    C7-   C10-    C8-    H6
    19    24    21    25     1  180.00   4.60240   2 ;    C7-   C11-    C9-    H7
    20    21    19    16     1  180.00   4.60240   2 ;    C8-    C9-    C7-    C6
    20    26    22    27     1  180.00   4.60240   2 ;    C8-   C12-   C10-    H8
    21    26    24    28     1  180.00   4.60240   2 ;    C9-   C12-   C11-    H9
    22    24    26    29     1  180.00   4.60240   2 ;   C10-   C11-   C12-   H10
```

SPG.gro

```
  70SPG      N  710   3.568   3.490   3.095
  70SPG      H  711   3.650   3.456   3.141
  70SPG     CA  712   3.582   3.552   2.964
  70SPG     HA  713   3.536   3.639   2.981
  70SPG     CB  714   3.727   3.577   2.925
  70SPG    HB1  715   3.733   3.624   2.837
  70SPG    HB2  716   3.778   3.491   2.921
  70SPG     OG  717   3.793   3.659   3.022
  70SPG     S1  718   4.192   3.726   3.176
  70SPG     C1  719   4.262   3.551   3.168
  70SPG     C2  720   4.142   3.464   3.118
  70SPG     N1  721   4.083   3.544   3.004
  70SPG     C3  722   4.059   3.687   3.055
  70SPG     C4  723   3.913   3.713   3.119
  70SPG     C5  724   3.803   3.658   3.022
  70SPG     O1  725   3.800   3.538   2.979
  70SPG     C6  726   4.378   3.549   3.063
  70SPG     C7  727   4.311   3.487   3.301
  70SPG     C8  728   4.189   3.302   3.085
  70SPG     O2  729   4.138   3.248   2.982
  70SPG     O3  730   4.269   3.255   3.178
  70SPG     N2  731   3.893   3.652   3.255
  70SPG     C9  732   3.904   3.745   3.366
  70SPG     O4  733   3.885   3.868   3.352
  70SPG    C10  734   3.934   3.671   3.502
  70SPG    C11  735   3.860   3.730   3.624
  70SPG    C12  736   3.830   3.649   3.736
  70SPG    C13  737   3.767   3.704   3.849
  70SPG    C14  738   3.732   3.841   3.852
  70SPG    C15  739   3.760   3.922   3.740
  70SPG    C16  740   3.824   3.867   3.627
  70SPG     H1  741   4.070   3.456   3.203
  70SPG     H2  742   3.986   3.505   2.982
  70SPG     H3  743   4.063   3.756   2.968
  70SPG     H4  744   3.896   3.822   3.133
  70SPG     H5  745   4.341   3.578   2.964
  70SPG     H6  746   4.459   3.618   3.092
  70SPG     H7  747   4.419   3.447   3.057
  70SPG     H8  748   4.411   3.522   3.330
  70SPG     H9  749   3.909   3.564   3.492
  70SPG    H10  750   4.043   3.677   3.519
  70SPG    H11  751   3.857   3.543   3.735
  70SPG    H12  752   3.744   3.640   3.936
  70SPG    H13  753   3.682   3.883   3.940
  70SPG    H14  754   3.732   4.028   3.741
  70SPG    H15  755   3.846   3.925   3.536
  70SPG    H16  756   3.949   3.564   3.267
  70SPG    H17  757   4.240   3.507   3.383
  70SPG    H18  758   4.306   3.375   3.268
  70SPG      C  759   3.505   3.484   2.850
  70SPG      O  760   3.494   3.539   2.741
```

SPG.top

```
[ defaults ]
; nbfunc        comb-rule       gen-pairs       fudgeLJ fudgeQQ
1               2               yes             0.5     0.8333

[ atomtypes ]
;name   bond_type     mass     charge   ptype   sigma         epsilon       Amb
 n       n          0.00000  0.00000   A     3.25000e-01   7.11280e-01 ; 1.82  0.1700
 hn      hn         0.00000  0.00000   A     1.06908e-01   6.56888e-02 ; 0.60  0.0157
 c3      c3         0.00000  0.00000   A     3.39967e-01   4.57730e-01 ; 1.91  0.1094
```

```
 h1      h1        0.00000  0.00000   A     2.47135e-01   6.56888e-02 ; 1.39  0.0157
 os      os        0.00000  0.00000   A     3.00001e-01   7.11280e-01 ; 1.68  0.1700
 ss      ss        0.00000  0.00000   A     3.56359e-01   1.04600e+00 ; 2.00  0.2500
 n3      n3        0.00000  0.00000   A     3.25000e-01   7.11280e-01 ; 1.82  0.1700
 c       c         0.00000  0.00000   A     3.39967e-01   3.59824e-01 ; 1.91  0.0860
 o       o         0.00000  0.00000   A     2.95992e-01   8.78640e-01 ; 1.66  0.2100
 ca      ca        0.00000  0.00000   A     3.39967e-01   3.59824e-01 ; 1.91  0.0860
 h2      h2        0.00000  0.00000   A     2.29317e-01   6.56888e-02 ; 1.29  0.0157
 hc      hc        0.00000  0.00000   A     2.64953e-01   6.56888e-02 ; 1.49  0.0157
 ha      ha        0.00000  0.00000   A     2.59964e-01   6.27600e-02 ; 1.46  0.0150

[ moleculetype ]
;name          nrexcl
 SPG           3

[ atoms ]
;   nr  type  resi  res  atom  cgnr    charge     mass      ; qtot   bond_type
710       N         70        SPG       N         1         -0.4157              14.01
711       H         70        SPG       H         2         0.2719               1.008
712       CT        70        SPG       CA        3         -0.0349              12.01
713       H1        70        SPG       HA        4         0.0853               1.008
714       CT        70        SPG       CB        5         0.1334               12.01
715       H1        70        SPG       HB1       6         0.0897               1.008
716       H1        70        SPG       HB2       7         0.0897               1.008
717       os        70        SPG       OG        8         -0.4439              16
718       ss        70        SPG       S1        9         -0.4702              32.06
719       c3        70        SPG       C1        10        0.0821               12.01
720       c3        70        SPG       C2        11        0.0145               12.01
721       n3        70        SPG       N1        12        -0.796201            14.01
722       c3        70        SPG       C3        13        0.2936               12.01
723       c3        70        SPG       C4        14        0.0877               12.01
724       c         70        SPG       C5        15        0.620101 12.01
725       o         70        SPG       O1        16        -0.554001            16
726       c3        70        SPG       C6        17        -0.0811              12.01
727       c3        70        SPG       C7        18        -0.0811              12.01
728       c         70        SPG       C8        19        0.935602 12.01
729       o         70        SPG       O2        20        -0.821301            16
730       o         70        SPG       O3        21        -0.821301            16
731       n         70        SPG       N2        22        -0.531901            14.01
732       c         70        SPG       C9        23        0.672101 12.01
733       o         70        SPG       O4        24        -0.660101            16
734       c3        70        SPG       C10       25        -0.0971   12.01
735       ca        70        SPG       C11       26        -0.1133   12.01
736       ca        70        SPG       C12       27        -0.133    12.01
737       ca        70        SPG       C13       28        -0.1215   12.01
738       ca        70        SPG       C14       29        -0.124    12.01
739       ca        70        SPG       C15       30        -0.1215   12.01
740       ca        70        SPG       C16       31        -0.133    12.01
741       h1        70        SPG       H1        32        0.0577    1.008
742       hn        70        SPG       H2        33        0.4038    1.008
743       h2        70        SPG       H3        34        0.0857    1.008
744       h1        70        SPG       H4        35        0.1137    1.008
745       hc        70        SPG       H5        36        0.0452    1.008
746       hc        70        SPG       H6        37        0.0452    1.008
747       hc        70        SPG       H7        38        0.0452    1.008
748       hc        70        SPG       H8        39        0.0452    1.008
749       hc        70        SPG       H9        40        0.0747    1.008
750       hc        70        SPG       H10       41        0.0747    1.008
751       ha        70        SPG       H11       42        0.132     1.008
752       ha        70        SPG       H12       43        0.1575    1.008
753       ha        70        SPG       H13       44        0.134     1.008
754       ha        70        SPG       H14       45        0.1575    1.008
755       ha        70        SPG       H15       46        0.132     1.008
756       hn        70        SPG       H16       47        0.3555    1.008
757       hc        70        SPG       H17       48        0.0452    1.008
758       hc        70        SPG       H18       49        0.0452    1.008
759       C         70        SPG       C         50        0.5973    12.01
760       O         70        SPG       O         51        -0.5679   16
```

```
[ bonds ]
;   ai    aj funct   r             k
714       717       1       1.4316E-01      2.5824E+05      ;       CB      -       OG
717       724       1       1.3584E-01      3.2702E+05      ;       OG      -       C5
718       719       1       1.8392E-01      1.8067E+05      ;       S1      -       C1
718       722       1       1.8392E-01      1.8067E+05      ;       S1      -       C3
719       720       1       1.5375E-01      2.5179E+05      ;       C1      -       C2
719       726       1       1.5375E-01      2.5179E+05      ;       C1      -       C6
719       727       1       1.5375E-01      2.5179E+05      ;       C1      -       C7
720       721       1       1.4647E-01      2.7271E+05      ;       C2      -       N1
720       728       1       1.5241E-01      2.6192E+05      ;       C2      -       C8
720       741       1       1.0969E-01      2.7665E+05      ;       C2      -       H1
721       722       1       1.4647E-01      2.7271E+05      ;       N1      -       C3
721       742       1       1.0190E-01      3.2836E+05      ;       N1      -       H2
722       723       1       1.5375E-01      2.5179E+05      ;       C3      -       C4
722       743       1       1.0961E-01      2.7757E+05      ;       C3      -       H3
723       724       1       1.5241E-01      2.6192E+05      ;       C4      -       C5
723       731       1       1.4619E-01      2.7506E+05      ;       C4      -       N2
723       744       1       1.0969E-01      2.7665E+05      ;       C4      -       H4
724       725       1       1.2183E-01      5.3363E+05      ;       C5      -       O1
726       745       1       1.0969E-01      2.7665E+05      ;       C6      -       H5
726       746       1       1.0969E-01      2.7665E+05      ;       C6      -       H6
726       747       1       1.0969E-01      2.7665E+05      ;       C6      -       H7
727       748       1       1.0969E-01      2.7665E+05      ;       C7      -       H8
727       757       1       1.0969E-01      2.7665E+05      ;       C7      -       H17
727       758       1       1.0969E-01      2.7665E+05      ;       C7      -       H18
728       729       1       1.2183E-01      5.3363E+05      ;       C8      -       O2
728       730       1       1.2183E-01      5.3363E+05      ;       C8      -       O3
731       732       1       1.3789E-01      3.5782E+05      ;       N2      -       C9
731       756       1       1.0129E-01      3.3740E+05      ;       N2      -       H16
732       733       1       1.2183E-01      5.3363E+05      ;       C9      -       O4
732       734       1       1.5241E-01      2.6192E+05      ;       C9      -       C10
734       735       1       1.5156E-01      2.6861E+05      ;       C10     -       C11
734       749       1       1.0969E-01      2.7665E+05      ;       C10     -       H9
734       750       1       1.0969E-01      2.7665E+05      ;       C10     -       H10
735       736       1       1.3984E-01      3.8585E+05      ;       C11     -       C12
735       740       1       1.3984E-01      3.8585E+05      ;       C11     -       C16
736       737       1       1.3984E-01      3.8585E+05      ;       C12     -       C13
736       751       1       1.0860E-01      2.8937E+05      ;       C12     -       H11
737       738       1       1.3984E-01      3.8585E+05      ;       C13     -       C14
737       752       1       1.0860E-01      2.8937E+05      ;       C13     -       H12
738       739       1       1.3984E-01      3.8585E+05      ;       C14     -       C15
738       753       1       1.0860E-01      2.8937E+05      ;       C14     -       H13
739       740       1       1.3984E-01      3.8585E+05      ;       C15     -       C16
739       754       1       1.0860E-01      2.8937E+05      ;       C15     -       H14
740       755       1       1.0860E-01      2.8937E+05      ;       C16     -       H15

[ pairs ]
;   ai    aj    funct
710       717       1       ;       N       -       OG
712       724       1       ;       CA      -       C5
713       717       1       ;       HA      -       OG
714       723       1       ;       CB      -       C4
714       725       1       ;       CB      -       O1
715       724       1       ;       HB1     -       C5
716       724       1       ;       HB2     -       C5
717       722       1       ;       OG      -       C3
717       731       1       ;       OG      -       N2
717       744       1       ;       OG      -       H4
717       759       1       ;       OG      -       C
718       724       1       ;       S1      -       C5
718       728       1       ;       S1      -       C8
718       731       1       ;       S1      -       N2
718       741       1       ;       S1      -       H1
718       742       1       ;       S1      -       H2
718       744       1       ;       S1      -       H4
718       745       1       ;       S1      -       H5
718       746       1       ;       S1      -       H6
718       747       1       ;       S1      -       H7
718       748       1       ;       S1      -       H8
```

718	757	1	;	S1	-	H17
718	758	1	;	S1	-	H18
719	723	1	;	C1	-	C4
719	729	1	;	C1	-	O2
719	730	1	;	C1	-	O3
719	742	1	;	C1	-	H2
719	743	1	;	C1	-	H3
720	723	1	;	C2	-	C4
720	743	1	;	C2	-	H3
720	745	1	;	C2	-	H5
720	746	1	;	C2	-	H6
720	747	1	;	C2	-	H7
720	748	1	;	C2	-	H8
720	757	1	;	C2	-	H17
720	758	1	;	C2	-	H18
721	724	1	;	N1	-	C5
721	726	1	;	N1	-	C6
721	727	1	;	N1	-	C7
721	729	1	;	N1	-	O2
721	730	1	;	N1	-	O3
721	731	1	;	N1	-	N2
721	744	1	;	N1	-	H4
722	725	1	;	C3	-	O1
722	726	1	;	C3	-	C6
722	727	1	;	C3	-	C7
722	728	1	;	C3	-	C8
722	732	1	;	C3	-	C9
722	741	1	;	C3	-	H1
722	756	1	;	C3	-	H16
723	733	1	;	C4	-	O4
723	734	1	;	C4	-	C10
723	742	1	;	C4	-	H2
724	732	1	;	C5	-	C9
724	743	1	;	C5	-	H3
724	756	1	;	C5	-	H16
725	731	1	;	O1	-	N2
725	744	1	;	O1	-	H4
726	728	1	;	C6	-	C8
726	741	1	;	C6	-	H1
726	748	1	;	C6	-	H8
726	757	1	;	C6	-	H17
726	758	1	;	C6	-	H18
727	728	1	;	C7	-	C8
727	741	1	;	C7	-	H1
727	745	1	;	C7	-	H5
727	746	1	;	C7	-	H6
727	747	1	;	C7	-	H7
728	742	1	;	C8	-	H2
729	741	1	;	O2	-	H1
730	741	1	;	O3	-	H1
731	735	1	;	N2	-	C11
731	743	1	;	N2	-	H3
731	749	1	;	N2	-	H9
731	750	1	;	N2	-	H10
732	736	1	;	C9	-	C12
732	740	1	;	C9	-	C16
732	744	1	;	C9	-	H4
733	735	1	;	O4	-	C11
733	749	1	;	O4	-	H9
733	750	1	;	O4	-	H10
733	756	1	;	O4	-	H16
734	737	1	;	C10	-	C13
734	739	1	;	C10	-	C15
734	751	1	;	C10	-	H11
734	755	1	;	C10	-	H15
734	756	1	;	C10	-	H16
735	738	1	;	C11	-	C14
735	752	1	;	C11	-	H12
735	754	1	;	C11	-	H14
736	739	1	;	C12	-	C15

```
736     749     1       ;       C12     -       H9
736     750     1       ;       C12     -       H10
736     753     1       ;       C12     -       H13
736     755     1       ;       C12     -       H15
737     740     1       ;       C13     -       C16
737     754     1       ;       C13     -       H14
738     751     1       ;       C14     -       H11
738     755     1       ;       C14     -       H15
739     752     1       ;       C15     -       H12
740     749     1       ;       C16     -       H9
740     750     1       ;       C16     -       H10
740     751     1       ;       C16     -       H11
740     753     1       ;       C16     -       H13
741     742     1       ;       H1      -       H2
742     743     1       ;       H2      -       H3
743     744     1       ;       H3      -       H4
744     756     1       ;       H4      -       H16
751     752     1       ;       H11     -       H12
752     753     1       ;       H12     -       H13
753     754     1       ;       H13     -       H14
754     755     1       ;       H14     -       H15

[ angles ]
;  ai   aj   ak   funct   theta       cth
712     714     717     1       1.0797E+02      5.6902E+02      ;       CA      -       CB      -
        OG
714     717     724     1       1.1598E+02      5.2969E+02      ;       CB      -       OG      -
        C5
715     714     717     1       1.0978E+02      4.2509E+02      ;       HB1     -       CB      -
        OG
716     714     717     1       1.0978E+02      4.2509E+02      ;       HB2     -       CB      -
        OG
717     724     723     1       1.1072E+02      5.7656E+02      ;       OG      -       C5      -
        C4
717     724     725     1       1.2325E+02      6.3011E+02      ;       OG      -       C5      -
        O1
718     719     720     1       1.1027E+02      5.1296E+02      ;       S1      -       C1      -
        C2
718     719     726     1       1.1027E+02      5.1296E+02      ;       S1      -       C1      -
        C6
718     719     727     1       1.1027E+02      5.1296E+02      ;       S1      -       C1      -
        C7
718     722     721     1       1.0738E+02      5.3890E+02      ;       S1      -       C3      -
        N1
718     722     723     1       1.1027E+02      5.1296E+02      ;       S1      -       C3      -
        C4
718     722     743     1       1.0833E+02      3.5229E+02      ;       S1      -       C3      -
        H3
719     718     722     1       9.9240E+01      5.0375E+02      ;       C1      -       S1      -
        C3
719     720     721     1       1.1104E+02      5.5229E+02      ;       C1      -       C2      -
        N1
719     720     728     1       1.1104E+02      5.2969E+02      ;       C1      -       C2      -
        C8
719     720     741     1       1.0956E+02      3.8828E+02      ;       C1      -       C2      -
        H1
719     726     745     1       1.0980E+02      3.8744E+02      ;       C1      -       C6      -
        H5
719     726     746     1       1.0980E+02      3.8744E+02      ;       C1      -       C6      -
        H6
719     726     747     1       1.0980E+02      3.8744E+02      ;       C1      -       C6      -
        H7
719     727     748     1       1.0980E+02      3.8744E+02      ;       C1      -       C7      -
        H8
719     727     757     1       1.0980E+02      3.8744E+02      ;       C1      -       C7      -
        H17
719     727     758     1       1.0980E+02      3.8744E+02      ;       C1      -       C7      -
        H18
720     719     726     1       1.1151E+02      5.2635E+02      ;       C2      -       C1      -
        C6
```

720	719	727	1	1.1151E+02	5.2635E+02	;	C2	-	C1	-
	C7									
720	721	722	1	1.1235E+02	5.3388E+02	;	C2	-	N1	-
	C3									
720	721	742	1	1.0929E+02	3.9664E+02	;	C2	-	N1	-
	H2									
720	728	729	1	1.2320E+02	5.6400E+02	;	C2	-	C8	-
	O2									
720	728	730	1	1.2320E+02	5.6400E+02	;	C2	-	C8	-
	O3									
721	720	728	1	1.1114E+02	5.5480E+02	;	N1	-	C2	-
	C8									
721	720	741	1	1.0988E+02	4.1422E+02	;	N1	-	C2	-
	H1									
721	722	723	1	1.1104E+02	5.5229E+02	;	N1	-	C3	-
	C4									
721	722	743	1	1.0935E+02	4.1505E+02	;	N1	-	C3	-
	H3									
722	721	742	1	1.0929E+02	3.9664E+02	;	C3	-	N1	-
	H2									
722	723	724	1	1.1104E+02	5.2969E+02	;	C3	-	C4	-
	C5									
722	723	731	1	1.1161E+02	5.5145E+02	;	C3	-	C4	-
	N2									
722	723	744	1	1.0956E+02	3.8828E+02	;	C3	-	C4	-
	H4									
723	722	743	1	1.1022E+02	3.8660E+02	;	C4	-	C3	-
	H3									
723	724	725	1	1.2320E+02	5.6400E+02	;	C4	-	C5	-
	O1									
723	731	732	1	1.2069E+02	5.3053E+02	;	C4	-	N2	-
	C9									
723	731	756	1	1.1768E+02	3.8325E+02	;	C4	-	N2	-
	H16									
724	723	731	1	1.0906E+02	5.6066E+02	;	C5	-	C4	-
	N2									
724	723	744	1	1.0822E+02	3.9330E+02	;	C5	-	C4	-
	H4									
726	719	727	1	1.1151E+02	5.2635E+02	;	C6	-	C1	-
	C7									
728	720	741	1	1.0822E+02	3.9330E+02	;	C8	-	C2	-
	H1									
729	728	730	1	1.3025E+02	6.5187E+02	;	O2	-	C8	-
	O3									
731	723	744	1	1.0888E+02	4.1673E+02	;	N2	-	C4	-
	H4									
731	732	733	1	1.2305E+02	6.2091E+02	;	N2	-	C9	-
	O4									
731	732	734	1	1.1518E+02	5.5898E+02	;	N2	-	C9	-
	C10									
732	731	756	1	1.1755E+02	4.0417E+02	;	C9	-	N2	-
	H16									
732	734	735	1	1.1101E+02	5.3304E+02	;	C9	-	C10	-
	C11									
732	734	749	1	1.0877E+02	3.9246E+02	;	C9	-	C10	-
	H9									
732	734	750	1	1.0877E+02	3.9246E+02	;	C9	-	C10	-
	H10									
733	732	734	1	1.2320E+02	5.6400E+02	;	O4	-	C9	-
	C10									
734	735	736	1	1.2077E+02	5.3137E+02	;	C10	-	C11	-
	C12									
734	735	740	1	1.2077E+02	5.3137E+02	;	C10	-	C11	-
	C16									
735	734	749	1	1.1047E+02	3.9162E+02	;	C11	-	C10	-
	H9									
735	734	750	1	1.1047E+02	3.9162E+02	;	C11	-	C10	-
	H10									
735	736	737	1	1.2002E+02	5.5731E+02	;	C11	-	C12	-
	C13									

```
735     736     751     1       1.1988E+02      4.0334E+02      ;       C11     -       C12     -
        H11
735     740     739     1       1.2002E+02      5.5731E+02      ;       C11     -       C16     -
        C15
735     740     755     1       1.1988E+02      4.0334E+02      ;       C11     -       C16     -
        H15
736     735     740     1       1.2002E+02      5.5731E+02      ;       C12     -       C11     -
        C16
736     737     738     1       1.2002E+02      5.5731E+02      ;       C12     -       C13     -
        C14
736     737     752     1       1.1988E+02      4.0334E+02      ;       C12     -       C13     -
        H12
737     736     751     1       1.1988E+02      4.0334E+02      ;       C13     -       C12     -
        H11
737     738     739     1       1.2002E+02      5.5731E+02      ;       C13     -       C14     -
        C15
737     738     753     1       1.1988E+02      4.0334E+02      ;       C13     -       C14     -
        H13
738     737     752     1       1.1988E+02      4.0334E+02      ;       C14     -       C13     -
        H12
738     739     740     1       1.2002E+02      5.5731E+02      ;       C14     -       C15     -
        C16
738     739     754     1       1.1988E+02      4.0334E+02      ;       C14     -       C15     -
        H14
739     738     753     1       1.1988E+02      4.0334E+02      ;       C15     -       C14     -
        H13
739     740     755     1       1.1988E+02      4.0334E+02      ;       C15     -       C16     -
        H15
740     739     754     1       1.1988E+02      4.0334E+02      ;       C16     -       C15     -
        H14
745     726     746     1       1.0758E+02      3.2970E+02      ;       H5      -       C6      -
        H6
745     726     747     1       1.0758E+02      3.2970E+02      ;       H5      -       C6      -
        H7
746     726     747     1       1.0758E+02      3.2970E+02      ;       H6      -       C6      -
        H7
748     727     757     1       1.0758E+02      3.2970E+02      ;       H8      -       C7      -
        H17
748     727     758     1       1.0758E+02      3.2970E+02      ;       H8      -       C7      -
        H18
749     734     750     1       1.0758E+02      3.2970E+02      ;       H9      -       C10     -
        H10
757     727     758     1       1.0758E+02      3.2970E+02      ;       H17     -       C7      -
        H18


[ dihedrals ] ; propers
; treated as RBs in GROMACS to use combine multiple AMBER torsions per quartet
;   i     j     k     l   func    C0          C1          C2          C3          C4          C5
710     712     714     717     3       0.65084     1.95253     0.00000     -2.60338    0.00000     0.00000     ;       N-
        CA-     CB-     OG
712     714     717     724     3       4.94967     8.15462     0.00000     -6.40989    0.00000     0.00000     ;       CA-
        CB-     OG-     C5
713     712     714     717     3       1.04600     -1.04600    0.00000     0.00000     0.00000     0.00000     ;       HA-
        CA-     CB-     OG
714     717     724     723     3       27.40520    14.43480    -22.59360               -19.24640               0.00000 0.00000
        ;       CB-     OG-     C5-     C4
714     717     724     725     3       28.45120    5.85760     -22.59360               0.00000     0.00000     0.00000 ;
        CB-     OG-     C5-     O1
715     714     717     724     3       1.60387     4.81160     0.00000     -6.41547    0.00000     0.00000     ;       HB1-
        CB-     OG-     C5
716     714     717     724     3       1.60387     4.81160     0.00000     -6.41547    0.00000     0.00000     ;       HB2-
        CB-     OG-     C5
717     724     723     722     3       0.00000     0.00000     0.00000     0.00000     0.00000     0.00000     ;       OG-
        C5-     C4-     C3
717     724     723     731     3       0.00000     0.00000     0.00000     0.00000     0.00000     0.00000     ;       OG-
        C5-     C4-     N2
717     724     723     744     3       0.00000     0.00000     0.00000     0.00000     0.00000     0.00000     ;       OG-
        C5-     C4-     H4
```

718	719	720	721	3	0.65084	1.95253	0.00000	-2.60338	0.00000	0.00000	;	S1-
	C1-	C2-	N1									
718	719	720	728	3	0.65084	1.95253	0.00000	-2.60338	0.00000	0.00000	;	S1-
	C1-	C2-	C8									
718	719	720	741	3	0.65084	1.95253	0.00000	-2.60338	0.00000	0.00000	;	S1-
	C1-	C2-	H1									
718	719	726	745	3	0.65084	1.95253	0.00000	-2.60338	0.00000	0.00000	;	S1-
	C1-	C6-	H5									
718	719	726	746	3	0.65084	1.95253	0.00000	-2.60338	0.00000	0.00000	;	S1-
	C1-	C6-	H6									
718	719	726	747	3	0.65084	1.95253	0.00000	-2.60338	0.00000	0.00000	;	S1-
	C1-	C6-	H7									
718	719	727	748	3	0.65084	1.95253	0.00000	-2.60338	0.00000	0.00000	;	S1-
	C1-	C7-	H8									
718	719	727	757	3	0.65084	1.95253	0.00000	-2.60338	0.00000	0.00000	;	S1-
	C1-	C7-	H17									
718	719	727	758	3	0.65084	1.95253	0.00000	-2.60338	0.00000	0.00000	;	S1-
	C1-	C7-	H18									
718	722	721	720	3	1.25520	3.76560	0.00000	-5.02080	0.00000	0.00000	;	S1-
	C3-	N1-	C2									
718	722	721	742	3	1.25520	3.76560	0.00000	-5.02080	0.00000	0.00000	;	S1-
	C3-	N1-	H2									
718	722	723	724	3	0.65084	1.95253	0.00000	-2.60338	0.00000	0.00000	;	S1-
	C3-	C4-	C5									
718	722	723	731	3	0.65084	1.95253	0.00000	-2.60338	0.00000	0.00000	;	S1-
	C3-	C4-	N2									
718	722	723	744	3	0.65084	1.95253	0.00000	-2.60338	0.00000	0.00000	;	S1-
	C3-	C4-	H4									
719	718	722	721	3	1.39467	4.18400	0.00000	-5.57867	0.00000	0.00000	;	C1-
	S1-	C3-	N1									
719	718	722	723	3	1.39467	4.18400	0.00000	-5.57867	0.00000	0.00000	;	C1-
	S1-	C3-	C4									
719	718	722	743	3	1.39467	4.18400	0.00000	-5.57867	0.00000	0.00000	;	C1-
	S1-	C3-	H3									
719	720	721	722	3	5.27184	3.76560	-4.01664	-5.02080	0.00000	0.00000	;	C1-
	C2-	N1-	C3									
719	720	721	742	3	1.25520	3.76560	0.00000	-5.02080	0.00000	0.00000	;	C1-
	C2-	N1-	H2									
719	720	728	729	3	0.00000	0.00000	0.00000	0.00000	0.00000	0.00000	;	C1-
	C2-	C8-	O2									
719	720	728	730	3	0.00000	0.00000	0.00000	0.00000	0.00000	0.00000	;	C1-
	C2-	C8-	O3									
720	719	718	722	3	1.39467	4.18400	0.00000	-5.57867	0.00000	0.00000	;	C2-
	C1-	S1-	C3									
720	719	726	745	3	0.66944	2.00832	0.00000	-2.67776	0.00000	0.00000	;	C2-
	C1-	C6-	H5									
720	719	726	746	3	0.66944	2.00832	0.00000	-2.67776	0.00000	0.00000	;	C2-
	C1-	C6-	H6									
720	719	726	747	3	0.66944	2.00832	0.00000	-2.67776	0.00000	0.00000	;	C2-
	C1-	C6-	H7									
720	719	727	748	3	0.66944	2.00832	0.00000	-2.67776	0.00000	0.00000	;	C2-
	C1-	C7-	H8									
720	719	727	757	3	0.66944	2.00832	0.00000	-2.67776	0.00000	0.00000	;	C2-
	C1-	C7-	H17									
720	719	727	758	3	0.66944	2.00832	0.00000	-2.67776	0.00000	0.00000	;	C2-
	C1-	C7-	H18									
720	721	722	723	3	5.27184	3.76560	-4.01664	-5.02080	0.00000	0.00000	;	C2-
	N1-	C3-	C4									
720	721	722	743	3	1.25520	3.76560	0.00000	-5.02080	0.00000	0.00000	;	C2-
	N1-	C3-	H3									
721	720	719	726	3	0.65084	1.95253	0.00000	-2.60338	0.00000	0.00000	;	N1-
	C2-	C1-	C6									
721	720	719	727	3	0.65084	1.95253	0.00000	-2.60338	0.00000	0.00000	;	N1-
	C2-	C1-	C7									
721	720	728	729	3	0.00000	0.00000	0.00000	0.00000	0.00000	0.00000	;	N1-
	C2-	C8-	O2									
721	720	728	730	3	0.00000	0.00000	0.00000	0.00000	0.00000	0.00000	;	N1-
	C2-	C8-	O3									
721	722	723	724	3	0.65084	1.95253	0.00000	-2.60338	0.00000	0.00000	;	N1-
	C3-	C4-	C5									

721	722 C3-	723 C4-	731 N2	3	0.65084	1.95253	0.00000	-2.60338	0.00000	0.00000	;	N1-
721	722 C3-	723 C4-	744 H4	3	0.65084	1.95253	0.00000	-2.60338	0.00000	0.00000	;	N1-
722	718 S1-	719 C1-	726 C6	3	1.39467	4.18400	0.00000	-5.57867	0.00000	0.00000	;	C3-
722	718 S1-	719 C1-	727 C7	3	1.39467	4.18400	0.00000	-5.57867	0.00000	0.00000	;	C3-
722	721 N1-	720 C2-	728 C8	3	1.25520	3.76560	0.00000	-5.02080	0.00000	0.00000	;	C3-
722	721 N1-	720 C2-	741 H1	3	1.25520	3.76560	0.00000	-5.02080	0.00000	0.00000	;	C3-
722	723 C4-	724 C5-	725 O1	3	0.00000	0.00000	0.00000	0.00000	0.00000	0.00000	;	C3-
722	723 C3-	731 C4-	732 N2-	3 C9	2.84512	-4.10032	16.73600	2.51040	-16.73600	0.00000	;	
722	723 C4-	731 N2-	756 H16	3	0.00000	0.00000	0.00000	0.00000	0.00000	0.00000	;	C3-
723	722 C3-	721 N1-	742 H2	3	1.25520	3.76560	0.00000	-5.02080	0.00000	0.00000	;	C4-
723	731 C4-	732 N2-	733 C9-	3 O4	20.92000	0.00000	-20.92000		0.00000	0.00000	0.00000	;
723	731 N2-	732 C9-	734 C10	3	6.27600	6.27600	0.00000	0.00000	0.00000	0.00000	;	C4-
724	723 C4-	722 C3-	743 H3	3	0.65084	1.95253	0.00000	-2.60338	0.00000	0.00000	;	C5-
724	723 C4-	731 N2-	732 C9	3	10.46000	-3.34720	-7.11280	0.00000	0.00000	0.00000	;	C5-
724	723 C4-	731 N2-	756 H16	3	0.00000	0.00000	0.00000	0.00000	0.00000	0.00000	;	C5-
725	724 C5-	723 C4-	731 N2	3	0.00000	0.00000	0.00000	0.00000	0.00000	0.00000	;	O1-
725	724 C5-	723 C4-	744 H4	3	3.68192	-4.35136	0.00000	1.33888	0.00000	0.00000	;	O1-
726	719 C1-	720 C2-	728 C8	3	0.65084	1.95253	0.00000	-2.60338	0.00000	0.00000	;	C6-
726	719 C1-	720 C2-	741 H1	3	0.65084	1.95253	0.00000	-2.60338	0.00000	0.00000	;	C6-
726	719 C1-	727 C7-	748 H8	3	0.66944	2.00832	0.00000	-2.67776	0.00000	0.00000	;	C6-
726	719 C1-	727 C7-	757 H17	3	0.66944	2.00832	0.00000	-2.67776	0.00000	0.00000	;	C6-
726	719 C1-	727 C7-	758 H18	3	0.66944	2.00832	0.00000	-2.67776	0.00000	0.00000	;	C6-
727	719 C1-	720 C2-	728 C8	3	0.65084	1.95253	0.00000	-2.60338	0.00000	0.00000	;	C7-
727	719 C1-	720 C2-	741 H1	3	0.65084	1.95253	0.00000	-2.60338	0.00000	0.00000	;	C7-
727	719 C1-	726 C6-	745 H5	3	0.66944	2.00832	0.00000	-2.67776	0.00000	0.00000	;	C7-
727	719 C1-	726 C6-	746 H6	3	0.66944	2.00832	0.00000	-2.67776	0.00000	0.00000	;	C7-
727	719 C1-	726 C6-	747 H7	3	0.66944	2.00832	0.00000	-2.67776	0.00000	0.00000	;	C7-
728	720 C2-	721 N1-	742 H2	3	1.25520	3.76560	0.00000	-5.02080	0.00000	0.00000	;	C8-
729	728 C8-	720 C2-	741 H1	3	3.68192	-4.35136	0.00000	1.33888	0.00000	0.00000	;	O2-
730	728 C8-	720 C2-	741 H1	3	3.68192	-4.35136	0.00000	1.33888	0.00000	0.00000	;	O3-
731	723 C4-	722 C3-	743 H3	3	0.65084	1.95253	0.00000	-2.60338	0.00000	0.00000	;	N2-
731	732 C9-	734 C10-	735 C11	3	0.00000	0.00000	0.00000	0.00000	0.00000	0.00000	;	N2-
731	732 C9-	734 C10-	749 H9	3	0.00000	0.00000	0.00000	0.00000	0.00000	0.00000	;	N2-
731	732 C9-	734 C10-	750 H10	3	0.00000	0.00000	0.00000	0.00000	0.00000	0.00000	;	N2-
732	731 N2-	723 C4-	744 H4	3	0.00000	0.00000	0.00000	0.00000	0.00000	0.00000	;	C9-

732	734 C10-	735 C11-	736 C12	3	0.00000	0.00000	0.00000	0.00000	0.00000	0.00000	;	C9-
732	734 C10-	735 C11-	740 C16	3	0.00000	0.00000	0.00000	0.00000	0.00000	0.00000	;	C9-
733	732 O4-	731 C9-	756 N2-	3 H16	29.28800	-8.36800	-20.92000		0.00000	0.00000	0.00000	;
733	732 C9-	734 C10-	735 C11	3	0.00000	0.00000	0.00000	0.00000	0.00000	0.00000	;	O4-
733	732 C9-	734 C10-	749 H9	3	3.68192	-4.35136	0.00000	1.33888	0.00000	0.00000	;	O4-
733	732 C9-	734 C10-	750 H10	3	3.68192	-4.35136	0.00000	1.33888	0.00000	0.00000	;	O4-
734	732 C10-	731 C9-	756 N2-	3 H16	20.92000	0.00000	-20.92000		0.00000	0.00000	0.00000	;
734	735 C10-	736 C11-	737 C12-	3 C13	30.33400	0.00000	-30.33400		0.00000	0.00000	0.00000	;
734	735 C10-	736 C11-	751 C12-	3 H11	30.33400	0.00000	-30.33400		0.00000	0.00000	0.00000	;
734	735 C10-	740 C11-	739 C16-	3 C15	30.33400	0.00000	-30.33400		0.00000	0.00000	0.00000	;
734	735 C10-	740 C11-	755 C16-	3 H15	30.33400	0.00000	-30.33400		0.00000	0.00000	0.00000	;
735	736 C11-	737 C12-	738 C13-	3 C14	30.33400	0.00000	-30.33400		0.00000	0.00000	0.00000	;
735	736 C11-	737 C12-	752 C13-	3 H12	30.33400	0.00000	-30.33400		0.00000	0.00000	0.00000	;
735	740 C11-	739 C16-	738 C15-	3 C14	30.33400	0.00000	-30.33400		0.00000	0.00000	0.00000	;
735	740 C11-	739 C16-	754 C15-	3 H14	30.33400	0.00000	-30.33400		0.00000	0.00000	0.00000	;
736	735 C11-	734 C10-	749 H9	3	0.00000	0.00000	0.00000	0.00000	0.00000	0.00000	;	C12-
736	735 C11-	734 C10-	750 H10	3	0.00000	0.00000	0.00000	0.00000	0.00000	0.00000	;	C12-
736	735 C12-	740 C11-	739 C16-	3 C15	30.33400	0.00000	-30.33400		0.00000	0.00000	0.00000	;
736	735 C12-	740 C11-	755 C16-	3 H15	30.33400	0.00000	-30.33400		0.00000	0.00000	0.00000	;
736	737 C12-	738 C13-	739 C14-	3 C15	30.33400	0.00000	-30.33400		0.00000	0.00000	0.00000	;
736	737 C12-	738 C13-	753 C14-	3 H13	30.33400	0.00000	-30.33400		0.00000	0.00000	0.00000	;
737	736 C13-	735 C12-	740 C11-	3 C16	30.33400	0.00000	-30.33400		0.00000	0.00000	0.00000	;
737	738 C13-	739 C14-	740 C15-	3 C16	30.33400	0.00000	-30.33400		0.00000	0.00000	0.00000	;
737	738 C13-	739 C14-	754 C15-	3 H14	30.33400	0.00000	-30.33400		0.00000	0.00000	0.00000	;
738	737 C14-	736 C13-	751 C12-	3 H11	30.33400	0.00000	-30.33400		0.00000	0.00000	0.00000	;
738	739 C14-	740 C15-	755 C16-	3 H15	30.33400	0.00000	-30.33400		0.00000	0.00000	0.00000	;
739	738 C15-	737 C14-	752 C13-	3 H12	30.33400	0.00000	-30.33400		0.00000	0.00000	0.00000	;
740	735 C11-	734 C10-	749 H9	3	0.00000	0.00000	0.00000	0.00000	0.00000	0.00000	;	C16-
740	735 C11-	734 C10-	750 H10	3	0.00000	0.00000	0.00000	0.00000	0.00000	0.00000	;	C16-
740	735 C16-	736 C11-	751 C12-	3 H11	30.33400	0.00000	-30.33400		0.00000	0.00000	0.00000	;
740	739 C16-	738 C15-	753 C14-	3 H13	30.33400	0.00000	-30.33400		0.00000	0.00000	0.00000	;
741	720 C2-	721 N1-	742 H2	3	1.25520	3.76560	0.00000	-5.02080	0.00000	0.00000	;	H1-
742	721 N1-	722 C3-	743 H3	3	1.25520	3.76560	0.00000	-5.02080	0.00000	0.00000	;	H2-
743	722 C3-	723 C4-	744 H4	3	0.65084	1.95253	0.00000	-2.60338	0.00000	0.00000	;	H3-
744	723 C4-	731 N2-	756 H16	3	0.00000	0.00000	0.00000	0.00000	0.00000	0.00000	;	H4-

```
751     736     737     752     3       30.33400 0.00000 -30.33400       0.00000 0.00000 0.00000 ;
        H11-    C12-    C13-    H12
752     737     738     753     3       30.33400 0.00000 -30.33400       0.00000 0.00000 0.00000 ;
        H12-    C13-    C14-    H13
753     738     739     754     3       30.33400 0.00000 -30.33400       0.00000 0.00000 0.00000 ;
        H13-    C14-    C15-    H14
754     739     740     755     3       30.33400 0.00000 -30.33400       0.00000 0.00000 0.00000 ;
        H14-    C15-    C16-    H15

[ dihedrals ] ; impropers
; treated as propers in GROMACS to use correct AMBER analytical function
;  i    j    k    l  func  phase     kd      pn
720     729     728     730     1       180.00000       4.60240  2       ;       C2-     O2-     C8-
        O3
723     725     724     717     1       180.00000       43.93200 2       ;       C4-     O1-     C5-
        OG
732     723     731     756     1       180.00000       4.60240  2       ;       C9-     C4-     N2-
        H16
734     731     732     733     1       180.00000       43.93200 2       ;       C10-    N2-     C9-
        O4
735     737     736     751     1       180.00000       4.60240  2       ;       C11-    C13-    C12-
        H11
735     739     740     755     1       180.00000       4.60240  2       ;       C11-    C15-    C16-
        H15
736     738     737     752     1       180.00000       4.60240  2       ;       C12-    C14-    C13-
        H12
736     740     735     734     1       180.00000       4.60240  2       ;       C12-    C16-    C11-
        C10
737     739     738     753     1       180.00000       4.60240  2       ;       C13-    C15-    C14-
        H13
738     740     739     754     1       180.00000       4.60240  2       ;       C14-    C16-    C15-
        H14
```

CTX.gro

```
  289CTX      C 4061   4.669   3.785   3.531
  289CTX     C1 4062   4.792   3.756   3.587
  289CTX     C2 4063   4.635   3.964   3.709
  289CTX      H 4064   4.708   4.037   3.673
  289CTX      S 4065   4.705   3.850   3.834
  289CTX      N 4066   4.582   3.871   3.609
  289CTX     C3 4067   4.488   4.012   3.734
  289CTX     H1 4068   4.463   4.102   3.676
  289CTX     C4 4069   4.449   3.882   3.652
  289CTX      O 4070   4.350   3.814   3.633
  289CTX     N1 4071   4.451   4.038   3.873
  289CTX     C5 4072   4.619   3.732   3.399
  289CTX     O1 4073   4.670   3.633   3.349
  289CTX     O2 4074   4.526   3.788   3.343
  289CTX     C6 4075   4.899   3.673   3.515
  289CTX     H2 4076   4.887   3.569   3.546
  289CTX     H3 4077   4.888   3.674   3.406
  289CTX     C7 4078   4.842   3.797   3.725
  289CTX     H4 4079   4.913   3.880   3.717
  289CTX     H5 4080   4.893   3.714   3.773
  289CTX     O3 4081   5.033   3.715   3.550
  289CTX     C8 4082   5.103   3.815   3.485
  289CTX     C9 4083   5.030   3.889   3.374
  289CTX     O4 4084   5.219   3.839   3.512
  289CTX     H6 4085   5.100   3.960   3.327
  289CTX     H7 4086   4.995   3.820   3.298
  289CTX     H8 4087   4.944   3.944   3.413
  289CTX    C10 4088   4.527   4.121   3.954
  289CTX     O5 4089   4.616   4.189   3.904
  289CTX     H9 4090   4.381   3.981   3.919
  289CTX    C11 4091   4.507   4.118   4.103
  289CTX     N2 4092   4.427   4.028   4.154
  289CTX     O6 4093   4.390   4.064   4.285
  289CTX    C12 4094   4.392   3.955   4.376
  289CTX    H10 4095   4.321   3.877   4.346
  289CTX    H11 4096   4.493   3.912   4.380
  289CTX    H12 4097   4.364   3.990   4.477
  289CTX    C13 4098   4.619   4.158   4.189
  289CTX    C14 4099   4.737   4.087   4.198
  289CTX    H13 4100   4.774   4.012   4.129
  289CTX    C15 4101   4.684   4.218   4.393
  289CTX     S1 4102   4.811   4.104   4.356
  289CTX     N3 4103   4.597   4.241   4.298
  289CTX     N4 4104   4.653   4.263   4.517
  289CTX    H14 4105   4.554   4.291   4.517
  289CTX    H15 4106   4.674   4.198   4.592
```

CTX.top

```
[ defaults ]
; nbfunc        comb-rule       gen-pairs       fudgeLJ fudgeQQ
1               2               yes             0.5     0.8333

[ atomtypes ]
;name   bond_type     mass     charge   ptype   sigma         epsilon       Amb
 ce       ce          0.00000  0.00000   A     3.39967e-01   3.59824e-01 ; 1.91  0.0860
 c2       c2          0.00000  0.00000   A     3.39967e-01   3.59824e-01 ; 1.91  0.0860
 cy       cy          0.00000  0.00000   A     3.39967e-01   3.59824e-01 ; 1.91  0.0860
 h2       h2          0.00000  0.00000   A     2.29317e-01   6.56888e-02 ; 1.29  0.0157
 ss       ss          0.00000  0.00000   A     3.56359e-01   1.04600e+00 ; 2.00  0.2500
 nj       nj          0.00000  0.00000   A     3.25000e-01   7.11280e-01 ; 1.82  0.1700
 h1       h1          0.00000  0.00000   A     2.47135e-01   6.56888e-02 ; 1.39  0.0157
 c        c           0.00000  0.00000   A     3.39967e-01   3.59824e-01 ; 1.91  0.0860
```

```
 o       o          0.00000  0.00000   A     2.95992e-01   8.78640e-01 ; 1.66  0.2100
 n       n          0.00000  0.00000   A     3.25000e-01   7.11280e-01 ; 1.82  0.1700
 c3      c3         0.00000  0.00000   A     3.39967e-01   4.57730e-01 ; 1.91  0.1094
 os      os         0.00000  0.00000   A     3.00001e-01   7.11280e-01 ; 1.68  0.1700
 hc      hc         0.00000  0.00000   A     2.64953e-01   6.56888e-02 ; 1.49  0.0157
 hn      hn         0.00000  0.00000   A     1.06908e-01   6.56888e-02 ; 0.60  0.0157
 n2      n2         0.00000  0.00000   A     3.25000e-01   7.11280e-01 ; 1.82  0.1700
 cc      cc         0.00000  0.00000   A     3.39967e-01   3.59824e-01 ; 1.91  0.0860
 cd      cd         0.00000  0.00000   A     3.39967e-01   3.59824e-01 ; 1.91  0.0860
 h4      h4         0.00000  0.00000   A     2.51055e-01   6.27600e-02 ; 1.41  0.0150
 na      na         0.00000  0.00000   A     3.25000e-01   7.11280e-01 ; 1.82  0.1700
 nh      nh         0.00000  0.00000   A     3.25000e-01   7.11280e-01 ; 1.82  0.1700
 nc      nc         0.00000  0.00000   A     3.25000e-01   7.11280e-01 ; 1.82  0.1700

[ moleculetype ]
;name            nrexcl
 CTX              3

[ atoms ]
;   nr  type  resi  res  atom  cgnr     charge       mass       ; qtot   bond_type
     1   ce     1   CTX     C     1     0.007400     12.01000 ; qtot 0.007
     2   c2     1   CTX    C1     2    -0.299400     12.01000 ; qtot -0.292
     3   cy     1   CTX    C2     3     0.104800     12.01000 ; qtot -0.187
     4   h2     1   CTX     H     4     0.091700      1.00800 ; qtot -0.096
     5   ss     1   CTX     S     5    -0.360200     32.06000 ; qtot -0.456
     6   nj     1   CTX     N     6    -0.333000     14.01000 ; qtot -0.789
     7   cy     1   CTX    C3     7     0.003700     12.01000 ; qtot -0.785
     8   h1     1   CTX    H1     8     0.114700      1.00800 ; qtot -0.670
     9   c      1   CTX    C4     9     0.700501     12.01000 ; qtot 0.030
    10   o      1   CTX     O    10    -0.502501     16.00000 ; qtot -0.472
    11   n      1   CTX    N1    11    -0.518901     14.01000 ; qtot -0.991
    12   c      1   CTX    C5    12     0.927802     12.01000 ; qtot -0.063
    13   o      1   CTX    O1    13    -0.790801     16.00000 ; qtot -0.854
    14   o      1   CTX    O2    14    -0.790801     16.00000 ; qtot -1.645
    15   c3     1   CTX    C6    15     0.198600     12.01000 ; qtot -1.446
    16   h1     1   CTX    H2    16     0.072700      1.00800 ; qtot -1.374
    17   h1     1   CTX    H3    17     0.072700      1.00800 ; qtot -1.301
    18   c3     1   CTX    C7    18     0.086900     12.01000 ; qtot -1.214
    19   h1     1   CTX    H4    19     0.072700      1.00800 ; qtot -1.141
    20   h1     1   CTX    H5    20     0.072700      1.00800 ; qtot -1.069
    21   os     1   CTX    O3    21    -0.441900     16.00000 ; qtot -1.511
    22   c      1   CTX    C8    22     0.638101     12.01000 ; qtot -0.872
    23   c3     1   CTX    C9    23    -0.200100     12.01000 ; qtot -1.073
    24   o      1   CTX    O4    24    -0.557001     16.00000 ; qtot -1.630
    25   hc     1   CTX    H6    25     0.089367      1.00800 ; qtot -1.540
    26   hc     1   CTX    H7    26     0.089367      1.00800 ; qtot -1.451
    27   hc     1   CTX    H8    27     0.089367      1.00800 ; qtot -1.361
    28   c      1   CTX   C10    28     0.609801     12.01000 ; qtot -0.752
    29   o      1   CTX    O5    29    -0.609101     16.00000 ; qtot -1.361
    30   hn     1   CTX    H9    30     0.346500      1.00800 ; qtot -1.014
    31   ce     1   CTX   C11    31     0.284300     12.01000 ; qtot -0.730
    32   n2     1   CTX    N2    32    -0.387200     14.01000 ; qtot -1.117
    33   os     1   CTX    O6    33    -0.163300     16.00000 ; qtot -1.280
    34   c3     1   CTX   C12    34     0.127700     12.01000 ; qtot -1.153
    35   h1     1   CTX   H10    35     0.050033      1.00800 ; qtot -1.103
    36   h1     1   CTX   H11    36     0.050033      1.00800 ; qtot -1.053
    37   h1     1   CTX   H12    37     0.050033      1.00800 ; qtot -1.003
    38   cc     1   CTX   C13    38     0.296000     12.01000 ; qtot -0.707
    39   cd     1   CTX   C14    39    -0.227400     12.01000 ; qtot -0.934
    40   h4     1   CTX   H13    40     0.211000      1.00800 ; qtot -0.723
    41   cd     1   CTX   C15    41     0.560301     12.01000 ; qtot -0.163
    42   ss     1   CTX    S1    42    -0.081300     32.06000 ; qtot -0.244
    43   nc     1   CTX    N3    43    -0.641001     14.01000 ; qtot -0.885
    44   nh     1   CTX    N4    44    -0.876501     14.01000 ; qtot -1.762
    45   hn     1   CTX   H14    45     0.380800      1.00800 ; qtot -1.381
    46   hn     1   CTX   H15    46     0.380800      1.00800 ; qtot -1.000

[ bonds ]
;   ai     aj funct   r             k
     1      2   1    1.3461e-01    4.5798e+05 ;      C - C1
```

```
    1     6   1    1.4250e-01    3.0861e+05 ;      C - N
    1    12   1    1.4825e-01    2.9665e+05 ;      C - C5
    2    15   1    1.5095e-01    2.7347e+05 ;     C1 - C6
    2    18   1    1.5095e-01    2.7347e+05 ;     C1 - C7
    3     4   1    1.0930e-01    2.8108e+05 ;     C2 - H
    3     5   1    1.8500e-01    1.7598e+05 ;     C2 - S
    3     6   1    1.4750e-01    2.6426e+05 ;     C2 - N
    3     7   1    1.5580e-01    2.3732e+05 ;     C2 - C3
    5    18   1    1.8392e-01    1.8067e+05 ;      S - C7
    6     9   1    1.4010e-01    3.3313e+05 ;      N - C4
    7     8   1    1.0950e-01    2.7874e+05 ;     C3 - H1
    7     9   1    1.5520e-01    2.4150e+05 ;     C3 - C4
    7    11   1    1.4330e-01    3.0091e+05 ;     C3 - N1
    9    10   1    1.2183e-01    5.3363e+05 ;     C4 - O
   11    28   1    1.3789e-01    3.5782e+05 ;    N1 - C10
   11    30   1    1.0129e-01    3.3740e+05 ;    N1 - H9
   12    13   1    1.2183e-01    5.3363e+05 ;     C5 - O1
   12    14   1    1.2183e-01    5.3363e+05 ;     C5 - O2
   15    16   1    1.0969e-01    2.7665e+05 ;     C6 - H2
   15    17   1    1.0969e-01    2.7665e+05 ;     C6 - H3
   15    21   1    1.4316e-01    2.5824e+05 ;     C6 - O3
   18    19   1    1.0969e-01    2.7665e+05 ;     C7 - H4
   18    20   1    1.0969e-01    2.7665e+05 ;     C7 - H5
   21    22   1    1.3584e-01    3.2702e+05 ;     O3 - C8
   22    23   1    1.5241e-01    2.6192e+05 ;     C8 - C9
   22    24   1    1.2183e-01    5.3363e+05 ;     C8 - O4
   23    25   1    1.0969e-01    2.7665e+05 ;     C9 - H6
   23    26   1    1.0969e-01    2.7665e+05 ;     C9 - H7
   23    27   1    1.0969e-01    2.7665e+05 ;     C9 - H8
   28    29   1    1.2183e-01    5.3363e+05 ;    C10 - O5
   28    31   1    1.4825e-01    2.9665e+05 ;    C10 - C11
   31    32   1    1.2874e-01    4.8735e+05 ;    C11 - N2
   31    38   1    1.4540e-01    3.2376e+05 ;    C11 - C13
   32    33   1    1.4015e-01    3.3999e+05 ;     N2 - O6
   33    34   1    1.4316e-01    2.5824e+05 ;     O6 - C12
   34    35   1    1.0969e-01    2.7665e+05 ;    C12 - H10
   34    36   1    1.0969e-01    2.7665e+05 ;    C12 - H11
   34    37   1    1.0969e-01    2.7665e+05 ;    C12 - H12
   38    39   1    1.3729e-01    4.1915e+05 ;    C13 - C14
   38    43   1    1.3694e-01    3.6911e+05 ;    C13 - N3
   39    40   1    1.0817e-01    2.9455e+05 ;    C14 - H13
   39    42   1    1.7562e-01    2.2242e+05 ;    C14 - S1
   41    42   1    1.7562e-01    2.2242e+05 ;    C15 - S1
   41    43   1    1.3172e-01    4.3965e+05 ;    C15 - N3
   41    44   1    1.3735e-01    3.6418e+05 ;    C15 - N4
   44    45   1    1.0121e-01    3.3857e+05 ;    N4 - H14
   44    46   1    1.0121e-01    3.3857e+05 ;    N4 - H15

[ pairs ]
;   ai    aj    funct
    1     4     1 ;      C - H
    1     5     1 ;      C - S
    1     7     1 ;      C - C3
    1    10     1 ;      C - O
    1    16     1 ;      C - H2
    1    17     1 ;      C - H3
    1    19     1 ;      C - H4
    1    20     1 ;      C - H5
    1    21     1 ;      C - O3
    2     3     1 ;     C1 - C2
    2     9     1 ;     C1 - C4
    2    13     1 ;     C1 - O1
    2    14     1 ;     C1 - O2
    2    22     1 ;     C1 - C8
    3    10     1 ;     C2 - O
    3    19     1 ;     C2 - H4
    3    20     1 ;     C2 - H5
    3    28     1 ;     C2 - C10
    3    30     1 ;     C2 - H9
    4     8     1 ;      H - H1
```

```
   4    9    1 ;    H - C4
   4   11    1 ;    H - N1
   4   18    1 ;    H - C7
   5    8    1 ;    S - H1
   5    9    1 ;    S - C4
   5   11    1 ;    S - N1
   5   15    1 ;    S - C6
   6    8    1 ;    N - H1
   6   11    1 ;    N - N1
   6   13    1 ;    N - O1
   6   14    1 ;    N - O2
   6   15    1 ;    N - C6
   6   18    1 ;    N - C7
   7   18    1 ;   C3 - C7
   7   29    1 ;   C3 - O5
   7   31    1 ;   C3 - C11
   8   10    1 ;   H1 - O
   8   28    1 ;   H1 - C10
   8   30    1 ;   H1 - H9
   9   28    1 ;   C4 - C10
   9   30    1 ;   C4 - H9
  10   11    1 ;    O - N1
  11   32    1 ;   N1 - N2
  11   38    1 ;   N1 - C13
  12    3    1 ;   C5 - C2
  12    9    1 ;   C5 - C4
  12   15    1 ;   C5 - C6
  12   18    1 ;   C5 - C7
  15   19    1 ;   C6 - H4
  15   20    1 ;   C6 - H5
  15   23    1 ;   C6 - C9
  15   24    1 ;   C6 - O4
  16   18    1 ;   H2 - C7
  16   22    1 ;   H2 - C8
  17   18    1 ;   H3 - C7
  17   22    1 ;   H3 - C8
  18   21    1 ;   C7 - O3
  21   25    1 ;   O3 - H6
  21   26    1 ;   O3 - H7
  21   27    1 ;   O3 - H8
  24   25    1 ;   O4 - H6
  24   26    1 ;   O4 - H7
  24   27    1 ;   O4 - H8
  28   33    1 ;  C10 - O6
  28   39    1 ;  C10 - C14
  28   43    1 ;  C10 - N3
  29   30    1 ;   O5 - H9
  29   32    1 ;   O5 - N2
  29   38    1 ;   O5 - C13
  30   31    1 ;   H9 - C11
  31   34    1 ;  C11 - C12
  31   40    1 ;  C11 - H13
  31   41    1 ;  C11 - C15
  31   42    1 ;  C11 - S1
  32   35    1 ;   N2 - H10
  32   36    1 ;   N2 - H11
  32   37    1 ;   N2 - H12
  32   39    1 ;   N2 - C14
  32   43    1 ;   N2 - N3
  33   38    1 ;   O6 - C13
  38   44    1 ;  C13 - N4
  39   44    1 ;  C14 - N4
  40   41    1 ;  H13 - C15
  40   43    1 ;  H13 - N3
  42   45    1 ;   S1 - H14
  42   46    1 ;   S1 - H15
  43   45    1 ;   N3 - H14
  43   46    1 ;   N3 - H15
```

[angles]

```
;  ai    aj    ak   funct   theta       cth
    1     2    15     1    1.2315e+02   5.3555e+02 ;    C - C1    - C6
    1     2    18     1    1.2315e+02   5.3555e+02 ;    C - C1    - C7
    1     6     3     1    1.1165e+02   5.4057e+02 ;    C - N     - C2
    1     6     9     1    1.3156e+02   5.1128e+02 ;    C - N     - C4
    1    12    13     1    1.2320e+02   5.7572e+02 ;    C - C5    - O1
    1    12    14     1    1.2320e+02   5.7572e+02 ;    C - C5    - O2
    2     1     6     1    1.1033e+02   5.9999e+02 ;   C1 - C     - N
    2     1    12     1    1.2042e+02   5.4810e+02 ;   C1 - C     - C5
    2    15    16     1    1.0996e+02   3.9413e+02 ;   C1 - C6    - H2
    2    15    17     1    1.0996e+02   3.9413e+02 ;   C1 - C6    - H3
    2    15    21     1    1.0856e+02   5.7321e+02 ;   C1 - C6    - O3
    2    18     5     1    1.0497e+02   5.2802e+02 ;   C1 - C7    - S
    2    18    19     1    1.0996e+02   3.9413e+02 ;   C1 - C7    - H4
    2    18    20     1    1.0996e+02   3.9413e+02 ;   C1 - C7    - H5
    3     5    18     1    9.4240e+01   5.1547e+02 ;   C2 - S     - C7
    3     6     9     1    9.4020e+01   5.9413e+02 ;   C2 - N     - C4
    3     7     8     1    1.1317e+02   3.7740e+02 ;   C2 - C3    - H1
    3     7     9     1    8.5160e+01   5.9496e+02 ;   C2 - C3    - C4
    3     7    11     1    1.1987e+02   5.3220e+02 ;   C2 - C3    - N1
    4     3     5     1    1.0966e+02   3.4811e+02 ;   H - C2    - S
    4     3     6     1    1.1454e+02   4.0334e+02 ;   H - C2    - N
    4     3     7     1    1.1679e+02   3.7154e+02 ;   H - C2    - C3
    5     3     6     1    1.0514e+02   5.4141e+02 ;   S - C2    - N
    5     3     7     1    1.1827e+02   4.9120e+02 ;   S - C2    - C3
    5    18    19     1    1.0876e+02   3.5229e+02 ;   S - C7    - H4
    5    18    20     1    1.0876e+02   3.5229e+02 ;   S - C7    - H5
    6     1    12     1    1.1853e+02   5.5229e+02 ;   N - C     - C5
    6     3     7     1    8.8640e+01   6.1170e+02 ;   N - C2    - C3
    6     9     7     1    9.1680e+01   6.1588e+02 ;   N - C4    - C3
    6     9    10     1    1.3306e+02   5.9078e+02 ;   N - C4    - O
    7     9    10     1    1.3523e+02   5.3053e+02 ;   C3 - C4   - O
    7    11    28     1    1.2171e+02   5.3388e+02 ;   C3 - N1    - C10
    7    11    30     1    1.1885e+02   3.8828e+02 ;   C3 - N1    - H9
    8     7     9     1    1.1297e+02   3.7907e+02 ;   H1 - C3    - C4
    8     7    11     1    1.0799e+02   4.2593e+02 ;   H1 - C3    - N1
    9     7    11     1    1.1738e+02   5.3974e+02 ;   C4 - C3    - N1
   11    28    29     1    1.2305e+02   6.2091e+02 ;   N1 - C10   - O5
   11    28    31     1    1.1522e+02   5.6819e+02 ;   N1 - C10   - C11
   13    12    14     1    1.3025e+02   6.5187e+02 ;   O1 - C5    - O2
   15     2    18     1    1.1565e+02   5.2635e+02 ;   C6 - C1    - C7
   15    21    22     1    1.1598e+02   5.2969e+02 ;   C6 - O3    - C8
   16    15    17     1    1.0846e+02   3.2803e+02 ;   H2 - C6    - H3
   16    15    21     1    1.0978e+02   4.2509e+02 ;   H2 - C6    - O3
   17    15    21     1    1.0978e+02   4.2509e+02 ;   H3 - C6    - O3
   19    18    20     1    1.0846e+02   3.2803e+02 ;   H4 - C7    - H5
   21    22    23     1    1.1072e+02   5.7656e+02 ;   O3 - C8    - C9
   21    22    24     1    1.2325e+02   6.3011e+02 ;   O3 - C8    - O4
   22    23    25     1    1.0877e+02   3.9246e+02 ;   C8 - C9    - H6
   22    23    26     1    1.0877e+02   3.9246e+02 ;   C8 - C9    - H7
   22    23    27     1    1.0877e+02   3.9246e+02 ;   C8 - C9    - H8
   23    22    24     1    1.2320e+02   5.6400e+02 ;   C9 - C8    - O4
   25    23    26     1    1.0758e+02   3.2970e+02 ;   H6 - C9    - H7
   25    23    27     1    1.0758e+02   3.2970e+02 ;   H6 - C9    - H8
   26    23    27     1    1.0758e+02   3.2970e+02 ;   H7 - C9    - H8
   28    11    30     1    1.1755e+02   4.0417e+02 ;   C10 - N1    - H9
   28    31    32     1    1.1441e+02   5.8492e+02 ;   C10 - C11    - N2
   28    31    38     1    1.1782e+02   5.3555e+02 ;   C10 - C11    - C13
   29    28    31     1    1.2320e+02   5.7572e+02 ;   O5 - C10    - C11
   31    32    33     1    1.1279e+02   5.9580e+02 ;   C11 - N2    - O6
   31    38    39     1    1.2805e+02   5.3304e+02 ;   C11 - C13    - C14
   31    38    43     1    1.2110e+02   5.6233e+02 ;   C11 - C13    - N3
   32    31    38     1    1.2096e+02   5.7572e+02 ;   N2 - C11    - C13
   32    33    34     1    1.0923e+02   5.5145e+02 ;   N2 - O6    - C12
   33    34    35     1    1.0978e+02   4.2509e+02 ;   O6 - C12    - H10
   33    34    36     1    1.0978e+02   4.2509e+02 ;   O6 - C12    - H11
   33    34    37     1    1.0978e+02   4.2509e+02 ;   O6 - C12    - H12
   35    34    36     1    1.0846e+02   3.2803e+02 ;   H10 - C12    - H11
   35    34    37     1    1.0846e+02   3.2803e+02 ;   H10 - C12    - H12
   36    34    37     1    1.0846e+02   3.2803e+02 ;   H11 - C12    - H12
```

```
   38    39    40     1   1.2848e+02   3.9581e+02 ;   C13 - C14   - H13
   38    39    42     1   1.1155e+02   5.4225e+02 ;   C13 - C14   - S1
   38    43    41     1   1.0549e+02   6.0082e+02 ;   C13 - N3    - C15
   39    38    43     1   1.1165e+02   6.0417e+02 ;   C14 - C13   - N3
   39    42    41     1   9.0240e+01   5.5396e+02 ;   C14 - S1    - C15
   40    39    42     1   1.1997e+02   3.5229e+02 ;   H13 - C14   - S1
   41    44    45     1   1.1563e+02   4.0920e+02 ;   C15 - N4    - H14
   41    44    46     1   1.1563e+02   4.0920e+02 ;   C15 - N4    - H15
   42    41    43     1   1.1451e+02   5.5229e+02 ;    S1 - C15   - N3
   42    41    44     1   1.2181e+02   5.3220e+02 ;    S1 - C15   - N4
   43    41    44     1   1.2065e+02   6.0584e+02 ;    N3 - C15   - N4
   45    44    46     1   1.1512e+02   3.3556e+02 ;   H14 - N4    - H15

[ dihedrals ] ; propers
; treated as RBs in GROMACS to use combine multiple AMBER torsions per quartet
;   i     j     k     l   func    C0         C1         C2         C3         C4         C5
    1     2    15    16     3    0.00000    0.00000    0.00000    0.00000    0.00000    0.00000 ;    C-    C1-   C6-   H2
    1     2    15    17     3    0.00000    0.00000    0.00000    0.00000    0.00000    0.00000 ;    C-    C1-   C6-   H3
    1     2    15    21     3    0.00000    0.00000    0.00000    0.00000    0.00000    0.00000 ;    C-    C1-   C6-   O3
    1     2    18     5     3    0.00000    0.00000    0.00000    0.00000    0.00000    0.00000 ;    C-    C1-   C7-   S
    1     2    18    19     3    0.00000    0.00000    0.00000    0.00000    0.00000    0.00000 ;    C-    C1-   C7-   H4
    1     2    18    20     3    0.00000    0.00000    0.00000    0.00000    0.00000    0.00000 ;    C-    C1-   C7-   H5
    1     6     3     4     3    0.00000    0.00000    0.00000    0.00000    0.00000    0.00000 ;    C-    N-    C2-   H
    1     6     3     5     3    0.00000    0.00000    0.00000    0.00000    0.00000    0.00000 ;    C-    N-    C2-   S
    1     6     3     7     3    0.00000    0.00000    0.00000    0.00000    0.00000    0.00000 ;    C-    N-    C2-   C3
    1     6     9     7     3   20.92000    0.00000  -20.92000    0.00000    0.00000    0.00000 ;    C-    N-    C4-   C3
    1     6     9    10     3   20.92000    0.00000  -20.92000    0.00000    0.00000    0.00000 ;    C-    N-    C4-   O
    2     1     6     3     3   13.80720    0.00000  -13.80720    0.00000    0.00000    0.00000 ;    C1-   C-    N-    C2
    2     1     6     9     3   10.46000    5.02080   -5.43920    0.00000    0.00000    0.00000 ;    C1-   C-    N-    C4
    2     1    12    13     3   18.20040    0.00000  -18.20040    0.00000    0.00000    0.00000 ;    C1-   C-    C5-   O1
    2     1    12    14     3   18.20040    0.00000  -18.20040    0.00000    0.00000    0.00000 ;    C1-   C-    C5-   O2
    2    15    21    22     3    1.60387    4.81160    0.00000   -6.41547    0.00000    0.00000 ;    C1-   C6-   O3-   C8
    2    18     5     3     3    1.39467    4.18400    0.00000   -5.57867    0.00000    0.00000 ;    C1-   C7-   S-    C2
    3     5    18    19     3    1.39467    4.18400    0.00000   -5.57867    0.00000    0.00000 ;    C2-   S-    C7-   H4
    3     5    18    20     3    1.39467    4.18400    0.00000   -5.57867    0.00000    0.00000 ;    C2-   S-    C7-   H5
    3     6     9     7     3   20.92000    0.00000  -20.92000    0.00000    0.00000    0.00000 ;    C2-   N-    C4-   C3
    3     6     9    10     3   20.92000    0.00000  -20.92000    0.00000    0.00000    0.00000 ;    C2-   N-    C4-   O
    3     7     9     6     3    0.00000    0.00000    0.00000    0.00000    0.00000    0.00000 ;    C2-   C3-   C4-   N
    3     7     9    10     3    0.00000    0.00000    0.00000    0.00000    0.00000    0.00000 ;    C2-   C3-   C4-   O
    3     7    11    28     3    0.00000    0.00000    0.00000    0.00000    0.00000    0.00000 ;    C2-   C3-   N1-   C10
    3     7    11    30     3    0.00000    0.00000    0.00000    0.00000    0.00000    0.00000 ;    C2-   C3-   N1-   H9
    4     3     5    18     3    1.39467    4.18400    0.00000   -5.57867    0.00000    0.00000 ;    H-    C2-   S-    C7
    4     3     6     9     3    0.00000    0.00000    0.00000    0.00000    0.00000    0.00000 ;    H-    C2-   N-    C4
    4     3     7     8     3    0.65084    1.95253    0.00000   -2.60338    0.00000    0.00000 ;    H-    C2-   C3-   H1
    4     3     7     9     3    0.65084    1.95253    0.00000   -2.60338    0.00000    0.00000 ;    H-    C2-   C3-   C4
    4     3     7    11     3    0.65084    1.95253    0.00000   -2.60338    0.00000    0.00000 ;    H-    C2-   C3-   N1
    5     3     6     9     3    0.00000    0.00000    0.00000    0.00000    0.00000    0.00000 ;    S-    C2-   N-    C4
    5     3     7     8     3    0.65084    1.95253    0.00000   -2.60338    0.00000    0.00000 ;    S-    C2-   C3-   H1
    5     3     7     9     3    0.65084    1.95253    0.00000   -2.60338    0.00000    0.00000 ;    S-    C2-   C3-   C4
    5     3     7    11     3    0.65084    1.95253    0.00000   -2.60338    0.00000    0.00000 ;    S-    C2-   C3-   N1
    5    18     2    15     3    0.00000    0.00000    0.00000    0.00000    0.00000    0.00000 ;    S-    C7-   C1-   C6
    6     1     2    15     3   55.64720    0.00000  -55.64720    0.00000    0.00000    0.00000 ;    N-    C-    C1-   C6
    6     1     2    18     3   55.64720    0.00000  -55.64720    0.00000    0.00000    0.00000 ;    N-    C-    C1-   C7
    6     1    12    13     3   18.20040    0.00000  -18.20040    0.00000    0.00000    0.00000 ;    N-    C-    C5-   O1
    6     1    12    14     3   18.20040    0.00000  -18.20040    0.00000    0.00000    0.00000 ;    N-    C-    C5-   O2
    6     3     5    18     3    1.39467    4.18400    0.00000   -5.57867    0.00000    0.00000 ;    N-    C2-   S-    C7
    6     3     7     8     3    0.65084    1.95253    0.00000   -2.60338    0.00000    0.00000 ;    N-    C2-   C3-   H1
    6     3     7     9     3    0.65084    1.95253    0.00000   -2.60338    0.00000    0.00000 ;    N-    C2-   C3-   C4
    6     3     7    11     3    0.65084    1.95253    0.00000   -2.60338    0.00000    0.00000 ;    N-    C2-   C3-   N1
    6     9     7     8     3    0.00000    0.00000    0.00000    0.00000    0.00000    0.00000 ;    N-    C4-   C3-   H1
    6     9     7    11     3    0.00000    0.00000    0.00000    0.00000    0.00000    0.00000 ;    N-    C4-   C3-   N1
    7     3     5    18     3    1.39467    4.18400    0.00000   -5.57867    0.00000    0.00000 ;    C3-   C2-   S-    C7
    7     3     6     9     3    0.00000    0.00000    0.00000    0.00000    0.00000    0.00000 ;    C3-   C2-   N-    C4
    7    11    28    29     3   20.92000    0.00000  -20.92000    0.00000    0.00000    0.00000 ;    C3-   N1-   C10-   O5
    7    11    28    31     3   20.92000    0.00000  -20.92000    0.00000    0.00000    0.00000 ;    C3-   N1-   C10-   C11
    8     7     9    10     3    0.00000    0.00000    0.00000    0.00000    0.00000    0.00000 ;    H1-   C3-   C4-   O
    8     7    11    28     3    0.00000    0.00000    0.00000    0.00000    0.00000    0.00000 ;    H1-   C3-   N1-   C10
    8     7    11    30     3    0.00000    0.00000    0.00000    0.00000    0.00000    0.00000 ;    H1-   C3-   N1-   H9
    9     7    11    28     3    0.00000    0.00000    0.00000    0.00000    0.00000    0.00000 ;    C4-   C3-   N1-   C10
    9     7    11    30     3    0.00000    0.00000    0.00000    0.00000    0.00000    0.00000 ;    C4-   C3-   N1-   H9
```

```
  10     9     7    11     3    0.00000    0.00000    0.00000    0.00000    0.00000    0.00000 ;     O-    C4-    C3-    N1
  11    28    31    32     3   18.20040    0.00000  -18.20040    0.00000    0.00000    0.00000 ;     N1-   C10-   C11-    N2
  11    28    31    38     3   18.20040    0.00000  -18.20040    0.00000    0.00000    0.00000 ;     N1-   C10-   C11-   C13
  12     1     2    15     3   55.64720    0.00000  -55.64720    0.00000    0.00000    0.00000 ;     C5-    C-    C1-    C6
  12     1     2    18     3   55.64720    0.00000  -55.64720    0.00000    0.00000    0.00000 ;     C5-    C-    C1-    C7
  12     1     6     3     3   13.80720    0.00000  -13.80720    0.00000    0.00000    0.00000 ;     C5-    C-    N-    C2
  12     1     6     9     3   10.46000    5.02080   -5.43920    0.00000    0.00000    0.00000 ;     C5-    C-    N-    C4
  15     2    18    19     3    0.00000    0.00000    0.00000    0.00000    0.00000    0.00000 ;     C6-    C1-    C7-    H4
  15     2    18    20     3    0.00000    0.00000    0.00000    0.00000    0.00000    0.00000 ;     C6-    C1-    C7-    H5
  15    21    22    23     3   27.40520   14.43480  -22.59360  -19.24640    0.00000    0.00000 ;     C6-    O3-    C8-    C9
  15    21    22    24     3   28.45120    5.85760  -22.59360    0.00000    0.00000    0.00000 ;     C6-    O3-    C8-    O4
  16    15     2    18     3    0.00000    0.00000    0.00000    0.00000    0.00000    0.00000 ;     H2-    C6-    C1-    C7
  16    15    21    22     3    1.60387    4.81160    0.00000   -6.41547    0.00000    0.00000 ;     H2-    C6-    O3-    C8
  17    15     2    18     3    0.00000    0.00000    0.00000    0.00000    0.00000    0.00000 ;     H3-    C6-    C1-    C7
  17    15    21    22     3    1.60387    4.81160    0.00000   -6.41547    0.00000    0.00000 ;     H3-    C6-    O3-    C8
  18     2    15    21     3    0.00000    0.00000    0.00000    0.00000    0.00000    0.00000 ;     C7-    C1-    C6-    O3
  21    22    23    25     3    0.00000    0.00000    0.00000    0.00000    0.00000    0.00000 ;     O3-    C8-    C9-    H6
  21    22    23    26     3    0.00000    0.00000    0.00000    0.00000    0.00000    0.00000 ;     O3-    C8-    C9-    H7
  21    22    23    27     3    0.00000    0.00000    0.00000    0.00000    0.00000    0.00000 ;     O3-    C8-    C9-    H8
  24    22    23    25     3    3.68192   -4.35136    0.00000    1.33888    0.00000    0.00000 ;     O4-    C8-    C9-    H6
  24    22    23    26     3    3.68192   -4.35136    0.00000    1.33888    0.00000    0.00000 ;     O4-    C8-    C9-    H7
  24    22    23    27     3    3.68192   -4.35136    0.00000    1.33888    0.00000    0.00000 ;     O4-    C8-    C9-    H8
  28    31    32    33     3    6.69440    0.00000   -6.69440    0.00000    0.00000    0.00000 ;     C10-   C11-    N2-    O6
  28    31    38    39     3    8.36800    0.00000   -8.36800    0.00000    0.00000    0.00000 ;     C10-   C11-   C13-   C14
  28    31    38    43     3    8.36800    0.00000   -8.36800    0.00000    0.00000    0.00000 ;     C10-   C11-   C13-    N3
  29    28    11    30     3   29.28800   -8.36800  -20.92000    0.00000    0.00000    0.00000 ;     O5-    C10-    N1-    H9
  29    28    31    32     3   18.20040    0.00000  -18.20040    0.00000    0.00000    0.00000 ;     O5-    C10-   C11-    N2
  29    28    31    38     3   18.20040    0.00000  -18.20040    0.00000    0.00000    0.00000 ;     O5-    C10-   C11-   C13
  30    11    28    31     3   20.92000    0.00000  -20.92000    0.00000    0.00000    0.00000 ;     H9-    N1-    C10-   C11
  31    32    33    34     3   25.10400    0.00000  -25.10400    0.00000    0.00000    0.00000 ;     C11-   N2-    O6-    C12
  31    38    39    40     3   33.47200    0.00000  -33.47200    0.00000    0.00000    0.00000 ;     C11-   C13-   C14-   H13
  31    38    39    42     3   33.47200    0.00000  -33.47200    0.00000    0.00000    0.00000 ;     C11-   C13-   C14-    S1
  31    38    43    41     3   39.74800    0.00000  -39.74800    0.00000    0.00000    0.00000 ;     C11-   C13-    N3-   C15
  32    31    38    39     3    8.36800    0.00000   -8.36800    0.00000    0.00000    0.00000 ;     N2-    C11-   C13-   C14
  32    31    38    43     3    8.36800    0.00000   -8.36800    0.00000    0.00000    0.00000 ;     N2-    C11-   C13-    N3
  32    33    34    35     3    1.60387    4.81160    0.00000   -6.41547    0.00000    0.00000 ;     N2-    O6-    C12-   H10
  32    33    34    36     3    1.60387    4.81160    0.00000   -6.41547    0.00000    0.00000 ;     N2-    O6-    C12-   H11
  32    33    34    37     3    1.60387    4.81160    0.00000   -6.41547    0.00000    0.00000 ;     N2-    O6-    C12-   H12
  33    32    31    38     3    6.69440    0.00000   -6.69440    0.00000    0.00000    0.00000 ;     O6-    N2-    C11-   C13
  38    39    42    41     3    9.20480    0.00000   -9.20480    0.00000    0.00000    0.00000 ;     C13-   C14-    S1-   C15
  38    43    41    42     3   39.74800    0.00000  -39.74800    0.00000    0.00000    0.00000 ;     C13-    N3-   C15-    S1
  38    43    41    44     3   39.74800    0.00000  -39.74800    0.00000    0.00000    0.00000 ;     C13-    N3-   C15-    N4
  39    38    43    41     3   39.74800    0.00000  -39.74800    0.00000    0.00000    0.00000 ;     C14-   C13-    N3-   C15
  39    42    41    43     3    9.20480    0.00000   -9.20480    0.00000    0.00000    0.00000 ;     C14-    S1-   C15-    N3
  39    42    41    44     3    9.20480    0.00000   -9.20480    0.00000    0.00000    0.00000 ;     C14-    S1-   C15-    N4
  40    39    38    43     3   33.47200    0.00000  -33.47200    0.00000    0.00000    0.00000 ;     H13-   C14-   C13-    N3
  40    39    42    41     3    9.20480    0.00000   -9.20480    0.00000    0.00000    0.00000 ;     H13-   C14-    S1-   C15
  42    39    38    43     3   33.47200    0.00000  -33.47200    0.00000    0.00000    0.00000 ;     S1-    C14-   C13-    N3
  42    41    44    45     3    8.78640    0.00000   -8.78640    0.00000    0.00000    0.00000 ;     S1-    C15-    N4-   H14
  42    41    44    46     3    8.78640    0.00000   -8.78640    0.00000    0.00000    0.00000 ;     S1-    C15-    N4-   H15
  43    41    44    45     3    8.78640    0.00000   -8.78640    0.00000    0.00000    0.00000 ;     N3-    C15-    N4-   H14
  43    41    44    46     3    8.78640    0.00000   -8.78640    0.00000    0.00000    0.00000 ;     N3-    C15-    N4-   H15

[ dihedrals ] ; impropers
; treated as propers in GROMACS to use correct AMBER analytical function
;   i     j     k     l   func   phase     kd      pn
    1     2    18    15     1   180.00   4.60240   2 ;     C-    C1-    C7-    C6
    1    13    12    14     1   180.00   4.60240   2 ;     C-    O1-    C5-    O2
    6     1     2    12     1   180.00   4.60240   2 ;     N-    C-    C1-    C5
    7     6     9    10     1   180.00  43.93200   2 ;     C3-    N-    C4-    O
    9     1     6     3     1   180.00   4.60240   2 ;     C4-    C-    N-    C2
   23    24    22    21     1   180.00  43.93200   2 ;     C9-    O4-    C8-    O3
   28     7    11    30     1   180.00   4.60240   2 ;     C10-    C3-    N1-    H9
   28    38    31    32     1   180.00   4.60240   2 ;     C10-   C13-   C11-    N2
   31    11    28    29     1   180.00  43.93200   2 ;     C11-    N1-    C10-    O5
   38    40    39    42     1   180.00   4.60240   2 ;     C13-   H13-   C14-    S1
   39    31    38    43     1   180.00   4.60240   2 ;     C14-   C11-   C13-    N3
   41    45    44    46     1   180.00   4.60240   2 ;     C15-   H14-    N4-   H15
   43    44    41    42     1   180.00   4.60240   2 ;     N3-    N4-   C15-    S1
```

SCX.gro

```
    70SCX      N  710   3.863   4.146   3.708
    70SCX      H  711   3.949   4.125   3.758
    70SCX     CA  712   3.871   4.207   3.573
    70SCX     HA  713   3.831   4.308   3.582
    70SCX     CB  714   4.018   4.219   3.527
    70SCX    HB1  715   4.019   4.263   3.428
    70SCX    HB2  716   4.062   4.119   3.520
    70SCX     OG  717   4.098   4.303   3.614
    70SCX     C2  718   4.159   4.248   3.724
    70SCX     O1  719   4.145   4.130   3.753
    70SCX     C3  720   4.267   4.339   3.788
    70SCX     C4  721   4.461   4.211   3.561
    70SCX     C5  722   4.605   4.234   3.579
    70SCX     C6  723   4.362   4.402   3.681
    70SCX     H4  724   4.314   4.493   3.644
    70SCX     S2  725   4.524   4.453   3.749
    70SCX     N1  726   4.382   4.315   3.564
    70SCX     H5  727   4.213   4.421   3.837
    70SCX     N2  728   4.343   4.264   3.891
    70SCX     C7  729   4.403   4.086   3.492
    70SCX     O2  730   4.464   3.979   3.489
    70SCX     O3  731   4.296   4.092   3.432
    70SCX     C8  732   4.699   4.171   3.505
    70SCX     H6  733   4.805   4.195   3.516
    70SCX     H7  734   4.674   4.097   3.429
    70SCX     C9  735   4.652   4.344   3.674
    70SCX     H8  736   4.722   4.409   3.620
    70SCX     H9  737   4.710   4.300   3.755
    70SCX    C10  738   4.389   4.316   4.010
    70SCX     O4  739   4.362   4.431   4.042
    70SCX    H10  740   4.354   4.164   3.881
    70SCX    C11  741   4.470   4.223   4.097
    70SCX     N3  742   4.537   4.125   4.042
    70SCX     O5  743   4.611   4.157   3.928
    70SCX    C12  744   4.732   4.079   3.927
    70SCX    H11  745   4.798   4.113   4.008
    70SCX    H12  746   4.708   3.974   3.943
    70SCX    H13  747   4.784   4.091   3.832
    70SCX    C13  748   4.469   4.237   4.243
    70SCX    C14  749   4.394   4.324   4.319
    70SCX    H14  750   4.322   4.397   4.283
    70SCX    C15  751   4.532   4.179   4.447
    70SCX     S1  752   4.423   4.309   4.490
    70SCX     N4  753   4.547   4.152   4.321
    70SCX     N5  754   4.607   4.107   4.534
    70SCX    H15  755   4.684   4.059   4.491
    70SCX    H16  756   4.616   4.141   4.629
    70SCX      C  757   3.789   4.138   3.462
    70SCX      O  758   3.778   4.191   3.351
```

SCX.top

```
[ moleculetype ]
; Name            nrexcl
SCX     3

[ defaults ]
; nbfunc        comb-rule       gen-pairs       fudgeLJ fudgeQQ
1               2               yes             0.5     0.8333

[ atomtypes ]
;name   bond_type     mass     charge   ptype   sigma         epsilon       Amb
```

```
n      n        0.00000  0.00000   A    3.25000e-01   7.11280e-01 ; 1.82  0.1700
hn     hn       0.00000  0.00000   A    1.06908e-01   6.56888e-02 ; 0.60  0.0157
c3     c3       0.00000  0.00000   A    3.39967e-01   4.57730e-01 ; 1.91  0.1094
h1     h1       0.00000  0.00000   A    2.47135e-01   6.56888e-02 ; 1.39  0.0157
os     os       0.00000  0.00000   A    3.00001e-01   7.11280e-01 ; 1.68  0.1700
c      c        0.00000  0.00000   A    3.39967e-01   3.59824e-01 ; 1.91  0.0860
o      o        0.00000  0.00000   A    2.95992e-01   8.78640e-01 ; 1.66  0.2100
ce     ce       0.00000  0.00000   A    3.39967e-01   3.59824e-01 ; 1.91  0.0860
h2     h2       0.00000  0.00000   A    2.29317e-01   6.56888e-02 ; 1.29  0.0157
ss     ss       0.00000  0.00000   A    3.56359e-01   1.04600e+00 ; 2.00  0.2500
n2     n2       0.00000  0.00000   A    3.25000e-01   7.11280e-01 ; 1.82  0.1700
c2     c2       0.00000  0.00000   A    3.39967e-01   3.59824e-01 ; 1.91  0.0860
ha     ha       0.00000  0.00000   A    2.59964e-01   6.27600e-02 ; 1.46  0.0150
cc     cc       0.00000  0.00000   A    3.39967e-01   3.59824e-01 ; 1.91  0.0860
cd     cd       0.00000  0.00000   A    3.39967e-01   3.59824e-01 ; 1.91  0.0860
h4     h4       0.00000  0.00000   A    2.51055e-01   6.27600e-02 ; 1.41  0.0150
nc     nc       0.00000  0.00000   A    3.25000e-01   7.11280e-01 ; 1.82  0.1700
nh     nh       0.00000  0.00000   A    3.25000e-01   7.11280e-01 ; 1.82  0.1700
hc     hc       0.00000  0.00000   A    2.64953e-01   6.56888e-02 ; 1.49  0.0157

[ atoms ]
;   nr  type  resi  res  atom  cgnr    charge     mass      ; qtot   bond_type
710       N        70       SCX      N        710       -0.4157              14.01
711       H        70       SCX      H        711       0.2719               1.008
712       CT       70       SCX      CA       712       -0.0349              12.01
713       H1       70       SCX      HA       713       0.0853               1.008
714       CT       70       SCX      CB       714       0.1414               12.01
715       H1       70       SCX      HB1      715       0.085205             1.008
716       H1       70       SCX      HB2      716       0.085205             1.008
717       os       70       SCX      OG       717       -0.3949              16
718       c        70       SCX      C2       718       0.621101             12.01
719       o        70       SCX      O1       719       -0.572001            16
720       c3       70       SCX      C3       720       0.0717               12.01
721       ce       70       SCX      C4       721       0.4466               12.01
722       ce       70       SCX      C5       722       -0.2338              12.01
723       c3       70       SCX      C6       723       0.2556               12.01
724       h2       70       SCX      H4       724       0.0987               1.008
725       ss       70       SCX      S2       725       -0.4452              32.06
726       n2       70       SCX      N1       726       -0.609901            14.01
727       h1       70       SCX      H5       727       0.1287               1.008
728       n        70       SCX      N2       728       -0.548901            14.01
729       c        70       SCX      C7       729       0.855301             12.01
730       o        70       SCX      O2       730       -0.806301            16
731       o        70       SCX      O3       731       -0.806301            16
732       c2       70       SCX      C8       732       -0.156               12.01
733       ha       70       SCX      H6       733       0.128                1.008
734       ha       70       SCX      H7       734       0.128                1.008
735       c3       70       SCX      C9       735       0.0599               12.01
736       h1       70       SCX      H8       736       0.0762               1.008
737       h1       70       SCX      H9       737       0.0762               1.008
738       c        70       SCX      C10      738       0.568801             12.01
739       o        70       SCX      O4       739       -0.575101            16
740       hn       70       SCX      H10      740       0.3395               1.008
741       ce       70       SCX      C11      741       0.2883               12.01
742       n2       70       SCX      N3       742       -0.3782              14.01
743       os       70       SCX      O5       743       -0.1793              16
744       c3       70       SCX      C12      744       0.1337               12.01
745       h1       70       SCX      H11      745       0.0477               1.008
746       h1       70       SCX      H12      746       0.0477               1.008
747       h1       70       SCX      H13      747       0.0477               1.008
748       cc       70       SCX      C13      748       0.317                12.01
749       cd       70       SCX      C14      749       -0.2464              12.01
750       h4       70       SCX      H14      750       0.217                1.008
751       cd       70       SCX      C15      751       0.532301             12.01
752       ss       70       SCX      S1       752       -0.0223              32.06
753       nc       70       SCX      N4       753       -0.640001            14.01
754       nh       70       SCX      N5       754       -0.871502            14.01
755       hn       70       SCX      H15      755       0.3763               1.008
756       hn       70       SCX      H16      756       0.3763               1.008
757       C        70       SCX      C        757       0.5973               12.01
```

```
758     O       70      SCX     O       758     -0.5679         16

[ bonds ]
;  ai    aj funct   r          k
714     717     1       1.4316E-01      2.5824E+05      ;       C1      -       O
717     718     1       1.3584E-01      3.2702E+05      ;       O       -       C2
718     719     1       1.2183E-01      5.3363E+05      ;       C2      -       O1
718     720     1       1.5241E-01      2.6192E+05      ;       C2      -       C3
720     723     1       1.5375E-01      2.5179E+05      ;       C3      -       C6
720     727     1       1.0969E-01      2.7665E+05      ;       C3      -       H5
720     728     1       1.4619E-01      2.7506E+05      ;       C3      -       N2
721     722     1       1.4574E-01      3.2033E+05      ;       C4      -       C5
721     726     1       1.2874E-01      4.8735E+05      ;       C4      -       N1
721     729     1       1.4825E-01      2.9665E+05      ;       C4      -       C7
722     732     1       1.3461E-01      4.5798E+05      ;       C5      -       C8
722     735     1       1.5159E-01      2.6836E+05      ;       C5      -       C9
723     724     1       1.0961E-01      2.7757E+05      ;       C6      -       H4
723     725     1       1.8392E-01      1.8067E+05      ;       C6      -       S
723     726     1       1.4661E-01      2.7154E+05      ;       C6      -       N1
725     735     1       1.8392E-01      1.8067E+05      ;       S       -       C9
728     738     1       1.3789E-01      3.5782E+05      ;       N2      -       C10
728     740     1       1.0129E-01      3.3740E+05      ;       N2      -       H10
729     730     1       1.2183E-01      5.3363E+05      ;       C7      -       O2
729     731     1       1.2183E-01      5.3363E+05      ;       C7      -       O3
732     733     1       1.0879E-01      2.8711E+05      ;       C8      -       H6
732     734     1       1.0879E-01      2.8711E+05      ;       C8      -       H7
735     736     1       1.0969E-01      2.7665E+05      ;       C9      -       H8
735     737     1       1.0969E-01      2.7665E+05      ;       C9      -       H9
738     739     1       1.2183E-01      5.3363E+05      ;       C10     -       O4
738     741     1       1.4825E-01      2.9665E+05      ;       C10     -       C11
741     742     1       1.2874E-01      4.8735E+05      ;       C11     -       N3
741     748     1       1.4540E-01      3.2376E+05      ;       C11     -       C13
742     743     1       1.4015E-01      3.3999E+05      ;       N3      -       O5
743     744     1       1.4316E-01      2.5824E+05      ;       O5      -       C12
744     745     1       1.0969E-01      2.7665E+05      ;       C12     -       H11
744     746     1       1.0969E-01      2.7665E+05      ;       C12     -       H12
744     747     1       1.0969E-01      2.7665E+05      ;       C12     -       H13
748     749     1       1.3729E-01      4.1915E+05      ;       C13     -       C14
748     753     1       1.3694E-01      3.6911E+05      ;       C13     -       N4
749     750     1       1.0817E-01      2.9455E+05      ;       C14     -       H14
749     752     1       1.7562E-01      2.2242E+05      ;       C14     -       S1
751     752     1       1.7562E-01      2.2242E+05      ;       C15     -       S1
751     753     1       1.3172E-01      4.3965E+05      ;       C15     -       N4
751     754     1       1.3735E-01      3.6418E+05      ;       C15     -       N5
754     755     1       1.0121E-01      3.3857E+05      ;       N5      -       H15
754     756     1       1.0121E-01      3.3857E+05      ;       N5      -       H16

[ pairs ]
;  ai    aj    funct
710     715     1       ;       N       -       H2
710     716     1       ;       N       -       H3
710     717     1       ;       N       -       O
710     758     1       ;       N       -       O6
711     713     1       ;       H       -       H1
711     714     1       ;       H       -       C1
711     757     1       ;       H       -       C16
712     718     1       ;       C       -       C2
713     715     1       ;       H1      -       H2
713     716     1       ;       H1      -       H3
713     717     1       ;       H1      -       O
713     758     1       ;       H1      -       O6
714     719     1       ;       C1      -       O1
714     720     1       ;       C1      -       C3
714     758     1       ;       C1      -       O6
715     718     1       ;       H2      -       C2
715     757     1       ;       H2      -       C16
716     718     1       ;       H3      -       C2
716     757     1       ;       H3      -       C16
717     723     1       ;       O       -       C6
717     727     1       ;       O       -       H5
```

717	728	1	;	O	-	N2
717	757	1	;	O	-	C16
718	724	1	;	C2	-	H4
718	725	1	;	C2	-	S
718	726	1	;	C2	-	N1
718	738	1	;	C2	-	C10
718	740	1	;	C2	-	H10
719	723	1	;	O1	-	C6
719	727	1	;	O1	-	H5
719	728	1	;	O1	-	N2
720	721	1	;	C3	-	C4
720	735	1	;	C3	-	C9
720	739	1	;	C3	-	O4
720	741	1	;	C3	-	C11
721	724	1	;	C4	-	H4
721	725	1	;	C4	-	S
721	733	1	;	C4	-	H6
721	734	1	;	C4	-	H7
721	736	1	;	C4	-	H8
721	737	1	;	C4	-	H9
722	723	1	;	C5	-	C6
722	730	1	;	C5	-	O2
722	731	1	;	C5	-	O3
723	729	1	;	C6	-	C7
723	736	1	;	C6	-	H8
723	737	1	;	C6	-	H9
723	738	1	;	C6	-	C10
723	740	1	;	C6	-	H10
724	727	1	;	H4	-	H5
724	728	1	;	H4	-	N2
724	735	1	;	H4	-	C9
725	727	1	;	S	-	H5
725	728	1	;	S	-	N2
725	732	1	;	S	-	C8
726	727	1	;	N1	-	H5
726	728	1	;	N1	-	N2
726	730	1	;	N1	-	O2
726	731	1	;	N1	-	O3
726	732	1	;	N1	-	C8
726	735	1	;	N1	-	C9
727	738	1	;	H5	-	C10
727	740	1	;	H5	-	H10
728	742	1	;	N2	-	N3
728	748	1	;	N2	-	C13
729	732	1	;	C7	-	C8
729	735	1	;	C7	-	C9
732	736	1	;	C8	-	H8
732	737	1	;	C8	-	H9
733	735	1	;	H6	-	C9
734	735	1	;	H7	-	C9
738	743	1	;	C10	-	O5
738	749	1	;	C10	-	C14
738	753	1	;	C10	-	N4
739	740	1	;	O4	-	H10
739	742	1	;	O4	-	N3
739	748	1	;	O4	-	C13
740	741	1	;	H10	-	C11
741	744	1	;	C11	-	C12
741	750	1	;	C11	-	H14
741	751	1	;	C11	-	C15
741	752	1	;	C11	-	S1
742	745	1	;	N3	-	H11
742	746	1	;	N3	-	H12
742	747	1	;	N3	-	H13
742	749	1	;	N3	-	C14
742	753	1	;	N3	-	N4
743	748	1	;	O5	-	C13
748	754	1	;	C13	-	N5
749	754	1	;	C14	-	N5
750	751	1	;	H14	-	C15

```
750     753     1       ;       H14     -       N4
752     755     1       ;       S1      -       H15
752     756     1       ;       S1      -       H16
753     755     1       ;       N4      -       H15
753     756     1       ;       N4      -       H16

[ angles ]
;  ai    aj    ak    funct   theta       cth
712     714     715     1       1.0956E+02      3.8828E+02      ;       C       -       C1      -
        H2
712     714     716     1       1.0956E+02      3.8828E+02      ;       C       -       C1      -
        H3
712     714     717     1       1.0797E+02      5.6902E+02      ;       C       -       C1      -
        O
712     757     758     1       1.2320E+02      5.6400E+02      ;       C       -       C16     -
        O6
713     712     714     1       1.0956E+02      3.8828E+02      ;       H1      -       C       -
        C1
713     712     757     1       1.0822E+02      3.9330E+02      ;       H1      -       C       -
        C16
714     712     757     1       1.1104E+02      5.2969E+02      ;       C1      -       C       -
        C16
714     717     718     1       1.1598E+02      5.2969E+02      ;       C1      -       O       -
        C2
715     714     716     1       1.0846E+02      3.2803E+02      ;       H2      -       C1      -
        H3
715     714     717     1       1.0978E+02      4.2509E+02      ;       H2      -       C1      -
        O
716     714     717     1       1.0978E+02      4.2509E+02      ;       H3      -       C1      -
        O
717     718     719     1       1.2325E+02      6.3011E+02      ;       O       -       C2      -
        O1
717     718     720     1       1.1072E+02      5.7656E+02      ;       O       -       C2      -
        C3
718     720     723     1       1.1104E+02      5.2969E+02      ;       C2      -       C3      -
        C6
718     720     727     1       1.0822E+02      3.9330E+02      ;       C2      -       C3      -
        H5
718     720     728     1       1.0906E+02      5.6066E+02      ;       C2      -       C3      -
        N2
719     718     720     1       1.2320E+02      5.6400E+02      ;       O1      -       C2      -
        C3
720     723     724     1       1.1022E+02      3.8660E+02      ;       C3      -       C6      -
        H4
720     723     725     1       1.1027E+02      5.1296E+02      ;       C3      -       C6      -
        S
720     723     726     1       1.0880E+02      5.5815E+02      ;       C3      -       C6      -
        N1
720     728     738     1       1.2069E+02      5.3053E+02      ;       C3      -       N2      -
        C10
720     728     740     1       1.1768E+02      3.8325E+02      ;       C3      -       N2      -
        H10
721     722     732     1       1.2326E+02      5.4727E+02      ;       C4      -       C5      -
        C8
721     722     735     1       1.1712E+02      5.3053E+02      ;       C4      -       C5      -
        C9
721     726     723     1       1.1867E+02      5.4810E+02      ;       C4      -       N1      -
        C6
721     729     730     1       1.2320E+02      5.7572E+02      ;       C4      -       C7      -
        O2
721     729     731     1       1.2320E+02      5.7572E+02      ;       C4      -       C7      -
        O3
722     721     726     1       1.1893E+02      5.7990E+02      ;       C5      -       C4      -
        N1
722     721     729     1       1.2098E+02      5.2802E+02      ;       C5      -       C4      -
        C7
722     732     733     1       1.2045E+02      4.1422E+02      ;       C5      -       C8      -
        H6
722     732     734     1       1.2045E+02      4.1422E+02      ;       C5      -       C8      -
        H7
```

722	735 S	725	1	1.1072E+02	5.1380E+02	;	C5	-	C9	-
722	735 H8	736	1	1.0954E+02	3.9330E+02	;	C5	-	C9	-
722	735 H9	737	1	1.0954E+02	3.9330E+02	;	C5	-	C9	-
723	720 H5	727	1	1.0956E+02	3.8828E+02	;	C6	-	C3	-
723	720 N2	728	1	1.1161E+02	5.5145E+02	;	C6	-	C3	-
723	725 C9	735	1	9.9240E+01	5.0375E+02	;	C6	-	S	-
724	723 S	725	1	1.0833E+02	3.5229E+02	;	H4	-	C6	-
724	723 N1	726	1	1.1020E+02	4.1338E+02	;	H4	-	C6	-
725	723 N1	726	1	1.0939E+02	5.3388E+02	;	S	-	C6	-
725	735 H8	736	1	1.0876E+02	3.5229E+02	;	S	-	C9	-
725	735 H9	737	1	1.0876E+02	3.5229E+02	;	S	-	C9	-
726	721 C7	729	1	1.1441E+02	5.8492E+02	;	N1	-	C4	-
727	720 N2	728	1	1.0888E+02	4.1673E+02	;	H5	-	C3	-
728	738 O4	739	1	1.2305E+02	6.2091E+02	;	N2	-	C10	-
728	738 C11	741	1	1.1522E+02	5.6819E+02	;	N2	-	C10	-
730	729 O3	731	1	1.3025E+02	6.5187E+02	;	O2	-	C7	-
732	722 C9	735	1	1.2253E+02	5.3555E+02	;	C8	-	C5	-
733	732 H7	734	1	1.1690E+02	3.1882E+02	;	H6	-	C8	-
736	735 H9	737	1	1.0846E+02	3.2803E+02	;	H8	-	C9	-
738	728 H10	740	1	1.1755E+02	4.0417E+02	;	C10	-	N2	-
738	741 N3	742	1	1.1441E+02	5.8492E+02	;	C10	-	C11	-
738	741 C13	748	1	1.1782E+02	5.3555E+02	;	C10	-	C11	-
739	738 C11	741	1	1.2320E+02	5.7572E+02	;	O4	-	C10	-
741	742 O5	743	1	1.1279E+02	5.9580E+02	;	C11	-	N3	-
741	748 C14	749	1	1.2805E+02	5.3304E+02	;	C11	-	C13	-
741	748 N4	753	1	1.2110E+02	5.6233E+02	;	C11	-	C13	-
742	741 C13	748	1	1.2096E+02	5.7572E+02	;	N3	-	C11	-
742	743 C12	744	1	1.0923E+02	5.5145E+02	;	N3	-	O5	-
743	744 H11	745	1	1.0978E+02	4.2509E+02	;	O5	-	C12	-
743	744 H12	746	1	1.0978E+02	4.2509E+02	;	O5	-	C12	-
743	744 H13	747	1	1.0978E+02	4.2509E+02	;	O5	-	C12	-
745	744 H12	746	1	1.0846E+02	3.2803E+02	;	H11	-	C12	-
745	744 H13	747	1	1.0846E+02	3.2803E+02	;	H11	-	C12	-
746	744 H13	747	1	1.0846E+02	3.2803E+02	;	H12	-	C12	-
748	749 H14	750	1	1.2848E+02	3.9581E+02	;	C13	-	C14	-

```
748     749     752     1     1.1155E+02     5.4225E+02     ;     C13     -     C14     -
        S1
748     753     751     1     1.0549E+02     6.0082E+02     ;     C13     -     N4      -
        C15
749     748     753     1     1.1165E+02     6.0417E+02     ;     C14     -     C13     -
        N4
749     752     751     1     9.0240E+01     5.5396E+02     ;     C14     -     S1      -
        C15
750     749     752     1     1.1997E+02     3.5229E+02     ;     H14     -     C14     -
        S1
751     754     755     1     1.1563E+02     4.0920E+02     ;     C15     -     N5      -
        H15
751     754     756     1     1.1563E+02     4.0920E+02     ;     C15     -     N5      -
        H16
752     751     753     1     1.1451E+02     5.5229E+02     ;     S1      -     C15     -
        N4
752     751     754     1     1.2181E+02     5.3220E+02     ;     S1      -     C15     -
        N5
753     751     754     1     1.2065E+02     6.0584E+02     ;     N4      -     C15     -
        N5
755     754     756     1     1.1512E+02     3.3556E+02     ;     H15     -     N5      -
        H16

[ dihedrals ] ; propers
; treated as RBs in GROMACS to use combine multiple AMBER torsions per quartet
;   i     j     k     l   func    C0          C1          C2          C3          C4          C5
710     712     714     717     3     6.5084E-01     1.95253     0     -2.60338     0     0     ;
        N-      C-      C1-     O
711     710     712     713     3     0.0000E+00     0     0     0     0     0     ;
        H-      N-      C-      H1
711     710     712     714     3     0.0000E+00     0     0     0     0     0     ;
        H-      N-      C-      C1
712     714     717     718     3     4.9497E+00     8.15462     0     -6.40989     0     0     ;
        C-      C1-     O-      C2
713     712     714     715     3     6.5084E-01     1.95253     0     -2.60338     0     0     ;
        H1-     C-      C1-     H2
713     712     714     716     3     6.5084E-01     1.95253     0     -2.60338     0     0     ;
        H1-     C-      C1-     H3
713     712     714     717     3     1.0460E+00     -1.046     0     0     0     0     ;
        H1-     C-      C1-     O
714     717     718     719     3     2.8451E+01     5.8576     -22.5936     0     0     0     ;
        C1-     O-      C2-     O1
714     717     718     720     3     2.7405E+01     14.4348     -22.5936     -19.2464     0     0     ;
        C1-     O-      C2-     C3
715     714     717     718     3     1.6039E+00     4.8116     0     -6.41547     0     0     ;
        H2-     C1-     O-      C2
716     714     717     718     3     1.6039E+00     4.8116     0     -6.41547     0     0     ;
        H3-     C1-     O-      C2
717     718     720     723     3     0.0000E+00     0     0     0     0     0     ;
        O-      C2-     C3-     C6
717     718     720     727     3     0.0000E+00     0     0     0     0     0     ;
        O-      C2-     C3-     H5
717     718     720     728     3     0.0000E+00     0     0     0     0     0     ;
        O-      C2-     C3-     N2
718     720     723     724     3     6.5084E-01     1.95253     0     -2.60338     0     0     ;
        C2-     C3-     C6-     H4
718     720     723     725     3     6.5084E-01     1.95253     0     -2.60338     0     0     ;
        C2-     C3-     C6-     S
718     720     723     726     3     6.5084E-01     1.95253     0     -2.60338     0     0     ;
        C2-     C3-     C6-     N1
718     720     728     738     3     1.0460E+01     -3.3472     -7.1128     0     0     0     ;
        C2-     C3-     N2-     C10
718     720     728     740     3     0.0000E+00     0     0     0     0     0     ;
        C2-     C3-     N2-     H10
719     718     720     723     3     0.0000E+00     0     0     0     0     0     ;
        O1-     C2-     C3-     C6
719     718     720     727     3     3.6819E+00     -4.35136     0     1.33888     0     0     ;
        O1-     C2-     C3-     H5
719     718     720     728     3     0.0000E+00     0     0     0     0     0     ;
        O1-     C2-     C3-     N2
```

720	723	725	735	3	1.3947E+00	4.184	0	-5.57867	0	0	;
	C3-	C6-	S-	C9							
720	723	726	721	3	0.0000E+00	0	0	0	0	0	;
	C3-	C6-	N1-	C4							
720	728	738	739	3	2.0920E+01	0	-20.92	0	0	0	;
	C3-	N2-	C10-	O4							
720	728	738	741	3	2.0920E+01	0	-20.92	0	0	0	;
	C3-	N2-	C10-	C11							
721	722	732	733	3	5.5647E+01	0	-55.6472	0	0	0	;
	C4-	C5-	C8-	H6							
721	722	732	734	3	5.5647E+01	0	-55.6472	0	0	0	;
	C4-	C5-	C8-	H7							
721	722	735	725	3	0.0000E+00	0	0	0	0	0	;
	C4-	C5-	C9-	S							
721	722	735	736	3	6.4015E+00	-9.58136	0	6.35968	0	0	;
	C4-	C5-	C9-	H8							
721	722	735	737	3	6.4015E+00	-9.58136	0	6.35968	0	0	;
	C4-	C5-	C9-	H9							
721	726	723	724	3	0.0000E+00	0	0	0	0	0	;
	C4-	N1-	C6-	H4							
721	726	723	725	3	0.0000E+00	0	0	0	0	0	;
	C4-	N1-	C6-	S							
722	721	726	723	3	6.6944E+00	0	-6.6944	0	0	0	;
	C5-	C4-	N1-	C6							
722	721	729	730	3	1.8200E+01	0	-18.2004	0	0	0	;
	C5-	C4-	C7-	O2							
722	721	729	731	3	1.8200E+01	0	-18.2004	0	0	0	;
	C5-	C4-	C7-	O3							
722	735	725	723	3	1.3947E+00	4.184	0	-5.57867	0	0	;
	C5-	C9-	S-	C6							
723	720	728	738	3	2.8451E+00	-4.10032	16.736	2.5104	-16.736	0	;
	C6-	C3-	N2-	C10							
723	720	728	740	3	0.0000E+00	0	0	0	0	0	;
	C6-	C3-	N2-	H10							
723	725	735	736	3	1.3947E+00	4.184	0	-5.57867	0	0	;
	C6-	S-	C9-	H8							
723	725	735	737	3	1.3947E+00	4.184	0	-5.57867	0	0	;
	C6-	S-	C9-	H9							
723	726	721	729	3	6.6944E+00	0	-6.6944	0	0	0	;
	C6-	N1-	C4-	C7							
724	723	720	727	3	6.5084E-01	1.95253	0	-2.60338	0	0	;
	H4-	C6-	C3-	H5							
724	723	720	728	3	6.5084E-01	1.95253	0	-2.60338	0	0	;
	H4-	C6-	C3-	N2							
724	723	725	735	3	1.3947E+00	4.184	0	-5.57867	0	0	;
	H4-	C6-	S-	C9							
725	723	720	727	3	6.5084E-01	1.95253	0	-2.60338	0	0	;
	S-	C6-	C3-	H5							
725	723	720	728	3	6.5084E-01	1.95253	0	-2.60338	0	0	;
	S-	C6-	C3-	N2							
725	735	722	732	3	0.0000E+00	0	0	0	0	0	;
	S-	C9-	C5-	C8							
726	721	722	732	3	8.3680E+00	0	-8.368	0	0	0	;
	N1-	C4-	C5-	C8							
726	721	722	735	3	8.3680E+00	0	-8.368	0	0	0	;
	N1-	C4-	C5-	C9							
726	721	729	730	3	1.8200E+01	0	-18.2004	0	0	0	;
	N1-	C4-	C7-	O2							
726	721	729	731	3	1.8200E+01	0	-18.2004	0	0	0	;
	N1-	C4-	C7-	O3							
726	723	720	727	3	6.5084E-01	1.95253	0	-2.60338	0	0	;
	N1-	C6-	C3-	H5							
726	723	720	728	3	6.5084E-01	1.95253	0	-2.60338	0	0	;
	N1-	C6-	C3-	N2							
726	723	725	735	3	1.3947E+00	4.184	0	-5.57867	0	0	;
	N1-	C6-	S-	C9							
727	720	728	738	3	0.0000E+00	0	0	0	0	0	;
	H5-	C3-	N2-	C10							
727	720	728	740	3	0.0000E+00	0	0	0	0	0	;
	H5-	C3-	N2-	H10							

728	738	741	742	3	1.8200E+01	0	-18.2004	0	0	0	;
	N2-	C10-	C11-	N3							
728	738	741	748	3	1.8200E+01	0	-18.2004	0	0	0	;
	N2-	C10-	C11-	C13							
729	721	722	732	3	8.3680E+00	0	-8.368	0	0	0	;
	C7-	C4-	C5-	C8							
729	721	722	735	3	8.3680E+00	0	-8.368	0	0	0	;
	C7-	C4-	C5-	C9							
732	722	735	736	3	6.4015E+00	-9.58136	0	6.35968	0	0	;
	C8-	C5-	C9-	H8							
732	722	735	737	3	6.4015E+00	-9.58136	0	6.35968	0	0	;
	C8-	C5-	C9-	H9							
733	732	722	735	3	5.5647E+01	0	-55.6472	0	0	0	;
	H6-	C8-	C5-	C9							
734	732	722	735	3	5.5647E+01	0	-55.6472	0	0	0	;
	H7-	C8-	C5-	C9							
738	741	742	743	3	6.6944E+00	0	-6.6944	0	0	0	;
	C10-	C11-	N3-	O5							
738	741	748	749	3	8.3680E+00	0	-8.368	0	0	0	;
	C10-	C11-	C13-	C14							
738	741	748	753	3	8.3680E+00	0	-8.368	0	0	0	;
	C10-	C11-	C13-	N4							
739	738	728	740	3	2.9288E+01	-8.368	-20.92	0	0	0	;
	O4-	C10-	N2-	H10							
739	738	741	742	3	1.8200E+01	0	-18.2004	0	0	0	;
	O4-	C10-	C11-	N3							
739	738	741	748	3	1.8200E+01	0	-18.2004	0	0	0	;
	O4-	C10-	C11-	C13							
740	728	738	741	3	2.0920E+01	0	-20.92	0	0	0	;
	H10-	N2-	C10-	C11							
741	742	743	744	3	2.5104E+01	0	-25.104	0	0	0	;
	C11-	N3-	O5-	C12							
741	748	749	750	3	3.3472E+01	0	-33.472	0	0	0	;
	C11-	C13-	C14-	H14							
741	748	749	752	3	3.3472E+01	0	-33.472	0	0	0	;
	C11-	C13-	C14-	S1							
741	748	753	751	3	3.9748E+01	0	-39.748	0	0	0	;
	C11-	C13-	N4-	C15							
742	741	748	749	3	8.3680E+00	0	-8.368	0	0	0	;
	N3-	C11-	C13-	C14							
742	741	748	753	3	8.3680E+00	0	-8.368	0	0	0	;
	N3-	C11-	C13-	N4							
742	743	744	745	3	1.6039E+00	4.8116	0	-6.41547	0	0	;
	N3-	O5-	C12-	H11							
742	743	744	746	3	1.6039E+00	4.8116	0	-6.41547	0	0	;
	N3-	O5-	C12-	H12							
742	743	744	747	3	1.6039E+00	4.8116	0	-6.41547	0	0	;
	N3-	O5-	C12-	H13							
743	742	741	748	3	6.6944E+00	0	-6.6944	0	0	0	;
	O5-	N3-	C11-	C13							
748	749	752	751	3	9.2048E+00	0	-9.2048	0	0	0	;
	C13-	C14-	S1-	C15							
748	753	751	752	3	3.9748E+01	0	-39.748	0	0	0	;
	C13-	N4-	C15-	S1							
748	753	751	754	3	3.9748E+01	0	-39.748	0	0	0	;
	C13-	N4-	C15-	N5							
749	748	753	751	3	3.9748E+01	0	-39.748	0	0	0	;
	C14-	C13-	N4-	C15							
749	752	751	753	3	9.2048E+00	0	-9.2048	0	0	0	;
	C14-	S1-	C15-	N4							
749	752	751	754	3	9.2048E+00	0	-9.2048	0	0	0	;
	C14-	S1-	C15-	N5							
750	749	748	753	3	3.3472E+01	0	-33.472	0	0	0	;
	H14-	C14-	C13-	N4							
750	749	752	751	3	9.2048E+00	0	-9.2048	0	0	0	;
	H14-	C14-	S1-	C15							
752	749	748	753	3	3.3472E+01	0	-33.472	0	0	0	;
	S1-	C14-	C13-	N4							
752	751	754	755	3	8.7864E+00	0	-8.7864	0	0	0	;
	S1-	C15-	N5-	H15							

752	751	754	756	3	8.7864E+00	0	-8.7864	0	0	0	;
	S1-	C15-	N5-	H16							
753	751	754	755	3	8.7864E+00	0	-8.7864	0	0	0	;
	N4-	C15-	N5-	H15							
753	751	754	756	3	8.7864E+00	0	-8.7864	0	0	0	;
	N4-	C15-	N5-	H16							

[dihedrals] ; impropers
; treated as propers in GROMACS to use correct AMBER analytical function

; i	j	k	l	func	phase	kd	pn						
720	719	718	717	1	180	4.6024	2	;	C3-	O1-	C2-	O
721	730	729	731	1	180	4.6024	2	;	C4-	O2-	C7-	O3
722	733	732	734	1	180	4.6024	2	;	C5-	H6-	C8-	H7
729	722	721	726	1	180	4.6024	2	;	C7-	C5-	C4-	N1
732	735	722	721	1	180	4.6024	2	;	C8-	C9-	C5-	C4
738	720	728	740	1	180	4.6024	2	;	C10-	C3-	N2-	H10
738	748	741	742	1	180	4.6024	2	;	C10-	C13-	C11-	N3
741	728	738	739	1	180	43.932	2	;	C11-	N2-	C10-	O4
748	750	749	752	1	180	4.6024	2	;	C13-	H14-	C14-	S1
749	741	748	753	1	180	4.6024	2	;	C14-	C11-	C13-	N4
751	755	754	756	1	180	4.6024	2	;	C15-	H15-	N5-	H16
753	754	751	752	1	180	4.6024	2	;	N4-	N5-	C15-	S1

Matlab Scripts –

"MMLam.m"

```
function [Km,kcat,y,residual,StErr]=MMLam(Data);
%"Data" is a 2-column matrix of x-values (1st column; sec), and y-values (2nd
%column; uM)for analytical fitting of steady-state time traces.
    t=Data(:,1); %Time (sec), t
    St=Data(:,2); %Substrate concentration (uM) at each time, t
    function W=Lambert(beta,t,St)
    S0=100.00; %Starting substrate concentration (uM)
    E0=1.0; %Enzyme concentration (uM)
    Km=beta(1);
    kcat=beta(2);

    W=Km*lambertw((exp((S0-kcat*E0*t)./Km)).*(S0/Km)); %General form for MM kinetics
    end
fun=@Lambert;
beta0=[50, 50]; %initial guess for KM (uM) and kcat (sec-1)
options=statset('FunValCheck','off');
[beta,R,J,CovB]=nlinfit(t,St,fun,beta0,options);

y=beta(1)*lambertw((exp((S0-beta(2)*E0*t)./beta(1))).*(S0/beta(1)));
format long
Km=beta(1);
kcat=beta(2);
residual=R;
plot(t,St,t,y,t,St-y)
StErr=(sqrt(diag(CovB)));
end
```

"KineticEstimator.m"

```
function [t,U]=KineticEstimator(KM,kcat,S0,E0);
%Analytic simulation of a progress curve for steady-state enzymatic catalysis given a
set of kinetic parameters. Useful for predicting the duration of various kinetic
regimes. Input parameters as follows: KM=Michaelis Constant (uM), kcat (sec-1),
%S0=time-zero substrate concentration (uM), E0=time-zero enzyme
%concentration (uM)
t=[0:1:600]; %time domain to simulate (sec)
F=(S0/KM)*(exp((S0-(E0*kcat*t))/KM));
U=KM*lambertw(F);
plot(t,U)
xlabel('Time (sec)')
```

```
ylabel('[Substrate] (uM)')
xlim([min(t), max(t)])
ylim([-50 max(U)])
```

"MassAnalysis_Gaussian.m"

```
%% MassAnalysis_Gaussian
% Script for analyzing steady-state MS data of protein charge envelope.
% Input intact mass of free and covalently-bound enzyme, in addition to x (Da), y
% (counts) data for analysis. Input is a .txt file with two column format,
% x-data is in the first column, y-data in the second. This version implements
% a Gaussian baselining protocol to be implemented in the fitting, see
% lines for details. Written by Sam Schneider (Revised Jan 2020) for
% evaluation of acyl-enzyme/Michaelis complex ratios in TEM B-lactamases.
%% Load Data and Input Nominal Masses and Desired Baseline
% load MS data (x,y) from .txt file
[fname,pname]=uigetfile('*.*','Load MS Spectrum','MultiSelect','on');
cd(pname);
Data=readtable(fname,'Delimiter',' ','Format','%f %f','ReadVariableNames',false);
Da=Data; %x-data
Counts=Data; %y-data

%input mass of free (E) and bound enzyme (EA)
dlgtitle='Input Information';
numLines=1;
prompt1={'E mass (Da)','EA mass (Da)'};
def1={'31500','31914'};
answer1=inputdlg(prompt1,dlgtitle,numLines,def1);
drawnow

%Input the approximate masses of E and EA complex for guiding the fits. If
%too far off (+-30Da) may yield errors.
E_mass=str2num(char(answer1(1)));
EA_mass=str2num(char(answer1(2)));

%% Initial Fitting Parameter Initialization
Intensities=zeros(20,8); %Initialize matrix containing the n, E/n, area_1, area_2,
EA/n, area_1, area_2 values
E=zeros(20,1); % starting conditions for mass_fracs for enzyme
EA=zeros(20,1); %starting conditions for mass_fracs for EA complex

%Determine the starting guesses/bounds for the peak position searches to
%bound the fits
for n=1:20;
    E(n,1)=E_mass/(40-n);
    EA(n,1)=EA_mass/(40-n);
    Intensities(n,1)=(40-n);
end

offset=1.5;
amplb=0.9*min(Counts);
```

```
ampub=1.1*max(Counts);
ampstart=max(Counts);

%% Gaussian Baselining
% Fit 1 - Fit Main Peak (bounds of shoulder set to 0)
fun=@(a,x)a(2)*exp(-((x-a(3)).^2)/(2*a(1)^2))+a(4)*exp(-((x-
a(5)).^2)/(2*a(1)^2))+a(6)*exp(-((x-a(7)).^2)/(2*a(1)^2))+a(8)*exp(-((x-
a(9)).^2)/(2*a(1)^2))+a(10)*exp(-((x-a(11)).^2)/(2*a(1)^2))+a(12)*exp(-((x-
a(13)).^2)/(2*a(1)^2))+a(14)*exp(-((x-a(15)).^2)/(2*a(1)^2))+a(16)*exp(-((x-
a(17)).^2)/(2*a(1)^2))+a(18)*exp(-((x-a(19)).^2)/(2*a(1)^2))+a(20)*exp(-((x-
a(21)).^2)/(2*a(1)^2))+a(22)*exp(-((x-a(23)).^2)/(2*a(1)^2))+a(24)*exp(-((x-
a(25)).^2)/(2*a(1)^2))+a(26)*exp(-((x-a(27)).^2)/(2*a(1)^2))+a(28)*exp(-((x-
a(29)).^2)/(2*a(1)^2))+a(30)*exp(-((x-a(31)).^2)/(2*a(1)^2))+a(32)*exp(-((x-
a(33)).^2)/(2*a(1)^2))+a(34)*exp(-((x-a(35)).^2)/(2*a(1)^2))+a(36)*exp(-((x-
a(37)).^2)/(2*a(1)^2))+a(38)*exp(-((x-a(39)).^2)/(2*a(1)^2))+a(40)*exp(-((x-
a(41)).^2)/(2*a(1)^2))+a(42)*exp(-((x-a(43)).^2)/(2*a(1)^2))+a(44)*exp(-((x-
a(45)).^2)/(2*a(1)^2))+a(46)*exp(-((x-a(47)).^2)/(2*a(1)^2))+a(48)*exp(-((x-
a(49)).^2)/(2*a(1)^2))+a(50)*exp(-((x-a(51)).^2)/(2*a(1)^2))+a(52)*exp(-((x-
a(53)).^2)/(2*a(1)^2))+a(54)*exp(-((x-a(55)).^2)/(2*a(1)^2))+a(56)*exp(-((x-
a(57)).^2)/(2*a(1)^2))+a(58)*exp(-((x-a(59)).^2)/(2*a(1)^2))+a(60)*exp(-((x-
a(61)).^2)/(2*a(1)^2))+a(62)*exp(-((x-a(63)).^2)/(2*a(1)^2))+a(64)*exp(-((x-
a(65)).^2)/(2*a(1)^2))+a(66)*exp(-((x-a(67)).^2)/(2*a(1)^2))+a(68)*exp(-((x-
a(69)).^2)/(2*a(1)^2))+a(70)*exp(-((x-a(71)).^2)/(2*a(1)^2))+a(72)*exp(-((x-
a(73)).^2)/(2*a(1)^2))+a(74)*exp(-((x-a(75)).^2)/(2*a(1)^2))+a(76)*exp(-((x-
a(77)).^2)/(2*a(1)^2))+a(78)*exp(-((x-a(79)).^2)/(2*a(1)^2))+a(80)*exp(-((x-
a(81)).^2)/(2*a(1)^2))+a(82)*exp(-((x-a(3)+a(122)).^2)/(2*a(1)^2))+a(83)*exp(-((x-
a(5)+a(122)).^2)/(2*a(1)^2))+a(84)*exp(-((x-a(7)+a(122)).^2)/(2*a(1)^2))+a(85)*exp(-
((x-a(9)+a(122)).^2)/(2*a(1)^2))+a(86)*exp(-((x-
a(11)+a(122)).^2)/(2*a(1)^2))+a(87)*exp(-((x-a(13)+a(122)).^2)/(2*a(1)^2))+a(88)*exp(-
((x-a(15)+a(122)).^2)/(2*a(1)^2))+a(89)*exp(-((x-
a(17)+a(122)).^2)/(2*a(1)^2))+a(90)*exp(-((x-a(19)+a(122)).^2)/(2*a(1)^2))+a(91)*exp(-
((x-a(21)+a(122)).^2)/(2*a(1)^2))+a(92)*exp(-((x-
a(23)+a(122)).^2)/(2*a(1)^2))+a(93)*exp(-((x-a(25)+a(122)).^2)/(2*a(1)^2))+a(94)*exp(-
((x-a(27)+a(122)).^2)/(2*a(1)^2))+a(95)*exp(-((x-
a(29)+a(122)).^2)/(2*a(1)^2))+a(96)*exp(-((x-a(31)+a(122)).^2)/(2*a(1)^2))+a(97)*exp(-
((x-a(33)+a(122)).^2)/(2*a(1)^2))+a(98)*exp(-((x-
a(35)+a(122)).^2)/(2*a(1)^2))+a(99)*exp(-((x-
a(37)+a(122)).^2)/(2*a(1)^2))+a(100)*exp(-((x-
a(39)+a(122)).^2)/(2*a(1)^2))+a(101)*exp(-((x-
a(41)+a(122)).^2)/(2*a(1)^2))+a(102)*exp(-((x-
a(43)+a(122)).^2)/(2*a(1)^2))+a(103)*exp(-((x-
a(45)+a(122)).^2)/(2*a(1)^2))+a(104)*exp(-((x-
a(47)+a(122)).^2)/(2*a(1)^2))+a(105)*exp(-((x-
a(49)+a(122)).^2)/(2*a(1)^2))+a(106)*exp(-((x-
a(51)+a(122)).^2)/(2*a(1)^2))+a(107)*exp(-((x-
a(53)+a(122)).^2)/(2*a(1)^2))+a(108)*exp(-((x-
a(55)+a(122)).^2)/(2*a(1)^2))+a(109)*exp(-((x-
a(57)+a(122)).^2)/(2*a(1)^2))+a(110)*exp(-((x-
a(59)+a(122)).^2)/(2*a(1)^2))+a(111)*exp(-((x-
a(61)+a(122)).^2)/(2*a(1)^2))+a(112)*exp(-((x-
a(63)+a(122)).^2)/(2*a(1)^2))+a(113)*exp(-((x-
a(65)+a(122)).^2)/(2*a(1)^2))+a(114)*exp(-((x-
a(67)+a(122)).^2)/(2*a(1)^2))+a(115)*exp(-((x-
a(69)+a(122)).^2)/(2*a(1)^2))+a(116)*exp(-((x-
a(71)+a(122)).^2)/(2*a(1)^2))+a(117)*exp(-((x-
a(73)+a(122)).^2)/(2*a(1)^2))+a(118)*exp(-((x-
a(75)+a(122)).^2)/(2*a(1)^2))+a(119)*exp(-((x-
a(77)+a(122)).^2)/(2*a(1)^2))+a(120)*exp(-((x-
a(79)+a(122)).^2)/(2*a(1)^2))+a(121)*exp(-((x-
a(81)+a(122)).^2)/(2*a(1)^2))+a(123)*exp(-((x-a(124)).^2)/(2*a(125)^2)); %a(1)=width
of all peaks, a(122)=shoulder offset, a(123-126) are for underlying polynomial (3rd-
order) baseline
```

```
a0=[0.3 ampstart E(1,1) ampstart EA(1,1) ampstart E(2,1) ampstart EA(2,1) ampstart
E(3,1) ampstart EA(3,1) ampstart E(4,1) ampstart EA(4,1) ampstart E(5,1) ampstart
EA(5,1) ampstart E(6,1) ampstart EA(6,1) ampstart E(7,1) ampstart EA(7,1) ampstart
E(8,1) ampstart EA(8,1) ampstart E(9,1) ampstart EA(9,1) ampstart E(10,1) ampstart
EA(10,1) ampstart E(11,1) ampstart EA(11,1) ampstart E(12,1) ampstart EA(12,1)
ampstart E(13,1) ampstart EA(13,1) ampstart E(14,1) ampstart EA(14,1) ampstart E(15,1)
ampstart EA(15,1)  ampstart E(16,1) ampstart EA(16,1)  ampstart E(17,1) ampstart
EA(17,1) ampstart E(18,1) ampstart EA(18,1) ampstart E(19,1) ampstart EA(19,1)
ampstart E(20,1) ampstart EA(20,1) 0 0 0 0 0 0 0 0 0 0 0 0 0 0 0 0 0 0 0 0 0 0 0 0 0 0 0 0
0 0 0 0 0 0 0 0 0 0 0 0 0 -1 2E5 950 200 ];
lb=[0.2 amplb E(1,1)-offset amplb EA(1,1)-offset amplb E(2,1)-offset amplb EA(2,1)-
offset amplb E(3,1)-offset amplb EA(3,1)-offset amplb E(4,1)-offset amplb EA(4,1)-
offset amplb E(5,1)-offset amplb EA(5,1)-offset amplb E(6,1)-offset amplb EA(6,1)-
offset amplb E(7,1)-offset amplb EA(7,1)-offset amplb E(8,1)-offset amplb EA(8,1)-
offset amplb E(9,1)-offset amplb EA(9,1)-offset amplb E(10,1)-offset amplb EA(10,1)-
offset amplb E(11,1)-offset amplb EA(11,1)-offset amplb E(12,1)-offset amplb EA(12,1)-
offset amplb E(13,1)-offset amplb EA(13,1)-offset amplb E(14,1)-offset amplb EA(14,1)-
offset amplb E(15,1)-offset amplb EA(15,1)-offset  amplb E(16,1)-offset amplb
EA(16,1)-offset  amplb E(17,1)-offset amplb EA(17,1)-offset amplb E(18,1)-offset amplb
EA(18,1)-offset amplb E(19,1)-offset amplb EA(19,1)-offset amplb E(20,1)-offset amplb
EA(20,1)-offset 0 0 0 0 0 0 0 0 0 0 0 0 0 0 0 0 0 0 0 0 0 0 0 0 0 0 0 0 0 0 0 0 0 0 0 0 0
0 0 0 0 0 -2.0 -Inf -Inf -Inf ];
ub=[0.3 ampub E(1,1)+offset ampub EA(1,1)+offset ampub E(2,1)+offset ampub
EA(2,1)+offset ampub E(3,1)+offset ampub EA(3,1)+offset ampub E(4,1)+offset ampub
EA(4,1)+offset ampub E(5,1)+offset ampub EA(5,1)+offset ampub E(6,1)+offset ampub
EA(6,1)+offset ampub E(7,1)+offset ampub EA(7,1)+offset ampub E(8,1)+offset ampub
EA(8,1)+offset ampub E(9,1)+offset ampub EA(9,1)+offset ampub E(10,1)+offset ampub
EA(10,1)+offset ampub E(11,1)+offset ampub EA(11,1)+offset ampub E(12,1)+offset ampub
EA(12,1)+offset ampub E(13,1)+offset ampub EA(13,1)+offset ampub E(14,1)+offset ampub
EA(14,1)+offset ampub E(15,1)+offset ampub EA(15,1)+offset  ampub E(16,1)+offset ampub
EA(16,1)+offset  ampub E(17,1)+offset ampub EA(17,1)+offset ampub E(18,1)+offset ampub
EA(18,1)+offset ampub E(19,1)+offset ampub EA(19,1)+offset ampub E(20,1)+offset ampub
EA(20,1)+offset 0 0 0 0 0 0 0 0 0 0 0 0 0 0 0 0 0 0 0 0 0 0 0 0 0 0 0 0 0 0 0 0 0 0 0 0 0
0 0 0 0 0 -0.5 Inf Inf Inf ];

options=optimset('MaxFunEvals',5000000,'TolFun',1e-10,'MaxIter',20000,'TolX', 1E-8);
%options parameters for fitting
[a,resnorm,residual,exitflag,output,lambda,jacobian] = lsqcurvefit(fun, a0, Da,
Counts,lb,ub,options);

% Fit 2 - Fit shoulder (fix main peak)
fun=@(a,x)a(2)*exp(-((x-a(3)).^2)/(2*a(1)^2))+a(4)*exp(-((x-
a(5)).^2)/(2*a(1)^2))+a(6)*exp(-((x-a(7)).^2)/(2*a(1)^2))+a(8)*exp(-((x-
a(9)).^2)/(2*a(1)^2))+a(10)*exp(-((x-a(11)).^2)/(2*a(1)^2))+a(12)*exp(-((x-
a(13)).^2)/(2*a(1)^2))+a(14)*exp(-((x-a(15)).^2)/(2*a(1)^2))+a(16)*exp(-((x-
a(17)).^2)/(2*a(1)^2))+a(18)*exp(-((x-a(19)).^2)/(2*a(1)^2))+a(20)*exp(-((x-
a(21)).^2)/(2*a(1)^2))+a(22)*exp(-((x-a(23)).^2)/(2*a(1)^2))+a(24)*exp(-((x-
a(25)).^2)/(2*a(1)^2))+a(26)*exp(-((x-a(27)).^2)/(2*a(1)^2))+a(28)*exp(-((x-
a(29)).^2)/(2*a(1)^2))+a(30)*exp(-((x-a(31)).^2)/(2*a(1)^2))+a(32)*exp(-((x-
a(33)).^2)/(2*a(1)^2))+a(34)*exp(-((x-a(35)).^2)/(2*a(1)^2))+a(36)*exp(-((x-
a(37)).^2)/(2*a(1)^2))+a(38)*exp(-((x-a(39)).^2)/(2*a(1)^2))+a(40)*exp(-((x-
a(41)).^2)/(2*a(1)^2))+a(42)*exp(-((x-a(43)).^2)/(2*a(1)^2))+a(44)*exp(-((x-
a(45)).^2)/(2*a(1)^2))+a(46)*exp(-((x-a(47)).^2)/(2*a(1)^2))+a(48)*exp(-((x-
a(49)).^2)/(2*a(1)^2))+a(50)*exp(-((x-a(51)).^2)/(2*a(1)^2))+a(52)*exp(-((x-
a(53)).^2)/(2*a(1)^2))+a(54)*exp(-((x-a(55)).^2)/(2*a(1)^2))+a(56)*exp(-((x-
a(57)).^2)/(2*a(1)^2))+a(58)*exp(-((x-a(59)).^2)/(2*a(1)^2))+a(60)*exp(-((x-
a(61)).^2)/(2*a(1)^2))+a(62)*exp(-((x-a(63)).^2)/(2*a(1)^2))+a(64)*exp(-((x-
a(65)).^2)/(2*a(1)^2))+a(66)*exp(-((x-a(67)).^2)/(2*a(1)^2))+a(68)*exp(-((x-
a(69)).^2)/(2*a(1)^2))+a(70)*exp(-((x-a(71)).^2)/(2*a(1)^2))+a(72)*exp(-((x-
a(73)).^2)/(2*a(1)^2))+a(74)*exp(-((x-a(75)).^2)/(2*a(1)^2))+a(76)*exp(-((x-
a(77)).^2)/(2*a(1)^2))+a(78)*exp(-((x-a(79)).^2)/(2*a(1)^2))+a(80)*exp(-((x-
a(81)).^2)/(2*a(1)^2))+a(82)*exp(-((x-a(3)+a(122)).^2)/(2*a(1)^2))+a(83)*exp(-((x-
a(5)+a(122)).^2)/(2*a(1)^2))+a(84)*exp(-((x-a(7)+a(122)).^2)/(2*a(1)^2))+a(85)*exp(-
```

```
((x-a(9)+a(122)).^2)/(2*a(1)^2))+a(86)*exp(-((x-
a(11)+a(122)).^2)/(2*a(1)^2))+a(87)*exp(-((x-a(13)+a(122)).^2)/(2*a(1)^2))+a(88)*exp(-
((x-a(15)+a(122)).^2)/(2*a(1)^2))+a(89)*exp(-((x-
a(17)+a(122)).^2)/(2*a(1)^2))+a(90)*exp(-((x-a(19)+a(122)).^2)/(2*a(1)^2))+a(91)*exp(-
((x-a(21)+a(122)).^2)/(2*a(1)^2))+a(92)*exp(-((x-
a(23)+a(122)).^2)/(2*a(1)^2))+a(93)*exp(-((x-a(25)+a(122)).^2)/(2*a(1)^2))+a(94)*exp(-
((x-a(27)+a(122)).^2)/(2*a(1)^2))+a(95)*exp(-((x-
a(29)+a(122)).^2)/(2*a(1)^2))+a(96)*exp(-((x-a(31)+a(122)).^2)/(2*a(1)^2))+a(97)*exp(-
((x-a(33)+a(122)).^2)/(2*a(1)^2))+a(98)*exp(-((x-
a(35)+a(122)).^2)/(2*a(1)^2))+a(99)*exp(-((x-
a(37)+a(122)).^2)/(2*a(1)^2))+a(100)*exp(-((x-
a(39)+a(122)).^2)/(2*a(1)^2))+a(101)*exp(-((x-
a(41)+a(122)).^2)/(2*a(1)^2))+a(102)*exp(-((x-
a(43)+a(122)).^2)/(2*a(1)^2))+a(103)*exp(-((x-
a(45)+a(122)).^2)/(2*a(1)^2))+a(104)*exp(-((x-
a(47)+a(122)).^2)/(2*a(1)^2))+a(105)*exp(-((x-
a(49)+a(122)).^2)/(2*a(1)^2))+a(106)*exp(-((x-
a(51)+a(122)).^2)/(2*a(1)^2))+a(107)*exp(-((x-
a(53)+a(122)).^2)/(2*a(1)^2))+a(108)*exp(-((x-
a(55)+a(122)).^2)/(2*a(1)^2))+a(109)*exp(-((x-
a(57)+a(122)).^2)/(2*a(1)^2))+a(110)*exp(-((x-
a(59)+a(122)).^2)/(2*a(1)^2))+a(111)*exp(-((x-
a(61)+a(122)).^2)/(2*a(1)^2))+a(112)*exp(-((x-
a(63)+a(122)).^2)/(2*a(1)^2))+a(113)*exp(-((x-
a(65)+a(122)).^2)/(2*a(1)^2))+a(114)*exp(-((x-
a(67)+a(122)).^2)/(2*a(1)^2))+a(115)*exp(-((x-
a(69)+a(122)).^2)/(2*a(1)^2))+a(116)*exp(-((x-
a(71)+a(122)).^2)/(2*a(1)^2))+a(117)*exp(-((x-
a(73)+a(122)).^2)/(2*a(1)^2))+a(118)*exp(-((x-
a(75)+a(122)).^2)/(2*a(1)^2))+a(119)*exp(-((x-
a(77)+a(122)).^2)/(2*a(1)^2))+a(120)*exp(-((x-
a(79)+a(122)).^2)/(2*a(1)^2))+a(121)*exp(-((x-
a(81)+a(122)).^2)/(2*a(1)^2))+a(123)*exp(-((x-a(124)).^2)/(2*a(125)^2)); %a(1)=width
of all peaks, a(122)=shoulder offset, a(123-126) are for underlying polynomial (3rd-
order) baseline
a0=a; %Uses the previously fit parameters as starting conditions for Fit 2, lb/ub for
1st peak fixed
lb=[0.3 a(2) a(3) a(4) a(5) a(6) a(7) a(8) a(9) a(10) a(11) a(12) a(13) a(14) a(15)
a(16) a(17) a(18) a(19) a(20) a(21) a(22) a(23) a(24) a(25) a(26) a(27) a(28) a(29)
a(30) a(31) a(32) a(33) a(34) a(35) a(36) a(37) a(38) a(39) a(40) a(41) a(42) a(43)
a(44) a(45) a(46) a(47) a(48) a(49) a(50) a(51) a(52) a(53) a(54) a(55) a(56) a(57)
a(58) a(59) a(60) a(61) a(62) a(63) a(64) a(65) a(66) a(67) a(68) a(69) a(70) a(71)
a(72) a(73) a(74) a(75) a(76) a(77) a(78) a(79) a(80) a(81) amplb amplb amplb amplb
amplb amplb amplb amplb amplb amplb amplb amplb amplb amplb amplb amplb amplb amplb
amplb amplb amplb amplb amplb amplb amplb amplb amplb amplb amplb amplb amplb amplb
amplb amplb amplb amplb amplb amplb amplb amplb -2.0 -Inf -Inf -Inf ];
ub=[0.3 a(2) a(3) a(4) a(5) a(6) a(7) a(8) a(9) a(10) a(11) a(12) a(13) a(14) a(15)
a(16) a(17) a(18) a(19) a(20) a(21) a(22) a(23) a(24) a(25) a(26) a(27) a(28) a(29)
a(30) a(31) a(32) a(33) a(34) a(35) a(36) a(37) a(38) a(39) a(40) a(41) a(42) a(43)
a(44) a(45) a(46) a(47) a(48) a(49) a(50) a(51) a(52) a(53) a(54) a(55) a(56) a(57)
a(58) a(59) a(60) a(61) a(62) a(63) a(64) a(65) a(66) a(67) a(68) a(69) a(70) a(71)
a(72) a(73) a(74) a(75) a(76) a(77) a(78) a(79) a(80) a(81) ampub ampub ampub ampub
ampub ampub ampub ampub ampub ampub ampub ampub ampub ampub ampub ampub ampub ampub
ampub ampub ampub ampub ampub ampub ampub ampub ampub ampub ampub ampub ampub ampub
ampub ampub ampub ampub ampub ampub ampub ampub -0.5 Inf Inf Inf ];

options=optimset('MaxFunEvals',5000000,'TolFun',1e-4,'MaxIter',20000,'TolX', 1E-4);
%options parameters for fitting
[a,resnorm,residual,exitflag,output,lambda,jacobian] = lsqcurvefit(fun, a0, Da,
Counts,lb,ub,options);

% Fit 3 - Final Fit, Relaxed Parameters
```

```
fun=@(a,x)a(2)*exp(-((x-a(3)).^2)/(2*a(1)^2))+a(4)*exp(-((x-
a(5)).^2)/(2*a(1)^2))+a(6)*exp(-((x-a(7)).^2)/(2*a(1)^2))+a(8)*exp(-((x-
a(9)).^2)/(2*a(1)^2))+a(10)*exp(-((x-a(11)).^2)/(2*a(1)^2))+a(12)*exp(-((x-
a(13)).^2)/(2*a(1)^2))+a(14)*exp(-((x-a(15)).^2)/(2*a(1)^2))+a(16)*exp(-((x-
a(17)).^2)/(2*a(1)^2))+a(18)*exp(-((x-a(19)).^2)/(2*a(1)^2))+a(20)*exp(-((x-
a(21)).^2)/(2*a(1)^2))+a(22)*exp(-((x-a(23)).^2)/(2*a(1)^2))+a(24)*exp(-((x-
a(25)).^2)/(2*a(1)^2))+a(26)*exp(-((x-a(27)).^2)/(2*a(1)^2))+a(28)*exp(-((x-
a(29)).^2)/(2*a(1)^2))+a(30)*exp(-((x-a(31)).^2)/(2*a(1)^2))+a(32)*exp(-((x-
a(33)).^2)/(2*a(1)^2))+a(34)*exp(-((x-a(35)).^2)/(2*a(1)^2))+a(36)*exp(-((x-
a(37)).^2)/(2*a(1)^2))+a(38)*exp(-((x-a(39)).^2)/(2*a(1)^2))+a(40)*exp(-((x-
a(41)).^2)/(2*a(1)^2))+a(42)*exp(-((x-a(43)).^2)/(2*a(1)^2))+a(44)*exp(-((x-
a(45)).^2)/(2*a(1)^2))+a(46)*exp(-((x-a(47)).^2)/(2*a(1)^2))+a(48)*exp(-((x-
a(49)).^2)/(2*a(1)^2))+a(50)*exp(-((x-a(51)).^2)/(2*a(1)^2))+a(52)*exp(-((x-
a(53)).^2)/(2*a(1)^2))+a(54)*exp(-((x-a(55)).^2)/(2*a(1)^2))+a(56)*exp(-((x-
a(57)).^2)/(2*a(1)^2))+a(58)*exp(-((x-a(59)).^2)/(2*a(1)^2))+a(60)*exp(-((x-
a(61)).^2)/(2*a(1)^2))+a(62)*exp(-((x-a(63)).^2)/(2*a(1)^2))+a(64)*exp(-((x-
a(65)).^2)/(2*a(1)^2))+a(66)*exp(-((x-a(67)).^2)/(2*a(1)^2))+a(68)*exp(-((x-
a(69)).^2)/(2*a(1)^2))+a(70)*exp(-((x-a(71)).^2)/(2*a(1)^2))+a(72)*exp(-((x-
a(73)).^2)/(2*a(1)^2))+a(74)*exp(-((x-a(75)).^2)/(2*a(1)^2))+a(76)*exp(-((x-
a(77)).^2)/(2*a(1)^2))+a(78)*exp(-((x-a(79)).^2)/(2*a(1)^2))+a(80)*exp(-((x-
a(81)).^2)/(2*a(1)^2))+a(82)*exp(-((x-a(3)+a(122)).^2)/(2*a(1)^2))+a(83)*exp(-((x-
a(5)+a(122)).^2)/(2*a(1)^2))+a(84)*exp(-((x-a(7)+a(122)).^2)/(2*a(1)^2))+a(85)*exp(-
((x-a(9)+a(122)).^2)/(2*a(1)^2))+a(86)*exp(-((x-
a(11)+a(122)).^2)/(2*a(1)^2))+a(87)*exp(-((x-a(13)+a(122)).^2)/(2*a(1)^2))+a(88)*exp(-
((x-a(15)+a(122)).^2)/(2*a(1)^2))+a(89)*exp(-((x-
a(17)+a(122)).^2)/(2*a(1)^2))+a(90)*exp(-((x-a(19)+a(122)).^2)/(2*a(1)^2))+a(91)*exp(-
((x-a(21)+a(122)).^2)/(2*a(1)^2))+a(92)*exp(-((x-
a(23)+a(122)).^2)/(2*a(1)^2))+a(93)*exp(-((x-a(25)+a(122)).^2)/(2*a(1)^2))+a(94)*exp(-
((x-a(27)+a(122)).^2)/(2*a(1)^2))+a(95)*exp(-((x-
a(29)+a(122)).^2)/(2*a(1)^2))+a(96)*exp(-((x-a(31)+a(122)).^2)/(2*a(1)^2))+a(97)*exp(-
((x-a(33)+a(122)).^2)/(2*a(1)^2))+a(98)*exp(-((x-
a(35)+a(122)).^2)/(2*a(1)^2))+a(99)*exp(-((x-
a(37)+a(122)).^2)/(2*a(1)^2))+a(100)*exp(-((x-
a(39)+a(122)).^2)/(2*a(1)^2))+a(101)*exp(-((x-
a(41)+a(122)).^2)/(2*a(1)^2))+a(102)*exp(-((x-
a(43)+a(122)).^2)/(2*a(1)^2))+a(103)*exp(-((x-
a(45)+a(122)).^2)/(2*a(1)^2))+a(104)*exp(-((x-
a(47)+a(122)).^2)/(2*a(1)^2))+a(105)*exp(-((x-
a(49)+a(122)).^2)/(2*a(1)^2))+a(106)*exp(-((x-
a(51)+a(122)).^2)/(2*a(1)^2))+a(107)*exp(-((x-
a(53)+a(122)).^2)/(2*a(1)^2))+a(108)*exp(-((x-
a(55)+a(122)).^2)/(2*a(1)^2))+a(109)*exp(-((x-
a(57)+a(122)).^2)/(2*a(1)^2))+a(110)*exp(-((x-
a(59)+a(122)).^2)/(2*a(1)^2))+a(111)*exp(-((x-
a(61)+a(122)).^2)/(2*a(1)^2))+a(112)*exp(-((x-
a(63)+a(122)).^2)/(2*a(1)^2))+a(113)*exp(-((x-
a(65)+a(122)).^2)/(2*a(1)^2))+a(114)*exp(-((x-
a(67)+a(122)).^2)/(2*a(1)^2))+a(115)*exp(-((x-
a(69)+a(122)).^2)/(2*a(1)^2))+a(116)*exp(-((x-
a(71)+a(122)).^2)/(2*a(1)^2))+a(117)*exp(-((x-
a(73)+a(122)).^2)/(2*a(1)^2))+a(118)*exp(-((x-
a(75)+a(122)).^2)/(2*a(1)^2))+a(119)*exp(-((x-
a(77)+a(122)).^2)/(2*a(1)^2))+a(120)*exp(-((x-
a(79)+a(122)).^2)/(2*a(1)^2))+a(121)*exp(-((x-
a(81)+a(122)).^2)/(2*a(1)^2))+a(123)*exp(-((x-a(124)).^2)/(2*a(125)^2)); %a(1)=width
of all peaks, a(122)=shoulder offset, a(123-126) are for underlying polynomial (3rd-
order) baseline
a0=a;
lb=[0.2 amplb E(1,1)-offset amplb EA(1,1)-offset amplb E(2,1)-offset amplb EA(2,1)-
offset amplb E(3,1)-offset amplb EA(3,1)-offset amplb E(4,1)-offset amplb EA(4,1)-
offset amplb E(5,1)-offset amplb EA(5,1)-offset amplb E(6,1)-offset amplb EA(6,1)-
offset amplb E(7,1)-offset amplb EA(7,1)-offset amplb E(8,1)-offset amplb EA(8,1)-
offset amplb E(9,1)-offset amplb EA(9,1)-offset amplb E(10,1)-offset amplb EA(10,1)-
```

```
offset amplb E(11,1)-offset amplb EA(11,1)-offset amplb E(12,1)-offset amplb EA(12,1)-
offset amplb E(13,1)-offset amplb EA(13,1)-offset amplb E(14,1)-offset amplb EA(14,1)-
offset amplb E(15,1)-offset amplb EA(15,1)-offset  amplb E(16,1)-offset amplb
EA(16,1)-offset  amplb E(17,1)-offset amplb EA(17,1)-offset amplb E(18,1)-offset amplb
EA(18,1)-offset amplb E(19,1)-offset amplb EA(19,1)-offset amplb E(20,1)-offset amplb
EA(20,1)-offset amplb amplb amplb amplb amplb amplb amplb amplb amplb amplb
amplb amplb amplb amplb amplb amplb amplb amplb amplb amplb amplb amplb amplb
amplb amplb amplb amplb amplb amplb amplb amplb amplb amplb amplb amplb amplb
amplb -2 -Inf -Inf -Inf ];
ub=[0.5 ampub E(1,1)+offset ampub EA(1,1)+offset ampub E(2,1)+offset ampub
EA(2,1)+offset ampub E(3,1)+offset ampub EA(3,1)+offset ampub E(4,1)+offset ampub
EA(4,1)+offset ampub E(5,1)+offset ampub EA(5,1)+offset ampub E(6,1)+offset ampub
EA(6,1)+offset ampub E(7,1)+offset ampub EA(7,1)+offset ampub E(8,1)+offset ampub
EA(8,1)+offset ampub E(9,1)+offset ampub EA(9,1)+offset ampub E(10,1)+offset ampub
EA(10,1)+offset ampub E(11,1)+offset ampub EA(11,1)+offset ampub E(12,1)+offset ampub
EA(12,1)+offset ampub E(13,1)+offset ampub EA(13,1)+offset ampub E(14,1)+offset ampub
EA(14,1)+offset ampub E(15,1)+offset ampub EA(15,1)+offset  ampub E(16,1)+offset ampub
EA(16,1)+offset  ampub E(17,1)+offset ampub EA(17,1)+offset ampub E(18,1)+offset ampub
EA(18,1)+offset ampub E(19,1)+offset ampub EA(19,1)+offset ampub E(20,1)+offset ampub
EA(20,1)+offset ampub ampub ampub ampub ampub ampub ampub ampub ampub ampub ampub
ampub ampub ampub ampub ampub ampub ampub ampub ampub ampub ampub ampub ampub ampub
ampub ampub ampub ampub ampub ampub ampub ampub ampub ampub ampub ampub ampub ampub
ampub -0.5 Inf Inf Inf ];

options=optimset('MaxFunEvals',5000000,'TolFun',1e-8,'MaxIter',20000,'TolX', 1E-8);
%options parameters for fitting
[a,resnorm,residual,exitflag,output,lambda,jacobian] = lsqcurvefit(fun, a0, Da,
Counts,lb,ub,options);
%% Store and Report Fit Data
%Store the individual mass fraction peaks and areas for the various ES and
%E peaks
Intensities(:,2)=a(3:4:79);%E_mass
Intensities(:,3)=a(2:4:78);%E_mass areas main peak
Intensities(:,4)=a(82:2:120);%E_mass areas shoulder
Intensities(:,5)=a(5:4:81);%EA_mass
Intensities(:,6)=a(4:4:80);%EA_mass areas main peak
Intensities(:,7)=a(83:2:121);%EA_mass areas shoulder

Ratio=(Intensities(:,6)+Intensities(:,7))./(Intensities(:,3)+Intensities(:,4)); %Ratio
EA/E
Intensities(:,8)=Ratio;
MeanRatio=mean(Ratio(2:19));%Average EA/ES ratio
StdRatio=std(Ratio(2:19)); %Std.dev of ratio
Resid=Counts-fun(a,Da);

%Direct to the variables where data is stored and display the avg and std.
%dev of EA/ES ratio
disp('Variables stored in "Intensities", "Ratio (EA/ES)", "MeanRatio" and "StdRatio"')
disp('Average EA/ES ratio is ...')
disp(MeanRatio)
disp('Std. dev of EA/ES ratio is ...')
disp(StdRatio)

%Plot the data and fits
plot(Da,Counts,Da,fun(a,Da),Da,Resid)
```

"RateDistribution.m"

```
%% RateDistribution: Use EA/ES ratios determined from steady-state MS and kcat (and
errors) to construct avg. and std dev. for k2 and k3. Written by Sam Schneider in June
2018 for utilization with TEM B-lactamases.
% load Ratio (EA/ES) data from .txt file (single column of ratios; no
% header)
[fname,pname]=uigetfile('*.*','Load MS Ratios','MultiSelect','on');
cd(pname);
Data=readtable(fname,'Delimiter',' ','Format','%f %f','ReadVariableNames',false);
x=Data{:,1}; %single column of Ratios from Steady-State MS analysis (MassAnalysis.m)

%input kcat (s-1), kcat std dev, and the # of bootstrap iterations to perform
dlgtitle='Input Information';
numLines=1;
prompt1={'kcat (sec^-1)','kcat Error','Iterations'};
def1={'4.2','1.3','1000000'};
answer1=inputdlg(prompt1,dlgtitle,numLines,def1);
drawnow

kcat=str2num(char(answer1(1))); %average value of kcat (s^-1)
kcat_error=str2num(char(answer1(2))); %standard deviations of kcat (s^-1)
Iter=str2num(char(answer1(3))); %number of iterations to sample

%% Determine k2 values
k2=zeros(length(x),Iter);
for i = 1:Iter;
kcatE=(kcat+(kcat_error*randn(1)));
k2_iter=kcatE.*(1+x);
k2(1:length(x),i)=k2_iter;
end
k2=k2(:);%convert matrix of k2 to single column vector

k2_avg=mean2(k2); %average over all elements of k2 matrix
k2_stddev=std2(k2); %std dev over all elements of k2 matrix
k2_median=median(k2);
yk2=quantile(k2,[0.01 0.025 0.05 0.15865 0.25 0.50 0.75 0.84135 0.95 0.975 0.99]);

disp('**********************************************************************************
*****************************')
AVG_k2 = sprintf('  The MEAN k2 (s-1) is   %d   with std. dev of %d (68CI) [  %d  ,
%d  ], 95CI of [  %d  ,  %d  ]', k2_avg,k2_stddev,(k2_avg-
k2_stddev),(k2_avg+k2_stddev),(k2_avg-2*k2_stddev),(k2_avg+2*k2_stddev));
disp(AVG_k2);
MEDIAN_k2 = sprintf('The MEDIAN k2 (s-1) is   %d   with std. dev of (68CI) [  %d  ,
%d  ], 95CI of [  %d  ,  %d  ]', k2_median,yk2(4),yk2(8),yk2(2),yk2(10));
disp(MEDIAN_k2);
disp(' ------------------------------------  k2 Quantiles  ---------------------------
--------- ')
disp('The 1.0, 2.5, 5, 15.865, 25, 50, 75, 84.135, 95, 97.5, and 99% quantiles:')
disp(yk2)
disp(' ----------------------------------------------------------------------------------
--------- ')
disp('**********************************************************************************
*****************************')

%% Determine k3 values (independent of k2)
k3=zeros(length(x),Iter);
for i = 1:Iter;
k3(1:length(x),i)=(kcat+(kcat_error*randn(1))).*(1+(1./x));
```

```
end
k3=k3(:);%convert matrix of k3 to single column vector

k3_avg=mean2(k3); %average over all elements of k2 matrix
k3_stddev=std2(k3); %std dev over all elements of k2 matrix
k3_median=median(k3);
yk3=quantile(k3,[0.01 0.025 0.05 0.15865 0.25 0.50 0.75 0.84135 0.95 0.975 0.99]);

disp('**********************************************************************************
*****************************')
disp(' FOR k3 INDEPENDENT OF k2 ')
AVG_k3 = sprintf('  The MEAN k3 (s-1) is   %d   with std. dev of %d [  %d  ,  %d  ],
95CI of [  %d  ,  %d  ]', k3_avg,k3_stddev,(k3_avg-
k3_stddev),(k3_avg+k3_stddev),(k3_avg-2*k3_stddev),(k3_avg+2*k3_stddev));
disp(AVG_k3);
MEDIAN_k3 = sprintf('The MEDIAN k3 (s-1) is   %d   with std. dev of [  %d  ,  %d  ],
95CI of [  %d  ,  %d  ]', k3_median,yk3(4),yk3(8),yk3(2),yk3(10));
disp(MEDIAN_k3);
disp(' ------------------------------------  k3 (k2 INDPENDENT) Quantiles  -----------
-------------------------- ')
disp('The 1.0, 2.5, 5, 15.865, 25, 50, 75, 84.135, 95, 97.5, and 99% quantiles:')
disp(yk3)
disp(' ------------------------------------------------------------------------------------
--------- ')
disp('**********************************************************************************
*****************************')

%% Histogram data of Normalized Probability for k2 and k3
%Plot the Normalized probability distribution of k2. Lines indicate 25, 50
%and 75% percentile
subplot(1,3,1)
j=histogram(k2,'Normalization','probability');
EdgesJ=j.BinEdges;
WidthJ=j.BinWidth;
LimitsJ=j.BinLimits;
BinsJX=[(LimitsJ(1)+(WidthJ/2)):WidthJ:(LimitsJ(2)-(WidthJ/2))];
CountsJ=j.Values;
title('k2 Distribution (s-1)')
xlabel('k2 (sec-1)')
ylabel('Norm. Prob.')
%xlim([-2,12])

line([k2_median, k2_median], [0, max(CountsJ)*1.1],'Color','red','LineStyle','-')
line([yk2(4), yk2(4)], [0, max(CountsJ)*1.1],'Color','red','LineStyle','--')
line([yk2(8), yk2(8)], [0, max(CountsJ)]*1.1,'Color','red','LineStyle','--')
line([yk2(2), yk2(2)], [0, max(CountsJ)]*1.1,'Color','red','LineStyle','-.')
line([yk2(10), yk2(10)], [0, max(CountsJ)]*1.1,'Color','red','LineStyle','-.')
line([k2_avg, k2_avg], [0, max(CountsJ)]*1.1,'Color','green','LineStyle','-')
legend('k2','Median','-1StdDev','+1StdDev','-2StdDev','+2StdDev','Average')

%Plot the Normalized probability distribution of k3. Lines indicate 25, 50
%and 75% percentile
subplot(1,3,2)
h=histogram(k3,'Normalization','probability');
Edges=h.BinEdges;
Width=h.BinWidth;
Limits=h.BinLimits;
BinsX=[(Limits(1)+(Width/2)):Width:(Limits(2)-(Width/2))];
Counts=h.Values;
hold on
%k=histogram(k3d,'Normalization','probability');
%EdgesK=k.BinEdges;
%WidthK=k.BinWidth;
```

```
%LimitsK=k.BinLimits;
%BinsKX=[(LimitsK(1)+(WidthK/2)):WidthK:(LimitsK(2)-(WidthK/2))];
%CountsK=k.Values;
hold off
title('k3 Distribution (s-1)')
xlabel('k3 (sec-1)')
ylabel('Norm. Prob.')
%legend('k3-Ind','k3-Dep')
xlim([-100,(yk3(10)*1.2)])
%xlim([-100,1200])

line([k3_median, k3_median], [0, max(Counts)*1.1],'Color','red','LineStyle','-')
line([yk3(4), yk3(4)], [0, max(Counts)*1.1],'Color','red','LineStyle','--')
line([yk3(8), yk3(8)], [0, max(Counts)]*1.1,'Color','red','LineStyle','--')
line([yk3(2), yk3(2)], [0, max(Counts)]*1.1,'Color','red','LineStyle','-.')
line([yk3(10), yk3(10)], [0, max(Counts)]*1.1,'Color','red','LineStyle','-.')
line([k3_avg, k3_avg], [0, max(Counts)]*1.1,'Color','green','LineStyle','-')

legend('k3-Ind','Median','-1StdDev','+1StdDev','-2StdDev','+2StdDev','Average')

%Plot the BoxPlot of the k3 distribution
subplot(1,3,3)
boxplot(k3,'Notch','on','Symbol','','DataLim',[-100,yk3(10)*1.2])
ylim([-100,(yk3(10)*1.2)])
%boxplot([k3,k3d],'Notch','on','Symbol','','DataLim',[0,yk3(10)*1.2],'Labels',{'k3-
Ind','k3-Dep'})
ylabel('k3 (sec-1)')
title('k3 Distributions (s-1)')

disp('&&&&&&&&&&&&&&&&&&&&&&&&&&&&&&&&&&&&&&&&&&&&&&&&&&&&&&&&&&&&&&&&&&&&&&&&&&&&&&&&&&&&&&
&&&&&&&&&&&&&&&&&&&&&&&&&&&&&&')
disp('(x,y) plot of k2 probability distribution can be made from
"plot(BinsJX,CountsJ)"')
disp('(x,y) plot of k3 probability distribution can be made from
"plot(BinsX,Counts)"')
disp('For reference, in a normal distribution, 1 std. dev contains 68.27% of the data
(2 is 95.45%, 3 is 99.73%)')
disp('&&&&&&&&&&&&&&&&&&&&&&&&&&&&&&&&&&&&&&&&&&&&&&&&&&&&&&&&&&&&&&&&&&&&&&&&&&&&&&&&&&&&&&
&&&&&&&&&&&&&&&&&&&&&&&&&&&&&&')
```